CEN2012

Carmona-Sevilla, Spain
October 01-04, 2012

Conferencia Española de Nanofotónica
Spanish NanoPhotonics Conference

Index

Foreword Page 1

Organisers/ Sponsors Page 2

Committees Page 3

Exhibitors Page 5

Speakers Page 7

Abstracts Page 17

Posters Page 99

Foreword

Following the spirit initiated by the first two editions of the "Conferencia Española de Nanofotónica", held respectively in Tarragona in 2008 and Segovia in 2010, we launch the 3rd edition that will be conducted in Carmona (Sevilla, Spain) during October 01-04, 2012. The Conference aims to gather all the groups carrying out research in Nanophotonics in Spain (as well as somewhere else with interest in the research in Nanophotonics performed here). It intends to spread the research results achieved by all the different Spanish groups and to promote the establishment or reinforcement of contacts between them, as a mean to help the community to become more visible and dynamic.

The Conference technical program aspires to address a wide area of research related to nanophotonics, metamaterials and subwavelength optics. Topics will include all aspects of the research, ranging from fundamental science to nanofabrication or applications.

The Conference will be organized in thematic sessions composed of plenary invited talks and contributed scientific communications (oral and poster).

The meeting will be structured in the following thematic lines, but interactions among them will be promoted:

1. Magnetoplasmonics and Optomechanical systems
2. Novel synthetic routes: materials aspects of photonic nanostructures
3. Colloidal nanophotonics and nanoplasmonics
4. Photonic nanostructures for energy efficient optoelectronic devices
5. Graphene and silicon photonics
6. New concepts and metamaterials
7. Near Field Optics: nanospectroscopy and nanoimaging
8. Nanophotonics for sensing

Finally, thanks must be directed to the staff of all organising institutions whose hard work has helped the smooth organisation and planning of this conference.

THE ORGANISING COMMITTEE

Organisers

Sponsors

Committees

Chair

Hernán Míguez (ICMS-CSIC)

Organizing Committee

Javier Aizpurua (CSIC-DIPC-UPV/EHU)
Antonio Correia (Fundación Phantoms)
María Ujué González (IMM-CSIC)
Cefe López (ICMM-CSIC)
Ricardo Marqués (US)
Lluís Marsal (URV)
Alejandro Martínez (NTC-UPV)
Jordi Martorell (ICFO)
Pablo Aitor Postigo (IMM-CSIC)
Juan José Sáenz (UAM)
Niek van Hulst (ICFO)

Technical Committee

Paloma García Escorial (Fundación Phantoms)
José Luis Roldan (Fundación Phantoms)

Local Committee

Mauricio Calvo (ICMS-CSIC)
Alberto Jiménez (ICMS-CSIC)
Silvia Colodrero (ICMS-CSIC)
Ana Borrás (ICMS-CSIC)
Ángel Barranco (ICMS-CSIC)

Scientific committee

Ramón Alcubilla (UPC)
Gonçal Badenes (ICFO)
Salvador Balle (UIB)
Alvaro Blanco (ICMM-CSIC)
José M. Calleja (UAM)
Enrique Calleja (UPM)
Francesc Díaz (URV)
Concepción Domingo (IEM-CSIC)
Antonio García Martín (IMM-CSIC)
Laura Lechuga (CIN2)
Javier Marti (CTN-UPV)
Luís Martín Moreno (UZ-CSIC)
Juan Martínez-Pastor (ICMUV)
Francisco Meseguer (UPV-CSIC)
Fernando Moreno (UC)
Manuel Nieto-Vesperinas (ICMM-CSIC)
Josep Pallarés (URV)
Roman Quidant (ICFO)
Jose Sánchez-Dehesa (UPV)
José A. Sánchez Gil (IEM-CSIC)
Jan Siegel (IO-CSIC)
Mario Sorolla (UN)
Clivia Sotomayor (ICN-CIN2)
Luis Viña (UAM)

Iberlaser was setup in 1993, and is based in Madrid-Spain. Our principal mission statement is provide research Spanish market with the novel instrumentation and highly qualified servicing.

Our lines of products include:

Bio-technology: Bio-AFM, Force Sensing Optical tweezers. Quantify Forces in Nanobiology. Cell Adhesion and Cell Mechanics Studies.
Microscopy systems (confocal), scientific cameras and live cell imaging software.
Laser Technology: Meets the needs of industry, aerospace, medicine, biomedicine and research. CW and pulsed lasers covering the range UV-VIS-IR. Tunable wavelength. Super continuum laser sources.
Low light Imaging: Ultra sensitive cameras (EMCCD sCMOS). Single photon sensitive and superior speed. Wide dynamic range, large field of view and high resolution. TE cooling.
Photovoltaics: ASTM, IEC, and JIS standards compliant Solar Simulators class AAA.
Completely self-contained systems and provided with certification of standards compliance for spectral match, temporal stability, and spatial uniformity.
Complete PV IV measurement systems. QE characterization.
Spectroscopy: Lamps sources, monochromators, spectrographs and detectors, mono and multi channel, (CCDs , EMCCD, time resolved and Xray cameras).
Microspectroscopy accessories. Modular approach to combined Microscopy & Spectroscopy.
LIBs and Raman systems. Time resolved (TCSPC) and steady state spectrofluorimeters.
Surface chemistry: Molecular interaction studies and Interface analysis (QCM-D and SPR). Monolayers preparation and thin films characterization. (Dip coaters, LB, BAM,IRRAS, Rheometer). Tensiometers optical and force measurements.
Vibrate Control for Sensitive Equipment. Workstations, Optical Tables and Support systems.
We complete our range of products with precision optical components, opto-mechanics and opto-electronics used in lasers, lasers systems and optical instruments.

Iberlaser
Avda. Pirineos, 7 - Oficina 2-8b
28700 San Sebastián de los Reyes (Madrid) Spain
Tel: 91 658 67 60 Fax: 91 654 17 00
www.iberlaser.com
info@iberlaser.com

Iberlaser, s.a.
Electro-Óptica Científica e Industrial
Instrumentación y Láseres

oerlikon
leybold vacuum

oerlikon
leybold vacuum

Oerlikon Leybold Vacuum offers a wide range of advanced vacuum solutions for research purposes and analytical processes, as well as for manufacturing processes.
The company's core capabilities centre on the development of application and customer specific systems for the creation of vacuum and extraction of process gases.
Oerlikon Leybold Vacuum's ability to meet highest requirements of most complex applications gives our customers the competitve edge to succeed. High duty processes in metallurgy, clean-room conditions at worldwide renowned institutes for research and development, or coating applications of minute dimensions – Oerlikon Leybold Vacuum offers highest performance.

Market Areas & Core Competencies: Areas of application are to be found in the every-day-life processes such as air conditioning, TV-tubes and automotive applications, heavy-duty applications in metallurgy and furnace, but also in high technological processes like coating of microchips, CDs and DVDs, as well as in the manufacturing of optical glass or analytical instruments.
With the experience of more than 162 years in vacuum technology, Oerlikon Leybold Vacuum uses the broad know how of processes and applications to optimize their customers' manufacturing processes, also offering additional services and customer proximity based on one of the largest world-wide sales and after sales network. Oerlikon Leybold Vacuum ranks among the top three providers in its specific business segments, which are Research & Development, Process Industry and Coating Technologies, Analytical Processes.
Products & Solutions: The product range of Oerlikon Leybold Vacuum comprises fore vacuum pumps, high vacuum pumps, vacuum systems, vacuum gauges, leak detecting instruments, flanges, fittings and valves, as well as consulting and engineering of complete vacuum solutions for specified customer applications.
A global, customized after sales service and network complements with multiple services all vacuum technology applications and represents the competencies of Oerlikon Leybold Vacuum.
Sales- & Customer Support: With 32 own locations and 48 agents and representatives Oerlikon Leybold Vacuum offers its customers one of the largest sales and after sales network of the vacuum technology industry.

Oerlikon Leybold Vacuum Spain

Marie Vaudolon
Marketing
C/ Huelva 7
E-08940 Cornellá de Llobregat (Barcelona)
Tel: 93 666 43 11 Fax: 93 666 43 70
marie.vaudolon@oerlikon.com
www.oerlikon.com/leyboldvacuum/spain

Speakers

Speakers

Index alphabetical order

I: Invited Lecture
O: Oral Presentation

		Page
Rafael Abargues Lopez (Intenanomat, Spain) *"Microplotter Printing of LSPR sensor based on Ag-PVA nancomposite for amine detection"*	O	**19**
Mohamed Ameen Poyli (Centro de Física de Materiales, CFM (CSIC-UPV/EHU) & DIPC, Spain) *"Multiscale Theoretical Modelling of Plasmonic Sensing of Hydrogen Uptake in Palladium Nanodisks"*	O	**21**
Gaspar Armelles (IMM-CSIC, Spain) *"Magnetoplasmonics: combining magnetic and plasmonic functionalities"*	I	**23**
Paloma Arroyo Huidobro (Universidad Autónoma de Madrid, Spain) *"Transformation Optics for Plasmonics"*	O	**24**
Victor Samuel Balderrama Vázquez (Universitat Rovira i Virgili /DEEEA, Spain) *"Organic Nanostructures with Low Band-Gap Materials: Manufacturing by Via Template-Assisted Method and Characterization for Optoelectronic Applications"*	O	**26**
Ana Isabel Becerro (ICMSE-CSIC, Spain) *"Multicolor and white light emission of $GdPO_4$ nanophosphors with a novel 3D architecture"*	O	**28**
Alvaro Blanco (ICMM-CSIC, Spain) *"Exploration and use of water in silica colloidal crystals"*	O	**30**
Alvaro Blanco (ICMM-CSIC, Spain) *"Presentation of the Nanophotonics for Energy network"*	O	**32**
Ana Borras (ICMSE-CSIC, Spain) *"A vacuum methodology for the fabrication of hybrid core@shell (ONWs@ZnO) nanowires"*	O	**33**
Antoine Brimont (Nanophotonics Technology Center, UPV, Spain) *"Recent progress on high contrast 40Gb/s and low drive voltage 10 Gb/s slow light-based silicon photonic modulators"*	O	**34**
Mauricio Calvo (ICMSE-CSIC, Spain) *"Integration of Gold Nanoparticles in Optical Resonators"*	O	**36**
Silvia Colodrero (ICMSE-CSIC, Spain) *"Two dimensional nanostructured surface relief patterns as optical diffraction gratings for enhanced photovoltaic performance"*	O	**37**
Nuno de Sousa (Universidad Autónoma de Madrid, Spain) *"Light emission statistics in correlated random photonic nanostructures"*	O	**38**
Vicente Delgado (Universidad de Sevilla, Spain) *"Simplified coupled-wave analysis for the characterization of extraordinary optical transmission in single and stacked metallic screens"*	O	**40**
Alberto Escudero (ICMSE-CSIC, Spain) *"Microwave assisted synthesis of Poly (acrylic acid) functionalised europium doped calcium hydroxyapatite and fluoroapatite nanospindles for biomedical application"*	O	**42**
André Espinha (ICMM-CSIC, Spain) *"Surface nano-structuration using composite colloidal monolayers"*	O	**44**
Zeno Gaburro (School of Engineering and Applied Sciences, Harvard University, USA) *"Molding light propagation with phase discontinuities"*	I	**46**

		Page
Juan Galisteo-López (ICMM-CSIC, Spain) *"Light propagation and emission in hybrid metallodielectric systems based on self-assembled structures"*	O	**47**
Francisco J. Garcia Vidal (Universidad Autonoma de Madrid, Spain) *"Graphene Nanophotonics"*	I	**48**
Blas Garrido (Universitat de Barcelona, Spain) *"Silicon nanocrystalls for all silicon tandem solar cells"*	O	**49**
Michael Giersig (Freie Universitat berlin, Germany) *"Electromagnetic waves interaction with various metallic nanomaterials"*	I	**51**
Raquel Gómez-Medina (Universidad Autonoma de Madrid, Spain) *"Negative scattering asymmetry parameter for dipolar particles: Unusual reduction of the transport mean free path and radiation pressure"*	O	**52**
Rainer Hillenbrand (CIC nanoGUNE, Spain) *"Infrared Nanospectroscopy - From Nanoscale Chemical Identification of Polymersto Real-space Imaging of Graphene Plasmons"*	I	**54**
Ignacio Iglesias (Universidad de Murcia, Spain) *"Light spin forces, polarization structuring and the trapping of small particles with optical tweezers"*	O	**56**
Tobias J. Kippenberg (EPFL, Switzerland) *"Cavity Optomechanics: Quantum coherent coupling of light and mechanical oscillators"*	I	**57**
Frank Koppens (ICFO, Spain) *"Graphene nano-optoelectronics for capturing and manipulating light at the nanoscale"*	I	**58**
Luis M. Liz-Marzan (CIC-biomaGUNE, Spain) *"Colloidal Plasmonic Nanostructures"*	I	**60**
Alejandro Manjavacas Arevalo (IQFR CSIC, Spain) *"Graphene plasmons and quantum emitters: from plasmon blockade to temporal control"*	O	**61**
Ricardo Marqués (Universidad de Sevilla, Spain) *"Babinet principle in optical nano-circuits and metamaterials"*	O	**62**
Lluis F. Marsal (Universitat Rovira i Virgili, Spain) *"Structural engineering of micro- and nanoporous silicon and nanoporous alumina for biosensing applications"*	O	**64**
Diana Martín-Becerra (IMM-CNM-CSIC, Spain) *"Theoretical analysis of magnetoplasmonic interferometers for sensing"*	O	**66**
Alejandro Martinez (Nanophotonics Technology Center – UPV, Spain) *"Strong magnetic field concentration in arrays of thick gold nanorings"*	O	**68**
Alejandro Martínez (Nanophotonics Technology Center – UPV, Spain) *"Report of the Nanophotonics Europe Association"*	O	**-**
Juan P. Martínez Pastor (Instituto de Ciencia de los Materiales de la Universidad de Valencia, Spain) *"Plasmonic layers based on noble metal nanoparticles embedded in oxides for photovoltaic applications"*	O	**69**
Agustín Mihi (ICFO, Spain) *"Coupling of Resonant Modes of Embedded Dielectric Microspheres in Solution-Processed Solar Cells"*	O	**71**
Fernando Moreno (Universidad de Cantabria, Spain) *"A study of the Near-Field of metallic materials for Plasmonics in the UV"*	O	**73**
Viktor Myroshnychenko (IQFR-CSIC, Spain) *"Plasmon spectroscopy and imaging of individual gold nanodecahedra: A combined optical microscopy, cathodoluminescence, and electron energy-loss spectroscopy study"*	O	**75**

		Page
Ramón Paniagua Domínguez (Instituto de Estrcutura de la Materia (CSIC), Spain) *"Exotic optical properties of metallo-dielectric core-shell nanospheres and nanowires. Applications to negative refraction"*	O	**76**
Francesco Pastorelli (ICFO-Institut de Ciències Fotòniques, Spain) *"Self assembled dimers of metallic nano-particles for enhanced light harvesting in organic solar cells"*	O	**78**
Pablo Aitor Postigo (IMM-CNM-CSIC, Spain) *"Fabrication of Photonic Crystal Chips for Biophotonic Applications"*	O	**80**
Mohammad Mahbubur Rahman (Universitat Rovira i Virgili, Spain) *"Nanoporous anodic alumina produced with variable voltages"*	O	**81**
Pablo Romero (ICFO – The Institute of Photonic Sciences, Spain) *"Photonic crystal back electrode design for highly efficient transparent polymer cells"*	O	**83**
Juan José Sáenz (Universidad Autónoma de Madrid, Spain) *"Non-conservative optical forces on nano particles"*	O	**85**
Mikolaj Schmidt (DIPC and Centro de Física Materiales CSIC-UPV/EHU, Spain) *"New pathways to control single emitter radiation in novel electric and magnetic antenna platforms"*	O	**87**
Lei Shi (ICMM/CSIC-UPV, Spain) *"A New Dielectric Metamaterial building block with a strong magnetic response below 1.5 micrometers region. Silicon Colloids nanocavities"*	O	**88**
Isaac Suárez (Instituto de Ciencia de los Materiales de la UVEG, Spain) *"Colloidal QDs/PMMA nanocomposites as material to provide gain in surface plasmon polaritons"*	O	**89**
Sukosin Thongrattanasiri (IQFR-CSIC, Spain) *"Quantum Junction Plasmons in Graphene Dimers"*	O	**91**
Aitor Velasco (Universidad Complutense, Spain) *"High Resolution Fourier-Transform Microspectrometers in Silicon-on-Insulator Waveguides"*	O	**92**
Alan Vitrey (IMM-CNM-CSIC, Spain) *"Rearrangement of the near-field landscape in heterogeneous nanoparticle arrays"*	O	**94**
Ondrej Vlasin (ICMAB-CSIC, Spain) *"Shaping Magneto-Optical Spectra with Plasmonic Resonances"*	O	**96**

Invited Speakers

Index alphabetical order

	Page
Gaspar Armelles (IMM-CSIC, Spain) *"Magnetoplasmonics: combining magnetic and plasmonic functionalities"*	**23**
Zeno Gaburro (School of Engineering and Applied Sciences, Harvard University, USA) *"Molding light propagation with phase discontinuities"*	**46**
Francisco J. Garcia Vidal (Universidad Autonoma de Madrid, Spain) *"Graphene Nanophotonics"*	**48**
Michael Giersig (Freie Universitat berlin, Germany) *"Electromagnetic waves interaction with various metallic nanomaterials"*	**51**
Rainer Hillenbrand (CIC nanoGUNE, Spain) *"Infrared Nanospectroscopy - From Nanoscale Chemical Identification of Polymersto Real-space Imaging of Graphene Plasmons"*	**54**
Tobias J. Kippenberg (EPFL, Switzerland) *"Cavity Optomechanics: Quantum coherent coupling of light and mechanical oscillators"*	**57**
Frank Koppens (ICFO, Spain) *"Graphene nano-optoelectronics for capturing and manipulating light at the nanoscale"*	**58**
Luis M. Liz-Marzan (CIC-biomaGUNE, Spain) *"Colloidal Plasmonic Nanostructures"*	**60**

Orals

Index alphabetical order

	Page
Rafael Abargues Lopez (Intenanomat, Spain) *"Microplotter Printing of LSPR sensor based on Ag-PVA nancomposite for amine detection"*	**19**
Mohamed Ameen Poyli (Centro de Física de Materiales, CFM (CSIC-UPV/EHU) & DIPC, Spain) *"Multiscale Theoretical Modelling of Plasmonic Sensing of Hydrogen Uptake in Palladium Nanodisks"*	**21**
Paloma Arroyo Huidobro (Universidad Autónoma de Madrid, Spain) *"Transformation Optics for Plasmonics"*	**24**
Victor Samuel Balderrama Vázquez (Universitat Rovira i Virgili /DEEEA, Spain) *"Organic Nanostructures with Low Band-Gap Materials: Manufacturing by Via Template-Assisted Method and Characterization for Optoelectronic Applications"*	**26**
Ana Isabel Becerro (ICMSE-CSIC, Spain) *"Multicolor and white light emission of $GdPO_4$ nanophosphors with a novel 3D architecture"*	**28**
Alvaro Blanco (ICMM-CSIC, Spain) *"Exploration and use of water in silica colloidal crystals"*	**30**
Alvaro Blanco (ICMM-CSIC, Spain) *"Presentation of the Nanophotonics for Energy network"*	**32**
Ana Borras (ICMSE-CSIC, Spain) *"A vacuum methodology for the fabrication of hybrid core@shell (ONWs@ZnO) nanowires"*	**33**
Antoine Brimont (Nanophotonics Technology Center, UPV, Spain) *"Recent progress on high contrast 40Gb/s and low drive voltage 10 Gb/s slow light-based silicon photonic modulators"*	**34**
Mauricio Calvo (ICMSE-CSIC, Spain) *"Integration of Gold Nanoparticles in Optical Resonators"*	**36**
Silvia Colodrero (ICMSE-CSIC, Spain) *"Two dimensional nanostructured surface relief patterns as optical diffraction gratings for enhanced photovoltaic performance"*	**37**
Nuno de Sousa (Universidad Autónoma de Madrid, Spain) *"Light emission statistics in correlated random photonic nanostructures"*	**38**
Vicente Delgado (Universidad de Sevilla, Spain) *"Simplified coupled-wave analysis for the characterization of extraordinary optical transmission in single and stacked metallic screens"*	**40**
Alberto Escudero (ICMSE-CSIC, Spain) *"Microwave assisted synthesis of Poly (acrylic acid) functionalised europium doped calcium hydroxyapatite and fluoroapatite nanospindles for biomedical application"*	**42**
André Espinha (ICMM-CSIC, Spain) *"Surface nano-structuration using composite colloidal monolayers"*	**44**
Juan Galisteo-López (ICMM-CSIC, Spain) *"Light propagation and emission in hybrid metallodielectric systems based on self-assembled structures"*	**47**

	Page
Blas Garrido (Universitat de Barcelona, Spain) *"Silicon nanocrystalls for all silicon tandem solar cells"*	**49**
Raquel Gómez-Medina (Universidad Autonoma de Madrid, Spain) *"Negative scattering asymmetry parameter for dipolar particles: Unusual reduction of the transport mean free path and radiation pressure"*	**52**
Ignacio Iglesias (Universidad de Murcia, Spain) *"Light spin forces, polarization structuring and the trapping of small particles with optical tweezers"*	**56**
Alejandro Manjavacas Arevalo (IQFR CSIC, Spain) *"Graphene plasmons and quantum emitters: from plasmon blockade to temporal control"*	**61**
Ricardo Marqués (Universidad de Sevilla, Spain) *"Babinet principle in optical nano-circuits and metamaterials"*	**62**
Lluis F. Marsal (Universitat Rovira i Virgili, Spain) *"Structural engineering of micro- and nanoporous silicon and nanoporous alumina for biosensing applications"*	**64**
Diana Martín-Becerra (IMM-CNM-CSIC, Spain) *"Theoretical analysis of magnetoplasmonic interferometers for sensing"*	**66**
Alejandro Martinez (Nanophotonics Technology Center – UPV, Spain) *"Strong magnetic field concentration in arrays of thick gold nanorings"*	**68**
Alejandro Martínez (Nanophotonics Technology Center – UPV, Spain) *"Report of the Nanophotonics Europe Association"*	**-**
Juan P. Martínez Pastor (Instituto de Ciencia de los Materiales de la Universidad de Valencia, Spain) *"Plasmonic layers based on noble metal nanoparticles embedded in oxides for photovoltaic applications"*	**69**
Agustín Mihi (ICFO, Spain) *"Coupling of Resonant Modes of Embedded Dielectric Microspheres in Solution-Processed Solar Cells"*	**71**
Fernando Moreno (Universidad de Cantabria, Spain) *"A study of the Near-Field of metallic materials for Plasmonics in the UV"*	**73**
Viktor Myroshnychenko (IQFR-CSIC, Spain) *"Plasmon spectroscopy and imaging of individual gold nanodecahedra: A combined optical microscopy, cathodoluminescence, and electron energy-loss spectroscopy study"*	**75**
Ramón Paniagua Domínguez (Instituto de Estrcutura de la Materia (CSIC), Spain) *"Exotic optical properties of metallo-dielectric core-shell nanospheres and nanowires. Applications to negative refraction"*	**76**
Francesco Pastorelli (ICFO-Institut de Ciències Fotòniques, Spain) *"Self assembled dimers of metallic nano-particles for enhanced light harvesting in organic solar cells"*	**78**
Pablo Aitor Postigo (IMM-CNM-CSIC, Spain) *"Fabrication of Photonic Crystal Chips for Biophotonic Applications"*	**80**
Mohammad Mahbubur Rahman (Universitat Rovira i Virgili, Spain) *"Nanoporous anodic alumina produced with variable voltages"*	**81**
Pablo Romero (ICFO – The Institute of Photonic Sciences, Spain) *"Photonic crystal back electrode design for highly efficient transparent polymer cells"*	**83**
Juan José Sáenz (Universidad Autónoma de Madrid, Spain) *"Non-conservative optical forces on nano particles"*	**85**
Mikolaj Schmidt (DIPC and Centro de Física Materiales CSIC-UPV/EHU, Spain) *"New pathways to control single emitter radiation in novel electric and magnetic antenna platforms"*	**87**

	Page
Lei Shi (ICMM/CSIC-UPV, Spain) *"A New Dielectric Metamaterial building block with a strong magnetic response below 1.5 micrometers region. Silicon Colloids nanocavities"*	**88**
Isaac Suárez (Instituto de Ciencia de los Materiales de la UVEG, Spain) *"Colloidal QDs/PMMA nanocomposites as material to provide gain in surface plasmon polaritons"*	**89**
Sukosin Thongrattanasiri (IQFR-CSIC, Spain) *"Quantum Junction Plasmons in Graphene Dimers"*	**91**
Aitor Velasco (Universidad Complutense, Spain) *"High Resolution Fourier-Transform Microspectrometers in Silicon-on-Insulator Waveguides"*	**92**
Alan Vitrey (IMM-CNM-CSIC, Spain) *"Rearrangement of the near-field landscape in heterogeneous nanoparticle arrays"*	**94**
Ondrej Vlasin (ICMAB-CSIC, Spain) *"Shaping Magneto-Optical Spectra with Plasmonic Resonances"*	**96**

Abstracts

Microplotter Printing of LSPR sensor based on Ag-PVA nancomposite for amine detection

R. Abargues[a], P.J. Rodríguez-Cantó[b], S. Albert[a], I. Suárez[b] and J. P. Martínez-Pastor[b]

[a]Intenanomat S.L., Catedrático José Beltrán 2, 46980 Paterna, Spain
[b]Instituto de Ciencia de los Materiales, Universidad de Valencia, P.O. Box 22085, 46071 Valencia, Spain

Rafael.Abargues@uv.es

Molecular sensing and detection based on localized surface plasmon resonance (LSPR) have attracted intense interest for detection of biomolecules with high sensitivity and low cost. LSPR of Au and Ag nanoparticles (NPs) strongly depends on the refractive index of the surrounding medium (substrate, solvent, and adsorbates) [1]. Recently, we proposed a novel LSPR sensing platform based on nanocomposite of Ag nanoparticles embedded on a polymer matrix such as PVA and Novolak for the detection of 2-mercaptoethanol [2,3]. The advantage of these materials is that Ag NPs are in situ synthesized inside the host polymers by a one-step procedure during the bake step of the formation of a nanocomposite thin film. Additionally, these materials can be patterned by e-beam and UV lithography [3,4,5], which may form the basis to the microfabrication of biochip sensors.

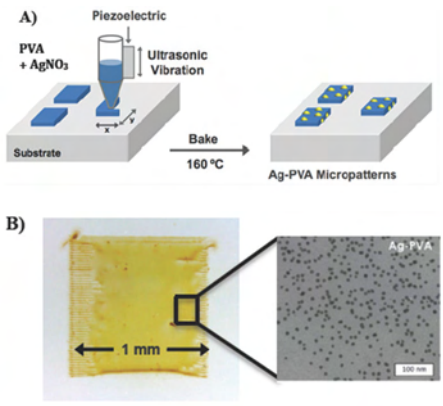

Figure 1: a) Scheme of the fabrication of Ag-PVA nanocomposite by microplotter printing. b) 1 mm-side pattern of Ag-PVA fabricated by microplotter printing and the corresponding TEM image.

In the present work we report on the fabrication of Ag-PVA sensors by a high-precision microplotter, a very promising direct-write technology developed for printing materials from solution, which may form the basis to the future microfabrication of LSPR sensors. Thus, we have formulated a novel nanoink based on a solution of the metallic NP precursor ($AgNO_3$) and the polymer (PVA). After the printing procedure, the patterns are bake and the NPs are synthesized inside the polymer. Figure 1.b shows an optical microscope image of 1 mm-side square Ag-PVA structure printed on a glass substrate from the optimized ink formulation and bake conditions and the corresponding TEM image.

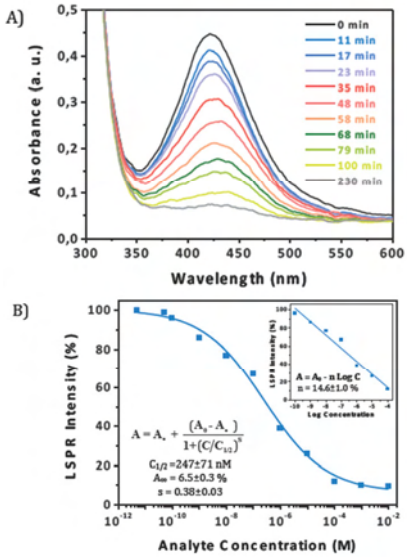

Figure 2: a) LSPR curve of a Ag-PVA thin film before and after immersing on an aqueous solution of 10^{-4} M ethylenediamine. b) Absorption decay response of Ag-PVA sensors as a function of the ethylenediamine concentration for immersing time of 1000 min. Inset: linear regresion of the calibration curve in the linear detection range.

Now, we extend the sensing capability of Ag nanocomposites to the detection of amine-basedanalytes both in solution and in vapor. Sensing of amine species in aqueous solutions is of great importance not only for environmental and industrial monitoring applications but also for the quality control of food products. Figure 2a exhibits the LSPR absorption curve of the Ag-PVA nanocomposites thin film after immersing into an aqueous solution of 10^{-4} M ethylenediamine for different times. We observed that LSPR intensity and LSPR shift evolve as a function of the immersing time. Analyte binding to Ag NPs is a strongly time-depending phenomenon. Figure 2b shows the LSPR absorption decay response of Ag-PVA sensors as a function of the EDA concentration for immersing time of 1000 min. Calibration curves for analyte binding assays are generally characterized by a sigmoidal relationship between the sensor response and the analyte concentration. Ag-PVA structures exhibit a limit of detection (LOD) of 0.1 nM. The maximum sensor response, this is the sensor saturation, is achieved for an analyte concentrations above 10^{-4} M. The linear detection range for EDA was estimated to be over an analyte concentration of six orders of magnitude, from 10^{-10} to 10^{-4} M. The sensitivity was determined to be 14.6±1.0 % from the slope of the linear regresion of the calibration curve shown in the inset of Figure 2b.

The response of the Ag-PVA was also performed by exposing the nanocomposite patterns to the vapors of several biogenic (putrescine, cadaverine) and synthetic (methylenediamine and ethylenediamine) amines. Because these amines are to a greater or lesser extent volatile, it is expected that a certain amount of diamines can be in the vapor phase. Figure 3 shows the real-time sensor response to different diamines and water. We measured a different sensor response to the amines tested. This can be mainly explained in terms of the analyte relative pressure in the vapor phase but also due to their different binding affinity for Ag NPs. The largest responses were obtained for shorter diamines (methylenediamine>ethylenediamine>>putrescine> cadaverine) because these molecules are more volatile and therefore their concentration in the vapor phase is higher.

This work confirms that a fully disposable sensing platform technology can be developed on this material because the proposed nanocomposite is easy-to-prepare, easy-to-use and low-cost and allows miniaturization.

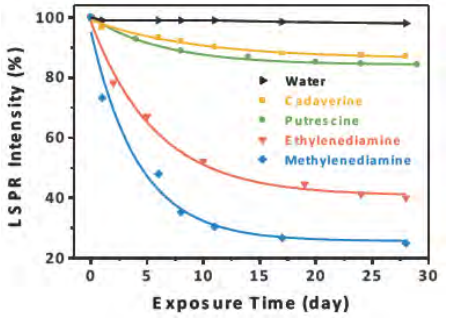

Figure 3: The real-time kinetic response of Ag-PVA exposed to the vapors of methylenediamine, ethylenediamine, putrescine and cadaverine.

References

[1] J. N. Anker, W. P. Hall, O. Lyandres, N. C. Shah, J. Zhao, R. P. Van Duyne, Nature Materials 7, (2008) 442.

[2] Gradess R., Abargues R., Habbou A., Canet-Ferrer J., Pedrueza E., Russell A., Valdés J. L., Martínez-Pastor J. P., J. Mater. Chem., 19, (2009), 9233-9240.

[3] Abargues R., Marques-Hueso J., Canet-Ferrer J., Pedrueza E., Valdes J.L., Jimenez E., Martınez-Pastor J. P., Nanotechnology, 19, (2009), 355308.

[4] Marqués-Hueso J., Abargues R., Canet-Ferrer J., Agouram S., Valdés J. L., Martínez-Pastor J. P., Langmuir 26, (2010), 2825-30.

[5] Marqués-Hueso J., Abargues R., Valdés J. L., Martínez-Pastor J. P., J. Mater. Chem. 20 (2010) 35, 7436.

Multiscale Theoretical Modelling of Plasmonic Sensing of Hydrogen Uptake in Palladium Nanodisks

M. Ameen Poyli[1,2], V. M. Silkin[2,3,4], I. P. Chernov[5], P. M. Echenique[1,2,3], R. Díez Muiño[1,2] and J. Aizpurua[1,2]

[1]Centro de Física de Materiales CFM (CSIC-UPV/EHU)-Materials Physics Center MPC, San Sebastián, Spain
[2]Donostia International Physics Center (DIPC), San Sebastián, Spain
[3]Departamento de Física de Materiales, Facultad de Químicas UPV/EHU, San Sebastián, Spain
[4]IKERBASQUE, Basque Foundation for Science, Bilbao, Spain
[5]Tomsk Polytechnical University, Tomsk, Russia

aizpurua@ehu.es

The study of Hydrogen uptake and its diffusion dynamics in metals has raised a lot of theoretical and experimental research because of its importance in a variety of relevant applications like efficient and safe hydrogen storage [1], hydrogen sensing [2] and nanocatalysis [3]. We analyse theoretically the optical properties of Palladium nanodisks during hydrogen uptake. The theoretical description of the optical response of Pd-H system is not an easy task due to (i) the presence of different phases (α and β phases) that H can adopt when absorbed into Pd and (ii) different length scales involved in the hydrogen uptake process. We first obtain the dielectric response of Pd-H using *ab initio* quantum mechanical calculations [4]. The quantum mechanical calculations consider the atomic scale changes occurring in Pd during hydrogen uptake. The crystal lattice used in the ab initio calculations is shown in Fig. 1(a). The calculated dielectric functions are then used in the full electrodynamical calculations of light scattering by H-modified Pd nanodisks. The electrodynamical calculations include the details of the size, shape and the environment affects of the mesoscopic system. Thus our multiscale theoretical approach address both the atomic level as well as the mesoscopic level changes responsible for the total optical response of the palladium hydride disks during hydrogen uptake.

Two different phases of Pd-H (α with low H concentration and β with higher H concentration) can coexist as the H concentration increases. We follow the spectral evolution of the localized surface plasmon peak of the disks for different admixtures of the Pd-H α and β phases (Fig. 1b) and reproduce the experimental [5] plasmon energy shift produced by the structural inhomogeneity upon hydrogen absorption (Fig. 1c). Our combined theoretical framework provides a solid background to describe plasmonic sensing in the dynamics of structural domains, as well as to identify hydrogen saturation conditions in metal-hydrides.

References

[1] L. Schlapbach and A. Zuttel, Hydrogen-storage materials for mobile applications. Nature, 414 (2001) 353-358.
[2] N. Liu, M. L. Tang, M. Hentschel, H. Giessen and A. P. Alivisatos, Nanoantenna-enhanced gas sensing in a single tailored nanofocus. Nat. Mater. 10 (2011), 631-636.
[3] M. Wilde, K. Fukutani, W. Ludwig, B. Brandt, J. H. Fischer, S. Schauermann, and H. J. Freund, Influence of carbon deposition on the hydrogen distribution in Pd nanoparticles and their reactivity in Olefin hydrogenation. Angew. Chem. Int. Ed., 47 (2008) 9289-9293.
[4] V. M. Silkin, R. Díez Muiño, I. P. Chernov, E. V. Chulkov, and P. M. Echenique, Tuning the plasmon energy of palladium–hydrogen systems by varying the hydrogen concentration, J. Phys.: Condens. Matter, 24 (2012) 104021.
[5] I. Zoríc, E. M. Larsson, B. Kasemo, and C. Langhammer, Localized surface plasmons shed light on nanoscale metal hydrides, Adv. Mater., 22 (2010) 4628.

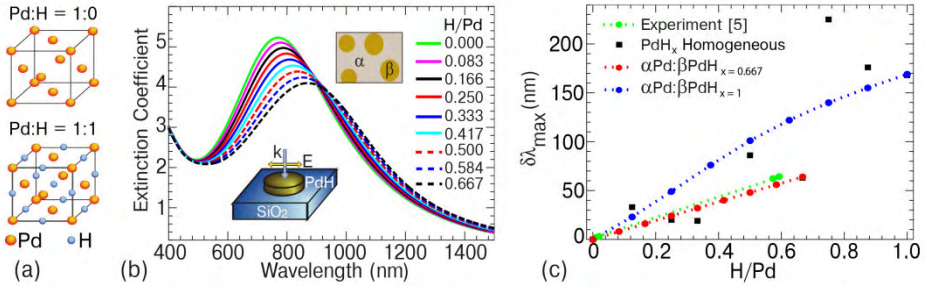

Figure 1: (a) Crystal lattice of $PdH_{x=0}$ and $PdH_{x=1}$ used in the ab initio calculations. (b) Extinction spectra for a PdH disk of 20 nm thickness and 190 nm diameter calculated using Bruggeman's effective dielectric function with α phase of $PdH_{x=0}$ and β of $PdH_{x=0.667}$ for different H/Pd ratios. (c) LSPR shifts calculated for a Pd-H disk of 20 nm thickness and 300 nm diameter placed on SiO_2 substrate plotted as a function of H/Pd using Bruggeman's effective dielectric function with the β phase taken as $PdH_{x=0.667}$ (red dots) and as $PdH_{x=1}$ (blue dots). A comparison with experimental results from Ref. [5] (green dots) is shown. The black dots give the spectral shift for a homogeneous distribution of H in Pd.

Magnetoplasmonics: combining magnetic and plasmonic functionalities

Gaspar Armelles, Juan Carlos Banthi, Alfonso Cebollada, Elias Ferreiro-Vila, Antonio García-Martín, Jose Miguel García-Martin, María Ujué González, Diana Martin-Becerra and David Meneses-Rodriguez

IMM-Instituto de Microelectrónica de Madrid (CNM-CSIC), Isaac Newton 8, PTM,
E-28760 Tres Cantos, Madrid, Spain

Nanosystems with combined magnetic and plasmonic functionalities have in recent years become an active topic of research. In these new structures, know as magneto-plasmonics, magnetic and plasmonic properties are intertwined, allowing for example plasmonic properties to become tunable upon de application of a magnetic field (active plasmonics) [1], or the Magneto-Optical (MO) effects to be largely increased by plasmon resonance excitation, as a consequence of the enhancement of the electromagnetic (EM) field in the MO active component of the structure [2]. In this last case, the study of the enhanced MO activity in structures with subwavelength dimensions is especially interesting since they may be viewed as nanoantennas in the visible range with MO functionalities. The light harvesting properties of these systems upon plasmon resonance excitation bring as a consequence an enhanced EM field in its interior, and more interestingly in the region where the MO active component is present [3]. At this stage, optimizing the EM field distribution within the structure by maximizing it in the MO components region while simultaneously minimizing it in all the other, non MO active, lossy components, will allow for the development of novel systems with even larger MO activity with reduced optical losses [4].

References

[1] V. V. Temnov, G. Armelles, U. Woggon, D. Guzatov, A. Cebollada, A. Garcia-Martin, J. M. Garcia-Martin, T. Thomay, A. Leitenstorfer, R. Bratschitsch, Nat. Photonics 4 (2010) 107–111.

[2] G. Armelles, A. Cebollada, A. García-Martín, J.M. García-Martín, M.U. González, J.B. González-Díaz, E. Ferreiro-Vila, and J.F. Torrado, Journal of Optics A: Pure and Applied Optics 11 (2009) 114023..

[3] D. Meneses-Rodríguez, E. Ferreiro-Vila, P. Prieto, J. Anguita, M.U. González, J.M. García-Martín, A. Cebollada, A. García-Martín, and G. Armelles, Small 7(2011), 7, 3317.

[4] J.C. Banthí, D. Meneses-Rodríguez, F. García, M.U. González, A. García-Martín, and G. Armelles, Advanced Materials 24(2012) OP36.

Transformation optics for plasmonics

V P. A. Huidobro[1], M.L. Nesterov[1], F.J. García-Vidal[1] and L. Martín-Moreno[2]

[1]Departamento de Física Teórica de la Materia Condensada, Universidad Autónoma de Madrid, E-28049 Madrid, Spain
[2]Instituto de Ciencia de Materiales de Aragón and Departamento de Física de la Materia Condensada, CSIC–Universidad de Zaragoza, E-50009 Zaragoza, Spain

paloma.arroyo@uam.es

In this talk I will present the concept of Transformation Optics (TO) as applied to Plasmonics, a new strategy to control the flow of surface plasmon polaritons (SPPs) at metal-dielectric interfaces. It is based on the application of the concept of TO, a theoretical framework proposed as a general technique to design complex electromagnetic (EM) media with unusual properties [1,2]. TO provides us with expressions for the dielectric permittivit ε, and the magnetic permeability, μ, that need to be implemented in order to obtain a medium with a desired functionality. This recent proposal has brought a novel way of controlling the flows of photons in any desired way. It is a very general technique that has yield many different optical devices and diverse functionalities.

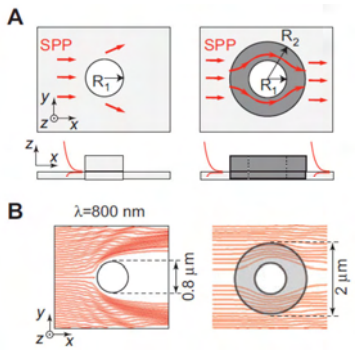

Figure 1: 3D cylindrical cloak for SPPs propagating along an airgold interface. (A) Sketch of the top and side views of the geometry. Left: scattering by a metallic cylinder. Right: the cloak is placed around the cylinder. (B) Power fl ow from 3D simulations. Left: a SPP experiences high scattering losses when it encounters the bare cylinder. Right: the cloak guides the SPP wave suppressing the scattering losses.

Recently [3], we have developed a general methodology for the design of Transformation-Optical devices for SPPs (see Fig. 1). We have shown that TO can also be used to effciently mould the flow of SPPs at metal-dielectric interfaces. Importantly, we have demonstrated that a simplified version of the TO recipes in which the optical parameters (ε and μ) are implemented only in the dielectric side of the interface leads to quasi-perfect functionalities [3,4].

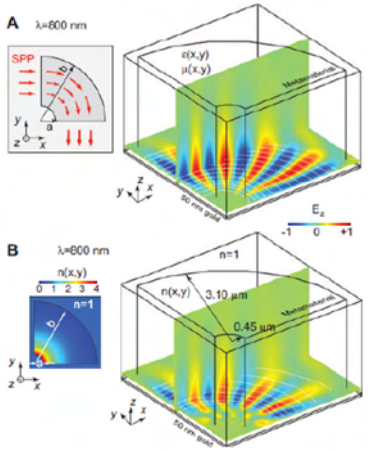

Figure 2: Simulation results for a SPP right-angle bend at = 800 nm. The curvature radius of the bend is ρ = 2 μm and the SPP has a Gaussian profi le of width Δ = 2.65 μm. (A) Anisotropic transformation medium. The propagation direction of a SPP is rotated by 90° by means of a metamaterial with anisotropic ε and μ. Inset: geometry layout in a top view. (B) Isotropic transformation medium. The SPP bend is characterized by the isotropic transformation medium n (x, y) shown in the inset panel. In both (A) and (B) the color scale plots the z component of the electric field of the SPP and the white lines correspond to power flow stream lines.

Additionally, we have shown that, thanks to the quasi two-dimensional character of SPPs and its inherent polarization, the application of conformal and quasi-conformal mapping techniques allows the design of plasmonic devices in which only the refractive index of the dielectric side needs to be engineered [5]. This leads to realistic models of plasmonic devices which can be fabricated with just isotropic dielectric materials (see Figs. 2 and 3) and, moreover, present a broadband response.

We study in detail several examples of plasmonic devices such as cloaks, bends, lenses and shifters. By means of numerical simulations, we quantify their efficiency as a function of the wavelength.

References

[1] J. B. Pendry, D. Schurig and D. R. Smith, Science, 312 (2006) 1780-1782.

[2] U. Leonhardt, Optical conformal mapping, Science, 312 (2006) 1777-1780.

[3] P. A. Huidobro, M. L. Nesterov, L. Martín-Moreno and F. J. García-Vidal, Nanoletters, 10(6) (2010)1985.

[4] Y. Liu, T. Zentgraf, G. Bartal and X. Zhang, Nanoletters, 10(6) (2010) 1991.

[5] P. A. Huidobro, M. L. Nesterov, L. Martín-Moreno and F. J. García-Vidal, New Journal of Physics, 13 (2011) 033011-31.

[6] M. Kadic, S. Guenneau, S. Enoch, P. A. Huidobro, L. Martín-Moreno, F. J. García-Vidal, J. Renger and R. Quidant, Nanophotonic (Review) 0(0) (2012) 1-14.

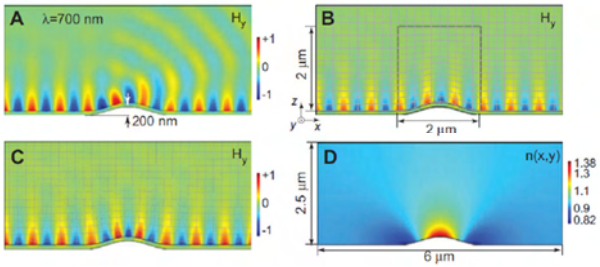

Figure 3: The scattering from a bump on a metal surface can be suppressed by means of a ground-plane cloak. (A) A SPP at 700 nm is scattered when it encounters a cos2 -shaped bump 200 nm high and 2 μm long in an air-gold interface. The SPP propagates in the x direction and the geometry is invariant in the y direction. (B) Scattering losses are suppressed when an anisotropic cloak (2 μm × 2 μm) is placed on top of the bump. The grid lines correspond to the coordinate map of the transfinite transformation used to derive the EM parameters of the cloak.

Organic Nanostructures with Low Band-Gap Materials: Manufacturing by Via Template-Assisted Method and Characterization for Optoelectronic Applications

V.S. Balderrama, P. Formentín, J. Pallarès and L.F. Marsal

Departament d'Enginyeria Electrònica, Elèctrica i Automàtica, Universitat Rovira i Virgili, Avda. Països Catalans 26, 43007 Tarragona, Spain

lluis.marsal@urv.cat

The fabrication of organic nanostructures (NS) in recently years have attracted interest due to potential application in many fields of research as flat panel displays, biological and chemical sensors, electronic and optoelectronic systems in special attention to devices such as polymer light-emitting diodes, transistors, and solar cells among others [1-3]. The organic NS can be manufactured by nanolithography [4], mechanical drawing [5], printing and spin-coating [6] and template-based methods [7]. The method frequently used to fabricate NS is the template synthesis due to its cost effective and versatile fabrication technique. The nanoporous anodic alumina templates (NAATs) is a material widely used as template because the template porous are hexagonally ordered, the geometric characteristics can be easily controlled (i.e. pore diameter, pore length, porosity, degree of hexagonal pore arrangement and thickness) and offer a higher thermal and mechanical stability. The control of its geometric characteristics previous mentioned are controllable by the anodization parameters (anodization voltage, temperature, and type and concentration of the acid electrolyte) [8]. The infiltration process of polymeric material inside of NAAT can be by wetting the template with a polymer solution or melt by direct polymerization of a monomer inside the pores of the template, etc. [9].

In this work, polymeric NS are manufactured with the used of NAATs. The fabrications of NAATs were prepared by two-step anodization process of aluminium metal in an acidic solution [8]. The first anodization step consists of applying the anodization voltage directly (194 V) in an electrolyte consisting of an aqueous solution of phosphoric acid (H_3PO_4) (0.3 M) by 24 hours at 0 ^{o}C while the second step was conducted under the same anodization conditions but for 7.5 min. The NAATs were characterized by environmental scanning electron microscopy (ESEM). Fig. 1 shows the ESEM image of the NAATs obtained with H3PO4 electrolyte. The cross section in Fig. 1 a) reveals a suitable average pore diameter of 180 nm. Fig. 1 b) is shown the top view for NAATs.

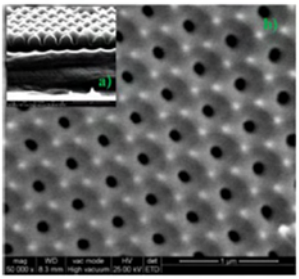

Figure 1: ESEM image of NAATs is shows the cross section view in a) and top view in b).

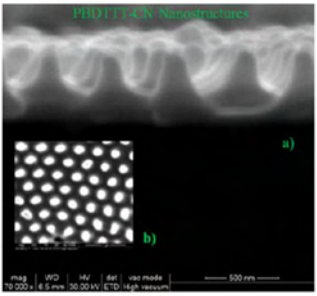

Figure 2: Cross-sectional a) and top view b) ESEM images of PBDTTT-CN nanostructures /PEDOT:PSS/ITO obtained using NAATs.

The low-bandgap polymer materials used to manufacture the NS were Poly[4,8-bis(2-ethylhexyloxy)-benzo[1,2-b:4,5-b']dithiophene-2,6-

diyl-alt-(4-octanoyl-5-fluoro-thieno[3,4-b]thiophene-2-carboxylate)-2,6-diyl] (PBDTTT-CF) [10] and Poly-(3-hexylthiophene-2,5-diyl) (P3HT). These polymers have their bandgap of 1.7 and 1.8 eV for the PBDTTT-CF and P3HT, respectively. The NS are fabricated onto Poly-(Ethylene dioxythiophene) doped with Poly-(Styrene Sulphonic acid) (PEDOT:PSS) (30 nm) /Indium-Tin-Oxide (ITO) (120 nm) / glass substrates by replicating from NAATs via spin-coating and melt-assisted wetting method. The organic NS were characterized by ESEM and UV/visible absorption spectra.

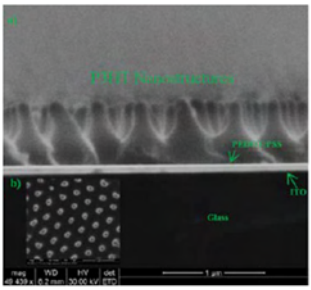

Figure 3: Cross-sectional a) and top view b) ESEM images of P3HT nanostructures /PEDOT:PSS/ITO obtained using NAATs.

The organic NS manufactured with the semiconductor polymers PBDTTT-CF and P3HT after the infiltration and removing the NAATs are show their cross sections in Fig. 2 a) and Fig.3 a), respectively. All the samples were fabricated under air atmosphere. Analysis by ESEM for PBDTTT-CF NS presents an average support base of 150 nm, pore length of 320 nm and an average interpillar distance of 460 nm and for P3HT NS has an average support base of 220 nm, pore length of 380 nm and interpillar distance of 490 nm. The pillar diameter for both structures has the similar value obtained of NAATs.

Fig. 4 shows the optical properties absorbance for the both polymer nanostructures. These NS are compared with their PBDTTT-CF and P3HT flat layers. Polymers nanostructures were obtained with an excellent replica process employing self-ordered NAATs. It is expected that these nanostructures will have potential applications as optoelectronic applications. The resulting PBDTTT-CF and P3HT nanopillars presented here these will be used to manufacture organic solar cells.

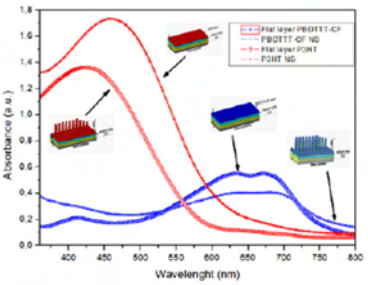

Figure 4: UV/visible absorption spectra of PBDTTT-CN and P3HT nanostructures. The NS were obtained with the used of the NAATs. These are compared with their respective flat layer made with the same semiconductor material and with similar process conditions.

This work was supported by the Spanish Ministry of Economy and Competitiveness (MINECO) under grant number TEC2009-09551, TEC2012-34397, CONSOLIDER HOPE project CSD2007-00007, by Catalan authority under project 2009 SGR 549.

References

[1] J. Meier, S. Doubail, R. Platz, P. Torres, U. Kroll, J.A. AnnaSelvan, N. Pellaton, Ch. Hof, D. Fischer, H. Keppner, R. Flückinger, A. Shah, V. Shklover, K.D. Ufert, Solar Energy Materials & Solar Cells 49 (1997) 35.

[2] B. Kippelen, J.L. Bredas, Energy & Environmental Science 2, (2009) 251.

[3] Y. Yang, K. Mielczarek, M. Aryal, A. Zakhidov, W. Hu, ACS Nano 6, No. 4 (2012) 2877.

[4] F. Buyukserin, M. Aryal, J. Gao, W. Hu, Small 5, (2009) 1632.

[5] S.A. Harfenist, S.D. Cambron, E.W. Nelson, S.M. Berry, A.W. Isham, M.M. Crain, K.M. Walsh, R.S. Keynton, R.W. Cohn, Nano Lett. 4, (2004) 1931.

[6] F.C. Krebs, Solar Energy Materials & Solar Cells 93, (2009) 394.

[7] L.F. Marsal, P. Formentín, R. Palacios, T. Trifonov, J. Ferré-Borrull, A. Rodriguez, J. Pallarès, R. Alcubilla, Physica Status Solidi (a) 205, (2008) 2437.

[8] R. Palacios, P. Formentín, E. Martínez-Ferrero, J. Ferre-Borrull, J. Pallarés, L.F. Marsal, Phys. Status Solidi A 208, No. 6, (2011) 1422.

[9] A. Santos, P. Formentín, J. Pallarés, J. Ferré-Borrull, L.F. Marsal, Solar Energy Materials & Solar Cells 94, (2010) 1247.

[10] Lijun Huo, Angew. Chem. Int. Ed. 49, (2010) 1500.

Multicolor and white light emission of $GdPO_4$ nanophosphors with a novel 3D architecture

Ana I. Becerro, Sonia Rodríguez-Liviano, Alberto J. Fernández-Carrión and Manuel Ocaña

Instituto de Ciencia de Materiales de Sevilla
(CSIC-Universidad de Sevilla)
c/ Américo Vespucio, 49. 41092 Sevilla, Spain

anieto@icmse.csic.es

Solid state lighting in the form of light emitting diodes (LEDs) has emerged in recent years as a high competent field and is therefore a subject of intensive research. LEDs combined with a phosphor can be used to produce visible light. Most white LEDs in production today are modified blue LEDs coated with a yellow emitting phosphor (YAG:Ce) [1]. However, such white LEDs present a low color rendering index and no full range of visible light. Another approach involves using a UV LED chip coated with three emitting blue, green, and red phosphors to generate warm white light. This, however, has a drawback that the blue emission efficiency is poor because of the strong reabsorption of the blue light by the green and red phosphors. The development of a single-phased white-light-emitting phosphor operating under UV excitation is of prime importance for a better performance of such LEDs. More importantly, compared to the multiple emitting components of the white LED system, the single-phased white-light-emitting phosphor for a UV-pumped white LED would enable easy fabrication with perfect stability and color. On the other hand, there has been recently an increase in interest and research into nanophosphors based on rare earth (RE) compounds including LnF_3[2], Ln_2O_3[3], $Ln(OH)_3$[4], $LnVO_4$[5] and $LnPO_4$[6], to mention a few. Among the large number of lanthanide compounds, lanthanide orthophosphates (LnPO4) represent an important class of materials because they possess a variety of favorable properties such as very high thermal stability (2300 °C), low solubility in water (Ksp = 10^{-25} - 10^{-27}) and high refractive index (n=1.5) that make them very useful in a large variety of applications as luminescent or laser materials, magnets, ceramics, catalysts, and also in medicine. The present contribution shows the synthesis and characterization of a single-phased $GdPO_4$ phosphor with a novel morphology, which emits white light under UV excitation.

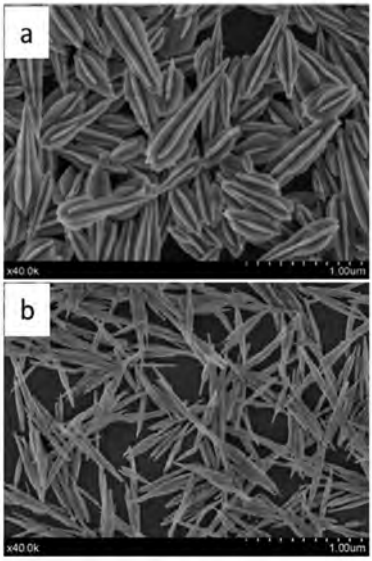

Figure 1: SEM micrographs of twin –like and rod-like GdPO4 particles synthesized using an EG/H_2O ratio of 90/10 (a) and 80/20 (b).

Homogeneous, monoclinic $GdPO_4$ particles consisting of three intersecting lance-shaped crystals forming a penetration (Figure 1a) twin were synthesized following a very simple and fast method consisting in the hydrothermal reaction of Gadolinium acetylacetonate with H_3PO_4 in a mixture of ethylene glycol and water at 180°C. The experimental conditions were found to have a strong effect on the morphological and structural features of the prepared particles. Thus, slightly increasing the amount of water in the solvent mixture leads to hexagonal rod-like $GdPO_4 \cdot 0.5H_2O$ nanoparticles (Figure 1b), while decreasing it only produces an amorphous gel-like precipitate. The

synthesis procedure is also successful for the preparation of Eu^{3+}-, Tb^{3+}- and Dy^{3+}-doped $GdPO_4$ particles with the same morphology and crystalline structure as the undoped materials. The effect of the doping level on the luminescent properties of the twin-like nanophosphors was evaluated (Figure 2). Likewise, the monoclinic twin-like GdPO4 nanophosphors were found to be much efficient than the hexagonal rod-like $GdPO_4$ ones in terms of emission intensity, especially the Eu- and Dy-doped particles. Finally, a solid state single-phase white light emitting nanophosphor has been fabricated for the first time in this system by triply doping the monoclinic $GdPO_4$ twined particles with appropriate concentrations of Eu^{3+}, Tb^{3+} and Dy^{3+} (Figure 3).

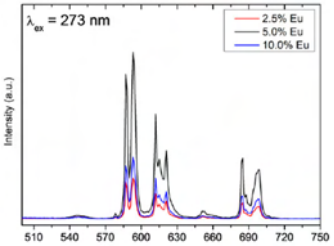

Figure 2: Emission spectra of different Eu-containing twin-like $GdPO_4$ nanophosphors recorded after exciting at 273 nm

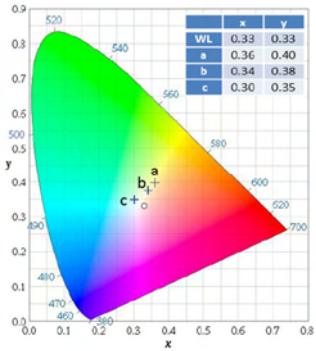

Figure 3: CIE chromaticity diagram of Eu/Tb/Dy triply doped twined GdPO4 particles and table displaying the corresponding CIE coordinates (Eu/Tb/Dy = 1.0/1.0/1.0 (a), 1.0/0.7/1.0 (b) and 0.5/0.7/1.0 (c).

References

[1] Bachmann, V.; Ronda, A.; Meijerink, C. Chem. Mater., 21 (2009) 2077.

[2] Lorbeer, C.; Cybinska, J.; Mudring, A.V. Chem Comm. 46 (2010) 571.

[3] Pedersen, H.; Ojamae, L. Nano Lett. 6 (2006) 2044.

[4] Mu, Q.Y.; Wang, Y.D. J. Alloys Comp. 509 (2011) 2060.

[5] Thirumalai, J.; Chandramohan, R.; Vijayan, T.A. Mater. Chem. Phys. 127 (2011) 259.

[6] Rodriguez-Liviano, S.; Aparicio, F.J.; Rojas, T.C.; Hungria, A.B.; Chinchilla, L.E.; Ocaña, M. Cryst. Growth Design 12 (2012) 635.

Exploration and use of internal water in silica colloidal crystals

A. Blanco, F. Gallego-Gómez, and C. López

Instituto de Ciencia de Ciencia de Materiales de Madrid ICMM-CSIC C/ Sor Juana Inés de la Cruz 3 28049 Madrid, Spain

ablanco@icmm.csic.es

Recently, it has been shown that silica artificial opals possess a PBG controlable by simple heating on a hot plate [1]. Submicrometer silica spheres easily form high-quality face-centered-cubic (fcc) structures displaying a Bragg peak (the lowest energy PBG) in the visible range. Given the hydrophilic character of silica, these opals inherently contain a substantial amount of molecular water (as much as 8 wt.% in as-grown samples) physisorbed on the silanol groups at the spheres surface. This water is partially placed between the spheres forming necks, leading to a nonclose-packed arrangement, so that the opal lattice parameter directly depends on the amount of water (figure 1). Thus, controlled desorption of this water upon moderate opal heating induced large effects in the opal photonic properties, mostly due to shrinking of the lattice parameter in up to ~ 12 nm. Complete water removal (achieved at ~ 120 °C) leads to a pronounced blueshift of the Bragg peak of 25 nm. PBG changes are reversible upon cooling down to room temperature (RT) by virtue of spontaneous water re-adsorption. By *in situ* measuring PBG behavior with temperature one can extract relevant fundamental knowledge regarding water morphology and adsorption in silica colloidal systems [2], [3]. Further, this internal water plays an important role in Azo-Molecules photo-alignment [4] or in the mechanical properties of these systems [5].

Once the presence of water is characterized we are able to use it for different means. The amount of adsorbed water and its distribution can be controlled by modifying the chemistry of the silica surface, from hydrophilic to hydrophobic through thermal annealing. By doing this we can acquire deep knowledge on silica chemistry and use it to tune the structure photonic response. Further, although thermal effects regarding the whole structure (sample size around some square centimeters) are usually rather slow (seconds) we can bring this response to the millisecond range by inducing local heating [6]. The opal was photoirradiated with a focused 488-nm Ar^{+}-laser while measuring the opal reflectance spectrum in order to monitor *in situ* the PBG changes. Photoirradiation significantly affected the spectrum of the infiltrated opal in a reversible fashion (Figure 2a). Under light exposure the Bragg peak shifted to shorter wavelengths (up to 13 nm) within a few milliseconds and rapidly shifted back to the original position after turning the light off (Figure 2). Simultaneously, the bandgap width decreased (up to 5%) during irradiation, also reversibly. Thus, the photoinduced PBG changes were fast and, without external stimulus, fully reversible, and the shift distance directly depended on the irradiation intensity I. Additionally, the overall performance was reproducible over millions of cycles. All these issues are greatly relevant for switching applications demanding not only spontaneous reverse effect but also accurate response and fidelity in a fast fashion.

References

[1] F. Gallego-Gómez, A. Blanco, V. Canalejas-Tejero and C. López, Small 2011, 7, 1838.
[2] F. Gallego-Gómez, A. Blanco, and C. López, Langmuir 2012, 37, 13992.
[3] F. Gallego-Gómez, A. Blanco, and C. López, J. of Phys. Chem. C (in press 2012)
[4] F. Gallego-Gómez, A. Blanco, D. Gomayo, and C. López, Adv. Funct. Mater. 2011, 21, 4109.
[5] F. Gallego-Gómez, V. Morales-Flórez, A. Blanco, De la Rosa-Fox, N. and C. López, Nano Letters (in press 2012).
[6] F. Gallego-Gómez, A. Blanco, and C. López, Advanced Materials (in press 2012).

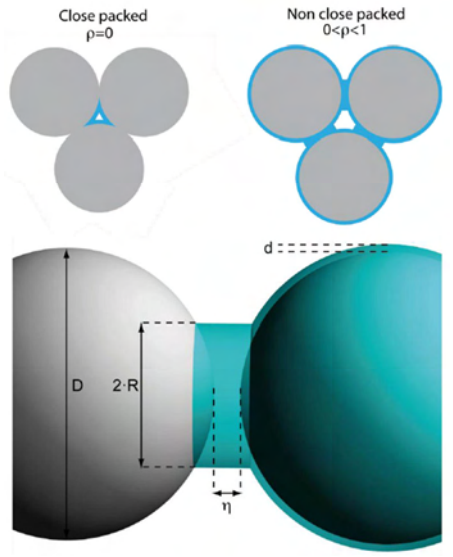

Figure 1: Proposed model for water distribution in as-grown silica opals at room temperature and about 35% humidity.

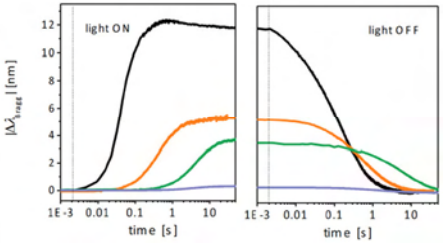

Figure 2: Temporal evolution of the Bragg peak position of infiltrated as-grown (black lines) and annealed (at 450, 525 and 600°C, orange, green and blue lines) opals. The laser was turned on/off 2 ms after beginning the measurement (denoted by the dashed lines). In all cases, the irradiated area S was 0.002 mm^2 and the laser intensity I was 30 W cm^{-2}.

Presentation of the Nanophotonics for Energy network

Alvaro Blanco

Instituto de Ciencia de Ciencia de Materiales de Madrid ICMM-CSIC
C/ Sor Juana Inés de la Cruz 3
28049 Madrid, Spain

ablanco@icmm.csic.es

How to boost energy efficiency to help curb climate change is a thorny scientific question that today's society must find answers to quickly. Photonics is set to be among the solutions. Photonics could thus help us design more efficient ways to convert electricity into light, and light into electricity, to meet our energy needs much more sustainably. Increasing the efficiency of light-matter interaction at the nanoscale, for example, could lead to important advances in the performance of both light-emitting and light-harvesting devices. With the sun sending to the Earth's surface, in less than an hour, an amount of solar energy equivalent to the energy consumed by the entire world population over a year, the potential for real solutions is huge.

Starting in January 2010, the Nanophotonics for Energy Efficiency Network of Excellence (N4E) aims to promote nanophotonics research in energy-efficient applications by bringing together different nanophotonic laboratories and research groups across Europe. To date, 9 institutions in 6 European countries are participating in the network, representing more than 130 scientists, engineers, technicians, and managers in the field. This is further enhanced by a comprehensive Advisory Board with participation of major companies, and an Associate Membership scheme open to all interested parties.

With the view to speed up the development of disruptive approaches to lighting and solar cell technology, N4E fosters collaborations for the exchange of scientific knowledge and best practices and paves the way for the establishment of common research agendas. N4E organizes workshops and summer schools for young researchers and technicians to learn about scientific and technological issues and hone their communication, entrepreneurship, and intellectual property skills. Every 6 months, the N4E Network also offers seed funding for collaborative projects to investigate disruptive nanophotonics concepts toward increased energy efficiency.

A vacuum methodology for the fabrication of hybrid core@shell (ONWs@ZnO) nanowires

Manuel Macias-Montero[1], A. Nicolas Filippin[1], Zineb Saghi[2], Francisco J. Aparicio[1], Angel Barranco[1], Agustín R. González-Elipe[1] and **Ana Borras**[1]

[1] Instituto de Ciencia de Materiales de Sevilla (ICMS, CSIC-US), Nanotechnology on Surfaces Lab., C/ Américo Vespucio 49, 41092, Sevilla, Spain
[2] Fundación Progreso y Salud BIONAND C/ Severo Ochoa 35, Parque Tecnológico de Andalucía, 29590 Malaga, Spain

anaisabel.borras@icmse.csic.es

In this communication we show the unprecedented fabrication of hybrid core@shell nanowires formed by an inner organic nanowire surrounded by a nanocrystalline ZnO layer. Single crystal organic nanowires made of small-molecules such as metal porphyrins, metal phthalocyanines and perylenes are fabricated by physical vapor deposition on organic and inorganic substrates with tailored microstructure [1, 2]. The conformal growth of the ZnO layer at low temperature allows the formation of the complex heterostructures keeping untouched the crystal structure of the organic part as demonstrated by HRTEM and SAED. As result, multifunctional hybrid core@shell architectures are fabricated on processable substrates. Examples of the ONWs@ZnO NWs as optical gas sensor and waveguides are presented.

References

[1] A. Borras, O. Groning, J, J. Koeble, P. Groening Adv. Mater. 21 (2010) 4816.
[2] M. Alcaire, J. R. Sanchez-Valencia, F. J. Aparicio, Z. Saghi, J. C. Gonzalez-Gonzalez, A. Barranco, Y. Oulad, A. R. Gonzalez-Elipe, P. Midgley, J. P. Espinos, P. Groening and A. Borras Nanoscale 3 (2011) 4554.

Recent Progress on High Contrast 40Gb/s and Low Drive Voltage 10 Gb/s Slow Light-Based Silicon Photonic Modulators

Antoine Brimont[1], Ana M. Gutierrez[1], Mariam Aamer[1], David J. Thomson[2], Frederic Y. Gardes[2],Jean-Marc Fedeli[3], Graham T. Reed[2], Javier Martí[1] and Pablo Sanchis[1]

[1]Nanophotonics Technology Center, Universitat Politècnica de València, Valencia, Spain
[2]School of Electronics and Computer Science, University of Southampton, Southampton, UK
[3]CEA, LETI, Minatec Campus, 17 Rue des Martyrs, 38054, GRENOBLE Cedex, France

abrimont@ntc.upv.es

The increasing need of more sophisticated means of communication is driving the demand for products and devices with high-speed and large bandwidth in data transfer along with low cost and high energy efficiency. Photonics technologies currently allow colossal amounts of data to be transmitted throughout the world via countless optical fiber links forming the global optical communication network. To address the ever increasing demand for bandwidth over shorter and shorter distances, silicon photonics seems to be the ideal candidate, solving in the near term the foreseeable electric interconnect bottleneck. As a result, integrated silicon photonics, which smartly benefits from the mature industrial complementary metal-oxide-semiconductor (CMOS) microelectronics technology, is expected to provide a very powerful, inexpensive and energy efficient platform to increase the interconnection bandwidth of processors (intra-chip), multi-core processors (intra-chip and chip-to-chip), boards and racks (off-chip).

In this context, silicon electro-optical modulators, which write electrical data onto an optical carrier at very high speeds, have attracted an increasing interest. Nevertheless, despite continuous efforts in realizing high performance devices, carrier depletion modulators remain subject to parametricadjustment trade-offs. In fact, fabricating a modulator that simultaneously features, high speed (40 Gb/s), small footprint (a few hundred microns), low insertion loss (<6dB) and low drive voltage (~1V) appears to be extremely challenging [1-6]. Fortunately, the well know slow light phenomenon is a good candidate to help mitigate these issues by significantly enhancing conventional "fast light" devices via enlarged light-matter interactions [4, 7].

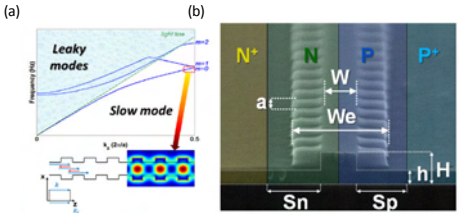

Figure 1: (a) Typical dispersion curve of a 1 dimensional corrugated waveguide. The slow forward movement is produced by the superposition (interference) of electromagnetic waves propagating back and forth in the direction indicated by the wave vector (slightly off-z-axis). (b) SEM picture of the corrugated waveguide.

In this paper, we showcase two attractive features of silicon slow wave modulators. Namely, we show their capacity to dramatically shrink the footprint of conventional rib waveguide based carrier depletion modulators while sustaining similar drive voltages and operating speed. Furthermore, we demonstrate that the use of slow light provides an attractive solution to reduce the drive voltage of carrier depletionbased Mach-Zehnder modulators fulfilling hence the consumption requirements of future CMOS electrophotonic transceivers.

Slow light propagation (Fig. 1 (b)) is achieved through the use of a corrugated waveguide whose parameters are indicated in Fig. 1 (b) (W=300nm; W_e=650nm; a=310nm). The slow wave modulator has been patterned in a standard CMOS fabrication line on a 220nm thick epilayer (designated H in Fig. 2 (b)) 8-inch wafer, using 193nm deep-UV lithography. The waveguide was shallow-etched, leaving a remaining slab thickness of height h=100nm. Electro-optical modulation is achieved via a carrier

depletion mechanism, that is, when the majority carriers are depleted from a reverse biased p-n junction, which in this case is positioned in the middle of the waveguide. The two *p*-type and *n*-type regions are connected to highly doped p^+ and n^+ regions, which are respectively situated at a distance of S_n=550nm and S_p=500nm from the edge of the narrow waveguide section. Low resistive and low microwave loss compound AlCu electrodes were finally deposited on top of the highly doped regions to ensure good ohmic contacts. Net doping concentrations in the *p*-type and *n*-type regions are respectively 4.10^{17} cm^{-3} and 5.10^{17} cm^{-3}.Highly p^+ and n^+ regions were implanted at a concentration of 1.10^{20} cm^{-3}.Two modulators of lengths 1000 µm and 500µm were used to demonstrate low drive voltage operation at 10Gb/s and high contrast performance at 40Gb/s, respectively.

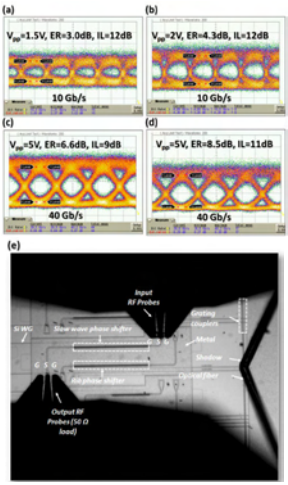

Figure 2: (a) 10 Gb/s eye diagrams for 1.5V and (b) 2V peak-to-peak drive voltages (1000-µm long modulator) (c) 40 Gb/s eye diagrams for a 5V peak-to-peak drive voltage at quadrature and (d) 2dB below quadrature (500-µm long modulator) (e) Optical microscope image of the slow-light modulator under test. V_{pp}= Voltage peak-to-peak; ER=Extinction ratio; IL=insertion loss.

To evaluate the high speed performance of the 1000µm slow wave modulator under low drive voltages, 10Gb/s eye diagrams were acquired at quadrature, as shown in Fig. 2 (b). The modulation efficiencies are 0.62V.cm and 0.70V.cm for 1.5V_{pp} and 2V_{pp} voltage swings, respectively. Extinction ratios of 3 dB and 4.3dB at 10 Gb/s were achieved. These results have been obtained for a group index of ~9.5. The insertion loss of the modulator is ~12dB [8]. Additionally, 40 Gb/s operation has been shown using the shorter version of the slow wave modulator (500µm), which exhibits a modulation efficiency of 0.85 V.cm for a 5V voltage swing and for a group index of ~8 [9]. Besides the lower optical losses, the choice of using such a group index value is motivated by the possibility of achieving a better electro-optical velocity matching and thus a higher modulation bandwidth. The device features an onchip insertion loss of only 6dB, including the 1dB loss of the two MMI structures. The extinction ratios at 40 Gb/s are 6.6 dB (respectively, 8.5 dB) achieved at quadrature (respectively, 2dB below quadrature) and with 9 dB (respectively, 11dB) optical loss.

In conclusion, low drive voltage 10 Gb/s and high contrast 40 Gb/s operation of compact slow light modulators have been demonstrated. The perspective of using engineered corrugated waveguide featuring a broad optical bandwidth [10] offer exciting prospects for slow light-based modulators.

References

[1] L. Liao, A. Liu, J. Basak, H. Nguyen, M. Paniccia, D. Rubin, Y. Chetrit, R. Cohen, and N. Izhaky." Electronics letters, vol. 43, 2007.

[2] F. Y. Gardes, D. J. Thomson, N. G. Emerson, and G. T. Reed." Opt. Express, vol. 19, 2011, pp. 11804-11814.

[3] D. J. Thomson, F. Y. Gardes, Y. Hu, G. Mashanovich, M. Fournier, P. Grosse, J. M. Fedeli, and G. T. Reed." Opt. Express, vol. 19, 2011, pp. 11507-11516.

[4] A. Brimont, D. J. Thomson, P. Sanchis, J. Herrera, F. Y. Gardes, J. M. Fedeli, G. T. Reed, and J. Martí." Opt. Express, vol. 19, 2011, pp. 20876-20885.

[5] M. Ziebell, D. Marris-Morini, G. Rasigade, J.-M. Fédéli, P. Crozat, E. Cassan, D. Bouville, and L. Vivien." Opt. Express, vol. 20, 2012, pp. 10591-10596.

[6] P. Dong, L. Chen, and Y.-k. Chen." Opt. Express, vol. 20, 2012, pp. 6163-6169.

[7] L. O'Faolain, D. M. Beggs, T. P. White, T. Kampfrath, K. Kuipers, and T. F. Krauss." Photonics Journal, IEEE, vol. 2, 2010, pp. 404-414.

[8] A. Brimont, A. M. Gutierrez, M. Aamer, D. J. Thomson, F. Y. Gardes, J.-M. Fedeli, G. T. Reed, J. Martí, and P. Sanchis." IEEE Phot. Journal, vol.4, 2012, pp.1306-1315.

[9] A. Brimont, D. J. Thomson, F. Y. Gardes, J. M. Fedeli, G. T. Reed, J. Martí, and P. Sanchis." Accepted in Optics Letters, 2012.

[10] A. Brimont, J. Vicente Galán, J. Maria Escalante, J. Martí, and P. Sanchis." Opt. Lett., vol. 35, 2010, pp. 2708-2710.

Integration of Gold Nanoparticles in Optical Resonators

Mauricio E. Calvo[1], Alberto Jiménez-Solano[1], Carmen López-López[1], Olalla Sánchez-Sobrado[1], Cristina Fernández-López[2], Ana Sánchez-Iglesias[2], Luis M. Liz-Marzán[2] and Hernán Míguez[1]

[1]Instituto de Ciencia de Materiales de Sevilla, Consejo Superior de Investigaciones Científicas - Universidad de Sevilla, Américo Vespucio 49, 41092, Seville, Spain
[2]Departamento de Química Física, Universidad de Vigo, 36310 Vigo, Spain

mauricio.calvo@icmse.csic.es

Herein we demonstrate the interplay between localized surface plasmons of gold nanoparticles and the field confinement effects that occur in porous one-dimensional photonic crystal based resonators [1,2] containing them (Figure 1). Experiments show the spectral modification of the optical absorption of one-dimensional photonic crystal based resonators containing different types of gold nanoparticles (rods and spheres of different sizes, Figure 2) [3]. We also demonstrate that the porous nature of the final hybrid material provides a means to precisely control the absorption spectrum of the multilayer as a function of the refractive index of the guest compounds Results are explained in terms of the calculated spatial distribution of the electric field intensity within the configurations under analysis [4].

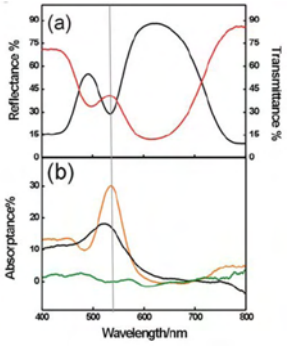

Figure 1

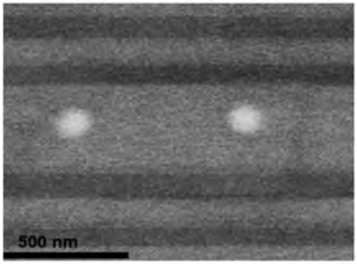

Figure 2

References

[1] Colodrero, S., Ocaña, M. and Míguez, H. Langmuir 24 (2008) 4430-4434.
[2] Calvo, M.E, Sánchez-Sobrado, O.; Colodrero, S. , Miguez, H. Langmuir 25 (2009) 2443
[3] Sánchez-Sobrado, O., Lozano, G., Calvo, M.E., Sánchez-Iglesias, A., Liz-Marzán, L.M. and Míguez, H. Adv. Mater. 23 (2011) 2108-2112.
[4] Jiménez-Solano, A., López-López, C., Sánchez-Sobrado, O., Luque, J.M., Calvo, M.E., Fernández-López, C., Sánchez-Iglesias, A., Liz-Marzán, L.M. and Míguez, H. Langmuir 28 (2012) 9161-9167.

Two dimensional nanostructured surface relief patterns as optical diffraction gratings for enhanced photovoltaic performance

S. Colodrero[1], M.C. López-López[1], L. Marsal[2] and H. Míguez[1]

[1]Instituto de Ciencia de Materiales de Sevilla, Consejo Superior de Investigaciones Científicas-Universidad de Sevilla, Américo Vespucio-49, Sevilla, Spain
[2]Departamento de Ingeniería Electrónica, Universitat Rovira i Virgili, Avda Paisos Catalans 26, Tarragona 43007, Spain

colodrero@icmse.csic.es

The use of surface relief gratings to boost the efficiency of active layers in different types of photovoltaic devices has received a great deal of attention in recent years. [1]-[3] Herein, the surface of nanocrystalline titania layers integrated in dye sensitized solar cells has been periodically patterned by means of a combined soft-lithography and micro-contact printing approach. A significant increase of the photogenerated current is observed as a result of the longer path travelled by light reflected back into the electrode by effect of the so built optical diffraction grating. Such surface relief patterns do not alter the porosity of the electrode, thus not hindering dye loading or electrolyte diffusion through the cell, preserving the rest of electrical parameters of the photovoltaic device intact.

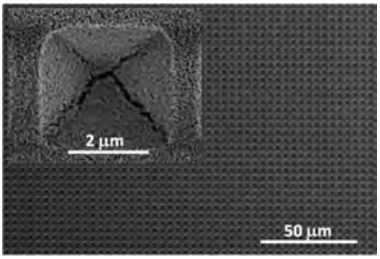

Figure 1: Top view SEM images of a 7.5 µm thick nanocrystalline TiO_2 film that has been periodically patterned to act as photoelectrode in dye sensitized solar cells.

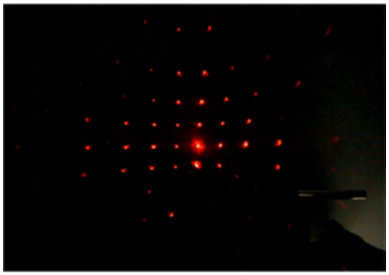

Figure 2: Diffraction pattern observed for the two dimensional array engraved on the surface of a nanocrytalline TiO_2 layer.

References

[1] S.I. Na, S.S. Kim, J. Jo, S.H. Oh, J. Kim, D.Y. Kim, Adv. Funct. Mater. 24 (2008) 3956.
[2] C. Battaglia, J. Escarré, K. Söderström, M. Charriére, M. Despeisse, F.J. Haug, C. Ballif, Nature Photonics, 9 (2011) 535.
[3] A. Mavrokefalos, S.E. Han, S. Yerci, M.S. Branham, G. Chen, Nano Lett. 6 (2012) 2792.

Light emission statistics in correlated random photonic nanostructures

N. de Sousa[1], J. J. Saenz[1], A. García-Martín[2] and L. S. Froufe-Pérez[3]

[1]Departamento de Física de la Materia Condensada, Universidad Autónoma de Madrid, Madrid, Spain
[2]Instituto de Microelectrónica de Madrid, CSIC, Tres Cantos, Madrid, Spain
[3]Instituto de Estructura de la Materia, CSIC, Madrid, Spain

nuno.teixeira@uam.es

The statistical properties of light transport and emission in disordered media has been a matter of intense research during the last century. Being the basis of coherent multiple scattering of waves well known, the phenomenon itself is not yet fully explored and understood. These multiple wave scattering effects are at the heart of emerging behaviors like Anderson localization of light and electrons, band structure in crystalline solids or photonic crystals (PhC), among many others.

Although the limits of perfectly ordered systems on the one hand, and uncorrelated and relatively weakly scattering systems on the other hand, are quite well understood. There is a gap between both limits which is largely unexplored. In particular, it has been shown in many different situations that disordered systems exhibiting certain structural correlations can share properties of both crystalline and fully disordered systems. For instance, the conductivity of liquid metals [1] or the cornea transparency [2] can be understood in the same footing: a disordered but correlated system can present spectral regions of high transparency for electron or light transport.

The effects of disorder in an initially ordered structure, such as a PhC, might lead to strong Anderson localization, as the scattering mean free path can be severely reduced in the band edges [3]. Also, strongly correlated charged colloids can scatter light in such a way that the transport mean free path presents a strong chromatic dispersion [4]. Even in the absence of practically any long range correlations, the structure of the scatterers itself can be used to modify the light emission and transport properties of a disordered system in such a way that transport parameters [5], or even the threshold of a random laser [6], can present resonances which can be tuned in advance.
The effect of correlations in a disordered structure regarding light emission properties of single fluorescent emitter has been a matter of much less intense research efforts. It is clear that the structure surrounding a single emitter can largely alter its emission dynamics [7]. In the last years, several groups considered such effects in a statistical way suitable for the description of disordered systems [7,8,9]. In particular, in ref.[9] it was shown that several structural properties near a phase transition can be accessed via fluorescence intensity fluctuations.

Has been theoretically proven that near field scattering in random systems alters fluorescence dynamics in such a way that microscopic information about the surroundings of a single emitter can be obtained from lifetime fluctuations or from the shape of the statistical distribution tails [10,11].

In this presentation, we theoretically show how, in the previous context, fluorescence emission rate statistics are largely altered due to the appearance of structural correlations in a disordered system.

We have developed a model of point resonant interacting scatterers which are placed at random. Emission dynamics of a single emitter is calculated for each sample of an ensemble of structural realizations of the system.

While keeping constant the scattering properties of single scatterers, the global geometry, and scatterers density, the structural correlations are controlled changing the temperature of the interacting set of scatterers.

It is shown that fluorescence decay rate statistics of a the single emitter correlates with the structural phase transitions of the system. In the low temperature limit, the structure freezes in an face center cubic lattice. This structure presents a gap (frequency range of low photonic density of states) corresponding to a vanishing fluorescence decay rate. As usual, it also presents narrow frequency windows of high density of states, corresponding to band edges of the perfect infinite crystalline structure, leading to high decay rates.

At frequencies corresponding to both a band gap and a band edge, we perform decay rate statistics varying the temperature of the system. It is shown that, at low temperature, decay rates hardly fluctuates and its average value corresponds to the crystalline one. On temperature raising, fluctuations of decay rate grow, and the averaged values undergoes a relatively sharp transition to a different value. This transition can be identified with a structural phase transition in the system.

References

[1] N. W. Aschcroft and J. Lekner, Phys. Rev. 145 (1966) 84.

[2] R. W. Hart and R. A. Farrell, J. Opt. Soc. Am. 59 (1969) 766.

[3] Sajeev John, Phys. Rev. Lett. 58 (1987) 2486.

[4] L. F. Rojas-Ochoa, J. M. Mendez-Alcaraz, J. J. Sáenz, P. Schurtenberger, and F. Scheffold, Phys. Rev. Lett. 93 (2004) 073903.

[5] P. D. García, R. Sapienza, A. Blanco, and C. López, Adv. Mater. 19, 2597 (2007); R. Sapienza, P.D. García, J. Bertolotti, M.D. Martín, A. Blanco, L. Viña and C. López, D.S. Wiersma, Phys. Rev. Lett. 99, (2007) 233902.

[6] S. Gottardo, R. Sapienza, P.D. Garcia, A. Blanco, D. S. Wiersma and C. Lopez, Nat. Phot. 2 (2008) 429.

[7] Jordi Hernando, Erik M. H. P. van Dijk, Jacob P. Hoogenboom, Juan-José García-López, David N. Reinhoudt, Mercedes Crego-Calama, María F. García-Parajó, and Niek F. van Hulst, Phys. Rev. Lett. 97 (2006) 216403.

[8] H. Gersen, M. F. García-Parajó, L. Novotny, J. A. Veerman, L. Kuipers, and N. F. van Hulst, Phys. Rev. Lett. 85 (2000) 5312.

[9] R. A. L. Vallee, M. Van der Auweraer W. Paul and K. Binder, Phys. Rev. Lett. 97 (2006) 217801.

[10] L. S. Froufe-Pérez, R. Carminati and J. J. Sáenz, Phys. Rev. A 76 (2007) 013835.

[11] L. S. Froufe-Pérez and R. Carminati, Phys. Stat. Sol. (a) 205 (2008) 1258.

Simplified coupled-wave analysis for the characterization of extraordinary optical transmission in single and stacked metallic screens

Vicente Delgado[1], Ricardo Marqués[1] and Lukas Jelinek[2]

[1]Dept. of Electronics and Electromagnetism, Av. Reina Mercedes S/N 41012, Univ. of Seville, Spain
[2]Dept. of Electromagnetic Field, Czech Technical Univ. in Prague 16627-Prague, Czech Republic

vdelgado @u s.es

We present a coupled-wave and surface-impedance method for the analysis of extraordinary optical transmission (EOT) through realistic metallic screens under normal and oblique incidence. Standard scattered matrix method is used to account for possible dielectric interlayers and stacked screens.

Extraordinary Optical Transmission (EOT) through metallic screens with a periodic array of subwavelength holes, first reported in [1], is a topic of intensive research with potential applications in photonic circuits [2] optical sensing [3] and fabrication of fishnet metamaterials [4]. EOT has been explained from different perspectives [5]-[7]. In our group we have proposed different waveguide models that account for EOT in the whole frequency range where it has been reported (e.g. [7], [8]). In this contribution we extend the previous work to the case of EOT screens made of realistic metals under oblique incidence. The model can also be applied to stacked and dielectric loaded of screens.

In the waveguide analysis, the problem is reduced to its unit cell (see Fig. 1) and the electromagnetic fields in the different regions are expanded in terms of Bloch and waveguide modes compatible with the boundary conditions imposed by the symmetry of the structure and the impinging wave. However, resolution of the whole problem in case of penetrable metals by these means would be inefficient. In order to overcome this difficulty, we make use of the surface impedance matrix [9] that relates the electromagnetic fields at both sides of a plain slab. If we neglect the perturbation introduced by the holes, the transverse components electromagnetic fields at both sides of the optically dense metallic screen are related through [8]

$$\begin{bmatrix} \boldsymbol{E}_{\parallel}^{(1)}(z=-t/2) \\ \boldsymbol{E}_{\parallel}^{(3)}(z=t/2) \end{bmatrix} \approx \overline{\overline{\boldsymbol{Z}}} \begin{bmatrix} \hat{\boldsymbol{z}} \times \boldsymbol{H}_{\parallel}^{(1)}(z=-t/2) \\ \hat{\boldsymbol{z}} \times \boldsymbol{H}_{\parallel}^{(3)}(z=t/2) \end{bmatrix} \quad (1)$$

where $\overline{\overline{\boldsymbol{Z}}}$ is the surface impedance matrix that can be diagonalized and is a function of the constitutive parameters of the material composing the screen and its tickness. Eq. (1) together with continuity of the fields in the cross section of the holes

$$\begin{bmatrix} \boldsymbol{E}_{\parallel}^{(1)}(z=-t/2) \\ \boldsymbol{H}_{\parallel}^{(1)}(z=-t/2) \end{bmatrix} = \begin{bmatrix} \boldsymbol{E}_{\parallel}^{(2)}(z=-t/2) \\ \boldsymbol{H}_{\parallel}^{(2)}(z=-t/2) \end{bmatrix} \text{ and}$$

$$\begin{bmatrix} \boldsymbol{E}_{\parallel}^{(2)}(z=t/2) \\ \boldsymbol{H}_{\parallel}^{(2)}(z=t/2) \end{bmatrix} = \begin{bmatrix} \boldsymbol{E}_{\parallel}^{(3)}(z=t/2) \\ \boldsymbol{H}_{\parallel}^{(3)}(z=t/2) \end{bmatrix} \quad (2)$$

provide a complete set of equations for the amplitudes of the different modes in which the fields are expanded after applying integral boundary conditions.

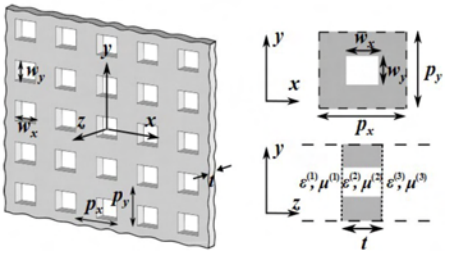

Figure 1: Metallic screen with a periodic array of holes (EOT screen) and fron and lateral views of the unit cell of the structure.

In Fig. 2 the transmission coefficients through a silver screen at infrared frequencies, for different polarizations and angles of incidence, obtained with the reported model are compared with electromagnetic simulations using *CST Microwave Studio*. In order to obtain meaningful results, the resolution of the highest mode inside the holes must be similar to that of the input and output regions. We employed higher order of 2 for modes inside the holes and 8 for modes in the cross section of the unit cell, which were enough to obtain accurate

results compared with full wave electromagnetic simulations. CPU time per frequency point was ~ 0.5 s vs ~ 4 min with the electromagnetic solver.

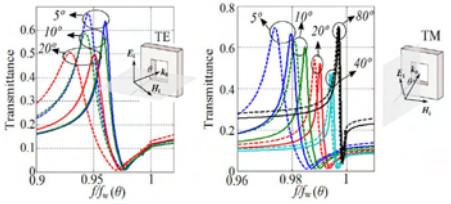

Figure 2: Transmission through an array of square holes in a silver screen at oblique incidence. Square periodicity is 1μm. Size of the holes is 250 nm and thickness of the screen is 50 nm. Wood's frequencies (fw) range from 150 THz to 220 THz. The metal is modeled by a Drude Lorentz permittivity. Solid lines correspond to the mode matching model and dashed lines to CST simulations.

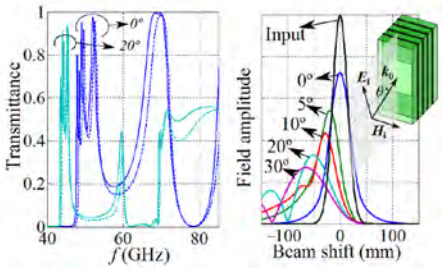

Figure 3: (Left) Transmission through four stacked copper screens at oblique incidence (TM incident wave). The four metallic screens are placed among a total of five dielectric slabs. Periodicities are 1.5 and 3.4 mm, size of the square holes is 1.1 mm, thickness of the metallic layer is 35 μm and thickness of each of the dielectric slabs is 0.49 mm. Continuous lines correspond to the mode matching model and dashed lines to the CST simulations. (Right) Electric field profiles of a 1D Gaussian beam impinging at different angles of incidence at the frequency of the maximum transmission. Deviation of the beam to the left is higher for increasing angles of incidence.

In case of a dielectric loaded or stacks with a finite number screens, the scattering matrix method is used in order to compute the complete scattering matrix (note that cascading of transmission matrix is ill conditioned due to the presence of positive and negative exponentials).

In Fig. 3 (left) we show the transmission coefficient for TM plane waves impinging at several angles over dielectric loaded stacked EOT screens, with an structure similar to those in [10]. Once the transmission coefficients for incident plane waves are known, we can analyze the behavior of incident Gaussian beams, which can be decomposed into plane waves. The profiles of the input and output TM beams impinging at different angles are shown in Fig. 3 (right) confirming the existence of negative refraction in accordance to the experimental results in [10].

References

[1] T. W. Ebbesen et al., Nature, vol. 391, pp. 667–669, 1998.

[2] E. Deveux et al., Appl. Phys. Lett., vol. 83, pp. 4396–4398, 2003.

[3] A. A. Yanik et al., Nano Lett., vol. 10, pp. 4962–4969, 2010.

[4] M. Beruete et al., Opt. Express, vol. 14, pp. 5445–5455, 2006.

[5] H. F. Ghaemi, et al. Phys. Rev. B, vol. 58, pp. 6779–6782, 1998.

[6] L. Martín-Moreno, et al. Appl. Phys. Lett., vol. 86, pp. 1114–1117, 2001.

[7] F. Medina, et al. IEEE Trans. Microw. Theory Tech., vol. 56, pp. 3108–3120, 2008.

[8] V. Delgado, et al. Opt. Express, vol. 18, pp. 6506–6515, 2010.

[9] S. Tretyakov, Analytical Modeling in Applied Electromagnetics, Edt. Artech House, 2003.

[10] M. Beruete, et al. Phys. Rev. B, vol. 79, pp. 195107(1)–195107(6), 2009.

Microwave assisted synthesis of Poly (acrylic acid) functionalised europium doped calcium hydroxyapatite and fluoroapatite nanospindles for biomedical applications

Alberto Escudero[1], Jesús M. de la Fuente[2] and Manuel Ocaña[1]

[1]Instituto de Ciencia de Materiales de Sevilla. CSIC - Unviersidad de Sevilla. C/ Américo Vespucio 49, E-41092 Seville, Spain
[2]Instituto de Nanociencia de Aragón, Universidad de Zaragoza, C/ Mariano Esquillor s/n, E-50018 Zaragoza, Spain.

aescudero@icmse.csic.es

Nanoparticles are attracting interest in nanomedicine not only due to their potential medical applications but also because they enable analyses and therapies that cannot be performed otherwise [1]. The clinical applications of nanoparticles range from optical biolabels and contrast agents for magnetic resonance imaging to carriers for drug and gene delivery for disease therapy. All these applications require uniform nanoparticles with controlled size, shape, composition, surface chemistry and other physicochemical properties. Calcium hydroxyapatite has attracted much research attention due to their high biocompatibility and good biodegradability [2]. This is caused by the fact that calcium phosphate is the inorganic mineral of human bone and teeth [3]. However, dispersions of calcium phosphate nanoparticles tend to agglomerate and sediment [4], hindering any possible biomedical application. A further functionalization process is thus required in order to achieve colloidal stability.

Europium-doped calcium hydroxyapatite and fluoroapatite nanophosphors functionalised with poly acryl acid (PAA) have been synthesised though a microwave-assisted hydrothermal method from aqueous basic solutions containing calcium nitrate, sodium phosphate monobasic and PAA. In both cases a spindle-like morphology was obtained, resulting from an aggregation process of smaller units which gave rise to high surface area particles. The size of the nanospindles was 191 (32) x 40 (5) nm for calcium hydroxyapatite and 152 (24) x 38 (6) nm for calcium fluoroapatite. This is the first time such a spindle morphology is reported for this system. The luminescent nanoparticles show the typical red luminescence of $Eu3^{+}$. Luminescence quantum yield measurements of both europium doped calcium hydroxyapatite and calcium fluoroapatite samples indicate that the fluoroapatite particles are more efficient than the hydroxyapatite, due to the presence of OH- quenchers in the latter. The nanophosphors show negligible toxicity for cells, although the hydroxyapatite nanophosphors were slightly more biocompatible than the fluoroapatite particles. Both PAA-functionalised nanophosphors showed a very high (up to several weeks) colloidal stability in MES at pH 6.5, which is a commonly-used buffer for physiological media. All these features make both kinds of apatite-based nanoparticles suitable for biomedical applications.

References

[1] Murthy, S. K. Int. J. Nanomed., 2 (2007) 129-141.
[2] Epple, M.; Ganesan, K.; Heumann, R.; Klesing, J.; Kovtun, A.; Neumann, S.; Sokolova, V. J. Mater.Chem., 20 (2010) 18-23.
[3] Dorozhkin, S. V.; Epple, M. Angew. Chem.-Int. Edit., 41 (2002) 3130-3146
[4] Sokolova, V.; Prymak, O.; Meyer-Zaika, W.; Colfen, H.; Rehage, H.; Shukla, A.; Epple, M. Materialwiss. Werkstofftech., 37 (2006) 441-445.

Figure 1: TEM micrograph of the 2% Eu doped calcium hydroxyapatite nanophosphors synthesized and functionalised with PAA.

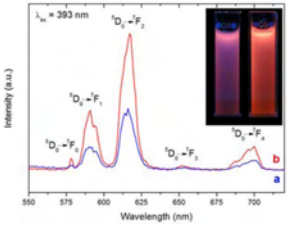

Figure 2: Emission spectra (λexc 393 nm) of aqueous suspensions of 2% doped calcium hydroxyapatite (a, blue line) and fluoroapatite (b, red line). The spectra were carried out with the same nanophosphors concentration. The image shows the luminescence of suspensions of 2% Eu calcium hydroxyapatite (left) and fluoroapatite (right) with the same nanoparticle concentration when irradiated with UV light.

Surface nano-structuration using composite colloidal monolayers

André Espinha, Marta Ibisate, Juan Galisteo-López, Álvaro Blanco, Cefe López

Instituto de Ciencia de Materiales de Madrid (CSIC)
Sor Juana Inés de la Cruz, 3, 28049 Madrid, Spain.

acmespinha@icmm.csic.es

Two dimensional (2D) photonic crystals (PC) have proven to be strong candidates for the control of the radiation/matter interaction and are a successful example of the research investment made by the photonics community. Furthermore, slab-like crystals based on the self-assembled arrangement of dielectric spheres are perhaps the most straightforward to fabricate [1]. These systems can be implemented in applications such as filters, waveguides and hybrid photonic-plasmonic devices. They can play an extraordinary role as masks, in nanosphere lithography or as templates for more complex colloidal structures and are also very effective for the production of nanoparticles.

The self-assembly methods are the simplest way to produce this kind of 2D PC, the most widespread being probably the vertical deposition starting from very dilute colloidal suspensions. Relying on convective particle assembly, this technique delivers crystals consisting of dielectric spheres, arranged in a hexagonal lattice. One of its important drawbacks is, nonetheless, polycrystalline domain structure. As so, the constant effort for improving the quality of the crystals resulted in several publications proposing alternative approaches for their fabrication, as well as reporting on the influence of different growth parameters.

A recent work [2] has shown that controlling the geometry of the three-phase contact line, at the meniscus of the suspension one can achieve better quality monolayers than those obtained by vertical deposition, in particular, single domain ones, centimeters across. The way to reach this is by confining the suspension in a wedge-shaped cell. The particularity of this kind of evaporation cell is that it permits an almost rectilinear interface between the three phases involved, during the evaporation.

Furthermore, there is also a significant demand on the fabrication of the inverse structures, that is, membranes composed of nanobowls or nanopore arrays or interconnected air voids [3]. Inverse structures are useful, for example, for the development of superhydrophobic surfaces, evaporation masks and templates for cell growth or protein self-assembly. Additionally, they are suitable systems for the study of photoluminescence manipulation [4]. Regarding fabrication, the inverse monolayers have been achieved mainly by infiltration with techniques such as electron beam evaporation, solution/sol-dipping, doctor blade technique or electrodeposition. Gas phase deposition can also be used for the infiltration, with additional advantages particularly, very good degree of conformality of the deposited material and fine tuning of the film thickness [5].

On the other hand, with respect to 3D PC, recent experiments pointed out that good quality, crack-free, inverse opals could be fabricated in a two-step method using co-assembly [6]. With this method, the composite (polymeric spheres immersed in a silica matrix) is obtained in a single step by adding a chemical precursor of the background material to the spheres' suspension. Therefore, the silica grows in the spheres' interstices, at the same time that the spheres assemble. Subsequently, the sacrificial spheres are removed using calcination or plasma etching and the inverse opal obtained.

In the work here presented, we tested the possibility of fabricating composite monolayers by combining the wedge shaped cell growth, on the one hand, with co-assembly on the other. By adopting this procedure, it was hoped that one might profit from the advantages that both techniques permit. Further thermal processing of the crystals permits one to attain the inverse porous membranes.

As so, composites were fabricated starting from colloidal suspensions of submicron spheres (diameters of 430 or 520 nm) in distilled water and added tetraethyl orthosilicate (TEOS) – the silica's

precursor. The suspensions are introduced in wedge shaped cells and left to evaporation in a climatic chamber with controlled temperature and humidity. A systematic study of the influence of TEOS concentration in the initial colloid (ranging from 1.0 to 6.0 vol%) was performed in order to improve the quality of the 2D crystals produced. The samples were characterized with scanning electron microscopy in order to ascertain the area of the perfect quality regions and filling fraction of the infiltrated silica. Figure 1 presents an example of a SEM image showing the surface of one of these monolayers. Furthermore, reflectance spectra of the obtained crystals were compared with the ones of similar crystals produced by infiltration of bare monolayers with chemical vapor deposition (CVD).

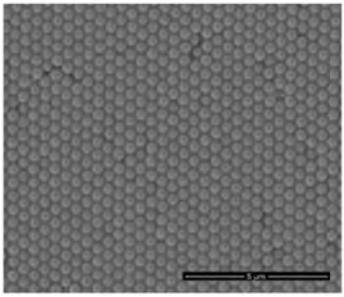

Figure 1: Example of SEM image exhibiting the surface aspect of the composite materials made of polystyrene spheres in a silica background.

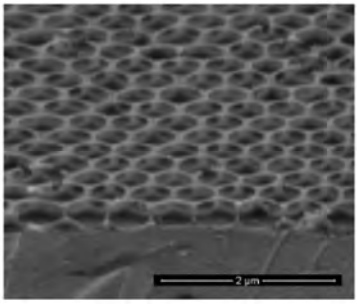

Figure 2: Example of SEM image, collected in cross section, exhibiting the aspect of the monolayers after calcination.

The effectiveness of the proposed fabrication method for the production of the composites was demonstrated. In a second phase of the work, the monolayers were calcinated in order to remove the polymer and achieve the inverse structure composed only of silica. An example of the crystals obtained with the referred procedure is shown in Figure 2. The results point out that the structures are robust enough to withstand the thermal treatments used in the inversion and, although defects are introduced, it is possible to obtain large area inverse monolayers of good quality.

The work described has been recently accepted for publication [7]. In comparison with similar experiments, previously carried out by other groups, our approach has the advantage of achieving the composite in one single step and also of improving the effective area of the final monolayers. We were able to obtain monodomain areas of the order of 1000 μm^2 with maximum perfect crack-free regions of approximately 120 μm^2. The procedure presented is expected to establish the route for an easier and quicker fabrication of inverse monolayers of higher refractive index materials, particularly silicon [8], with applications in light control.

References

[1] J. Galisteo-López et al. Advanced Materials, 23 (2011) 30-69.

[2] J. Sun, C. Tang, P. Zhan, Z. Han, Z. Cao, Z. Wang. Langmuir, 26 (2010) 7859–7864.

[3] J. Zhang, Y. Li, X. Zhang, B. Yang. Advanced Materials, 22 (2010) 4249–69.

[4] Y. Li, W. Cai, G. Duan, F. Sun, B. Cao, F. Lu, Q. Fang. Applied Physics A, 81 (2005) 269–273.

[5] A. Blanco, C. López. Advanced Materials, 18 (2006) 1593–1597.

[6] B. Hatton et al. Proc. Natl. Acad. Sci. U. S. A, 107 (2010) 1–6.

[7] A. Espinha, M. Ibisate, J. Galisteo-López, A. Blanco, C. López. Langmuir, DOI: 10.1021/la302395x.

[8] Z. Bao, M. Weatherspoon, S. Shian, Y. Cai. Nature, 446 (2007) 172–175.

Molding light propagation with phase discontinuities

Zeno Gaburro

Dipartimento di Fisica,
Università degli Studi di Trento
CNSC - Istituto Italiano di Tecnologia (IIT)
SEAS, Harvard University

sukosin@gmail.com

Conventional optical components rely on gradual phase shifts accumulated during light propagation to shape light beams. New degrees of freedom are attained by introducing abrupt phase changes over the scale of the wavelength. A two-dimensional array of optical resonators with spatially varying phase response and subwavelength separation can imprint such phase discontinuities on propagating light as it traverses the interface between two media. Anomalous reflection and refraction phenomena are observed in this regime in optically thin arrays of metallic antennas on silicon with a linear phase variation along the interface, in excellent agreement with generalized laws derived from Fermat's principle. Phase discontinuities provide great flexibility in the design of light beams as illustrated by the generation of optical vortices, lenses and axicons using planar designer metallic interfaces.

References

[1] N. Yu et al., Science 334, 333, 2011 (featured on cover),
[2] P. Genevet et al., Appl. Phys. Lett. 100, 13101, 2012 (featured on cover),
[3] F. Aieta et al., NanoLetters 12, 1702, 2012,
[4] R. Blanchard et al., Phys. Rev. B 85, 155457, 2012,
[5] F. Aieta et al., NanoLetters 12, 4932, 2012.

Light propagation and emission in hybrid metallodielectric systems based on self-assembled structures

J.F. Galisteo-López[1], M. López-García[1], A. García-Martín[2], C. López[1]

[1]Instituto de Ciencia de Materiales de Madrid (ICMM-CSIC), Sor Juana Inés de la Cruz, 3, 28049 Madrid, Spain.
[2]Instituto de Microelectrónica de Madrid (IMM-CSIC), c/ Isaac Newton 8, 28760 Tres Cantos, Madrid, Spain

galisteo@icmm.csic.es

The fields of photonic crystals and plasmonics have been actively explored over the past two decades as a means to exert control on light propagation and emission in ways not permitted by conventional materials. While photonic crystals have achieved unprecedented control over the guiding and generation of light, the nanoscale confinement of electromagnetic radiation allowed by metallic nanostructured systems remains unparalleled. Recently, the possibility of combining the two fields in hybrid metallodielectric structures has paved the way to strongly confine electromagnetic radiation while avoiding losses associated with metals [1,2].

Over the past two years the potential of hybrid metallodielectric systems fabricated by means of selfassembly methods has been demonstrated through their use to strongly modify the spontaneous emission of internal light sources [3], as chemical sensors [4] or as a route to improve the efficiency of solar cells [5]. In this work we combine spectroscopic techniques together with k-space (Fourier) imaging [6] to characterize light propagation in this kind of structures. We have studied 2D arrays of organic spheres containing light emitters and considered first the role of the substrate in the light confinement capabilities of these systems (see Figure 1). [7] Further, a complete experimental study comprising dispersion relations together with equifrequency surfaces is presented and the way light coupled to or emitted from this kind of systems propagates within them is discussed (see Figure 2) [8].

References

[1] J. Grandidier, S. Massenot, G. Colas des Francs, A. Bouhelier, J.-C. Weeber, L. Markey, A. Dereux, J. Renger, M. U. González, and R. Quidant, Physical Review B 78 (2008) 245419.
[2] R.F. Oulton, V. J. Sorger, V. J. Zentgraf, R.M. Ma, C. Gladden, L. Dai, G. Bartal, X. Zhang, Nature 461 (2009) 629.
[3] M. López-García, J.F. Galisteo-López, A. Blanco, J. Sánchez-Marcos, C. López and A. García-Martín, Small 6 (2010) 1757.
[4] X. Yu, L. Shi, D. Han, J. Zi and P.V. Braun, Advanced Functional Matererials 20 (2010) 1910.
[5] J. Grandidier, D.M. Callahan, J.N. Munday, and H.A. Atwater, Advanced Materials 23 (2011) 1171.
[6] M. López-García, J.F. Galisteo-López and C. López, Submitted (2012).
[7] M. López-García, J.F. Galisteo-López, C. López and A. García-Martín, Physical Review B 85 (2012) 235145.
[8] J.F. Galisteo-López, M. López-García, A. Blanco and C. López, Langmuir 28 (2012) 9174.

Graphene Nanophotonics

Francisco J. García-Vidal

Departamento de Física Teórica de la Materia Condensada and IFIMAC,
Universidad Autónoma de Madrid,
Madrid 28049, Spain

fj.garcia@uam.es

In this talk I will resume our work on graphene nanophotonics during the last two years. First I will analyze the electromagnetic fields radiated by a nanoemitter placed in the close proximity of a graphene sheet, which present a rich dependence on frequency, distance to the source and orientation of the dipole moment [1]. Then, I will study the propagating characteristics of the two types of graphene surface plasmons (waveguide and edge modes) supported by one-dimensional graphene ribbons [2]. When these graphene ribbons are placed in a periodic fashion, resonant features that lead to enhanced absorption and suppressed transmission emerge in the spectrum [3]. I will also address the coupling between graphene surface plasmons in graphene sheet arrays and the emergence of collective surface plasmons that present anomalous dispersion [4]. In the final part of the talk the capabilities of graphene both to act as a mediator in different light-matter coupling scenarios [5] and to support very deep-subwavelength optical solitons [6] will be discussed.

References

[1] A. Yu. Nikitin et al., Phys. Rev. B 84, 195446 (2011).
[2] A. Yu. Nikitin et al., Phys. Rev. B 84, 161407(R) (2011).
[3] A. Yu. Nikitin et al., Phys. Rev. B 85, 081405(R) (2012).
[4] B. Wang et al., Phys. Rev. Lett. 109, 073901 (2012).
[5] P. A. Huidobro et al., Phys. Rev. B 85, 155438 (2012).
[6] M. L. Nesterov et al. (to be published).

Silicon nanocrystals for all silicon tandem solar cells

J. López-Vidrier[1], S. Hernández[1], O. Blázquez[1], D. Hiller[2], S. Gutsch[2], A.M. Hartel[2], M. Canino[3], M. Allegrezza[3], M. Bellettato[3], M. Schnabel[4], P. Löper[4], J. Valenta[5], L. López-Conesa[1], S. Estradé[1,6], F. Peiró[1], M. Zacharias[2], C. Summonte[3], S. Janz[4] and **B. Garrido**[1]

[1]MIND-IN2UB, Departament d'Electrònica, Universitat de Barcelona, Barcelona, Spain
[2]IMTEK, Faculty of Engineering, Albert-Ludwigs-University Freiburg, Freiburg, Germany
[3]CNR-IMM, Consiglio Nazionale delle Richerche – Istituto per la Microelettronica e Microsistemi, Bologna, Italy.
[4]Fraunhofer Institute for Solar Energy Systems ISE, Freiburg, Germany
[5]CUNI, Faculty of Mathematics and Engineering, Charles University, Prague, Czech Republic
[6]TEM-MAT, CCiT-UB, Centre Científic i Tecnològic, Universitat de Barcelona, Barcelona, Spain

bgarrido@el.ub.edu

For years, silicon solar cells have attracted the attention of the industry due to their low fabrication and commercialization costs, as well as the favourable electrical properties of Si. However, although Si presents an almost optimum band gap energy (1.12 eV) for the solar spectrum absorption, the conversion efficiency of such material is very low (reaching a theoretical maximum of 33 %), mainly due to thermalization loses [1]. Tandem solar cells are able to avoid this drawback by combining two or more different band-gap systems. Recent studies have been focused on the performance of an all-Si tandem solar cell, consisting of a bulk crystalline Si solar cell and a different configuration of the same element on the top (see the scheme in Fig. 1), reaching theoretical conversion efficiencies up to 42.5% [2]. Silicon nanocrystals (Si-NCs) embedded in different Si-related dielectric matrices (such as SiO_2, Si_3N_4 or SiC) have proved to be a suitable candidate for the top material of such a structure, because of their outstanding properties, arisen from the quantum confinement of the carriers inside the nanostructures when reducing their size [3].

The control of the NC size is then crucial for obtaining the desired electronic properties. Many studies have been reported on Si-NCs embedded in SiO_x/SiO_2 superlattices, showing a good control of the multilayer thickness and the NC size [4]. Therefore, by means of this approach, a vertical confinement of the NC size is easily achieved. Other authors have focused in the growth of Si_xC_{1-x}/SiC multilayers containing Si-NCs [5]. SiC partially solves the electron transport problem in an insulator like SiO_2, and its lower band gap energy allows for a better absorption of the solar spectrum. However, the deposition process of the superlattices is not well established yet, and therefore the NC size cannot be fully controlled (see Fig. 2). For the performance of an efficient solar cell, both a good photon absorption and photogenerated carriers extraction are required, in order to obtain photocurrent. Then, the study and optimization of the SiO_2 and SiC matrices becomes crucial.

In this work, we present the characterization work performed over SiO_x/SiO_2 and Si_xC_{1-x}/SiC superlattices, deposited on crystalline Si or fused silica substrates by means of plasma-enhanced chemical-vapour deposition. After a post-deposition annealing process, the Si excess present in the Si-rich layers precipitates and crystallizes forming Si-NCs. Different structural parameters (silicon content, thickness of the layers and annealing temperature) have been changed to study their structural, optical and electrical properties. By means of energy-filtered transmission electron microscopy, the presence of nanocrystals after the annealing process was corroborated in both matrices. We made use of the Raman scattering

technique in order to determine the crystalline degree of the samples. For this, a previously developed phonon confinement model was employed [6]. Photoluminescence and UV-absorption studies were also carried out, in order to obtain information about the band gap energy the samples present, checking this way the quantum confinement of the carriers inside the NCs. Finally, electrical measurements have been performed under dark and illumination conditions, to deduce the NCs presence on the electrical properties of the systems. The photocurrent generation has been proved in both systems, which shows the potential of these materials for developing all silicon tandem solar cells.

References

[1] F. Meillaud, A. Shah, C. Droz, E. Vallat-Sauvain et al., Sol. Energy Mater. & Sol. Cells 90 (2006) 2952.

[2] Conibeer, G., Green, M., Cho, E.-C., König, D., et al., Thin Solid Films 516 (2008) 6748.

[3] Godefroo, S., Hayne, M., Jivanescu, M., Stesmans, A., et al., Nat. Nanotechnol. 3 (2008) 174.

[4] Zacharias, M., Bläsing, J., Veit, P., Tsybeskov, et al., Appl. Phys. Lett. 74 (1999) 2614.

[5] Song, D., Cho, E.-C., Conibeer, G., Flynn, C,. et al., Sol. Energy Mater. & Sol. Cells 92 (2008) 474.

[6] Hernández, S. Martínez, A., Pellegrino, P., Lebour, Y., et al.: J. Appl. Phys. 104 (2008) 044304.

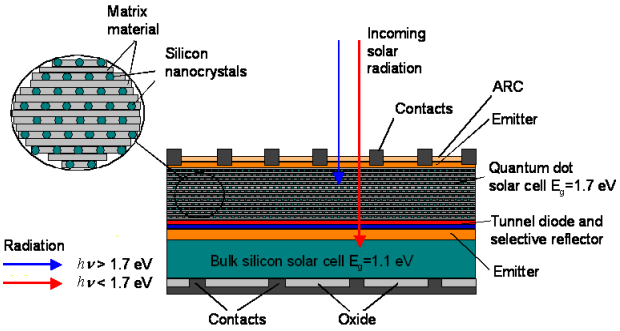

Figure 1: Cross-section scheme of an all-Si tandem solar cell, consisting of a multilayer structure containing Si-NCs on the top of a crystalline Si solar cell. A tunnel junction links both structures.

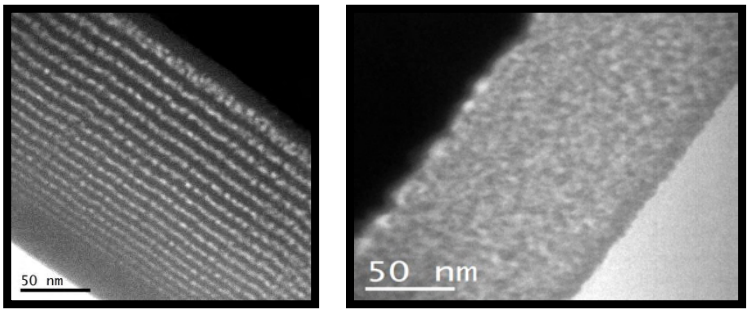

Figure 2: Cross-section energy-filtered transmission electron microscopy images of the multilayer structures studied in this work for (left) SiO_2 and (right) SiC dielectric matrices. Both samples underwent an annealing treatment. Bright dots are attributed to Si-NCs. Notice that, after annealing, the multilayer structure is lost for the SiC matrix sample.

Electromagnetic waves interaction with various metallic nanomaterials

Michael Giersig

Institute for Experimental Physics
Arnimallee 14, 14195 Berlin, Germany

giersig@physik.fu-berlin.de

In the last decade the possibility of active interaction of light with the nanosized plasmonic materials has been tremendously growth. The metallic nanoparticles can effectively confine the radiation to nanoscale in the proximity of Plasmon resonance whereby the position of this resonance is controlled by the morphology (size and shape) of the nanostructures. In this lecture we will discussed the physical and chemical preparations methods of various nanostructures and their structural and optical characterization.

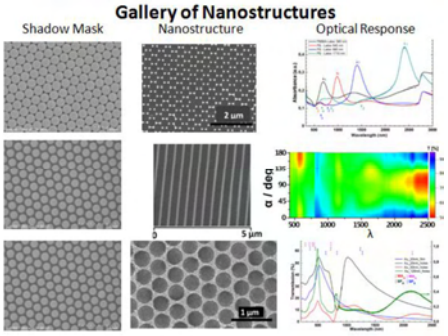

Figure 1

References

[1] A. Kosiorek, W. Kandulski, P. Chudzinski, K. Kempa, and M. Giersig, NanoLetters 4, 7, 1359–1363, 2004.

[2] A. Kosiorek, W. Kandulski, H. Glaczynska, M.Giersig, Small 1, 4, 439-444, 2005.

[3] P. Patoka ,T. Skeren, M. Hilgendorff , K. Kempa and M. Giersig, Small 7, 21, 3096-3100, 2011

[4] P. Patoka and M. Giersig, J. Mater. Chem., 21, 16783-16796, 2011.

[5] P. Patoka, T. Sun, M. Giersig and K. Kempa, Advanced Materials 24, 22, 3042-3045, 2012.

Negative scattering asymmetry parameter for dipolar particles: Unusual reduction of the transport mean free path and radiation pressure

R. Gómez-Medina[1], L. S. Froufe-Pérez[2], M. Yépez1, F. Scheffold[3], M. Nieto-Vesperinas[4] and J.J. Sáenz[1]

[1]Condensed Matter Physics Dept. and Centro de Investigación en Física de la Materia Condensada (IFIMAC), Universidad Autónoma de Madrid, Madrid, Spain
[2]Instituto de Estructura de la Materia, Consejo Superior de Investigaciones Científicas CSIC, Madrid, Spain
[3]Department of Physics, University of Fribourg, Fribourg, Switzerland
[4]Instituto de Ciencia de Materiales de Madrid, Consejo Superior de Investigaciones Científicas (CSIC), Madrid, Spain

r.gomezmedina@uam.es

Propagation of light and image formation in turbid media has long been a subject of great interest [1] and constitutes the core of powerful techniques with countless applications including biomedical imaging [2, 3] and dynamic spectroscopy techniques [4-6], characterization of composite materials and complex fluids [7], remote sensing or telecommunications [8] to mention a few.

Lossless dielectric nanospheres (made of nonmagnetic materials) with relatively low refraction index may present strong electric and magnetic dipolar resonances [9-11].

We establish a relationship between the optical force [12,13] from a plane wave on small electric and magnetic dipolar particles, the transport cross section, and the scattering asymmetry parameter g [14].

In this way we predict negative g (that minimize the transport mean free path below values of the scattering mean free path) for a dilute suspension of both perfectly reflecting spheres as well as of lossless dielectric nanospheres made of moderate permittivity materials, e.g., silicon or germanium nanospheres in the infrared region. Lossless dielectric Mie spheres of relatively low refraction index (as low as 2.2) are shown to present negative g in specific spectral ranges [14].

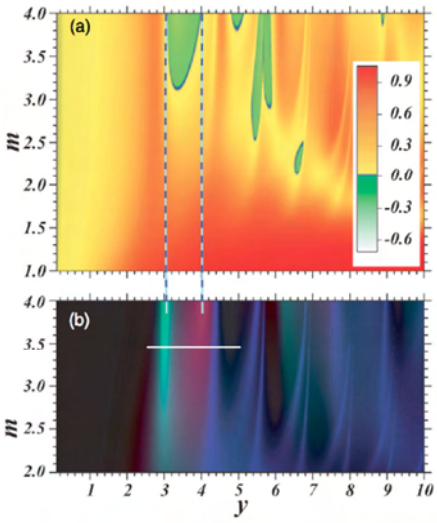

Figure 1: (a) Color map of the g factor for spherical absorptionless particles as a function of their refractive index m and size parameter y = mka. As seen in the attached scale, green areas correspond to negative values of g. (b) Color map of the sphere scattering cross section. Red corresponds to dominant electric dipole contributions to the scattering cross section. Green corresponds to dominant magnetic dipole contributions, while blue sums up all higher-order multipole terms. Vertical dashed lines coincide with y parameter for maximum electric dipole contribution (right vertical line) and maximum magnetic dipole contribution (left vertical line). The white horizontal line at m ≈ 3.5 which corresponds to a silicon sphere. (After Ref.[14]).

References

[1] Waves and Imaging through Complex Media, edited by P. Sebbah (Kluwer Academic, Dordrecht, 2001); in Wave Scattering in Complex Media: From Theory to Applications, edited by B. A. van Tiggelen and S. E. Skipetrov, NATO Science Series II: Mathematics, Physics and Chemistry,Vol. 107 (Kluwer Academic, Dordrecht, 2003).

[2] A. Yodh and B. Chance, Phys. Today 48(3), 34 (1995); S. K. Gayen and R. R. Alfano, Opt. Photon. News 7 (1996) 17.

[3] J. Ripoll, V. Ntziachristos, J. P. Culver, D. N. Pattanayak, A. G. Yodh, and M. Nieto-Vesperinas, J. Opt. Soc. Am. A 18 (2001) 821.

[4] D. A. Weitz and D. J. Pine, in Dynamic Light Scattering, edited by W. Brown (Oxford University Press, New York, 1993).

[5] G. Maret and P. E. Wolf, Z. Phys. B 65 (1987) 409; D. J. Pine, D. A. Weitz, P. M. Chaikin, and E. Herbolzheimer, Phys. Rev. Lett. 60 (1988) 1134.

[6] R. Lenke and G. Maret, in Multiple Scattering of Light: Coherent Backscattering and Transmission, edited by W. Brown (Gordon & Breach, Reading, UK, 2000).

[7] F. Scheffold and P. Schurtenberger, Soft Mater. 1 (2003) 139.

[8] A. Derode, A. Tourin, J. de Rosny, M. Tanter, S. Yon, and M. Fink, Phys. Rev. Lett. 90 (2003) 14301; G. Lerosey, J. de Rosny, A. Tourin, and M. Fink, Science 315 (2007) 1120.

[9] A. García-Etxarri, R. Gómez-Medina, L. S. Froufe-Pérez, C. López, L. Chantada, F. Scheffold, J. Aizpurua, M. Nieto-Vesperinas and J. J. Sáenz, Opt. Express, 19 (2011) 4815-4826.

[10] R. Gómez-Medina, B. García-Cámara, I. Suárez-Lacalle, F. González, F. Moreno, M. Nieto-Vesperinas and J. J. Sáenz, J. Nanophoton. 5 (2011) 053512.

[11] M. Nieto-Vesperinas, R. Gómez-Medina, and J. J. Sáenz, J. Opt. Soc. Am. A, 28 (2011) 54-60.

[12] M. Nieto-Vesperinas, J. J. Sáenz, R. Gómez-Medina, and L. Chantada, Opt. Express, 18 (2010) 11428-11443.

[13] R. Gómez-Medina, M. Nieto-Vesperinas and J. J. Sáenz, Phys. Rev. A, 83 (2011) 033825.

[14] R. Gómez-Medina, L. S. Froufe- Pérez, M. Yépez, F. Scheffold, M. Nieto-Vesperinas and J. J. Sáenz, Phys. Rev. A, 85 (2012) 035802.

Infrared Nanospectroscopy - From Nanoscale Chemical Identification of Polymers to Real-space Imaging of Graphene Plasmons

R. Hillenbrand

CIC nanoGUNE Consolider, San Sebastian, Spain
Ikerbasque, Basque Science Foundation, Bilbao, Spain

r.hillenbrand@nanogune.eu

Optical spectroscopy has tremendous impact in science and technology, particularly in the infrared (IR) and terahertz (THz) spectral range, where photons can probe molecule vibrations, phonons, as well as plasmons and electrons in non-metallic conductors. However, diffraction limits the spatial resolution to the micrometer scale, thus strongly limiting its application in nano- and biosciences. To overcome this drawback, we developed near-field microscopy based on elastic light scattering from atomic force microscope tips (scattering-type scanning near-field optical microscopy, s-SNOM) [1]. Collection of the tip-scattered light yields nanoscale resolved IR and THz [2] images, beating the diffraction limit in the terahertz spectral range by more than three orders of magnitude.

For nanoscale infrared dielectric mapping and vibrational spectroscopy we employ metalized AFM tips acting as infrared antennas. The illuminating light is converted into strongly concentrated near fields at the tip apex (nanofocus), which provides a means for localized excitation of molecule vibrations, plasmons or phonons in the sample surface. Spectroscopic mapping of the scattered light thus allows for nanoscale chemical recognition of (bio)materials, mapping of free-carrier concentration in semiconductor nanodevices [2] and nanowires [3] or nanoimaging of strain.

Using broadband IR illumination and Fourier-transform (FT) spectroscopy of the tip-scattered light, we are able to record IR spectra with nanoscale spatial resolution (nano-FTIR), even when employing the weak radiation from an incoherent thermal source [4]. Particularly, we demonstrate that nano-FTIR can acquire near-field absorption spectra of molecular vibrations throughout the mid-infrared fingerprint region at a spatial resolution of 20 nm. To that end, we employ a novel laser-based continuum source and perform spectroscopic imaging and identification of polymer nanostructures [5].

s-SNOM also enables the launching and detecting of propagating and localized plasmons in graphene nanostructures (Fig. 1). Spectroscopic real-space images of the plasmon modes allow for direct measurement of the ultrashort plasmon wavelength and for visualizing plasmon control by gating the graphene structures.

Another application of s-SNOM is the imaging of the vectorial infrared near-field distribution of plasmonic nanostructures. In this application, a dielectric tip scatters the near fields at the sample surface, allowing for mapping the hot spots in plasmonic infrared gap antennas [8] or for verifying IR energy transport and compression in nanoscale transmission lines [9]. With these studies we establish a basis for the development of nanoscale infrared circuits based on antennas and transmission lines, which could have interesting application potential for the development of ultra-compact infrared sensors, spectrometers and novel near-field probes.

References

[1] F. Keilmann, R. Hillenbrand, Phil. Trans. R. Soc. Lond. A 362, 787 (2004)
[2] A. J. Huber, et al., Nano Lett. 8, 3766 (2008)
[3] J. M. Stiegler, et al., Nano Lett. 10, 1387 (2010)
[4] F. Huth, M. Schnell, J.Wittborn, N. Ocelic, R. Hillenbrand, Nature Mater. 10, 352 (2011)
[5] F. Huth, et al., Nano Lett. 12, 3973 (2012)
[6] J. Chen, et al., Nature 487, 77 (2012)
[7] Z. Fei, et al., Nature 487, 82 (2012)
[8] P. Alonso-González, et al., Nat. Commun. 3:684 doi: 10.1038/ncomms1674 (2012)
[9] M. Schnell, et al., Nature Photon. 5, 283 (2011)

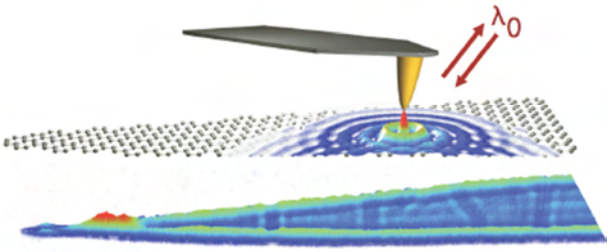

Figure 1: Optical nanoimaging of graphene plasmons. Upper panel: Sketch of the imaging method. A laser illuminated scanning tip launches plasmons on graphene. Detection is by recording the light backscattered from the tip. Lower panel: Optical image of graphene, where the fringes visualize the interference of the graphene plasmons.

Light spin forces, polarization structuring and the trapping of small particles with optical tweezers

Ignacio Iglesias[1] and
Juan José Sáenz[2]

[1]Departmento de Física, Universidad de Murcia, Campus de Espinardo, E-30100, Murcia, Spain
[2]Departmento de Física de la Materia Condensada, Universidad Autónoma de Madrid, E-28049, Madrid, Spain

iic@um.es

The force generated by the light spin on Rayleigh particles in optical tweezers increases with the numerical aperture of the microscope altering the trapping potential structure [1]. As happen with the radiation pressure, the spatial distribution of the spin force deeply changes when the polarization of the incident beam is modified. For certain polarizations, the spin force can be comparable in magnitude with the radiation pressure.

To improve the trapping efficiency of metallic particles [2] by minimizing the scattering forces, it has been proposed the use of radial polarized beams [3, 4]. The reason is that the radial pupil plane polarization generates an intensity distribution around the focal point whereas the axial component of the radiation pressure surrounds the optical axis. Thanks to that, it is assumed that the stability region generated by the gradient forces becomes free from scattering.

In this presentation we will describe the different forces acting in a high numerical aperture optical trap for different polarization structures and how, if the spin forces are considered, radial polarization does not reduce the scattering on small metallic particles [5] although it may have other advantages.

References

[1] I. Iglesias and J. J. Sáenz, Opt. Comm. 284, 2430-2436 (2011).
[2] K. Svoboda and S. M. Block, Opt. Lett. 19, 930-932 (1994).
[3] Q. Zhan, Opt. Express 12, 3377-3382 (2004).
[4] Q. Zhan, Adv. Opt. Photon. 1, 1-57 (2009).
[5] I. Iglesias and J. J. Sáenz, Opt. Express 20, 2832-2834 (2012).

Cavity Optomechanics: Quantum coherent coupling of light and mechanical oscillators

Tobias J. Kippenberg

EPFL , Switzerland

The mutual coupling of optical and mechanical degrees of freedom via radiation pressure has been a subject of interest in the context of quantum limited displacements measurements for Gravity Wave Detection for many decades, however light forces have remained experimentally unexplored in such systems. Recent advances in nano- and micro-mechanical oscillators have for the first time allowed the observation of radiation pressure phenomena in an experimental setting and constitute the emerging research field of cavity optomechanics [1].

Using on-chip micro-cavities that combine both optical and mechanical degrees of freedom in one and the same device [2], radiation pressure back-action of photons is shown to lead to effective cooling [3-6] of the mechanical oscillator mode using dynamical backaction, which has been predicted by Braginsky as early as 1969 [4]. This back-action cooling exhibits many close analogies to atomic laser cooling. With this novel technique the quantum mechanical ground state of a micromechanical oscillator has been prepared with high probability using both microwave and optical fields. In our research this is reached using cryogenic precooling to ca. 700 mK in conjunction with laser cooling, allowing cooling of micro-mechanical oscillator to only 1.7 quanta. – implying the oscillator resides more than 1/3 of its time in the quantum ground state. Moreover it is possible in this regime to observe quantum coherent coupling in which the mechanical and optical mode hybridize and the coupling rate exceeds the mechanical and optical decoherence rate [7]. This accomplishment enables a range of quantum optical experiments, including state transfer from light to mechanics using the phenomenon of optomechanically induced transparency [8].

From a broader perspective the described experiments that exploit optomechanical coupling are motivated both by the effort to realize quantum measurement schemes on mechanical systems and establish mechanical oscillator as a quantum technology, following atoms, ions and molecules in a first and electrical circuits in a third wave of developments.

References

[1] T. J. Kippenberg, K. J. Vahala, Cavity Optomechanics: Backaction at the mesoscale. Science 321, 1172 (2008, 2008).

[2] T. J. Kippenberg, H. Rokhsari, T. Carmon, A. Scherer, K. J. Vahala, Analysis of Radiation-Pressure Induced Mechanical Oscillation of an Optical Microcavity. Physical Review Letters 95, 033901 (2005).

[3] V. B. Braginsky, S. P. Vyatchanin, Low quantum noise tranquilizer for Fabry-Perot interferometer. Physics Letters A 293, 228 (Feb 4, 2002).

[4] V. B. Braginsky, Measurement of Weak Forces in Physics Experiments. (University of Chicago Press, Chicago, 1977).

[5] A. Schliesser, P. Del'Haye, N. Nooshi, K. J. Vahala, T. J. Kippenberg, Radiation pressure cooling of a micromechanical oscillator using dynamical backaction. Physical Review Letters 97, 243905 (Dec 15, 2006).

[6] A. Schliesser, R. Riviere, G. Anetsberger, O. Arcizet, T. J. Kippenberg, Resolved-sideband cooling of a micromechanical oscillator. Nature Physics 4, 415 (May, 2008).

[7] E. Verhagen, S. Deleglise, S. Weis, A. Schliesser, T.J. Kippenberg, Nature (2012)

[8] S. Weis et al., Optomechanically Induced Transparency. Science 330, 1520 (Dec, 2010).

Graphene nano-optoelectronics for capturing and manipulating light at the nanoscale

F. Koppens[1], M. Badioli[1], J. Osmond[1], L. Gaudreau[1], M. Bernechea[1], P. Garcia de Arquer[1], F. Gatti[1], M. Spasenovic[1], G. Konstantatos[1], J. Chen[2], F. Huth[2], P. Alonso-González[2], R. Hillenbrand[2], A. Centeno[3], A. Pesquera[3], A. Zurutuza[3], P. Godignon[4], N. Camara[4], S. Thongrattanasiri[5] and J. Garcia de Abajo[5]

[1]ICFO, The institute of photonic Sciences, Barcelona, Spain
[2]CIC nanoGUNE, San Sebastian, Spain
[3]Graphenea S.A., San Sebastian, Spain
[4]CNM-IMB, Barcelona, Spain and GREMAN, Tours, France
[5]IQFR-CSIC, Madrid, Spain

Graphene, a two-dimensional sheet of carbon atoms, has recently emerged as a novel material with unique electrical and optical properties, with great potential for opto-electronic applications, such as ultrafast photo-detection and optical switches. In this talk, I will review recent experimental work on exploiting graphene as a host for guiding, switching and manipulating light and electrons at the nanoscale [1,2]. This is achieved by exploiting surface plasmons: surface waves coupled to the charge carrier excitations of the conducting sheet. Due to the unique characteristics of graphene, light can be squeezed into extremely small volumes and thus facilitate strongly enhanced light-matter interactions. I will discuss recent observations of propagating and localized optical plasmons in graphene nano-structures. The plasmon wavelength can be tuned and plasmon propagation can even be switched on and off in-situ, simply by tuning the carrier density by electrostatic gates. These results pave the way towards ultrafast modulation of nanoscale optical fields, resonantly confined in graphene nano-structures or propagating along graphene ribbons.

The second part of the talk is devoted to a novel hybrid graphene-quantum dot photodetector [3] which exhibits a gain mechanism that can generate multiple charge carriers from one incident photon. Strong and tunable light absorption in the quantum-dot layer creates electric charges that are transferred to the graphene, where they recirculate many times due to graphene's high charge mobility and long trapped-charge lifetimes in the quantum-dot layer. We demonstrate a gain of 10^8 electrons per photon and a record-high responsivity of 10^7 A/W. Our devices also benefits from gate-tunable sensitivity and speed, spectral selectivity from the short-wavelength infrared to the visible, and compatibility with current circuit technologies.

References

[1] J. Chen, M. Badioli, P. Alonso-González, S Thongrattanasiri, F Huth, J Osmond, M. Spasenović, A. Centeno, A. Pesquera, P. Godignon, A. Zurutuza, N. Camara, J. Garcia de Abajo, R. Hillenbrand, F. Koppens, "Optical nano- imaging of gate-tuneable graphene plasmons", Nature (2012).

[2] F. Koppens, D. Chang, J. García de Abajo, "Graphene Plasmonics: A Platform for Strong Light–Matter Interactions", Nano Letters 11, 3370–3377 (2011).

[3] G. Konstantatos, M. Badioli, L. Gaudreau, J. Osmond, M. Bernechea, P. Garcia de Arquer, F. Gatti, F. Koppens, "Hybrid graphene-quantum dot phototransistors with ultrahigh gain", Nature Nanotechnology (2012).

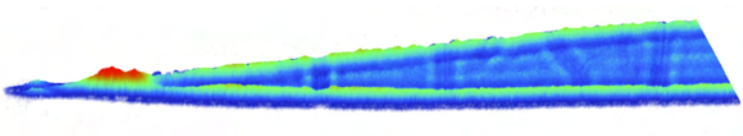

Figure 1

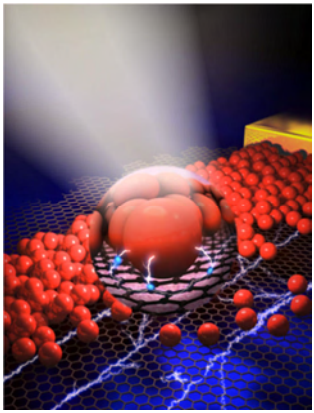

Figure 2

Colloidal Plasmonic Nanostructures

Luis M. Liz-Marzán

Departamento de Química Física,
Universidade de Vigo, 36310 Vigo, Spain,

The assembly of nanoparticle building blocks is a pre-requisite for the amplification of the properties of the components and/or the generation of new features unique to the ensemble [1]. Usually, nanoparticles employed for these assemblies are spherical and lack a geometrical preference toward directional self-assembly, thus limiting their potential applications. In contrast, controlled self-assembly of non-spherical nanoparticles, such as gold nanorods, enables these arrays to form defined 1D, 2D or 3D structures with a vectorial dependence of the desired properties. I will present in this lecture several examples of directional assembly of gold nanoparticles, resulting in unusual optical properties, which are a consequence of the particular configuration within the assembly [2, 3].

Standing 2D and 3D superlattices made of gold nanorods can be obtained through the use of gemini surfactants as capping agents in aqueous solution. The extreme directionality of these assemblies is reflected in the anisotropic optical properties of the crystalline superlattices, which additionally display extraordinary antenna effects, rendering them excellent SERS substrates [4].

A completely different type of self-assembly in solution has been recently found for PVP-coated gold nanorods, when dispersed in N-methylpyridine and irradiated with UV light. In this case, the assembly invariably results in ladder-like structures that display novel plasmon resonance modes that were typically restricted to gold nanostructures on solid substrates [5].

Alternatively, the assembly can be directed by using different types of templates. For example, when gold nanorods are adsorbed on chiral fibers, special arrangements are obtained that display extremely high optically activity, even in solution.

These and other recent examples of directed nanoparticle assembly will pave the way toward the design of novel devices based on the remarkable plasmonic properties characteristic of the assemblies.

References

[1] M. Grzelczak, J. Vermant, E. Furst, L.M. Liz-Marzán, ACS Nano 2010, 4, 3591-3605.
[2] A. Guerrero-Martínez, E. Carbó-Argibay, J. Pérez-Juste, G. Tardajos, L.M. Liz-Marzán, Angew. Chem. Int. Ed. 2009, 48, 9484-9488.
[3] R.A. Alvarez-Puebla et al., PNAS 2011, 108, 8157-8161.
[4] M. Grzelczak et al., Langmuir 2012, 28, 8826-8833.
[5] A. Guerrero-Martínez et al., Angew. Chem. Int. Ed. 2011, 50, 5499-5503.

Graphene plasmons and quantum emitters: from plasmon blockade to temporal control

A. Manjavacas[1], S. Thongrattanasiri[1], P. Nordlander[2], D. E. Chang[3] and F. J. García de Abajo[1]

[1]IQFR - CSIC, Serrano 119, Madrid, Spain
[2]Department of Physics and Astronomy, M.S. 61, Rice University, Houston, Texas 77005-1892, United States
[3]ICFO-Institut de Ciencies Fotoniques, Mediterranean Technology Park, 08860 Castelldefels (Barcelona), Spain

alejandro.manjavacas@gmail.com

Among the many extraordinary properties of graphene, its optical response allows one to easily tune its interaction with nearby molecules via electrostatic doping. The large confinement displayed by plasmons in graphene nanodisks makes it possible to reach the strong-coupling regime with a nearby quantum emitter, such as a quantum dot or a molecule. In this limit, the quantum emitter can introduce a significant plasmon-plasmon interaction, which gives rise to a plasmon blockade effect. This produces, in turn, strongly nonlinear absorption and modified statistics of the bosonic plasmon mode. In the first part of this work [1], we characterize these phenomena by studying the optical absorption cross section and he equal-time second-order correlation function $g^{(2)}(0)$, which plunges below a value of 1, thus revealing the existence of nonclassical plasmon states.

The plasmon-emitter coupling can be efficiently controlled by tuning the doping level of the graphene nanodisks. Therefore, the time modulation of the doping opens the possibility of achieving full temporal control of the quantum emitter dynamics. In the second part of this work [2] we explore such possibility, analyzing the temporal evolution of a single quantum emitter placed in the vicinity of a graphene nanodisk, under different doping profiles. We also demonstrate theoretically the possibility of temporal controlling the coupling of two quantum emitters mediated by the graphene plasmons.

The proposed systems based on graphene nanostructures emerge as a new promising platform to realize quantum plasmonic devices [3] capable of commuting optical signals at the single-photon/plasmon level with full temporal control.

References

[1] A. Manjavacas, P. Nordlander, and F. J. García de Abajo, ACS Nano. 6, (2012) 1724.
[2] A. Manjavacas, F. J. García de Abajo, and P. Nordlander, Nano Lett. 11, (2011) 2318.
[3] A. Manjavacas, S Thongrattanasiri, D E Chang, and F. J. García de Abajo, arXiv:1207.5903, (2012).

(a)

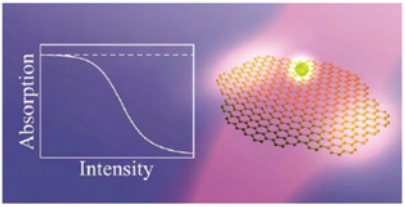

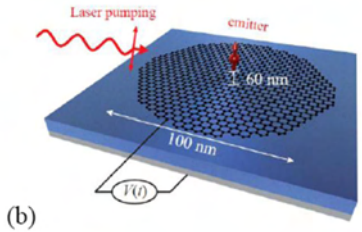

(b)

Figure 1: (a) Artistic view of the system under study composed of a quantum emitter placed near a graphene nanodisk, and plot of the absorption cross section as a function of the illumination intensity showing the non-linear optical response of the system. (b) Schematic view of the system considered to study the temporal control of a quantum emitter.

Babinet principle in optical nano-circuits and metamaterials

Ricardo Marqués[1], Juan Domingo Baena[2], Vicente Delgado[1] and Julián David Ortiz[2]

[1]Dept. of Electronics and Electromagnetism, Av. Reina Mercedes S/N 41012, Univ. of Seville, Spain
[2]Dept. of Physics, Universidad Nacional de Colombia, Bogota, Colombia

marques @u s.es

Classical Babinet principle is only rigorous for infinitely thin perfect conducting screens. A different "Babinet theorem" applicable to penetrable and thick plasmonic screens is presented in this contribution.

We will consider the quasi-static 2D problem shown in Fig.1, consisting in a 2D piecewise homogeneous region filled by some media with relative dielectric constants ε_i, which supports a quasielectrostatic electric field $\mathbf{E} = -\nabla_t\phi(x, y) = -\mathbf{u}_x\partial_x\phi - \mathbf{u}_y\partial_y\phi$, where $\phi(x, y)$ satisfies Laplace's equation $\nabla_t^2\phi = 0$. Surface plasmons and bound solutions for $\phi(x, y)$ may exist if there is at least one ε_i with $\mathrm{Re}(\varepsilon_i) < 0$, and at least one ε_j with $\mathrm{Re}(\varepsilon_j) > 0$. In such case, the electric field inside each region must satisfy $\nabla_t \times \phi = 0$ and $\nabla_t \cdot \mathbf{E}_i = 0$, as well as the boundary conditions at the border between i and j media $\mathbf{n}\times(\mathbf{E}_i - \mathbf{E}_j) = 0$ and $\mathbf{n}\cdot(\varepsilon_i\mathbf{E}_i - \varepsilon_j\mathbf{E}_j) = 0$, where n is the unit vector normal to this border and contained in the *xy* plane.

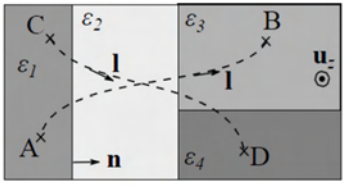

Figure 1: Illustration of a planar nanocircuit like those analyzed in this contribution.

The "complementary" structure is obtained by substituting the permittivities ε_i by the "complementary" ones $\varepsilon'_i = C_1/\varepsilon_i$ where C_1 is an arbitrary constant (for the particular case of a two-phase planar region we can choose $C_1 = \varepsilon_1\varepsilon_2$ in order to recover conventional complementarity). The "complementary" fields $\mathbf{E}'_i$ inside each region of the complementary structure are defined by:

$$\mathbf{E}'_i = C_2\,\varepsilon_i\,\mathbf{u}_z \times \mathbf{E}_i \qquad (1)$$

where C_2 is an arbitrary constant. It is shown that these fields also satisfy the quasi-electrostatic equations. Let be *A, B, C* and *D* some fixed points in the original and the complementary structures (see Fig.1). Let us define the voltage integral between *A* and *B* and the current integral through the path *C–D* as:

$$V_{AB} = \int_A^B \mathbf{E}\cdot\mathrm{l}dl; \text{ and } I_{CD} = j\omega\varepsilon_0 h\int_C^D \varepsilon(\mathbf{r})\mathbf{E}\cdot(\mathbf{u}_z\times\mathbf{l})dl \quad (2)$$

where h is the thickness of the circuit board. Let us assume that we can define some meaningful impedances $Z = V_{AB}/I_{CD}$ for the structure of Fig.1 and $Z' = V'_{AB}/I'_{CD}$ for its complementary one. By using (1) in (2) we obtain: $h^2k^2C_1ZZ' = -Z_0^2$ (3)

where $k = \sqrt{\varepsilon_0/\mu_0}$ is the phase constant and $Z_0 = \sqrt{\varepsilon_0/\mu_0}$ is the vacuum impedance. Let us now consider a diffraction screen made of a periodic planar nano-circuit [1]-[3]. Since nano-circuits must be electrically small [1], the periodicity must be small too. Therefore, we can describe the screen as a surface impedance sheet. This surface impedance will be, in general, a 2D symmetric tensor whose main values are related with the nano-circuit impedances. The surface impedance along a main axis of this tensor can be computed as $Z_s = Zl_{CD}/l_{AB}$ with Z defined above with the paths *A–B* and *C–D* chosen as straight lines going across the whole unit cell and directed along the proper main axes of the surface impedance tensor (l_{AB} and l_{CD} are the lengths of the corresponding paths). Specifically, this surface impedance Z_s describes the behavior of the screen for incident light polarized along the *A→B* direction. For the "complementary" screen, the surface impedance for incident light of orthogonal polarization is $Z'_s = Z'l_{CD}/l_{AB}$, with Z' defined above. The transmission coefficient for the first screen and the considered incident light is:

$$t = \frac{2Z_s}{Z_0 + 2Z_s} \qquad (4)$$

and the transmission coefficient for the complementary screen:

$$t' = \frac{2Z'_s}{Z_0 + 2Z'_s} = \frac{Z_0}{Z_0 + 2KZ_s}; \quad K = \pi h^2 k^2 C_1/4 \quad (5)$$

which for $K = 1$ reproduces the well known Babinet relation $t+t'= 1$ for infinitely thin perfect conducting complementary screens. If $K \neq 1$, Eqs. 4-5 still reproduce many of the main predictions of Babinet principle. For lossless media, the transmittance $|t|^2$ has a zero when and $|t'|^2$ has a maximum when $|Z| \to 0$. For lossy media $|Z|$ never goes to zero, and the minimum of $|t|^2$ occurs at the minimum of $|Z|$, whereas the maximum of $|t'|^2$ occurs at the minimum of $|KZ|$. This may lead to some deviation between the minimum of $|t|^2$ and the maximum of $|t'|^2$. Eqs. 4-5 can be considered as the generalization of Babinet principle for planar nano-circuits. However, they are still approximate and valid in the quasi electrostatic limit and as far as the effects of fringing fields can be neglected. Since these constrains are approximately fulfilled by many planar nano-circuit [1]-[3] and metallic metamaterial "atoms" [4]-[5], this theory is expected to be useful for the analysis of these structures.

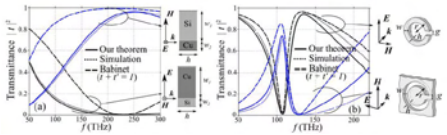

Figure 2: Left: transmission through two complementary 1D diffraction screens made of alternating layers of copper and silicon (unit cells shown aside). Dimensions are $w1$ = 50 nm, $w2$ = 10 nm and h = 25 nm. Right: transmission through complementary silver SRR and CSRR screens with r = 100 nm, g = 10 nm, w = 30 nm and h = 60 nm. Periodicity is 250 nm.

We have applied our theory to the analysis of the structure shown in the inset of Fig.2 (left). It is a 1D diffraction screen made of alternating layers of copper and silicon ($\varepsilon \approx 11.9$) which can be seen as the realization of an optical nano-circuit [6]. We first computed the transmittance through the screen using the commercial solver CST Microwave Studio, and then obtained the transmittance through the complementary screen from (4)-(5) after elimination of the common variable Z. The results are shown in Fig.2, where a very good agreement between our theory and the electromagnetic simulations can be observed. The results coming from conventional Babinet principle ($t + t' = 1$), also plotted, show a significant deviation from the computed ones, as expected from the properties of the media involved in the screen. Our theory has also been applied to the computation of the transmittance through screens made of conventional and complementary SRRs operating in the optical range (Fig.2 (right)), and also approaches reality better than conventional Babinet principle ($t + t' = 1$), in spite of the fact that SRRs can not be considered as purely quasi-electrostatic entities except at very high frequencies, i.e. beyond saturation [7]. Finally, we have computed the transverse components of the electric field displacement and the electric field in the middle plane of the SRR and the CSRR studied in Fig. 2 (right), respectively. According to our theory the orthogonal components of these fields must show a similar behavior. This fact is confirmed in Fig. 3 where the results of the aforementioned computations are shown.

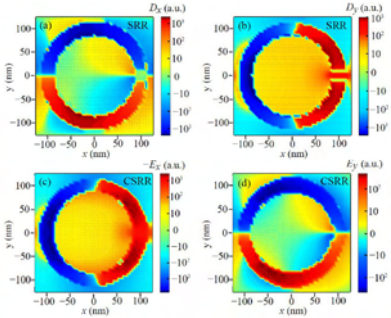

Figure 3: Electric field displacement components in the middle plane of the SRR (a), (b) and electric field components in the middle plane of the CSRR (c), (d) at a frequency of 100THz. The resemblance between the distribution of the cross components of the displacement and electric field in both structures is in accordance with the hypothesis of the theorem reflected in equation (2).

References

[1] N. Engheta, A. Salandrino, and A. Alu, Phys. Rev. Lett., 95, 095504 (2005).

[2] M. Silveirinha, A. Alu, J. Li, and N. Engheta, J. Appl. Phys., 103, 064305 (2008).

[3] A. Alu, and N. Engheta, Phys. Rev. Lett., 103, 143902 (2009).

[4] T. Zentgraf et al., Phys. Rev. B, 76, 033407 (2007).

[5] C. Rocksthul, and F. Lederer, Phys. Rev. B, 76, 125426 (2007).

[6] Y. Sun, B. Edwards, A. Alu, and N. Engheta, Nature Materials 11, 208 (2012).

[7] J. Zhou et al., Phys. Rev. Lett., 95, 23902 (2005).

Structural engineering of micro- and nanoporous silicon and nanoporous alumina for biosensing applications

L. F. Marsal[1], A. Santos[2], P. Formentin[1], L. Hernández[1], G. Macias[1], M. Alba[1], J. Pallares[1] and J. Ferré-Borrull[1]

[1]Departament d'Enginyeria Electrònica, Elèctrica i Automàtica, Universitat Rovira i Virgili, Avda. Països Catalans 26, 43007 Tarragona, Spain
[2]School of Chemical Engineering, The University of Adelaide, Engineering North Building, 5005 Adelaide, Australia

lluis.marsal@urv.cat

In the last years, a new generation of optical biosensors based on micro- and nanoporous silicon and nanoporous alumina structures has been proposed with promising results. These porous materials are produced by electrochemical anodization of silicon or aluminium in different acid electrolytes and their pore morphology can be effectively modified by adjusting the anodizing conditions such as the acid electrolyte, temperature, voltage or time. For example, many innovative pore architectures such as funnel-like [1], modulated, serrated-like, hierarchical, three-dimensional, tip-like, etc. have emerged from different electrochemical approaches [2-6].

These pore structures also have an exclusive set of optical properties (e.g. photoluminescence, transmittance, reflectance, absorbance and so on) and their performance has been successfully tested in such optical devices as microcavities, filters, resonators or waveguides. Notice that, anodization is based on a cost-effective technology and is fully compatible with current semiconductor processing technologies.

Furthermore, the surface chemistry of these porous materials can be modified at will. Therefore, the functionality of nanoporous silicon and alumina can be tuned for different chemical and biological environments. Their particular surface structure can be easily modified and used as a label-free enzymatic or immunosensors. All this brings an opportunity to design and fabricate nanoporous materials with special features for multiple biotechnological purposes (e.g. cell culture, molecular separation–adsorption, drug delivery, optical sensors and so forth).

Herein, we report on the experimental procedures and results of fabrication, characterization and optimization of new structures based on nanoporous anodic alumina and micro-nanoporous silicon obtained by different anodization strategies. The fabricated structures were characterized by different structural and optical methods such as scanning electron microscopy (SEM), Atomic Force Microscopy (AFM), confocal microscopy, photoluminescence (PL), UV-Vis-NIR spectroscopy, spectroscopic ellisometry, etc.

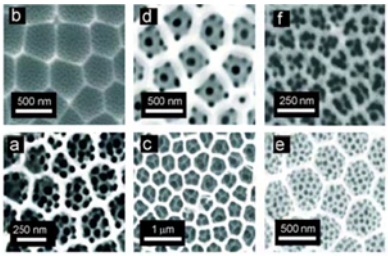

Figure 1: SEM top view images of the different types of HNAATs fabricated by the asymmetric two-step anodization process.

Figure 1 shows a set of SEM images of the fabricated hybrid nanoporous anodic alumina (HNAA). An asymmetric two-step anodization process makes it possible to fabricate HNAAs with a wide range of geometric characteristics such as interconcavity and interpore distance and concavity and pore diameter. These structures can be useful for molecule separation or drug delivery purposes. Figure 2a shows an example of nanoporous anodic alumina (NAA) used in a PL characterization. Figure 2b shows photoluminescence spectra as a function of the porosity (i.e. time of pore widening, T_{pw}) for a pore

length of 6.8 µm. As can be seen, the PL oscillations can be adjusted by changing the porosity (i.e. pore diameter) [7,8]. Consequently, the combination of nanoporous anodic alumina with PL spectroscopy allows us to generate multiple photonic barcodes, which can be used as an objective biosensing system for detecting and quantifying substances infiltrated within the nanopores. Finally, macroporous silicon produced by electrochemical etching of silicon has been proved to be a promising material in a broad range of applications due to its versatility and remarkable characteristics (e.g. well-controlled geometry, biocompatibility, etc.). One example is the fabrication of silicon dioxide (SiO_2) micropillars, which can be obtained from the oxidation of macroporous silicon templates and subsequent etching steps. The geometry and uniformity can be accurately controlled by the etching conditions. Figure 3 shows two examples of high-aspect ratio random and ordered silicon dioxide micropillars. Several bioapplications can be proposed for macroporous silicon based structures, such as microneedles from drug delivery [9] or SiO_2 pillars for DNA separation [10].

This work was supported by the Spanish Ministry of Economy and Competitiveness (MINECO) under grant number TEC2009-09551, TEC2012-34397, CONSOLIDER HOPE project CSD2007-00007, by Catalan authority under project 2009 SGR 549.

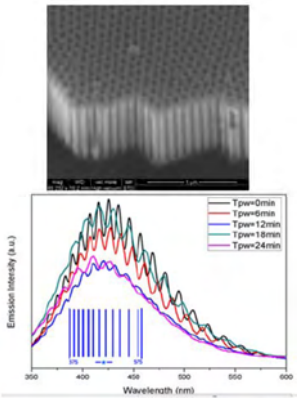

Figure 2: a) Top and cross section view of nanoporous alumina sample with a pore length of 6.8 µm and 40 nm pore diameter. b) PL spectrums for different porosities of nanoporous alumina: 11% (T_{pw}=0 min), 16% (T_{pw}=6 min), 22% (T_{pw}=12 min), 34% (T_{pw}=18 min) and 40% (T_{pw}=24 min).

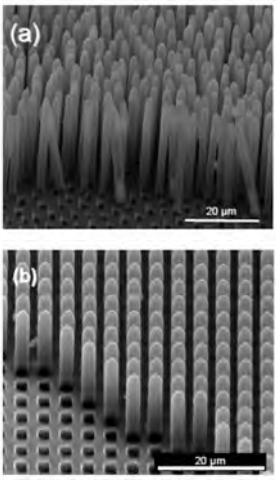

Figure 3: ESEM micrographs of (a) random and (b) ordered SiO_2 micropillars based onmacroporous silicon.

References

[1] A. Santos, P. Formentín, J. Pallarès, J. Ferré-Borrull, L. F. Marsal, Journal of Electroanalytical Chemistry, 655 (2011) 73.
[2] W. Lee, R. Ji, U. Gösele, K. Nielsch, Nature Materials, 5 (2006) 741.
[3] W. Lee, K. Nielsch, U. Gösele, Nanotechnology, 18 (2007) 475713.
[4] D. Losic, D. Jr. Losic, Langmuir, 25 (2009) 5426.
[5] K. Pitzschel, J. M. Montero-Moreno, J. Escrig, O. Albrecht, K. Nielsch, J. Bachmann, ACS Nano, 3 (2009) 3463.
[6] K. Schwirn, W. Lee, R. Hillebrand, M. Steinhart, K. Nielsch, U. Gösele, ACS Nano, 2 (2008) 302.
[7] A. Santos, V. S. Balderrama, M. Alba, P. Formentín, J. Ferré-Borrull, J. Pallarès, L. F. Marsal, Advanced Materials, 24 (2012) 1050.
[8] A. Santos, G. Macías, J. Ferré-Borrull, J. Pallarès, L. F.Marsal, L.F. ACS Applied Materials & Interfaces, 4 (2012) 3584.
[9] A. Rodríguez, D. Molinero, E. Valera, T. Trifonov, L.F. Marsal, J. Pallarès, R. Alcubilla, Sensors and Actuators B, 109 (2005) 135.
[10] S. Izuo, H. Ohji, P. French, K. Tsutsumi, M. Kimata, Sens. Mater., 14 (2002) 239.

Theoretical analysis of magnetoplasmonic interferometers for sensing

D. Martín-Becerra[1,2], G. Armelles[1], M. U. González[1] and A. García-Martín[1]

[1]IMM-Instituto de Microelectrónica de Madrid (CNM-CSIC), Isaac Newton 8, PTM, E-28760 Tres Cantos, Madrid, Spain
[2]International Iberian Nanotechnology Laboratory, 4710-229 Braga, Portugal

diana.martin@imm.cnm.csic.es

Surface plasmon polaritons (SPP) are evanescent waves that propagate along a metal-dielectric interface. Its wavevector is defined as: $k = k_0\sqrt{\frac{\varepsilon_d\varepsilon_m}{\varepsilon_d+\varepsilon_m}}$, being k_0 the wavevector of light in vacuum, and ε_d and ε_m the dielectric constants of the dielectric and the metal respectively. SPP have the ability to confine the light beyond the diffraction limit, which makes them appropriate for miniaturized optical devices. Besides, due to the dependency of the SPP with the dielectric constants of the materials of the interface, they have been broadly applied for sensing techniques, being the prism-based Surface Plasmon Resonance (SPR) with propagating SPP one of the most popular ones [1]. On the other hand, interferometry is in general known as a very sensitive and reliable technique and plasmonic interferometry for sensing has been recently demonstrated, both theoretically and experimentally [2-4]. Nevertheless, a precise theoretical comparison with the traditional SPR has not been done. Following the path inspired by these results, in this work tilted slit-groove plasmonic interferometry [5] is being proposed as a promising sensing device, and it will be compared with SPR systems based on prism coupling.

Furthermore, it has also put forward that this plasmonic interferometric device can be magnetically modulated [6,7], and that this modulation presents quite a large dependence on ε_d [8]. This has encouraged us to also analyze its sensitivity with small variations in ε_d and its potential for sensing applications, and compare its performance with purely plasmonic interferometers.

In our particular set-up, the plasmonic interferometers are arranged in a tilted slit-groove geometry (Fig. 1). When the interferometers are illuminated with a p-polarized laser, the light collected at the other side of the slit consists of the interference between the light directly transmitted through the slit and a SPP excited in the groove and decoupled back to radiative light in the slit. When the refractive index of the dielectric present at the interface changes (Δn), the wavevector of the SPP will change ($\Delta^{\varepsilon}k$), and so will do the Intensity of the interference ($\Delta^{\varepsilon}I_p$). In fact, this change of the intensity $\Delta^{\varepsilon}I_p$ is proportional to the product $\Delta^{\varepsilon}k\ d$, where d is the groove-slit distance. In a SPR system, on the other hand, the SPP wavevector change with Δn modifies the reflectivity (ΔR). By comparing ΔR with $\Delta^{\varepsilon}I_p$ under the same amount of Δn, our results show that the sensitivity of the plasmonic interferometric configuration can be higher than that of the SPR one for large enough d (see Fig. 2a).

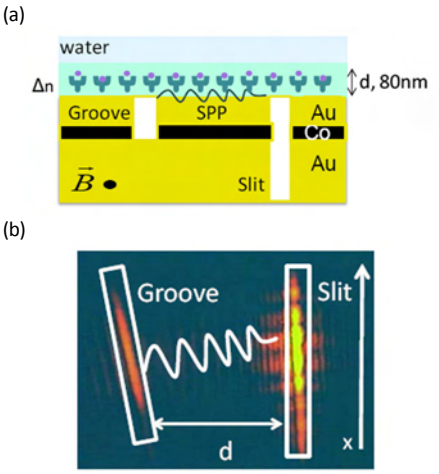

Figure 1: (a): Sketch of the proposed interferometer for sensing in transversal section. (b): Upper view of an actual interferometer.

On the other hand, the magnetoplasmonic devices are basically equal to the above plasmonic interferometer but with a magnetic field applied. Under application of an external oscillating magnetic field, the SPP wavevector is modified ($\Delta^m k$, that we are going to name k_m to simplify) therefore synchronously changing the interference intensity ($\Delta^m I_{mp}$). Moreover, under Δn, both k and k_m change in this magnetoplasmonic interferometer ($\Delta^\varepsilon k$, $\Delta^\varepsilon k_m$). As can be seen in Fig. 2b, the relative change induced by Δn is higher for km than for the SPP wavevector k. This suggests that the magnetoplasmonic interferometers are a promising alternative for SPP-based sensing.

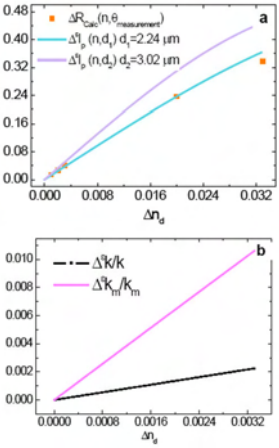

Figure 2: a) Comparison between the variation of the reflectivity in an SPR and the variation of the plasmonic intensity in a plasmonic interferometer as a function of the change of refractive index of the dielectric layer. Two different distances for the interferometers are shown. The calculations correspond to a wavelength of 633 nm. b) Comparison between the relative variation of the main parameters involved in a plasmonic and a magnetoplasmonic interferometer as a function of the change of refractive index n of the dielectric layer.

References

[1] Homola, J. Anal. Bioanal.Chem. 377, (2003) 528–539.

[2] Yongkang Gao, Q. G. & Bartoli, F. J. ACS Nano 5, 12, (2011) 9836–9844.

[3] Feng, J. et al. Nano Lett. 12, (2012) 602–609.

[4] Li, X., Tan, Q., Bai, B. & Jin, G. Opt. Express 19, (2011) 20691–20703.

[5] Temnov, V. V., et al. Opt. Lett. 32-10, (2007) 1235–1237.

[6] Temnov, V. V. et al. Nat. Photonics 4, (2010) 107–111.

[7] Martin-Becerra, D. et al. Phys. Rev. B 86, (2012) 035118.

[8] Martin-Becerra, D. et al. Appl. Phys. Lett. 97, (2010) 183114.

Strong magnetic field concentration in arrays of thick gold nanorings

María Lorente-Crespo[1], Li Wang[2], Rubén Ortuño[1], Carlos García-Meca[1], Yasin Ekinci[2,3] and **Alejandro Martínez**[1]

[1]Nanophotonics Technology Center, Universitat Politècnica de València, Camino de Vera, s/n, 46022, Valencia, Spain
[2]Laboratory for Micro- and Nanotechnology, Paul Scherrer Institute, 5232 Villigen PSI, Switzerland
[3]Laboratory of Metal Physics and Technology, Department of Materials, ETH Zurich, Switzerland

amartinez@ntc.upv.es

We show that the coupled-bonding plasmon resonance in coupled gold nanorings changes its character from electric to magnetic when increasing the height of the nanorings, giving rise to magnetic plasmons in the near infrared regime. Numerical simulations show that a virtual current loop appears at resonance for sufficiently thick nanorings (> 250 nm), causing a strong concentration of the magnetic field in the gap region (magnetic hot spot). There is an optimum thickness over spacing ratio that provides the maximum magnetic intensity enhancement (over 100-fold) and give an explanation of this observation. A red-shift of the plasmonic resonance is observed when the nanorings height is increased, which is confirmed both numerically and experimentally for arrays of coupled nanorings built on quartz substrates. Our structure works as an array of magnetic nanoantennas. The arrangement in an array will provides a very dense periodic structure of magnetic hot spots (about 500 million per cm^2 in the fabricated samples) when illuminating the nanorings with unpolarized light at the resonant wavelength. Each nanoantenna will be formed by two closely-spaced nanorings whose performance mimics a magnetic nanoloop. Indeed, a loop antenna is at resonance at a wavelength equal to its perimeter. In our case, the resonance (see Fig. 2(c)) occurs at wavelength about 1.5-2 times the perimeter (obtained as $2s+2t$). However, this can be explained by the penetration of the fields inside both the metal and the dielectric substrate, which is well-known to produce an increase in the wavelength of the LSPR, as in the case of dipole nanoantennas. Therefore, we argue that our structure performs as an array of resonant nanoloop antennas. The nanoring arrays could be used to build optical metamaterials as well as to observe a large variety of magnetic-based plasmonic effects at optical frequencies.

This work has been supported by Spanish Government and European Union (EU) funds under contracts CSD2008-00066 and TEC2011-28664-C02-02, and Universitat Politecnica de Valencia (program INNOVA 2011).

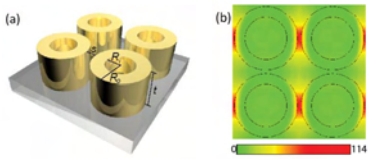

Figure 1: Transmission through an array of square holes in a silver screen at oblique incidence. Square periodicity is 1μm. Size of the holes is 250 nm and thickness of the screen is 50 nm. Wood's frequencies (fw) range from 150 THz to 220 THz. The metal is modeled by a Drude Lorentz permittivity. Solid lines correspond to the mode matching model and dashed lines to CST simulations.

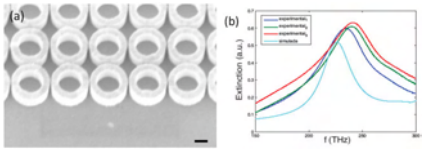

Figure 2: (a) SEM image of a fabricated sample with t = 325 nm and s = 30 nm (scale bar 200 nm). (b) Measured spectra of a three fabricated samples and comparison with a numerical result obtained by CST Microwave Studio (R_o = 300 nm, R_i = 200 nm, t = 350 nm, s = 60 nm; substrate: quartz).

Plasmonic layers based on noble metal nanoparticles embedded in oxides for photovoltaic applications

Esteban Pedrueza, Diana Fragua, Rafael Abargues, José L. Valdés and **Juan P. Martinez-Pastor**

UMDO www.uv.es/umdo
Instituto de Ciencia de los Materiales, Universidad de Valencia, PO Box 22085, 46071 Valencia, Spain

juan.mtnez.pastor@uv.es

Metal-dielectric nanocomposite (MNC) thin films have attracted much attention in the last years due to its unique electromagnetic behavior and high potential in diverse fields like photovoltaics [1] and sensing [2], other than metamaterials, photodetectors, catalysis, sub-wavelenght imaging, … The special electromagnetic properties of the MNC are predominantly dominated by the localized surface plasmon resonance (LSPR) typical of noble metal nanoparticles (NPs). The control of the size, shape and density of these NPs embedded in a given solid matrix is needed for most of these applications.

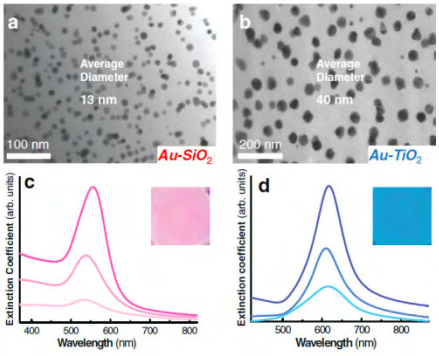

Figure 1

Recently, we have developed a novel sol-gel method implemented for spin-coating technique, in which metal NPs are synthesized in situ and their average size and density can be varied up to a certain extent with the concentration of the Au precursor solution [3]. MNC films doped with Ag and Au NPs have been successfully fabricated until date following this procedure over different substrates (glass and silicon) in order to investigate their optical properties. Figure 1 shows TEM images of SiO_2 (Fig. 1a) and TiO_2 (Fig. 1b) thin films containing Au NPs, other than the visual aspect and LSPR spectra (Figs. 1c-d). Larger Au NPs were synthesized (about 40 nm) in the TiO_2 matrix than in SiO_2; this may be important for photovoltaic applications because light scattering predominates over light absorption for larger metal NPs. Antireflective (AR) coatings are needed to increase light absorption by most solar cell designs. The inclusion of metal NPs in AR films can further reduce reflectance and increase light trapping at the short wavelength side of the LSPR. Further AR effect can be achieved by introducing a weak chemical etching process that leads to the formation of pores in the TiO_2 matrix (see SEM image in Fig. 2a). We obtain a minimum in the overall reflectance spectra in MNC films on Si-substrate (Fig. 2b). In glass-substrate samples we observe an intensity decrease and blue-shift of the LSPR, which is attributed to the reduction of the matrix effective refractive index associated to pore formation.

Given the extensive use of TiO_2 and ZnO materials as transparent conductive electrodes in organic and Si thin/ultrathin film solar cells we have also extended our sol-gel/spin-coating method to in situ synthesize Au NPs in ZnO. The conductivity of the so prepared ZnO layers is around $3.4 \times 10^{-2}\ \Omega^{-1}cm^{-1}$, whereas that in Au:ZnO films decreased by a factor two.

This work was supported by the EU-FP7 project NANOPV and the project PROMETEO/2009/074 from the Generalitat Valenciana.

(a)

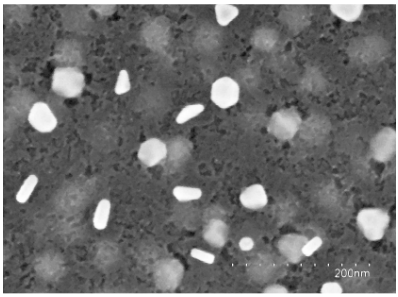

(b)

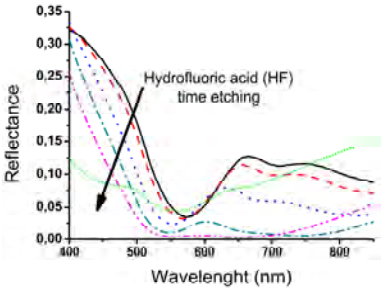

Figure 2

References

[1] Atwater, H. A,; Polman, A. Nat. Mater. 2010, 9, 205.

[2] Gradess, R.; Abargues, R.; Habbou, A.; Canet-Ferrer, J.; Pedrueza, E.; Russell, A.; Valdes, J. L.; Martinez-Pastor, J. P. J. Mater. Chem. 209, 19, 9233.

[3] Pedrueza, E.; Valdés, J. L.; Chirvony, V.; Abargues, R.; Hernández-Saz, J.; Herrera, M.; Molina, S. I.; Martínez-Pastor, J. P. Adv. Funct. Mater. 2011, 21, 3502.

Coupling of Resonant Modes of Embedded Dielectric Microspheres in Solution-Processed Solar Cells

Agustín Mihi, María Bernechea and Gerasimos Konstantatos*

ICFO- Instituto de Ciencias Fotónicas,
Parque Mediterráneo de la tecnología,
08860 Castelldefels, Barcelona. Spain

gerasimos.konstantatos@icfo.es

Either from a cost saving or improved carrier collection perspective, thin absorber layers are increasingly becoming part of novel photovoltaic technologies. To maintain or boost the efficiency, light trapping strategies are being developed to capture photons in the widest spectral range and with the smallest quantity of absorbing material. From textured surfaces to complex plasmonic nanostructures, many approaches are being investigated to increase the optical path within solar cells [1]. Particularly interesting is the use of optical resonators to boost light absorption in the active material [2]. Resonances from these architectures have successfully been employed in sensors and lasers, exploiting the large amount of energy stored within the optical cavities due to total internal reflection. Grandidier et al. theoretically studied the benefits of coupling whispering gallery modes of submicrometric dielectric spheres into an amorphous silicon solar cell. By choosing wisely the sphere diameter, diffractively excited resonant modes of the spheres couple into the high dielectric constant substrate, increasing the photogenerated current [3]. Several groups have studied the use of dielectric microspheres to enhance the optical absorption, but the incorporation of these resonators in actual solar cells has been elusive so far [4,5].

In this work, we combine inexpensive optical resonators such as dielectric colloidal spheres with solution processed PbS-TiO_2 solar cells. These heterojunctions are currently leading the race towards high performance colloidal quantum dot solar cells and [6], we have chosen them to study the ideal configuration of the sphere monolayer within the solar cell, leading to the largest number of resonant modes coupled into the absorbing layer. The PbS quantum dots (QDs) layer is built by alternatively spin casting solutions of the p-type semiconductor and an organic ligand onto a nanocrystalline titania (nc-TiO_2) substrate. This deposition method allows the infiltration of the QDs into the voids between spheres, completely embedding them. The higher refractive index of the PbS (n=2.4) versus that of the silica spheres (n=1.425) favors the leakage of the resonant modes into the semiconductor film. The optimum configuration of the spheres within a colloidal PbS-TiO_2 bulk heterojunction solar cell is investigated. A monolayer of hexagonally packed silica spheres is placed in three different locations within the PbS layer of the heterojunction (figure 1a,b). Enhancements in photocurrent are found in the cases where the spheres are partially or completely infiltrated with PbS and are explained in terms of the coupling of resonant modes of the silica spheres within the semiconductor layer according to FDTD simulations (figure 1c).

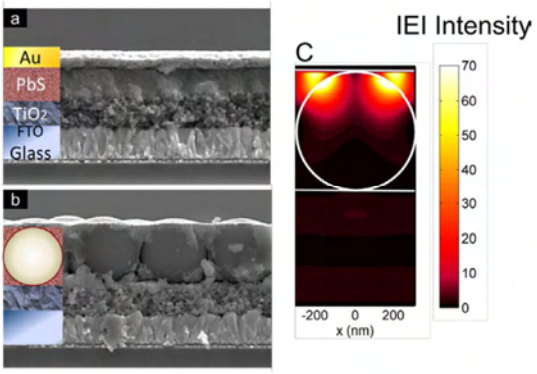

Figure 1: Crossectional SEM images from (a) a reference PbS-TiO_2 cell and (b) a similar heterojunction with a SiO_2 sphere monolayer embedded within the PbS film. (c) Calculated spatial distribution of the electric field intensity at λ=1037nm for the architecture depicted in (b).

References

[1] Polman, A. & Atwater, H. A. Photonic design principles for ultrahigh-efficiency photovoltaics. Nature materials 11(2012) 174

[2] Mendes, M. J., Tobías, I., Martí, A. & Luque, A. Light concentration in the near-field of dielectric spheroidal particles with mesoscopic sizes. Optics Express 19 (2011) 16207

[3] Grandidier, J., Callahan, D. M., Munday, J. N. & Atwater, H. a Light absorption enhancement in thin-film solar cells using whispering gallery modes in dielectric nanospheres. Advanced materials (Deerfield Beach, Fla.) 23 (2011)1272

[4] Yao, Y. et al. Broadband light management using low-Q whispering gallery modes in spherical nanoshells. Nature communications 3 (2012) 664.

[5] López-García, M., Galisteo-López, J. F., Blanco, Á., López, C. & García-Martín, A. High Degree of Optical Tunability of Self-Assembled Photonic-Plasmonic Crystals by Filling Fraction Modification. Advanced Functional Materials 20 (2010) 4338

[6] Barkhouse, D. A. R. et al. Depleted bulk heterojunction colloidal quantum dot photovoltaics. Advanced materials (Deerfield Beach, Fla.) 23 (2011) 3134

A study of the Near-Field of metallic materials for Plasmonics in the UV

Dolores Ortiz, Juan M. Sanz, Rodrigo Alcaraz de la Osa, Jose Mª Saiz, Francisco González and **Fernando Moreno**

Group of Optics. Department of Applied Physics. University of Cantabria. 39005 Santander, Spain

morenof@unican.es

The last decade has seen an explosion in the development and exploitation of nanometer scale metallic structures because of their remarkable plasmonic ability to locally enhance electromagnetic fields and cross-section efficiencies [1-6]. The degree of enhancement strongly depends on the conductivity and geometry (size and shape) of the nanostructure. In the case of metallic nanoparticles, some of the plasmonic applications are based on the generation of Localized Plasmon Resonances (LPR's), whose spectral location and width are sensitive to their size, shape and optical properties as well as to those of the surrounding medium [7]. Visible and Near IR have been the most important spectral regions where Plasmonics has contributed to nanotechnology. However, UV deserves also some attention due to fundamental applications in biotechnology (bioimaging), Raman spectroscopy, device engineering and nano-material science [8,9]. Pursuing this objective, the aim of this research is to numerically analyze, by using the Discrete Dipole Approximation (DDA) method [10], the near field distribution shown in the UV by some metals like Magnesium, Titanium, Chromium, Tungsten, Ruthenium, Rhodium, Palladium, Platinum, Copper, and Indium, in order to find more possibilities in the UV. The plasmonic response of small hemispherical nanoparticles located on a dielectric substrate has been compared with others already characterized such as Au, Ag, Ga and Al [11].

The near field distribution is analysed on a hemispherical surface surrounding the nanoparticle. In order to do it properly, a mesh shell was made in the nanoparticle surface boundary. The electric field intensity was obtained for each intersection point in the mesh, and the average intensity over the particle surface was evaluated by assigning the appropriate weight to each point (given by $sin\theta$, in the inset of Fig. 1). For the incident wavelength for which the electric field enhancement factor is maximum [12], a typical dipolar field distribution is observed (Figure 1 for Mg) with high intensity lobes appearing close to the nanoparticle surface. Their centerline is shifted to an oblique direction due to both nanoparticle geometry and substrate effects. Usually, the highest intensity values are located on the boundary layer between the hemispherical particle and the substrate, and the hot spots are placed in the meeting point of the polarization plane, the substrate and the nanoparticle surface. Observing the spectral location and values of the near field maxima (Figure 2), and considering the electric field enhancement factor for a hemispherical particle of 20 nm radius, Mg, Al, Rh, Cr, Ru and Ti show LPR's in the UV range (3-5 eV), whereas for the rest of metals, they are located in the VIS range.

This research was supported by the Ministry of Education of Spain and USAITCA under projects FIS2010-21984 and R&D 1390-PH-01 respectively. R. Alcaraz de la Osa also thanks the Ministry of Education of Spain for his FPU grant.

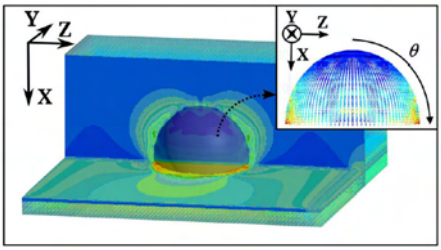

Figure 1: Near-field color map for a hemispherical Mg nanoparticle (R=20 nm) located over a sapphire substrate. Incident field Z-polarized.

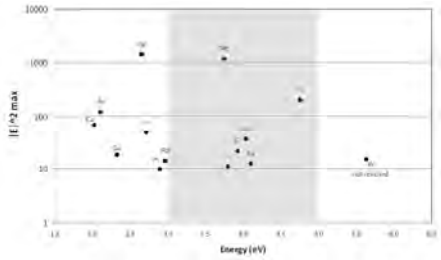

Figure 2: Maximum electric field enhancement factor ($|E|^2$ max) vs. energy values of the LPR for all the metals. The gray zone indicates the UV range (3 – 5 eV).

References

[1] W. Barnes, J. Lightwave Tech. 17 (1999) 2170–2182.

[2] C. Haynes and R. van Duyne, J. Phys. Chem. B 105 (2001) 5599–5611.

[3] J. Jackson and N. Halas, Proc. Natl. Acad. Sci. U. S. A. 101 (2004) 17930–17935.

[4] K. Kneipp, Phys. Today 60, 40–46 (2007).

[5] S. Lal, N. K. Grady, J. Kundu, C. S. Levin, J. B. Lassiter, and N. J. Halas, Chem. Soc. Rev. 37 (2008) 898–911.

[6] Z. Wang, S. Pan, T. Krauss, H. Du, and L. Rothberg, Proc. Natl. Acad. Sci. U. S. A. 100 (2003) 8638–8643.

[7] M. Stockman, Opt. Express 19, 22029 (2011)

[8] I. Lieberman, G. Shemer, T. Fried, E. M. Kosower, and G. Markovich, Angewandte Chemie 120, 4933 (2008).

[9] Taguchi A, Hayazawa N, Furusawa K, Ishitobia H, Kawata S, J. Raman Spectroscopy 40:1324 (2010)

[10] Draine, B.T., & Flatau, P.J. User Guide to the Discrete Dipole Approximation Code DDSCAT 7.2, http://arXiv.org/abs/1202.3424 (2012).

[11] P. Albella, B. García-Cueto, F. González, F. Moreno, et al. Nano Lett. 11, 3531 (2011).

[12] M. Moskovits, Rev. Mod. Phys., 57 3 (1985) 783-826.

Plasmon spectroscopy and imaging of individual gold nanodecahedra: A combined optical microscopy, cathodoluminescence, and electron energy-loss spectroscopy study

V. Myroshnychenko and
J. F. García de Abajo

IQFR - CSIC,
Serrano 119, 28006 Madrid, Spain

viktor.myroshnychenko@gmail.com

Imaging localized plasmons in noble-metal nanoparticles is of fundamental importance for applications such as ultrasensitive sensing and detection. Here, we demonstrate the combined use of optical dark-field microscopy (DFM), cathodoluminescence (CL), and electron energy-loss spectroscopy (EELS) to study localized surface plasmons on individual gold nanodecahedra. By exciting surface plasmons with either external light or an electron beam, we experimentally resolve a prominent dipole-active plasmon band in the far-field radiation acquired via DFM and CL, whereas EELS reveals an additional plasmon mode associated with a weak dipole moment. We present measured spectra and intensity maps of plasmon modes in individual nanodecahedra in excellent agreement with boundary-element method simulations, including the effect of the substrate. A simple tight-binding model is formulated to successfully explain the rich plasmon structure in these particles encompasing bright and dark modes, which we predict to be fully observable in less lossy silver decahedra. Our work provides useful insight into the complex nature of plasmon resonances in nanoparticles with pentagonal symmetry.

References

[1] V.Myroshnychenko et al., Nano Lett., 2012, 12 (8), pp 4172–4180.

Exotic optical properties of metallo-dielectric core-shell nanospheres and nanowires. Application to negative refraction

R. Paniagua-Domínguez[1], D. R. Abujetas[1], F. López-Tejeira[1], L. Froufe-Pérez[1], R. Marqués[2] and J. A. Sánchez-Gil[1]

[1]Instituto de Estructura de la Materia (CSIC), Serrano 121, 28006 Madrid, Spain
[2]Departamento de Electrónica y Electromagnetismo, Universidad de Sevilla, Sevilla, Spain

ramon.paniagua@iem.cfmac.csic.es

Artificial materials showing electromagnetic properties not attainable in naturally occurring media, the so called metamaterials, are among the most active fields of research in optical and material physics. One of the major challenges found is to obtain truly three-dimensional isotropic negative index metamaterials (NIM) at optical frequencies.

We report the possibility to use a certain class of core-shell (CS) nanospheres as building blocks of such NIM, operating in the near infrared. These CS, made of a metallic core and a high permittivity shell, are doubly-resonant, allowing for a spectral overlap of their first electric and magnetic dipolar resonances. The strong diamagnetic response is due to the lowest, dipolar magnetic resonance of the shell, where the electric field is forced to rotate as a consequence of the abrupt continuity conditions between the shell and the surrounding medium. The electric resonance is due to the excitation of a localized surface plasmon resonance in the core (see Fig. 1).

Since the responses do not depend on the interaction between constituents, no particular arrangement is needed to build the metamaterial, which is, moreover, intrinsically isotropic and polarization independent. We study realistic designs with silver in the core, and silicon or germanium in the shell. We show that, for certain geometrical parameters and filling fractions, metamaterials composed by such CS nanospheres can have simultaneously negative permittivity and permeability between 1.2 µm-1.55 µm [1].

Moreover, we have extended our study to metallo-dielectric core-shell nanowires, revealing similar properties when incident light wavevector and polarization are both normal to the nanowire axis. The metallic core (localized surface plasmon) resonance provides again the negative electric response; the dielectric shell yields a magnetic resonance, which nonetheless does not exhibit a proper magnetic dipolar character. The resulting metamaterial then behaves in certain frequency range as a 2D isotropic NIM, though polarization dependent [2].

Finally, the far-field scattering properties of a single core-shell nanosphere or nanowire are also explored in the spectral region where both (electric and magnetic) resonances overlap [3]. Particular attention is paid to the occurrence of zero-backward or zero-forward scattering (Kerker's conditions); the former has been recently proposed as means for broadband focusing [4].

Acknowledgements: Spanish "Ministerio de Economía y Competitividad" (CSD2008-00066 and FIS2009-11264), "Comunidad de Madrid" (S2009/TIC-1476), and CSIC (JAE-Pre grant).

References

[1] R. Paniagua-Domínguez, F. López-Tejeira, R. Marqués and J. A. Sánchez-Gil, New. J. Phys. 13, 123017 (2011).
[2] D. R. Abujetas, R. Paniagua-Domínguez, and J. A. Sánchez-Gil, preprint.
[3] D. R. Abujetas, R. Paniagua-Domínguez, L. S. Froufe-Pérez, J. J. Sáenz, and J. A. Sánchez-Gil, preprint. [4] W. Liu, A. E. Miroshnichenko, D. N. Neshev, and Yu. S. Kivshar, ACS Nano 6, 5489-97 (2012).

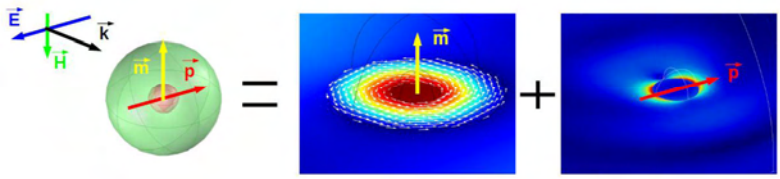

Figure 1: Scheme of the underlying physical mechanism operating in the doubly-resonant metallo-dielectric core-shell nanosphere considered in this work.

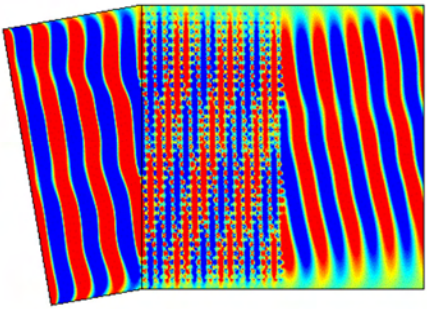

Figure 2: A negative-refraction-index slab operating at λ_0=1350 nm.

Self assembled dimers of metallic nano-particles for enhanced light harvesting in organic solar cells

Francesco Pastorelli[1,2], Sebastien Bidault[3], Nicolas Bonod[2] and Jordi Martorell[1,4]

[1]ICFO-Institut de Ciències Fotòniques, Mediterranean Technology Park, Castelldefels (Barcelona), Spain
[2]Institut Fresnel, Aix-Marseille Université, CNRS, Domaine Universitaire de St Jérôme, Marseille, France
[3]Institut Langevin, CNRS, ESPCI Paris Tech, INSERM, 1 rue Jussieu, Paris, France
[4]Departament de Fisica i Enginyeria Nuclear, Universitat Politecnica de Catalunya, Terrassa, Spain

francesco.pastorelli@icfo.es

Organic based photovoltaics (OPVs) is one of the solar technologies that has the potential to become cost effective while providing added functionality such as transparency and flexibily. However, for an efficient charge collection in materials with a rather low charge mobility, one must fabricate devices with very thin active layers. Such thin layers imply that an efficient light harvesting is difficult to achieve. One approach to enhance light harvesting has been to consider the inclusion of metallic nano-particles (NPs) to enhance the scattering of sunlight within the active material [1-2].

In the current work we consider the inclusion, in between the transparent electrode and the active material, of single 40 nm gold nano-particles (NPs) and groups of the same NPs forming a dimer nano-structure. To obtain the dimers we used a simple self-assembly based method which lead to the controlled formation of strongly coupled particles. The two NPs in the dimer remain linked to a fix distance by Dithiothreitol (DTT) molecules, as shown in the SEM image from Figure 1.

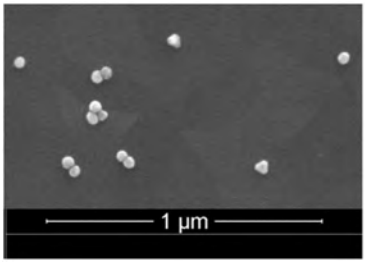

Figure 1: SEM image of Self-assebmled gold Nanoparticles on an ITO substrate showing dimers NPs.

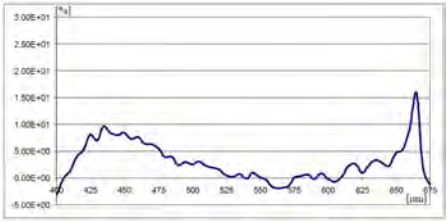

Figure 2: Plot of the percentage change in the EQE function of a plasmonic solar cell with monomer and dimer 40 nm in diameter Au NPs inclusions relative to a plasmonic solar cell with single 40 nm in diameter Au NPs inclusions.

We fabricated three types of OPV devices, a standard inverted OPV planar device with the following architecture ITO/TiO_2/P_3HT:PCBM/MoO_3/Ag. A similar type of device where single nano-particles were dispersed at the ITO/TiO_2 interface and, one last type of device including the dimer nano-structures at the same interface. The latter one exhibited a photoconversion of 3.2% and a short circuit current that we measured to be 11% times larger than the efficiency of the standard one, while for the single NPs device the increase in short circuit current was only 8%. Such enhanced performance of the dimer device can be understood when considering that the scattering cross section is almost twice at short wavelengths below 540 nm, it has a comparable behavior in the middle wavelengths range (540-650nm), while it exhibits a resonance peak at around 665nm. These wavelength dependent enhancements are clearly visible in the external quantum efficiency (EQE) percentage change measurements shown in Figure 2. The increase in EQE at the short wavelengths

range (from 420 nm to 510 nm) is about 18%, while at the long wavelength range (from 630 nm to 670 nm) is about 23% relative to the standard cell without NPs.

In conclusion, we showed that dimers of gold nanoparticles have a larger capability than monomers to lead to an effective photon absorption at those wavelengths where the optical absorption constant of the majority of photovoltaic polymers is smaller.

References

[1] J. Wu, F. Chen, Y. Hsiao, F. Chien, P. Chen,C. Kuo, M. H. Huang, C. Hsu, "Surface Plasmonic Effects of Metallic Nanoparticles on the Performance of Polymer Bulk Heterojunction". ACSnano, vol. 5(2), (2011), 959-967.

[2] Wang, D. H., Park, K. H., Seo, J. H., Seifter, J., Jeon, J. H., Kim, J. K., Park, J. H., et al., "Enhanced Power Conversion Efficiency in PCDTBT/PC70BM Bulk Heterojunction Photovoltaic Devices with Embedded Silver Nanoparticle Clusters", Advanced Energy Materials, 1(5), (2011), 766-770.

Fabrication of Photonic Crystal Chips for Biophotonic Applica

P.A. Postigo[1], R. Alvaro[1], A. Juarros[2] and S. Merino[2]

[1]IMM-Instituto de Microelectrónica de Madrid, IMM-CNM-CSIC, Isaac Newton 8,
PTM, E-28760 Tres Cantos, Madrid, Spain
[2]Dpto. Microtecnologías y Nanotecnologías, TEKNIKER, Otaola 20, P.K. 44, 20600 EIBAR, Gipuzkoa, Spain

pabloaitor.postigo@imm.cnm.csic.es

Stretching luminescent molecules by confinement in nanofluidic channels has attracted a great interest during the last few years for the study of physical and biological properties of these molecules, like DNA [1, 2]. In this work, we present the fabrication of a sealed micro/nanofluidic chip for molecule stretching applications and enhanced fluorophore detection, based on the use of photonic crystal technology combined with anodic bonding of the silicon base and Pyrex cover. The photonic crystal is composed of arrays of nanoholes that enhance light emission (see Fig.1). Fabrication is made by high-resolution focused ion beam (FIB) etching on a 100nm thick Si_3N_4 layer. This layer is on top of a 500-nm thick SiO_2 layer on a Si substrate. Using this chip we have performed fluorescence intensity measurements of a fluorophore inserted in the microchannels. The liquid flows through the nanochannels that have been fabricated with and without the photonic crystals. Enhancements of light intensity up to 2.5 times have been found for the nanochannels with the photonic crystal structures.

References

[1] H. Cao, Z. Yu, J. Wang, J.O. Tegenfelt, R. Austin, E. Chen, W. Wu, S. Chou, "Fabrication of 10 nm enclosed nanofluidic channels". App. Phys. Lett. 81, 1, 174-176 (2002).

[2] E. Abad, S. Merino, A. Retolaza, A. Juarros, R. Marie, A. Kristensen."Single molecule DNA stretching in nanofluidic chips fabricated by thermal imprinting and anodic bonding". Microel. Enginee. 88, 300 (2011).

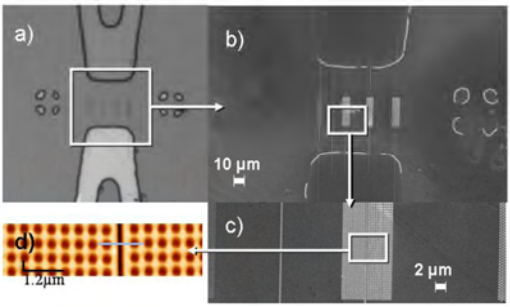

Figure 1: Scanning electron microscopy (SEM) images of the chips fabricated by FIB etching showing greater magnifictions of the areas marked by the white boxes (a ,b and c). The images in (d) is an atomic force microscopy (AFM) image of the area marked by the white box in c).

Nanoporous anodic alumina produced with variable voltages

Mohammad Mahbubur Rahman, Gerard Macias Sotuela, Maria Alba, Lluís F. Marsal, Josep Pallarès and Josep Ferré-Borrull*

Departament d'Enginyeria Electrònica, Elèctrica i Automàtica, Universitat Rovira i Virgili, Tarragona, Spain

josep.ferre@urv.cat

Nanoporous anodic alumina (NAA) is a very interesting material in nanotechnology due to its selfassembled nanoscale-ranged porous structure. In the adequate fabrication conditions the interpore distance is of the order of the wavelength of visible light [1,2]. We have recently demonstrated that this fact in combination with the quasi-ordered structure of the pores makes it possible the existence of stop bands inside the material[3,4]. Recently, three-dimensional structuring of NAA has been introduced, where attention was paid on the fabrication of Bragg mirrors based on NAA having cyclic porosity with the depth by applying a cyclic voltage with carefully chosen voltage profiles[5,6]. However, the control over the optical properties of the layers obtained on every cycle is not studied in depth. If the 2D inplane confinement properties cited above can be combined with confinement in the direction parallel with the pores by means of a cavity surrounded by Bragg mirrors, 3D confinement of light could be achieved.

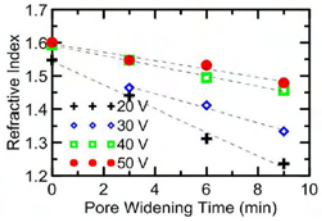

Figure 1: Effective refractive index of the NAA layer for the wavelength λ=750nm as a function of the pore widening time, for NAA made under different anodization voltages.

In this communication we report on the efforts being carried out at our group to achieve this 3D confinement. With our approach, it is possible to obtain photonic stop bands for light propagating along the direction of the pores by an in-depth structuring of NAA. In contrast with previous works of other authors, besides applying a periodic voltage to obtain a Bragg structure, we introduce a subsequent pore widening step which increases the refractive index contrast between the different layers, what permits to improve the optical performance of the structure.

In order to obtain the maximum refractive index contrast between the different layers in the NAA we have investigated the dependence of the pore widening rate of single-layer NAA with the voltage applied to obtain them. Figure (1) shows the effective refractive index of the porous NAA estimated from ellipsometric measurements of single-layer structures as a function of the pore widening time. The structures were fabricated by anodization in 0.3M oxalic acid at 4°C and at applied voltages of 20 V, 30V, 40V and 50 V, at which 2D self-assembly of the pores takes place. It can be seen that the refractive index is very similar for all voltages and for the as-produced layers, while the refractive index decreases and the differences between voltages increase with increasing pore widening time. This indicates that if a cyclic voltage is applied in the fabrication of NAA, layers with different porosity can be obtained, and that this differences in porosity can be enlarged with a subsequent pore widening step.

Figure 2a) shows the first three anodization voltage cycles and the corresponding current transient for an in-depth structured NAA. After the first anodization at 40 V and removal of the alumina layer to obtain the self-ordering of the pores, a second anodization starts at 20 V and it lasts until a charge of 2 C has flowed through the system. In this way, a self-ordered layer of vertical pores is obtained. After this, a voltage cycle is applied for 150 times. Each cycle consists of i) a linear ramp from 20 V to 50 V, at a rate of 0.5 V/, ii) an interval

of constant voltage at 50V that lasts until a charge of 2C has flowed through the system, and iii) a subsequent ramp from 50 V to 20 V at 0.1V/s. Whit this cyclic voltage we aim at obtaining alternating layers with different porous structure. After this process, a subsequent pore widening step is applied. This pore widening step provides an increase in refractive index contrast that improves the optical properties of the cyclic-layered structure.

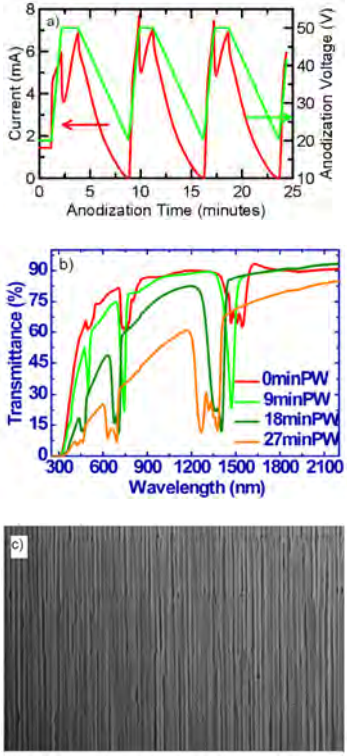

Figure 2: a) First three cycles of periodic anodization voltage used to produce an in-depth structured NAA with DBR structure and the corresponding current. b) reflectance spectra of the as-produced indepth structured NAA and for the same structure after different pore widening times as indicated in the graph. c) FE-SEM cross-section picture of four cycles of the sample.

Figure 2b) depicts the reflectance spectra of the NAA structure obtained with this cyclic voltage for the as-produced structure and for the same structure after different steps of pore widening with a solution of 5%wt H_3PO_4. The spectrum of the as-produced sample shows a decrease in transmittance in three intervals centred approximately at 1500 nm, 750 nm and 375 nm. This is clearly related to the existence of a Bragg mirror structure. The successive pore widening steps produce an increase in the depth of the transmittance stop bands as well as in their width, together with a decrease in the centre wavelength. This is a clear consequence of the increase of refractive index contrast between layers. Finally, in figure 2c) a FE-SEM picture of a cross section of the sample is depicted, showing the layered structure.

This in-depth nanostructuring of NAA with a fairly good control over the optical properties of the constitutive layer opens the possibility of building new devices based on 3D optical confinement in such structures.

This work was supported by the Spanish Ministry of Science under the projects TEC2009-09551, TEC2012-34397, HOPE CSD2007-00007 (Consolider-Ingenio 2010).

References

[1] A. P. Li, F. Müller, A. Birner, K. Nielsch, and U. Gösele, J. Appl. Phys. 84 (1998) 6023.

[2] L. Vojkuvka, L. F. Marsal, J. Ferre-Borrull, P. Formentin, and J. Pallares, Superlattices Microstruct. 44 (2008) 577.

[3] I. Maksymov, J. Ferré-Borrull, J. Pallarès, L. F. Marsal, Photonics and Nanostructures - Fundamentals and Application, http://dx.doi.org/10.1016/j.photonics.2012.02.003

[4] Mohammad Mahbubur Rahman, Josep Ferré-Borrull, Josep Pallarès, Lluis F. Marsal, Phys. Status Solidi C 8 (2011) 1066–1070.

[5] Dusan Losic, Mickael Lillo, and Dusan Losic Jr, Small 5 (2009) 1392–1397.

[6] Yan Su, Guang Tao Fei, Yao Zhang, Peng Yan, Hui Li, Guo Liang Shang, Li De Zhang, Materials Letters 65 (2011) 2693–2695.

Photonic crystal back electrode design for highly efficient transparent polymer cells

Pablo Romero-Gómez, Alberto Martínez-Otero, Rafael Betancur, Xavier Elias, and Jordi Martorell

ICFO – The Institute of Photonic Sciences
Mediterranean Technology Park Av. Carl Friedrich Gauss 3 08860 Castelldefels (Barcelona), Spain

pablo.romero@icfo.es

The specific properties of organic photovoltaic (OPV) cells make them suitable for a large variety of applications where the traditional inorganic semiconductor based photovoltaic technology cannot be used. The inherent semi-transparency of the thin active material layer in an OPV cell may turn out to be very useful in the development of a technology well integrated in building window panes. However, such transparency for the active layer is a necessary but not sufficient condition to develop transparent solar modules. Indeed, a high photo-conversion efficiency (PCE) in organic photovoltaics requires a thick non-transparent metal back electrode. Several attempts have been made to substitute such thick metal layer by a transparent electrode [1,2]. However, transparencies above 25% in the visible range invariably lead to PCEs below 4 %.

In the current paper we consider the combined use of a thin transparent silver layer and an ad hoc photonic crystal designed to enhance the performance of the photovoltaic cell for the infrared wavelengths while simultaneously maintain the transparency in the visible. The starting point was an organic cell with an average PCE of 8.1%, fabricated using a bulk hetero-junction of PTB7:PC71BM and finished with a thick silver layer as back electrode. When thinning down such back silver electrode to 10 nm, light trapping provided by the back reflector is essentially lost and we observe a reduction in short circuit current that results in PCEs of 4.8% approximately. To recover the lost light harvesting efficiency we thermally evaporated several dielectric layers to form a one-dimensional non-periodic photonic crystal on top of the thin electrode. The evaporation procedure followed introduced a minimal damage to the organic cell and we succeeded at maintaining the open circuit voltage and fill factor of the original cell. As shown in Figure 1a, infrared light trapping induced by the photonic crystal leads to a 15% recovery for the short circuit current. In such conditions, the short circuit current recovery is sufficient to obtain cells with PCEs above 5.6%, while the transparency, shown in Figure 1b, is above 40 % in a broad range of visible wavelengths, corresponding to a luminosity through the cell above 30%. The photonic crystal also offers the possibility to tune the cell color, as shown in Figure 2, while maintaining the efficiency. To conclude, we report on a competitive transparent solar technology based on organics. Using the light trapping provided by a thin metal layer combined with an ad hoc photonic crystal, efficient transparent solar cells can be fabricated.

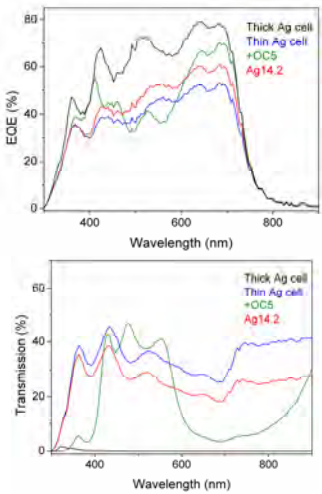

Figure 1: (a) External quantum efficiency and (b) transmission spectra for the device incorporing a five-layers photonic crystal (green) compared to the original device with a 10 nm thin Ag electrode (blue) and a device with a back electrode of 14.2 nm Ag that provides the same performance but lower transmission than the device with the integrated photonic control.

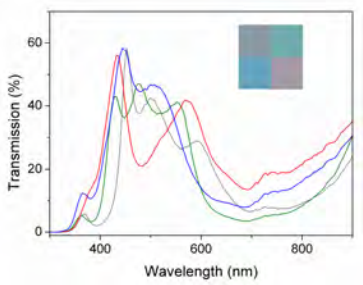

Figure 2: Color tuning using ad hoc photonic crystals and keeping the luminosity over 30%.

References

[1] R. R. Lunt and V. Bulovic, Appl. Phys. Lett., 98 (2011) 113305.

[2] A. Colsmann, A. Puetz, A. Bauer, J. Hanisch, E. Ahlswede and U. Lemmer, Adv. Energy Mater. 1, (2011) 599.

Non-conservative Optical Forces on Nanoparticles

M.I. Marqués[1,2], S. Albaladejo[3], R. Gómez-Medina[2,3], L.S. Froufe-Pérez[4], M. Yépez[2,3], M. Nieto-Vesperinas[5] and **J.J. Sáenz**[2,3]

[1]Departamento de Física de Materiales, Universidad Autónoma de Madrid, Madrid, Spain
[2]Centro de Investigación en Física de la Materia Condensada (IFIMAC), UAM, Madrid, Spain
[3]Departamento de Física de la Materia Condensada, Universidad Autónoma de Madrid, Madrid, Spain
[4]Instituto de Estructura de la Materia, CSIC, Madrid, Spain
[5]Instituto de Ciencia de Materiales de Madrid, CSIC, Madrid, Spain

juanjo.saenz@uam.es

We will address some basic questions related to the light forces on small (Rayleigh) particles, which are usually described as the sum of two terms: the dipolar or gradient force and the scattering or radiation pressure force. The scattering force is traditionally considered proportional to the Poynting vector, which gives the direction and magnitude of the momentum flow. However, as we will show, when the light field has a non-uniform spatial distribution of spin angular momentum, an additional scattering force arises as a reaction of the particle against the rotation of the spin. This non-conservative force term is proportional to the curl of the spin angular momentum of the light field [1].

We analyze the forces on a small dipolar particle and the electromagnetic momentum density in a configuration consisting in two perpendicular linear [1,2] and circularly [3] polarized stationary waves. The field distribution shows regions in which the electric and magnetic fields are parallel corresponding to a null Poynting vector. Although the average value of the momentum density, proportional to the Poynting vector, is zero in these regions, there are scattering forces acting on small particles due to light's spin force. The total scattering force suggests a new definition of the average value of the momentum density for free propagating electromagnetic fields [3].

The unusual properties of the optical forces acting on nanoparticle chains [4] as well as on particles with both electric and magnetic response [5] will also be analyzed. We will see that a chain made of metallic nanoparticles can be used as a resonant light sail, attached by one end point to a transparent object and propelling it by the use of electromagnetic radiation. Interestingly, there is a window in the frequency spectrum in which null torque equilibrium configuration, with minimum geometric cross section, corresponds to a maximum in the driving force. We finally focus on nanometer-sized spheres of conventional semiconductor materials, like Silicon (Si) or Germanium (Ge), which have extraordinary electric and magnetic optical properties in the infrared-telecom range of the electromagnetic spectrum [6-8]. These particles play a key role as pulling probes in the recent proposal of Laser Tractor Beams [9,10].

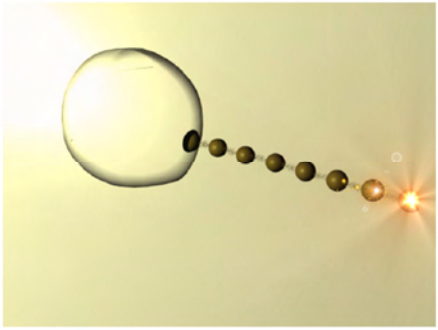

Figure 1: Sketch representing a light sail composed of a gold nanoparticle chain. (After Ref.[4]).

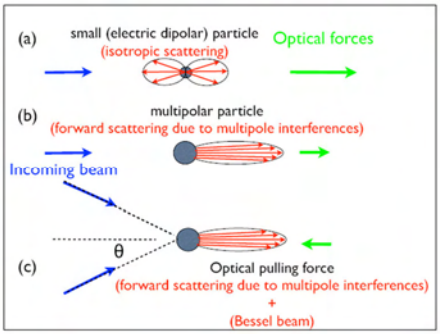

Figure 2: (a) For small dipolar particles scattering is isotropic. There is a net force on the particle along the forward direction (the same direction of the incoming beam) due to the conservation of the total momentum. (b) Due to the interference between multipolar fields, the scattering can be strongly focused in the forward direction. The total force forward is reduced. (c) As the angle between the beams increases, the traditional radiation force goes to zero as the cosine of the angle, whilst the contribution to the force coming from the strongly focused forward scattering remains finite. Above a given angle, there is an optical pulling force against the photon stream. (After Ref.[10]).

References

[1] S. Albaladejo, M. Laroche, M. Marqués, J.J. Sáenz, Phys. Rev. Lett. 102 , 113602 (2009).

[2] S. Albaladejo, M.I. Marqués, F. Scheffold, J.J. Sáenz, Nano Letters 9, 3527 (2009); I. Zapata et al., Phys. Rev. Lett. 103, 130601 (2009).

[3] M.I. Marqués and J.J. Sáenz, Opt. Lett. 37, 2787 (2012).

[4] S. Albaladejo, J.J. Sáenz and M.I. Marqués, Nano Letters 11, 4597 (2011).

[5] M. Nieto-Vesperinas et al. , Opt. Express 18, 1149 (2010).

[6] A. Garcia-Etxarri et al., Opt. Express 19, 4815 (2011).

[7] M. Nieto-Vesperinas, R. Gómez-Medina, J.J. Sáenz, J. Opt. Soc. Am. A 28, 54 (2011).

[8] R. Gómez-Medina et al., J. Nanophoton. 5, 053512 (2011); Phys. Rev. A 83, 033825 (2011); Phys. Rev. A 85, 035802 (2012).

[9] J. Chen, J. Ng, Z. Lin, C.T. Chan, Optical pulling force, Nature Photon. 5, 531 (2011); A. Novitsky, C.-W. Qiu, H. Wang, Phys. Rev. Lett. 107, 203601 (2011); S. Sukhov, A. Dogariu, Phys. Rev. Lett. 107, 203602 (2011).

[10] J.J. Sáenz, Nature Photon. 5, 514 (2011).

New pathways to control single emitter radiation in novel electric and magnetic antenna platforms

M. K. Schmidt[1], R. Esteban[1], J. J. Sáenz[1,2], S. Mackowski[3] and J. Aizpurua[1]

[1]Donostia International Physics Center DIPC and Centro de Física de Materiales CSIC-UPV/EHU, P. Manuel de Lardizabal, 5, Donostia-San Sebastián, Spain.
[2]Departamento de Física de la Materia Condensada and Instituto Nicolás Cabrera, Universidad Autónoma de Madrid, 28049 Madrid, Spain
[3]Institute of Physics, Nicolaus Copernicus University, Grudziadzka 5/7, Torun, Poland.

mikolaj_schmidt@ehu.es

Nano-antennas, commonly used in research, are mostly designed for controlling the radiation from electric dipolar emitters by exciting elementary dipolar modes in plasmonic nanostructures [1]. Recently however, two new notions have emerged, bearing a potential for novel paradigms in the design of nanophotonics devices: excitation of dark modes in plasmonic linear antennas by a radiating dipolar emitter [2,3] and tunable magnetic resonances of dielectric submicron spheres [4,5]. We report on our findings regarding these new antenna designs and propose pathways to achieve a versatile control of their performance and efficiency.

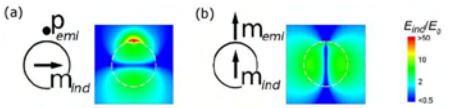

Figure 1: Near-field intensity of the electric field induced by (a) an electric dipolar (p_{emi}) and (b) a magnetic dipolar (m_{emi}) emitters in the proximity of a silicon spherical nanoparticle (m_{ind}).

Modification of the decay rates of a single dipolar electric emitter can be achieved by positioning it in the vicinity of a metallic linear nanoantenna in which higher-order plasmonic excitations are induced. We show that it is possible to effectively tune the enhancement or suppression of both the radiative and non-radiative decay processes by controlling the position and orientation of the dipole with respect to the antenna.

Furthermore, we consider the decay of an electric or magnetic dipolar emitter positioned in the vicinity of a spherical submicron dielectric particle. As we show, silicon nanospheres, with strong magnetic dipolar resonances in the near infrared, provide a canonical example of dielectric antennas that can be used to selectively enhance the magnetic dipolar emission. Near the magnetic resonance, we find a strong enhancement of the decay rate of magnetic emitters which resembles the enhancement of electric dipole emission near a resonant plasmonic particle.

Our results show new important phenomena that emerge from the system comprising canonic nano-optical elements, such as linear plasmonic antennas, dipolar emitters and dielectric nanospheres. The magnetic response from high-refractive index materials can stand as a building block of novel metamaterials and infrared communication platforms.

References

[1] R. Esteban, T. V. Teperik, and J. J. Greffet, Physical Review Letters 104 (2010) 026802.
[2] M. K. Schmidt, S. Mackowski, and J. Aizpurua, Optics Letters 37 (2012) 1017.
[3] M. Liu, T.-W. Lee, S. K. Gray, P. Guyot-Sionnest, and M. Pelton, Physical Review Letters 102 (2009) 107401.
[4] A. García-Etxarri, R. Gómez-Medina, L. S. Froufe-Pérez, C. López, L. Chantada, F. Scheffold, J. Aizpurua, M. Nieto-Vesperinas, and J. J. Sáenz, Optics Express 19 (2011) 4815.
[5] M. K. Schmidt, R. Esteban, J. J. Sáenz, I. Suárez-Lacalle, S. Mackowski, and J. Aizpurua, Optics Express 20 (2012) 13636.

A New Dielectric Metamaterial building block with a strong magnetic response below 1.5 micrometers region. Silicon Colloids nanocavities

Lei Shi, T. Umut Tuzer, Roberto Fenollosa and Francisco Meseguer*

Centro de Tecnologias Fisicas, Unidad Asociada ICMM/CSIC-UPV Av. Los Naranjos s/n, Valencia, 46022, Spain
Instituto de Ciencia de Materiales de Madrid CSIC

fmese@fis.upv.es

A new dielectric metamaterial building block has been processed and characterized (Fig. 1 inset). It is based on high refractive index silicon spherical nanocavities with Mie resonances appearing in the near infrared optical region. Both, experiments and theoretical calculations (Fig. 1) clearly show that a single silicon nanocavity supports well defined and robust magnetic resonances, even in a liquid medium environment, at wavelength values up to six times larger than the cavity radius [1].

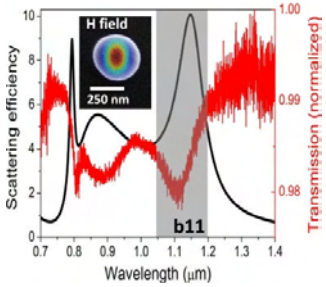

Figure 1: Scattering (black) efficiency as a function of wavelength and the experiment transmission spectra (red line) of single silicon nanocavity (diameter: 306 nm) are shown. The SEM image and the magnetic field distribution inside the nanocavity are also shown inset.

Furthermore, based on those "optical magnetism" silicon nanocavities, strong magnetic interaction between optical waveguide and silicon nanocavities are also reported [2]. The magnetic field component of light in dielectric materials generally plays a negligible role at optical frequency values. However, it is a key component of metamaterials with optical magnetism [3]. Here, the analytical method, as well as the finite difference time domain (FDTD) simulation, shows a three dimensional (3D) magnetic trap effect when the magnetic like Mie resonances of the silicon nanocavities are excited (Fig. 2).

References

[1] Lei Shi, T. Umut Tuzer, Roberto Fenollosa and Francisco Meseguer, Adv. Mater., DOI: 10.1002/adma. 201201987, (2012) accepted.
[2] Lei Shi and Francisco Meseguer, Opt. Express, (2012) accepted.
[3] R. Merlin , Proc. Natl. Acad. Sci. USA, 106, 1693, (2009).

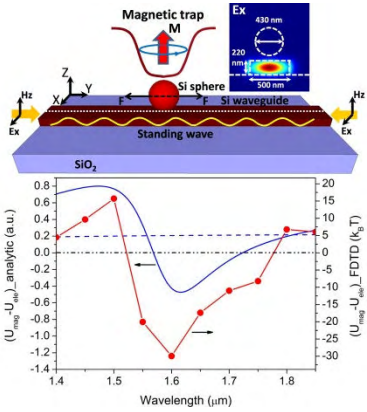

Figure 2: Upper, schematic view of a spherical silicon nanocavity located above the top side of a silicon waveguide. The waveguide cross section and the field distribution of Ex in the waveguide is shown inset. Lower, the potential difference between the high magnetic field region and high electric field region at the waveguide as a function of wavelength for both the analytical model (blue line) and FDTD simulation (red line). For comparison purposes, we have also plotted the PS sphere as a blue dash line. The diameter of silicon and PS spheres are 430 nm, and the intensity of guided light in waveguide is 0.9 mW.

Colloidal QDs/PMMA nanocomposites as material to provide gain in surface plasmon polaritons

I. Suárez[1], E. P. Fitrakis[2], P. Rodriguez-Cantó[1], R. Abargues[1], H. Gordillo[1], I. Tomkos[2] and J. Martinez-Pastor[1]

[1]UMDO (Unidad Asociada al CSIC-IMM), Instituto de Ciencia de los Materiales, Universidad de Valencia, PO Box 22085, 46071 Valencia, Spain
[2]Athens Information Technology (AIT)
P.O. Box 68 19,5 klm, Markopoulo Ave.
GR – 19002, Peania Attikis, Greece

isaac.suarez@uv.es

Surface plasmon polaritons (SPPs) are hybrid electromagnetic waves and charge surface states propagating in the boundary between a metal and a dielectric [1]. They receive much interest nowadays because the present unique properties as subwavelength confinement, strong near electromagnetic field enhancement or high sensitivity to the environment [2], leading to a broad range of potential applications, like subwavelength photonics, metamaterials or biosensing. However, although devices based on the propagation of surface plasmon can achieve exceptional properties, SPPs suffer from high attenuation because of the absorption losses in the metal, limiting the application of this technology. Nevertheless, this limitation can be overcome by providing the material adjacent to the metal with optical gain. Under these conditions, the problem of absorption losses is alleviated. Consequently, the propagation length of SPPs [3] is increased or SPPs are even amplified [4]. In the literature different materials like dyes [3], fluorescent polymers [4], rare earths [5] or PbSe quantum dots [6] have been proposed as gain medium for wavelengths between 600 and 1500 nm.

In this work a novel material based on the incorporation of colloidal quantum dots in a polymer matrix is proposed as a dielectric medium to provide gain in plasmonic waveguides. This kind of nanocomposite (polymer+quantum dots) is a useful material because it combines the novel properties of colloidal quantum dots (temperature independent emission and color tuning with the base material) with the technological feasibility of polymers (spin coating, UV and e-beam lithography...). Indeed, the application of CdSe/PMMA in the development of active dielectric waveguides has already been demonstrated at 600 nm [7]. Furthermore, wavelength tunability of the device (from 400 nm to more than 2 μm) can be achieved just by changing the material of the dots and their size [8] without modifying the fabrication conditions. In this manuscript, CdSe-PMMA nanocomposite films are deposited on a gold surface to compensate the losses of the SPP propagating at the interface at 600 nm [9]. First, a suitable design of the amplifier is presented, making a thoroughly study of the propagation of SPP under amplification. The effect of the concentration of CdSe in PMMA nanocomposites on the gain is analyzed. Then, plasmonic waveguides are fabricated by spin coating CdSe-PMMA nanocomposites on gold layers evaporated on a SiO_2/Si substrate. When the structures are optically pumped (see figure 1 a) the photoluminescence (PL) of the CdSe can be coupled to the SPP mode, making it possible to characterize the waveguided PL (figure 1 b) or modes (figure 1 c) by collecting the light at the output of the waveguide. If the pumping laser is focused in the shape of a stripe line the optical gain can be estimated by measuring the photoluminescence as a function of the pumping length [10]. Figure 2a shows the characterization of the gain for three different filling factors of QDs in the polymer. In all cases there is an exponential dependence on saturation for stripe lengths longer than 500 μm. By fitting the curve with an exponential law, net gains of around 25 cm have been estimated for the highest filling factor studied. In the same way propagation losses can be characterized by keeping the length of the stripe constant and moving it away from the edge of the sample. Then, propagation losses can be fitted by approximating the dependence of the output intensity as a function of the distance between the stripe and the edge of the

sample with an exponential decrease. In addition, figure 2b shows that propagation losses increase with the concentration of QDs in the PMMA due to reabsorption effects, presenting a compromise between high gain and low reabsorption.

References

[1] T.W. Ebbesen et al., Physics Today, 61 (2008) 44.

[2] P. Berini, Advances in Optics and Photonics 1 (2009) 484.

[3] I. De Leon and P. Berini, Nature Photonics, 4 (2010) 382.

[4] M.C. Gather et al., Nature Photonics 4 (2010) 457.

[5] M. Ambati et al., Nanoletters, 8 (2008) 3998.

[6] J. Grandidier et al., Nanoletters, 9 (2009) 2935.

[7] I. Suárez et al., Nanotechnology, 22 (2011) 435202.

[8] H. Gordillo et al., Journal of Nanomaterials, 2012 (2012) 960201.

[9] I. Suárez et al., ICTON Proceedings (2012).

[10] L. Dal Negro et al., Optics Communications, 229 (2004) 337.

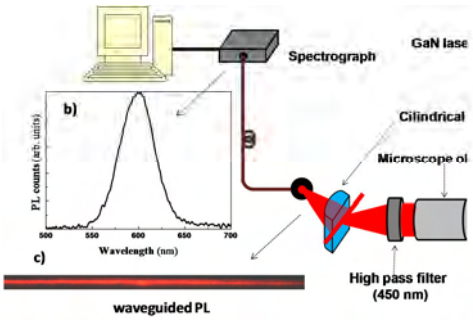

Figure 1

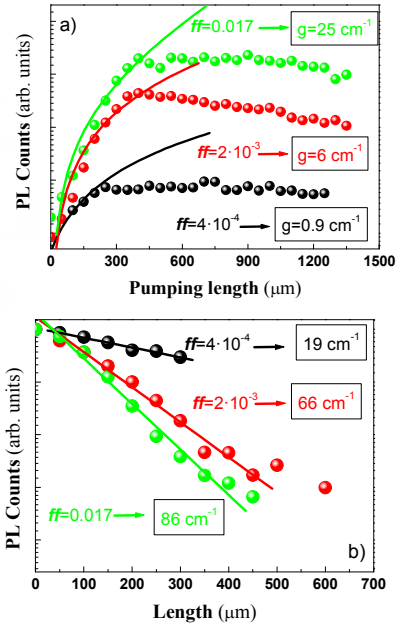

Figure 2

Quantum Junction Plasmons in Graphene Dimers

Sukosin Thongrattanasiri[1], Alejandro Manjavacas[1], Peter Nordlander[2], and F. Javier García de Abajo[1]

[1]ICFO – C SIC, Serrano 119, 28006 Spain
[2]Department of Physics and Astronomy, M.S. 61, Rice University, Houston 77005-1892, United States

sukosin@gmail.com

The interaction between doped graphene nanoislands connected by narrow junctions constitutes an ideal testbed to probe quantum effects in plasmonic systems. Here, we predict that the interaction between graphene plasmons in neighboring nanoislands is extremely sensitive to the size and shape of the junctions [1]. Due to the two-dimensional character of this material, the addition of a small number of atoms (<10) is sufficient to dramatically modify the absorption spectrum of the entire dimer. Our ab initio calculations predict three different regimes of interactions: For narrow bridges (<4 carbon-atom rows) the conductance of the junction is too low to allow electron transport and the optical response is a characteristic bonding dipolar dimer mode that also appear in a classical description; for wider junctions (4-8 carbon rows), a pronounced charge polarization is induced across the junction which gives rise to a novel "junction plasmon" that has no counterpart in a classical description; for wider junctions (>8 rows) the conductance of the junction is sufficiently large to allow charge transport between the two graphene islands, resulting in a pronounced charge transfer plasmon which can also be described classically. The intermediate regime between the classical narrow and wide junction regimes is marked by a plasmon localized at the junction that is absent in classical-electrodynamics calculations [2]. Also in contrast to classical theory, our quantum description predicts a minor dependence on the length of the junction and a strong dependence on its width, thus confirming the importance of a quantum mechanical description of the optical properties of bridged graphene dimers.

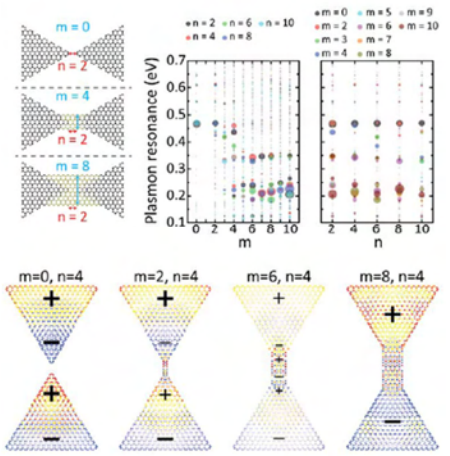

Figure 1

References

[1] S. Thongrattanasiri, A. Manjavacas, P. Nordlander, and F.J. García de Abajo, submitted (2012).

[2] R. Esteban, A.G. Borisov, P. Nordlander, and J. Aizpurua, Nature Commun. 3, 825 (2012).

High Resolution Fourier-Transform Microspectrometers in Silicon-on-Insulator Waveguides

Aitor V. Velasco[2], Pavel Cheben[1], Przemek Bock[1], Jens H. Schmid[1], Jean Lapointe[1], André Delâge[1], María L. Calvo[2], Siegfried Janz[1], Dan-Xia Xu[1] and Mirosław Florjańczyk[1]

[1]National Research Council Canada, Ottawa, Ontario K1A 0R6, Canada
[2]Dpto de Óptica, Facultad de Ciencias Físicas, Universidad Complutense, 28040 Madrid, Spain

avillafranca@pdi.ucm.es

In the past years, there has been an increasing amount of attention paid to the development of compact high-resolution spectrometers for a wide range of applications such as optical communication networks, health diagnosis, environmental sensing and space instrumentation, to name a few [1]. In particular, planar waveguide Fourier-Transform (FT) spectrometers based on the principle of Spatial Heterodyne Spectroscopy (SHS) have been recently proposed [2,3], overcoming the light throughput (etendue) limitation of other devices such as Arrayed Waveguide Gratings [4]. The SHS interferometric technique is based on the principle Michelson interferometer [5], and it allows simultaneously obtaining the outputs for a plurality of sampled path by replacing moving mirrors with diffraction gratings [6]. It is also possible to implement the SHS concept with a waveguide array of Mach-Zehnder interferometers (MZI) with increasing path differences [2,7]. The stationary patterns at the output of the MZI array $F(x_i)$ are then numerically analyzed with Fourier Transform techniques, obtaining full retrieval of the input spectrum (p_{in}) within the Free Spectral Range (FSR) of the device with a single measurement. Additionally, the output of each MZI can be analyzed individually to compensate the amplitude and phase errors associated with waveguide loss and dimensional inaccuracies of the fabrication. In this work, we present two types of SHS-FT spectrometers for the submicron silicon-on-insulator (SOI) platform, demonstrating their high performance by accurately retrieving the spectra of experimental input signals.

The first SHS-FT spectrometer is based on an array of N silicon wire waveguide MZIs with an increasing path length difference ΔL_i (Fig. 1a). Each MZI comprises an arm with a straight waveguide and another arm with a spiral waveguide of increasing radius. The high contrast index of the SOI platform allows implementing long optical path lengths within a compact footprint. In particular, SHS-FT spectrometers comprising spiral waveguides up to 1.13 cm long were implemented within a footprint of only 12 mm^2. In the spirals, a minimum waveguide bend radius of 5 µm is used.

In the second device (Fig. 1b), the increasing optical path differences along the interferometer array are implemented with subwavelength grating (SWG) delays [8]. By periodically alternating along the waveguide thin transversal segments of silicon core and cladding material with a period below one half of the wavelength of the guided light, the effective index of the waveguide can be modified by design over a wide range. The optical path difference can thus be adjusted by varying the length of the SWG delays sections, or by modifying its duty cycle. In particular, the fabricated device comprises 32 MZI with SWG sections ranging from 0.46 mm to 1.5 cm. The periodic SWG structures were designed with a 400 nm pitch, a width of 300 nm, and a constant duty cycle of 50%. One of the main advantages of this device is that all the MZI present the same physical length and similar losses, thus achieving a more stable visibility of the MZI outputs along the array.

For both devices, the same spectral retrieval technique was used. The oscillations at the output of each MZI were calibrated by a high-resolution wavelength scan within the free spectral range (FSR) of the device, and used to define a transformation matrix T such that $F(x_i)=p_{in}\times T$. The input spectrum of the actual measurement was obtained by

multiplying the output pattern by a pseudoinverse T^+ of the transformation matrix, computed by Single Value Decomposition [9]. The matrix T^+ includes all the fabrication errors of the device and corresponding fluctuations in both amplitude and phase of the optical signal. This yields more robust results than the traditional cosine transform, which requires an active compensation of the phase errors before the spectral retrieval can be performed [7]. Figure 2 shows signal spectra experimentally retrieved using both types of devices. The spiral waveguide SHS-FT spectrometer has a spectral resolution of 42 pm and a FSR of 0.75 nm. The SHS-FT spectrometer with SWG delays has a resolution of 50 pm and a FSR of 0.78 nm. For both cases, the original spectrum is retrieved with low crosstalk. Truncation ripple is reduced by applying an apodization window on the output pattern.

In conclusion, two planar waveguide SHS-FT spectrometers have been demonstrated in submicron silicon-on-insulator waveguides, showing high spectral resolution, low crosstalk and a compact footprint.

References

[1] P. Cheben, "Wavelength dispersive planar waveguide devices: Echelle gratings and arrayed waveguide gratings," in Optical Waveguides: From Theory to Applied Technologies, Eds. M. L. Calvo and V. Laksminarayanan, Chapter 5, CRC Press, London, 2007.

[2] P. Cheben, I. Powell, S. Janz, and D.-X. Xu, Opt. Lett., 30 (2005) 1824.

[3] M. Florjanczyk, P. Cheben, S. Janz, A. Scott, B. Solheim, and D. X. Xu, Opt. Express, 15 (2007) 18176.

[4] P. Cheben, J. H. Schmid, A. Delâge, A. Densmore, S. Janz, et al., Opt. Express, 15 (2007) 2299.

[5] P. Jacquinot, J. Opt. Soc. Am., 44 (1954) 761.

[6] J. M. Harlander, F. L. Roesler, J. G. Cardon, C. R. Englert, and R. R. Conway, Appl. Opt., 41 (2002) 1343.

[7] K. Okamoto, H. Aoyagi, and K. Takada, Opt. Lett., 35 (2010), 2103.

[8] P. Cheben, P. J. Bock, J. H. Schmid, J. Lapointe, S. Janz, et al, Opt. Lett., 35 (2010) 2526.

[9] G. H. Golub and C. Reinsch, Numerische Mathematik, 14 (1970), 430.

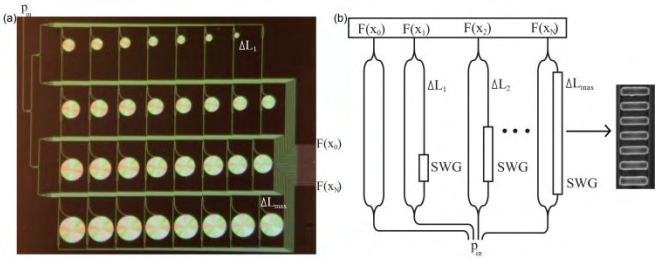

Figure 1: (a) Spatial-Heterodyne Fourier-Transform (SHFT) spectrometer implemented with planar spiral waveguides. (b) Schematics of a SHFT spectrometer implemented with subwavelength grating (SWG) phase delays, and SEM micrograph of a SWG section.

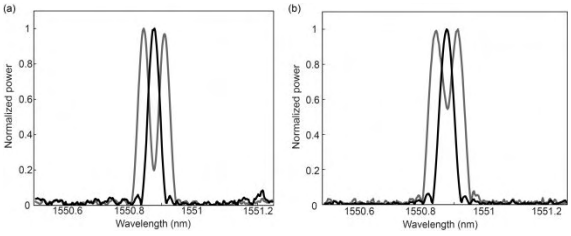

Figure 2: Spectra of a single narrowband laser source (black) and a doublet of two monochromatic lines separated 65 pm (grey) retrieved from the experimental measurements of Spatial-Heterodyne Fourier-Transform spectrometers implemented with (a) planar spiral waveguides; and (b) subwavelength grating (SWG) phase delays.

Rearrangement of the near-field landscape in heterogeneous nanoparticle arrays

A. Vitrey, P. Prieto, A. García-Martín, J.M. García-Martín and M. U. González

IMM-Instituto de Microelectrónica de Madrid (CNM-CSIC), Isaac Newton 8, E-28760 Tres Cantos, Madrid (Spain)

alan.vitrey@imm.cnm.csic.es

Geometric resonances in nanostructure arrays sustaining localized surface plasmons have received increasing attention in the last few years [1]. These geometric resonances exhibit narrower peaks than the purely plasmonic ones, therefore these systems are promising candidates for sensing applications [2]. Moreover, they provide new features in the near-field distribution patterns. Heterogeneous nanoparticle arrays offer a way to tune both the near and far-field response by using nanoparticles of different sizes, shapes or materials [3], but there is a lack of experimental studies in this context.

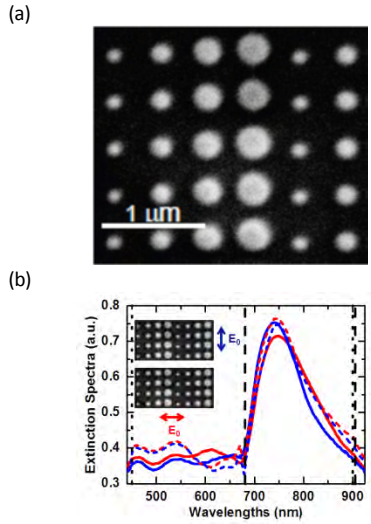

Figure 1: (a) SEM image of the studied sample, consisting of 120 nm height Au nanodiscs with four different diameters deposited on glass. (b) Experimental (solid lines) and numerical (dashed lines) extinction spectra; Inset: Polarization of the incident light.

In this work, we will present a theoretical and experimental analysis of the near-field modification induced by the presence of heterogeneity and collective resonances. We have investigated a two dimensional array of gold nanodiscs with four different diameters and located 3º off-axis (see Fig. 1 (a)), which also allows studying the effect of a small alteration in the geometrical arrangement [4]. We present zero-order extinction spectra acquired in far-field, as well as measurements of the near field distribution using SNOM technique in collection mode with two orthogonal polarizations and different wavelengths. Far and near-field characterizations are understood with the help of FDTD numerical results. The far-field spectra (Fig. 1 (b)) corroborate the existence of geometric resonances in our heterogeneous system, as predicted theoretically [3]. Moreover, from our numerical analysis it will be shown that heterogeneity has little influence on the far-field response. However, in clear contrast, the near-field shows a complex redistribution induced by the heterogeneity, as can be seen in Fig. 2. As illustrated in more detail by the simulated field maps of Fig. 3, the main effect is a dramatic break of the axial symmetry of the field pattern typically generated by nanodiscs, and more generally, the suppression or the enhancement of the field surrounding the nanostructures, mainly when the polarization is aligned along the heterogeneous direction. We attribute this to constructive and destructive interferences arising from the phase contribution of the field scattered from each kind of nanodiscs. Our results offer a deeper insight on the interplay between individual and collective resonances.

(a)

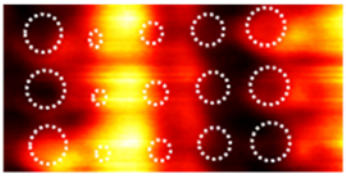

(b)

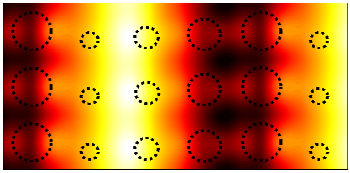

Figure 2: (a) SNOM image of the sample shown in Fig. 1(a). (b) Calculated distribution of the near-field. For (a) and (b) the wavelength is 860 nm and the incident polarization is aligned along the heterogeneous direction (represented with a red arrow in the inset of figure 1(b)). For (b) the near field distribution is calculated at an altitude similar to that of the SNOM scans, i.e. 100 nm above the nanodiscs.

(a)

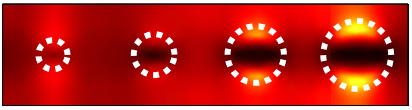

(b)

Figure 3: Simulated field maps at 860 nm wavelength for incident light polarized perpendicularly (a) or parallel (b) to the heterogeneous direction (blue and red arrows respectively in the inset of figure 1(b)). The field maps are calculated at 30 nm above the discs to show in detail the break of symmetry in the near field dipolar pattern when the polarization is aligned in the heterogeneous direction.

References

[1] B. Auguié and W. L. Barnes, Phys. Rev. Lett., 101 (2008) 143902.

[2] P. Offermans, M.C. Schaafsma, S.R.K. Rodriguez, Y. Zhang, M. Crego-Calama, S.H. Brongersma, and J. Gómez Rivas, ACS Nano, 5 (2011) 5151.

[3] J. Li, Y. Gu, and Q. Gong, Opt. Express, 18 (2010) 17684.

[4] S. Zou and G.C. Schatz, J. Chem. Phys., 121 (2004) 12606.

Shaping Magneto-Optical Spectra with Plasmonic Resonances

Miguel Rubio-Roy[1], **Ondrej Vlasin**[1], José Manuel Caicedo[1], Oana Pascu[1], Nicolás G. Tognalli[2],Alejandro Fainstein[2], Malte Schmidt[1], Alejandro Goñi[1,3], Anna Roig[1] and Gervasi Herranz[1*]

[1]Institut de Ciència de Materials de Barcelona, ICMAB-CSIC Campus de la UAB, Catalonia, Spain
[2]Centro Atómico Bariloche, Instituto Balseiro, Comisión Nacional de Energía Atómica, Argentina
[3]Institució Catalana de Recerca i Estudis Avançats, Barcelona, Catalonia, Spain

*gherranz@icmab.es

The magneto-optical activity results from the interaction of polarized light with magnetized media. This is revealed by an induced rotation and ellipticity of the polarization as the light is transmitted or reflected from a medium in the presence of a magnetic field and/or magnetization. Thus, the interaction of light with magnetic materials provides a way to manipulate the polarization of light and to exploit this phenomenology for characterization as well as applications. Indeed, the cross link between light and magnetism affords the basis for potentially novel devices in data control of optical communications, optical storage data and sensing. This has, in turn, spurred the research on new materials exhibiting large magneto-optical responses at the operating wavelengths, in particular in the visible. The strategies towards magneto-optical enhancement are essentially based on the dramatic intensification of the lightmatter interaction when media are nanostructured intentionally to couple predominantly with photons of certain wavelengths.

In previous works, we have demonstrated the efficiency of coupling magneto-optics to photonic bandedge effects in magnetophotonic crystals [1, 2], where at frequencies close to the band edges the group velocity of light is dramatically slowed down and, therefore, photons of those wavelengths couple very intensively with the medium. Exploiting this mechanism, we have achieved enhanced magneto-optical responses at near-band edge wavelengths in three-dimensional magneto-photonic crystals (3D-MPCs) (see Figure 1a). Here we envisage an alternative strategy to boost magneto-optic signals by coupling to plasmonic resonances. Thus, the incorporation of magnetic nanoparticles into plasmonic structures provides an alternative pathway to modulate the magneto-optical spectra and enhance the response at specific wavelengths. In this case, we have exploited the huge increase of the electromagnetic energy density associated with plasmons that are excited in extremely confined regions around metal/dielectric interfaces. With this in mind, we have coated corrugated gold/dielectric interfaces with magnetic (nickel and iron oxide) nanoparticles [3]. We have found that the magneto-optical spectra at visible wavelengths are strongly modified when the magnetic nanoparticles are incorporated into plasmonic structures formed either by Au voids or Au nanodisk arrays. In particular, we find that the magnetooptical activity is enhanced by up to around one order of magnitude (Figure 1b) for wavelengths that are correlated to the excitation of either propagating or localized surface plasmons. In addition, we demonstrate that this strong magneto-optical activity is not merely the result of the reflectance modification associated to diagonal terms of the permittivity tensor, but to an intrinsic huge enhancement of the optical activity related to the off-diagonal permittivity coefficients.

Our results demonstrate the potential of exploiting light polarization in plasmonic and photonic structures as a powerful strategy to customize the magneto-optical spectral response of magnetic materials and to obtain optimized materials for

applications such as sensing or optical communications.

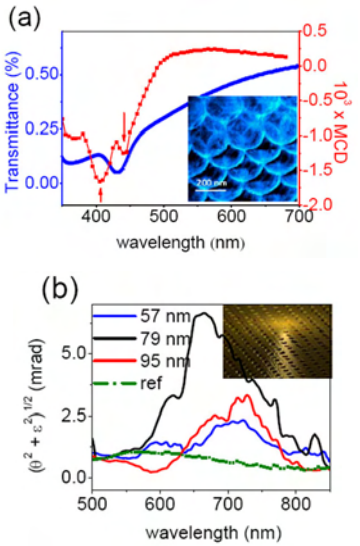

Figure 1: (a) Spectral response of the optical transmission (blue) and the magnetic circular dichroism (red) of a direct opal infiltrated with $MnFe_2O_4$ of nanoparticles (see a SEM image in the inset). (b) Magneto-optical spectra (θ = rotation, ε = ellipticity) of iron oxide nanoparticles deposited on nanodisks arrays with diameter *d* = 57, 79 and 95 nm and on a flat surface. The inset shows a SEM picture of one of the nanodisk arrays.

References

[1] J.M. Caicedo et al., ACS Nano, 5 (2011) 2957.
[2] O. Pascu et al., Nanoscale, 3 (2011) 4811.
[3] M. Rubio-Roy et al., Langmuir, 28 (2012) 9010.

Posters

Posters

Index alphabetical order

		Page
Maria Alba Martin (Universitat Rovira i Virgili, Spain) *"Label-free enzyme biosensor based on porous silicon microcavities"*	*applications: multifunctional structures*	**103**
Miguel Anaya Martín (ICMSE-CSIC, Spain) *"Enhanced Light-to-Electron Conversion in Photoconducting Nanostructured Multilayers by Optical Field Confinement Effects"*	*photonic structures*	**105**
Paloma Arroyo Huidobro (Universidad Autónoma de Madrid, Spain) *"Superradiance mediated by graphene surface plasmons"*	*plasmonics*	**107**
Ramón Bernardo Gavito (UAM/IMDEA Nanociencia, Spain) *"Near-field study of localized and extended surface plasmon resonance on gold nanoislands"*	*near field optics*	**109**
Antoine Brimont (Nanophotonics Technology Center - UPV, Spain) *"Increased sensitivity of delay-interferometer receiver for 10G DPSK for SOI platform"*	*photonic structures*	**110**
Blanca Caballero (IMM-CNM-CSIC, Spain) *"Magneto-optical properties of nanostructured ferromagnetic films mediated by surface plasmon polaritons"*	*plasmonics*	**112**
José Raúl Castro Smirnov (ICMSE-CSIC, Spain) *"Novel approaches to ultraviolet radiation protecting thin films based on nanoparticle multilayers"*	*applications: multifunctional structures*	**114**
Arnau Coll Valentí (Universitat Politècnica de Catalunya / MNT, Spain) *"Angle emission properties of complex colloidal nanostructures for energy efficiency applications"*	*photonic structures*	**115**
Diana Fragua (Instituto de Ciencia de los Materiales. Universidad de Valencia, Spain) *"Nanocomposite based on gold nanoparticles embedded into ZnO films"*	*plasmonics*	**117**
Luis S. Froufe-Pérez (Instituto de Estructura de la Materia-CSIC, Spain) *"Parabolic antennae at telecommunication infrared wavelengths"*	*photonic structures*	**119**
Francisco Gallego-Gomez (ICMM-CSIC, Spain) *"Photoinduced Local Heating in Silica Photonic Crystals for Fast and Reversible Switching"*	*photonic structures*	**121**
Francisco Gallego-Gomez (ICMM-CSIC, Spain) *"Water-Dependent Micromechanical and Rheological Properties of Silica Colloidal Crystals Studied by Nanoindentation"*	*photonic structures*	**123**
Blas Garrido (Universitat de Barcelona, Spain) *"Silicon nanostructures and devices for advanced LEDs"*	*photonic structures*	**125**
Maria Ujue Gonzalez (IMM-CNM-CSIC, Spain) *"High magneto optical activity and low optical losses in metal–dielectric Au/Co/Au-SiO_2 magnetoplasmonic nanodisks"*	*plasmonics*	**126**
Maria Ujue Gonzalez (IMM-CNM-CSIC, Spain) *"Magnetic modulation of surface plasmon modes in magnetoplasmonic Metal-Insulator-Metal cativies"*	*plasmonics*	**128**
Henry Gordillo Millán (Universidad de Valencia, Instituto de Ciencia de Materiales, Spain) *"Waveguides based on colloidal QDs embedded in PMMA and SU8"*	*applications: multifunctional structures*	**130**
Pedro Granero (Universitat Rovira i Virgili, Spain) *"2D and 3D light absorption modeling of interdigitated full organic solar cells"*	*photonic structures*	**132**
Peilin Han (Universitat Rovira i Virgili, Spain) *"Annealing effect on the performance of PTB1: PCBM bulk heterojunction solar cells"*	*photonic structures*	**134**
Laura P Hernandez Eguia (URV/ Escla tècnica superior d'enginyeria/ DEEEA, Spain) *"Tailoring the optical properties of nanoporous anodic alumina with geometry modification for further sensing applications"*	*applications: multifunctional structures*	**136**

		Page
Alberto Jiménez-Solano (ICMSE-CSIC, Spain) *"Integration of gold nanoparticles in photonic crystals: effect of the interplay between plasmonic and optical cavity resonances"*	*plasmonics*	**138**
M Carmen López López (ICMSE-CSIC, Spain) *"Optimized integration of one-dimensional photonic crystals in dye solar cells"*	*applications: multifunctional structures*	**139**
Gerard Macias Sotuela (Universitat Rovira i Virgili, Spain) *"Fabrication and characterization of nanoporous anodic alumina bilayers for biosensing applications"*	*applications: multifunctional structures*	**140**
Alejandro Martinez (Nanophotonics Technology Center - UPV, Spain) *"Experimental demonstration of photonic confinement in suspended square-lattice silicon photonic crystal cavities"*	*photonic structures*	**142**
Mariluz Martínez-Marco (Universidad de Valencia, Instituto de Ciencia de Materiales, Spain) *"In-situ synthesis of conducting polymers and gold nanoparticles into PMMA"*	*applications: multifunctional structures*	**144**
Alberto Martinez Otero (ICFO-Institut de Ciencies Fotoniques, Spain) *"Optical optimization for high performance polymer solar cells"*	*applications: multifunctional structures*	**146**
Daniel Navarro Urrios (Catalan Institute of Nanotechnology (ICN), Spain) *"Optical characterization of 1D and 2D Silicon PhoXonic crystals with an evanescent light coupling technique"*	*photonic structures*	**147**
Maksym Nesterov (University of Zaragoza, Spain) *"Graphene supports the propagation of subwavelength optical solitons"*	*photonic structures*	**148**
Alejandro Ortega-Moñux (Universidad de Málaga, Spain) *"Silicon sub-wavelength structures for refractive index and dispersion engineering"*	*photonic structures*	**150**
Reyes Ortiz Marchena (ICMSE-CSIC, Spain) *"Optical analysis of 1D diffraction gratings patterned on nanocrystalline titania electrodes for enhanced photovoltaic conversion"*	*applications: multifunctional structures*	**152**
Esteban Pedrueza Villalmanzo (Instituto de Ciencia de los Materiales - Universidad de Valencia, Spain) *"Au and Ag nanoparticle-doped-TiO_2 thin films: structural and optical characterization and antireflective properties"*	*plasmonics*	**153**
Carmen Rial (Universidade de Santiago de Compostela, Spain) *"Direct ink writing of ZnO three-dimensional terahertz photonic crystals"*	*photonic structures*	**155**
David Rivas (Intituto de Ciencia de los Materiales, Spain) *"Single photons emitted by quantum dots: towards all-optical q-gates"*	*photonic structures*	**156**
Manuel Rodrigo (DAS Photonics, S.L., Spain) *"Application of nanophotonic biosensors for the detection of traces of DMMP"*	*applications: multifunctional structures*	**158**
Pedro Rodríguez Cantó (Univ. de Valencia, Instituto de Ciencia de Materiales, Spain) *"Plasmonic layers of colloidal Ag nanoparticles for enhancement of light trapping in silicon solar cells"*	*plasmonics*	**160**
Elisabetta Romano (Universitat Rovira i Virgili, DEEEA, Spain) *"Disordered macroporous silicon as optical filter in the medium infrared region"*	*applications: multifunctional structures*	**162**
Jose A. Sánchez-Gil (Instituto de Estructura de la Materia (CSIC), Spain) *"Plasmonic Fano resonances on single nanorods: Application to refractive index sensing"*	*plasmonics*	**164**
Fernando Villate (Universdidad de Zaragoza, Spain) *"Light Harvesting at the Infrared"*	*plasmonics*	**165**
Miztli Yolotzin Yépez (UAM, Spain) *"Perturbative approach for the statistical scattering of waves in disordered waveguides: closed channels contributions and the effective medium approximation"*	*photonic structures*	**167**

Label-free enzyme biosensor based on porous silicon microcavities

M. Alba, P. Formentín, J. Ferré-Borrull, J. Pallarès and L. F. Marsal*

Departament d'Enginyeria Electrònica, Elèctrica i Automàtica, Universitat Rovira i Virgili,
Avda. Països Catalans 26, 43007 Tarragona, Spain

*lluis.marsal@urv.cat

Herein, we present a porous silicon (PSi) microcavity designed for the immobilization and detection of trypsin enzyme. The extraordinary optical and morphological features of PSi multilayer structures make them an advantageous support for label-free biosensing. Surface modification and enzyme confinement are monitored based on changes in the optical reflectance spectrum. The narrow resonance peak of the microcavity shifts to the red due to an increase in the effective refractive index caused by the attached molecules [1]. Label-free sensors based on optical measurements can be tailored for the detection of molecular binding events. Particularly, the detection of enzymes is of special interest as their levels are indicators of various diseases, such as cancer, diabetes or hyperthension [2,3]. Here, trypsin was selected as a test biomolecule to evaluate the feasibility of the method.

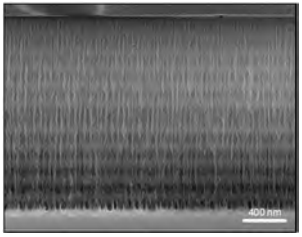

Figure 1: Cross-sectional FESEM of the λ/2 microcavity after oxidation. Each mirror stack is composed by 5 periods of alternating high and low porosity.

A PSi microcavity (PSiMc) is composed of two multilayer λ/4 Bragg mirror stacks (alternating low and high porosity layers) spaced by an active layer (microcavity) [4]. The optical thickness (nd) of the active layer is twice the high-porosity layer (λ/2), where n is the refractive index, d the physical thickness and λ the Bragg wavelength. PSiMc were fabricated by anodic electrochemical etching of a p^{++} silicon (100) wafer (0.002-0.004 Ωcm) using an electrolyte containing hydrofluoric acid (48%), ethanol (98%) and glycerol (98%) in the volumetric ratio 3:7:1 [5]. By alternating a low (25 $mA{\cdot}cm^{-2}$) and high (70 $mA{\cdot}cm^{-2}$) current densities, low (65%) and high (80%) porosity layers were obtained. Anodization times of 6.4 s (high porosity) and 11.5 s (low porosity) were chosen to obtain an optical thickness of λ/4 in each layer. The microcavity structure consisted of two 5-period Bragg mirrors and a defect layer of λ/2 optical thickness, for a wavelength range 780-820 nm. After anodization, the microcavities were thermally oxidized at 800 °C for 1 h.

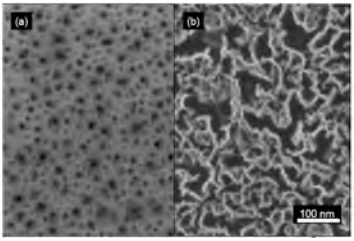

Figure 2: Top view FESEM of the oxidized (a) low (25 mA/cm^2) and (b) high (70 mA/cm^2) porosity layers.

A cross-sectional field emission scanning electron micrograph (FESEM) of the PSiMc (Fig. 1) shows a thickness of 3.7 μm. Fig. 2a and 2b show top-views of the low and high porosity layers after oxidation, respectively. Optical reflectance spectra were recorded using a Perkin Elmer Lambda 950 UV-Vis-NIR spectrometer with a reflection accessory at 15°. The PSiMc spectra before and after oxidation are presented in Fig. 3. The spectrum blue shifted approximately 50 nm due to the formation of silicon oxide, which has lower refractive index.

The surface of the PSiMc was modified using standard silane and glutaraldehyde coupling chemistry to make it suitable for the enzyme

attachment. First, the samples were incubated in 0.5% (3-aminopropyl)triethoxysilane (APTES) solution in toluene at 70 ºC for 2 h. After rinsing with toluene and drying with a N_2 flow, the samples were annealed at 100 °C for 15 min. Following the silanization, the activation of the amine group was performed by incubation in 2.5% glutaraldehyde (GTA) solution in phosphate buffer (PBS).Then the trypsin was immobilized by dipping the samples in 1 mg·mL^{-1} trypsin solution in PBS containing 50 mM benzamidine (to restrict the trypsin autolysis) for 4.5 h at 4 °C. After removing the non-specifically bounded trypsin by rinsing with PBS, the trypsin-immobilized PSiMc was immersed in 1 M tris(hydroxymethyl)aminomethane (Tris-HCl) for 2 h to deplete the residual aldehyde groups.

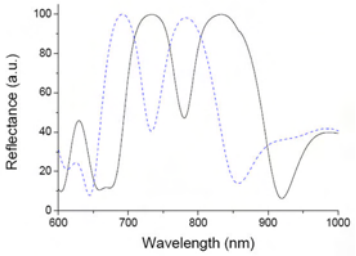

Figure 3: Reflectance spectra of a porous silicon microcavity structure. The solid line correspond sto the as-produced PSiMc and dotted on to the oxidized PSiMc.

The surface modification process (i.e. silanization, activation and enzyme binding) was monitored by recording the optical reflectance spectrum of the PSiMc. The characteristic narrow resonance of the spectrum is very sensitive to changes in the effective optical thickness. The consecutive bindings of the target species cause an increase in the refractive index, revealing a gradual red shift of resonance. The spectrum shift is related to the total amount of analyte immobilized by the PSi structure [1]. Fig. 4 shows how the resonance peak wavelength increases after each functionalization step. The increase of the refractive index after the incubation in APTES and GTA caused a 21 and 18 nm shift, respectively. Finally, after the selective immobilization of trypsin, there was a resonance wavelength increase of 20 nm.

In summary, we proposed a label-free enzymatic biosensor based on porous silicon microcavities. Psi microcavities were designed in porosity, thickness and geometry to obtain the desired optical behaviour. Biological functionalization was performed via silane-gluteraldehyde chemistry to ensure a covalent binding of the enzyme. The optical reflectance spectrum is very sensitive to changes in the effective optical thickness. Thus, the surface modification and the trypsin immobilization were followed by monitoring the optical reflectance before and after the functionalization. The red shift in the spectra confirms the confinement of the enzyme.

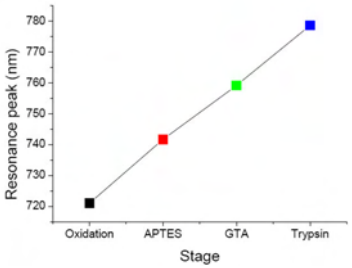

Figure 4: Red shift of the resonance peak wavelength as a result of the different functionalization stages.

This work was supported by the Spanish Ministry of Science and Innovation (MICINN) under grands Nº TEC2009-09551and TEC2012-34397, CONSOLIDER HOPE project CSD2007-00007 and AGAUR 2009 SGR 549.

References

[1] H. Ouyang, L. A. DeLouise, B. L. Miller, P. M. Fauchet, Anal. Chem, 79 (2007) 1502.

[2] Y. Shang, W. Zhao, E. Xu, C. Tong, J. Wu, Biosensors and Bioelectronics 25 (2010) 1056.

[3] A. Santos, G. Macías, J. Ferré-Borrull, J. Pallarès, L. F. Marsal, ACS Appl. Mater. Interfaces 4 (2012) 3584.

[4] E. Xifré-Pérez, L. F. Marsal, J. Ferré-Borrull, J. Pallarès, J. Appl. Phys 102 (2007) 063111.

[5] G. Palestino, V. Agarwal, R. Aulombard, E. Pérez. C. Gergely, Langmuir, 24 (2008) 13765.

Enhanced Light-to-Electron Conversion in Photoconducting Nanostructured Multilayers by Optical Field Confinement Effects

Miguel Anaya, Mauricio E. Calvo, José Miguel Luque and Hernán Míguez

Instituto de Ciencia de Materiales de Sevilla (CSIC-US), Calle Américo Vespucio 49, 41092 Sevilla, Spain

knaya38@hotmail.com

Herein we show experimental evidence of resonant photocurrent generation in dye sensitized periodically nanostructured photoconductors, which is achieved by spectral matching of the sensitizer absorption band to different types of localized photon modes present in either periodical or broken symmetry structures. Results are explained in terms of the calculated spatial distribution of the electric field intensity within the configurations under analysis.

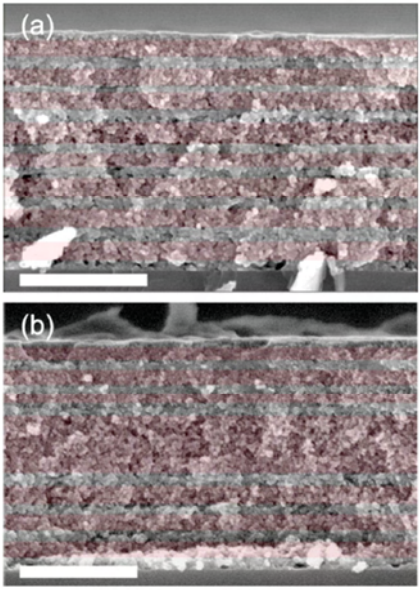

Figure 1: FESEM images of cross sections of (a) a periodic multilayer and (b) a multilayer in which a thicker middle layer has been deposited. Each type of layer has been shaded with a different color for the sake of clarity (grey, thinner lower porosity layer; purple, thicker higher porosity layer). The scale bar is 500nm in both (a) and (b).

Photo-electro-chemical devices may largely benefit from the electromagnetic field localization occurring within periodic photonic nanostructures [1]. Different studies show that both photocatalytic and photovoltaic cells improve their efficiency when such materials, capable of enhancing radiation-matter interactions at specific locations and wavelengths, are introduced [2-6]. However, proofs of concept so far reported are based on the observation of performance parameters whose improvement cannot be unambiguously linked to increased electron photogeneration resulting from optical field confinement [7-9]. The reason for this lies in the sort of materials that have been employed so far for these experiments. In some cases, the modulation of the refractive index can be realized employing different stacks of nanostructures of similar composition but with different porosity [10-14]. Such ensembles preserve the intensive properties of the bulk material and at the same time present new optical properties of structural origin. When the molded material is photoconducting, as it is the case of TiO_2 or SnO_2, then the possibility opens up to modify the spectral response of the photocurrent by means of the optical design of the multilayer. However, in lattices of uniform chemical composition and alternated porosity, the refractive index contrast is usually low, large number of periods being required in order to observe strong scattering phenomena. This has prevented the observation of clear field confinement effects on the photocurrent spectrum of photoconducting multilayers so far. Alternative approaches based on inverse opal photoconducting structures lead to photonic crystal lattices with larger dielectric contrast but high density of intrinsic defects, as the low intensity scattering related to order indicates [2, 3, 5, 15], again being difficult to relate the observed enhancement with specific photon resonances.

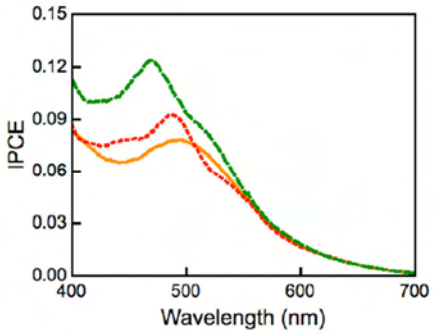

Figure 2: Incident photon to collected electron efficiency measured for a dye sensitized periodic multilayer (green dotted line), a dye sensitized multilayer in which a thicker middle layer has been deposited (red dashed line) and a nanostructured TiO_2 reference cell with no photonic properties (orange solid line).

References

[1] Chen, J.I.L.; von Freymann, G.; Choi, S.Y.; Kitaev, V.; Ozin, G.A. Adv. Mater. 2006, 18, 1915–1919.

[2] Nishimura,S.; Abrams,N.; Lewis,B.A.; Halaoui,L.I.; Mallouk,T.E.; Benkstein,K.D.; van de Lagemaat,J.; Frank,A.J.; J. Am. Chem. Soc. 2003, 125, 6306- 6310.

[3] Li, Y.; Kunitake, T.; Fujikawa, S. J. Phys. Chem. B 2006, 110,13000-13004.

[4] Ramiro-Manzano,F.; Atienzar,P.; Rodriguez,I.; Meseguer,F.; Garcia,H.; Corma,A. Chem. Commun. 2007, 242–244.

[5] Chen, H.; Chen, S.; Quan, X. ; Zhang, Y. Environ. Sci. Technol. 2010, 44, 451–455.

[6] Sordello, F.; Duca, C.; Maurinoa, V.; Minero, C. Chem. Commun. 2011, 47, 6147–6149.

[7] Mihi, A.; Míguez, H. J. Phys. Chem. B 2005, 109, 15968-15976.

[8] Halaoui, L.I.; Abrams, N.M.; Mallouk, T.E. J. Phys. Chem. B 2005, 109, 6334-6342.

[9] Chen, J.I.L.; von Freymann, G.; Kitaev, V.; Ozin, G.A. J. Amer. Chem. Soc. 2007, 129, 1196-1202.

[10] Steele, J.J.; van Popta, A.C.; Hawkeye, M.M.; Sit, J.C.; Brett, M.J. Sens. Actuators B 2006, 120, 213-219.

[11] Guo, D.L.; Fan, L.X.; Wang, F.H.; Huang, S.Y.; Zou, X.W. J. Phys. Chem. C 2008, 112, 17952-17956.

[12] Schubert, M.F.; Xi, J.Q.; Kim, J.K.; Schubert, E.F. Appl. Phys. Lett. 2007, 90, 141115.

[13] Calvo, M.E.; Colodrero,S.; Rojas, T.C.; Anta,J.A.; Ocaña, M.; Míguez,H. Adv. Func. Mater. 2008, 18, 2708-2715.

[14] Guldin,S.; Kolle,M.; Stefik,M.; Langford,R.; Eder,D.; Wiesner,U.; Steiner,U. Adv. Mater. 2011, 23, 3664-3668.

[15] Chen, X.; Ye, J.; Ouyang,S.; Kako,T.; Li,Z.; Zou,Z. ACS Nano 2011, 5, 4310–4318.

Superradiance mediated by graphene surface plasmons

V P. A. Huidobro[1], A. Y. Nikitin[2,3], C. González-Ballestero[1], L. Martín-Moreno[2] and F.J. García-Vidal[2]

[1]Departamento de Física Teórica de la Materia Condensada, Universidad Autónoma de Madrid, E-28049 Madrid, Spain
[2]Instituto de Ciencia de Materiales de Aragón and Departamento de Física de la Materia Condensada, CSIC–Universidad de Zaragoza, E-50009 Zaragoza, Spain
[3]A. Ya. Usikov Institute for Radiophysics and Electronics, NAS of Ukraine, Kharkov, Ukraine

paloma.arroyo@uam.es

As it has been recently shown, a graphene sheet can support Surface Plasmon Polaritons (SPPs) in the THz regime [1-3]. Compared to conventional SPPs in metals, the properties of graphene surface plasmons (GSP) can be tuned by means of a gate potential that modifies the conductivity of the electrons in graphene.

In our work [4], we first study the emission properties of an emitter close to a graphene sheet and, in particular, the decay through GSP. Within a certain range of distances to the graphene sheet, the decay rate of one emitter can be fully dominated by the GSP channel. Due to this efficient coupling, the enhancement of the decay rate of the emitter, known as Purcell factor, can be enhanced by several orders of magnitude.

We show that this efficient coupling to GSP can be used to tailor the interaction between two emitters. When two emitters are close to a graphene sheet a superradiant state can be achieved where the collective emission is greater than the sum of the individual emissions. Remarkably, due to graphene's properties, the interaction between the emitters can be tuned by means of a gate potential, allowing to change from subradiance to superradiance by modifying the gate. This means that the coupling between the emitters can be strongly enhanced or supressed. Moreover, we also study the interaction between two emitters mediated by one-dimensional (1D) graphene ribbons supporting waveguide modes [5], which provide a very efficient coupling between the two emitters

For both the two-dimensional (2D) graphene sheets and the 1D graphene ribbons, we investigate the super- and subradiant regimes in the reflection and transmission configurations. Importantly, the length scale of the coupling between emitters, which in vacuum is fixed by the free-space wavelength, is now determined by the wavelength of the GSP, which can be extremely. Additionally, confinement in 2D or 1D results in an interaction with a larger decay length as compared to interaction in free-space.

References

[16] A. H. Castro Neto, F. Guinea, N. M. R. Peres, K. S. Novoselov, and A. K. Geim, Rev. Mod. Phys., 81 (2009) 109.
[17] M. Jablan, H. Buljan, and M. Soljaci´c, Phys. Rev. B, 80 (2009) 245435.
[18] A. A. Dubinov, V. Y. Aleshkin, V. Mitin, T. Otsuji, and V. Ryzhii, J. Phys. Condens. Matter, 23 (2011) 145302.
[19] P. A. Huidobro, A. Y. Nikitin, C. González-Ballestero, L. Martín-Moreno and F. J. García-Vidal, Phys. Rev. B, 85 (2012) 155438.
[20] A. Y. Nikitin, F. Guinea, F. J. García-Vidal, and L. Martín-Moreno, Phys. Rev. B (R), 84 (2011) 161407.

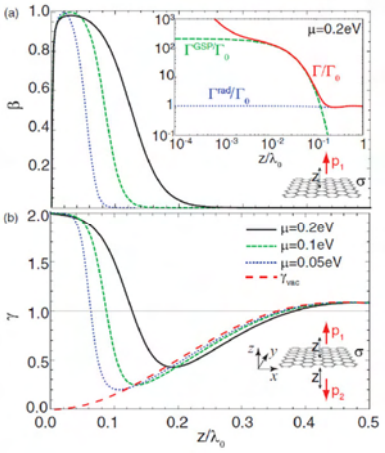

Figure 1: (a) β factor for an emitter at ν = 2.4 THz as a function of the distance to the graphene sheet, z. Inset panel: total decay rate and decay rates through the plasmonic and radiative channels. (b) Tuning superradiance between two emitters mediated by a graphene sheet by means of the chemical potential. The emitters are placed in a transmission configuration.

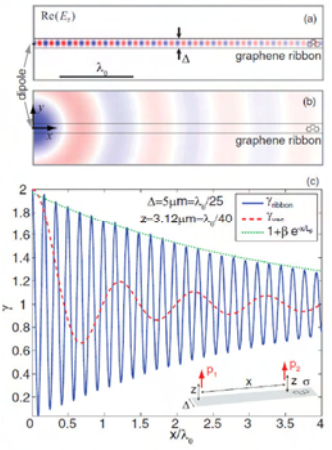

Figure 2: Interaction between two emitters mediated by 1D graphene ribbons. (a)–(b) Electric field profile for a dipole decaying to the ribbon GSP. The dipole is placed at x = 0, y = 0, and z = λ_0/40 in panel (a) and at z = λ_0/10 in panel (b) [the same would be obtained for z >λ_0/10]. (c) Superradiance mediated by the ribbon-GSP mode shown in panel (a). The dotted green line shows the exponential decay of the interaction.

Near-field study of localized and extended surface plasmon resonance on gold nanoislands

R. Bernardo-Gavito[1,2], A. Serrano[3,4], M.A. García[3], R. Miranda[1,2,5] and D. Granados[2]

[1]Dpto. Fís. de la Materia Condensada, UAM, Facultad de Ciencias, Madrid, Spain
[2]Fundación IMDEA Nanociencia, Faraday 9, Madrid, Spain
[3]Instituto de Cerámica y Vidrio (ICV-CSIC), Madrid, Spain
[4]Dpto Física de Materiales, UCM, Madrid, Spain
[5]Instituto de Ciencia de Materiales "Nicolás Cabrera", Facultad de Ciencias, Madrid, Spain.

ramon.bernardo@uam.es

We present a study of localized and extended surface plasmons on size-tunable gold nano-islands by scanning near-field optical microscopy (SNOM). The gold nanoislands are self-assembled by a thermal annealing process of an Au thin film. The morphology and density of the nanoislands can be controlled by modifying the initial thickness of the Au thin film and the thermal treatment conditions [1].

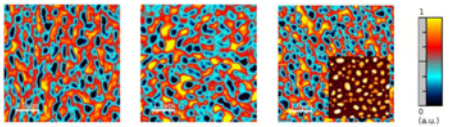

Figure 1: 5umx5um SNOM images of three different samples of gold nanoislands annealed at 300°C, 400°C and 500°C (left to right). Inset: 2.5umx2.5umAFM topography of the corresponding sample.

A surface plasmon (SP) resonance is a collective oscillation of the conduction electrons in a metallic-dielectric interface. It leads to a huge absorption cross-section at a specific frequency. SPs behave as travelling charge waves in the interface between a dielectric and a noble metal film (extended SPs), or can be spatially confined in the boundaries of nanoparticles (localized SPs). Localized SPs in nanoparticles can be easily excited by incoming light, leading to an easily recognizable peak in a routine absorbance spectrum. On the other hand, extended SPs require special matching techniques in order to be coupled to light. While this can be done in different ways, the only method capable of giving local information on the nanoscale is near-field coupling, in which a SNOM tip is used as a surface plasmon point source [2].

In this work we present a systematic study of gold nanoislands fabricated under different annealing temperatures or initial Au thin film thickness. We use SNOM to show how the surface plasmon behavior depends on the islands size and inter-particle distance. We will also show preliminary results on SNOM spectroscopy. Our aim is to understand the SP resonance frequency shifts and find the frontier between localized and extended surface plasmons.

References

[1] A. Serrano, O. Rodríguez de la Fuente, and M. A. García, Journal of Applied Physics 108, 074303 (2010).

[2] S. A. Maier, Plasmonics, Fundamentals and Applications (Springer Science+Bussines Media LLC, New York, 2007), pp. 39-50.

Increased sensitivity of delay-interferometer receiver for 10G DPSK for SOI platform

M. Aamer[1*], A. Griol[1], **A. Brimont**[1], A. M. Gutierrez[1], P. Sanchis[1], and A. Håkansson[2]

[1]Nanophotonics Technology Center, Universitat Politecnica Valencia, Camino de Vera s/n, 46022, Valencia, Spain
[2]DAS Photonics, Camino de Vera s/n Ed 8F 2ª pta, 46022 Valencia, Spain

*maaa@ntc.upv.es

Differential-phase-shift-keyed (DPSK) format exhibits several advantageous qualities [1]. It enables 3-dB improved receiver sensitivity with balanced detection, and has higher tolerance to nonlinear degradation if compared with OOK. The detection of the phase at the receiver can either be implemented using coherent or differential (non-coherent) detection. A coherent receiver uses carrier tracking by phase-locked loops to estimate the absolute phase, while in differential encoded PSK the information is in the phase transition and can be demodulated using a passive delay-interferometer. The simplicity of the differential detection and the elimination of a local oscillator (LO) and digital signal processor (DSP) makes differential detection advantageous for low cost links. However this comes with a loss, the differential detection has an intrinsic lower sensitivity of approximately 2dB [2]. Moreover, if the receiver isn't well balanced further losses in sensitivity could be produced.

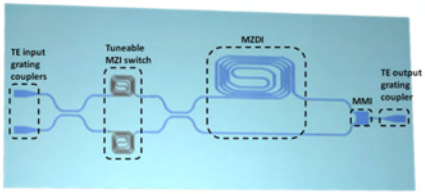

Figure 1: Schematic of the proposed DPSK demodulator. From left to right in the figure: Two input TE grating couplers with waveguide tapers, 2x2 unbalanced MZI switch, MZDI with a 10GHz delay-line, a 2x1 MMI, taper, and an output grating coupler.

As a technological platform, SOI presents a low-cost and compact solution for mass-production of highly integrated photonic devices and has shown good potential for implementing various formats of DPSK demodulation [3-9]. The small bending radius of about 5 microns, alongside the monolithic integration of Ge photo detectors by using CMOS compatible process makes this technology very attractive for low-cost differential receivers. Specifically in access networks at lower data speeds, such as 5Gbps or 10Gbps. Also, by implementing a polarization diversity scheme [3], the TE and TM polarization can be completely separated and processed individually in order to deal with problems such as polarization dependent loss.
Mainly two designs of the SOI receiver have been addressed in the literature, either using more standard MZDI [3-5] or by using micro ring-resonators [6-9]. There are mainly two advantages of using a ring resonator in the demodulation circuit; the size and the tolerance in bit-rate deviation. However, the optimal performance is reached for an optimized Q-factor and at the same time maximized extinction ratio, which usually requires adding some tuning mechanism as in [10] and therefore increases power consumption and complexity. MZDI still seems to be the most used implementation in more complete system such as presented in [4,5].

In this paper we demonstrate a simple approach to enhance the sensitivity of a MZDI while at the same time minimizing the power consumption by using wavelength tuning. The standard implementation of the MZDI suffers from unbalanced performance due to the propagation losses in the delay line. We here achieve optimized performance by modifying the input to a SOI 10Gbps DPSK differential receiver. We also show how the footprint can drastically be reduced by using compact spirals and so minimize the size of the receiver to just a few times larger than a ring resonator based implementation.

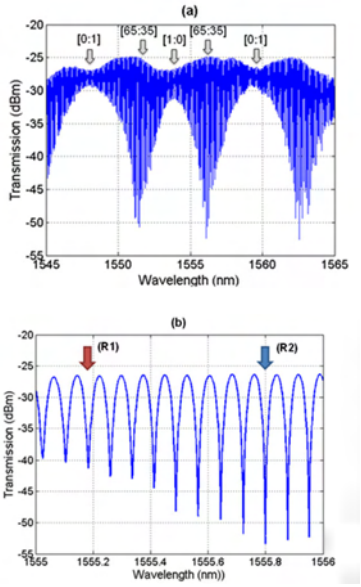

Figure 2: Measured spectral response at the DPSK demodulator. (a) Transmission spectrum of the full experimental wavelength band. The arrows mark the different states of the MZI switch at the input of the MZDI. (b) A zoom with 1pm resolution on the wavelength range where resonances have higher ER ratio. Two resonances are marked in the figure R1 for 16dB ER and R2 with optimized 28dB ER.

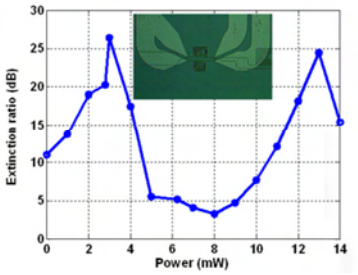

Figure 3: ER variation for different powers applied to the micro-heater on the MZI switch. The inset shows an optical image of the microheaters on top of the MZI switch

References

[1] A. H. Gnauck and P. J. Winzer, "Optical phase-shift-keyed transmission," J. Lightwave Technol., vol. 23, pp. 115-130, 2005.

[2] J. Proakis and M. Salehi, Dig. Comm. (2008)

[3] C. R. Doerr, L. Chen, B. Labs, and H. Road, "Monolithic PDM-DQPSK receiver in silicon," 36th European conference and Exhibition on Optical Communication (ECOC), p1-3, 2010

[4] C. R. Doerr, N. Fontaine, L. Buhl, "PDM DQPSK silicon receiver with integrated monitor and minimum number of controls," IEEE Photon. Technol. Lett., vol. 24, no. 8, pp. 697-699, Apr. 2012.

[5] K. Suzuki, H. C. Nguyen, T. Tamanuki, F. Shinobu, Y. Sakai, and T. Baba, "Slow-light-based variable symbol-rate silicon photonics DQPSK receiver," Optics Express, vol. 20, no. 4, pp. 4796-4804, 2012.

[6] L. Zhang et al., "Microring-based modulation and demodulation of DPSK signal," Optics express, vol. 15, no. 18, pp. 11564-9, Sep. 2007.

[7] S. Park et al., "Demodulation of 10-Gbps DPSK signals with silicon micro-ring resonators," 23rd Annual Meeting of the IEEE Photonics Society, pp. 264-265, 2010.

[8] L. Xu, C. Li, C. Y. Wong, and H. K. Tsang, "DQPSK demodulation using integrated silicon microring resonators," Optics Communications, vol. 284, no. 1, pp. 172-175, Jan. 2011.

[9] Y. Ding et al., "Multi-Channel 40 Gbit/s NRZ-DPSK Demodulation Using a Single Silicon Microring Resonator," Journal of Lightwave Technology, vol. 29, no. 5, pp. 677-684, Mar. 2011.

[10] L. Chen, N. Sherwood-droz, and M. Lipson, "Compact bandwidth-tunable microring resonators," Optics Letters, vol. 32, no. 22, pp. 3361-3363, 2007.

Magneto-optical properties of nanostructured ferromagnetic films mediated by surface plasmon polaritons

Blanca Caballero[1,2], J. C. Cuevas[2], A. García-Martín[1], E. Melander[3], E. Östman[3], J. Keller[3], J. Schmidt[3], E.Th. Papaioannou[3], V. Kapaklis[3], U.B. Arnalds[3] and B. Hjörvarsson[3]

[1]IMM-Instituto de Microelectrónica de Madrid (CNM-CSIC), Isaac Newton 8, PTM, Tres Cantos, E-28760 Madrid, Spain;
[2]Departamento de Física Teórica de la Materia Condensada, Universidad Autónoma de Madrid, 28049, Madrid, Spain
[3]Department of Physics and Astronomy, Uppsala University, Box 516, SE-751 20 Uppsala, Sweden

blanca.caballero@imm.cnm.csic.es

Magneto-optics offers unique possibilities to manipulate light by making use of an external magnetic field. Recently, this research area has benefited a lot from the connection to the field of plasmonics, producing novel ways of manipulating light at the nanoscale [1]. The main idea is based around using nanostructures made of magnetic materials that simultaneously support plasmon excitations. This can concentrate light in reduced volumes, resulting in an amplification of the electric field, which in turn enhances the magneto-optical response. This increase of the magneto-optical signals, in particular of the Kerr and Faraday effects, paves the way for new applications, for instance, in sensing and biosensing devices [2].

One particular case of interest is the transverse magneto-optical Kerr effect (TMOKE) in periodically patterned ferromagnetic nanostructures. We choose ferromagnetic metals for our research since they combine both, plasmon resonances and magneto-optical activity. In particularly, we focus on the study of hexagonal anti-dot array systems in transverse configuration for Fe [3,4] and Ni [5] (Figs. 1a and 2a). In both cases, experiments show an enhancement of the TMOKE signal, likely mediated by the excitation of surface plasmon polaritons (SPPs). We prove this to be the case, and reproduce quite accurately the experimental results by making use of the dedicated scattering matrix formalism aimed to describe magneto-optical systems for arbitrary orientation of the sample magnetization [4].

In Figs. 1b and 2b the calculated reflectivity and TMOKE are presented, where the dashed lines correspond to the resonant conditions for SPPs. A clear correlation between reflectivity minima and TMOKE maxima and plasmon excitations can be observed.

References

[1] G. Armelles, A. Cebollada, A. García-Martín, J.M. García-Martín, M.U. González, J.B. González-Díaz, E. Ferreiro-Vila, and J.F. Torrado, J. Opt. A: Pure Appl. Opt., 11 (2009) 114023.
[2] B. Sepúlveda, A. Calle, L. M. Lechuga, and G. Armelles, Opt. Lett., 31, (2006) 1085
[3] J. F. Torrado, E. Th. Papaioannou, G. Ctistis, P. Patoka, M. Giersig, G. Armelles, and A. Garcia-Martin, Phys. Status Solidi (RRL), 4, (2010) 271
[4] B. Caballero, A. García-Martín, and J.C. Cuevas, Phys. Rev. B, 85 (2012) 245103.
[5] E. Melander, E. Östman, J. Keller, J. Schmidt, E.Th. Papaioannou, V. Kapaklis, U.B. Arnalds, B. Caballero, A. García-Martín, J.C. Cuevas, and B. Hjörvarsson, Appl. Phys. Lett., 101 (2012) 063107.

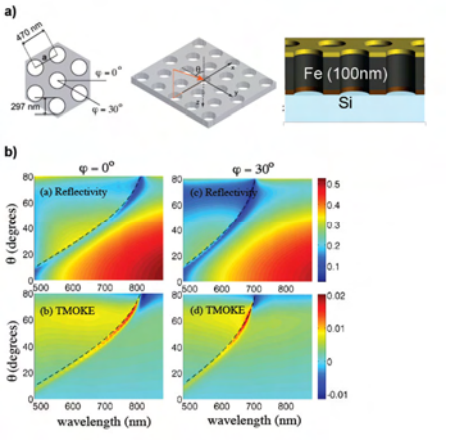

Figure 1: Fe

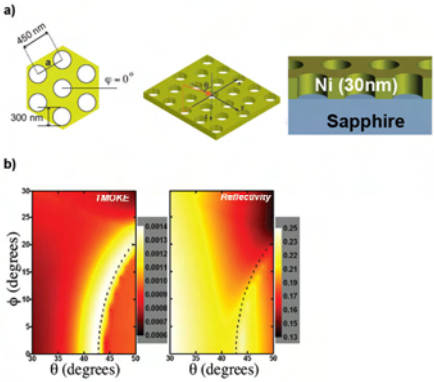

Figure 2: Ni

Novel approaches to ultraviolet radiation protecting thin films based on nanoparticle multilayers

J.R. Castro Smirnov, Mauricio E. Calvo and Hernán Míguez

Instituto de Ciencia de Materiales de Sevilla,
Consejo Superior de Investigaciones Científicas-Universidad de Sevilla,
Américo Vespucio 49, 41092, Seville, Spain.

jrcastro@icmse.csic.es

Herein we introduce a novel porous one-dimensional photonic crystal with strong reflectance in the ultraviolet (UV) region of the electromagnetic spectrum. These periodic nanostructures are built by spin-coating assisted layer by layer deposition of colloidal suspensions of non UV absorbing nanoparticles of ZrO_2 and SiO_2 (electronic band gap at λ<220 nm). The UV shielding effect takes place totally from optical interference phenomena and is related with the number of deposited layers and the difference of the refractive index values of the two materials that form the unit cell. Interference filters are designed consequently to block specific wavelength ranges in UVA, UVB and UVC regions of the electromagnetic spectrum. In addition, we show that the accessible pore network of the as-deposited multilayer allows preparing flexible, self-standing, selective UV filters without losing considerably reflectance intensity, i.e., preserving the dielectric contrast. We prove that these films outperform layers of similar thickness made of only absorbing materials in terms of the degree of radiation protection achieved.

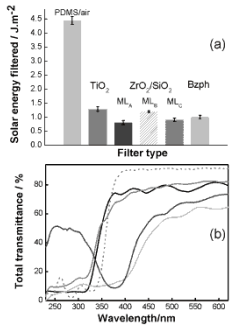

Figure 1: (a) Energy received by identical UV sensitive strips covered with different flexible protective films. Height of the bar represents the media value, black line represents the standard deviation. MLA , MLB , MLC belong to different ZrO_2 /SiO_2 films. (see figure 6b)(b) Total transmittance spectra of the protecting films used in Figure 6a. TiO_2 (black solid line), MLA (light gray solid line), MLB (grey solid line), MLC (dark grey solid line),benzophenone-3 (grey short dashed line).

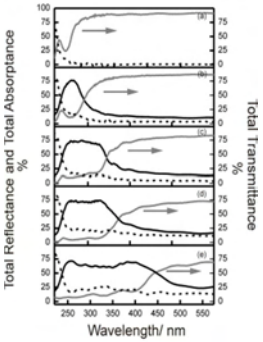

Figure 2: Total reflectance (black solid line), total transmittance (grey solid line) and absorptance (black dotted line) spectra of stacking flexible films prepared from samples shown in figure 4a. The number of stacking samples is 1 (a), 2 (b), 3 (c), 5 (d) and 7 (e). (black solid line), MLA (light gray solid line), MLB (grey solid line), MLC (dark grey solid line),benzophenone-3 (grey short dashed line).

References

[1] M.E. Calvo, J.R. Castro Smirnov, H. Miguez, J. Pol. Sci part B: pol.Phys, 50, (2012), 945.
[2] M.E. Calvo, H. Miguez, Chem. Mater., 22, (2010), 3909–3915.

Angle emission properties of complex colloidal nanostructures for energy efficiency applications

A. Coll[1], D. Hernández[1], S. Bermejo[1], A. Blanco[2], J. F. Galisteo-López[2], C. López[2], L. Castañer[1] and R. Alcubilla[1]

[1]Universitat Politècnica de Catalunya, Jordi Girona 1-3, 08034 Barcelona, Spain
[2]ICMM-CSIC, Sor Juana Inés de la Cruz, 3, Cantoblanco, 28049 Madrid, Spain

arnau.coll@upc.edu

The optical properties of ordered colloidal structures, or colloidal crystals, have been studied for more than 20 years due to their unique control of the propagation of visible light through it [1]. One of the most representative properties of these 3D periodic structures is their ability to forbid the transmittance of frequency bands through the crystal, making these wavelengths to reflect back whichever the incident angle. On the other hand, 2D nanostructures and gratings have been analyzed in a lot of different applications [2], showing their ability to affect the light in single incoming angles.

The purpose of this work is to study the effects of "coupling" different types of gratings on 3D colloidal crystals, looking for both an angle selective and frequency selective propagation of light across the nanostructure. 3D polystyrene colloidal crystals were made using an Electrospray deposition technique [3] which consists in a pump that introduces the colloidal solution into a needle electrically polarized. The sample is also polarized with an opposite signal to attract the droplets formed in the needle's tip.

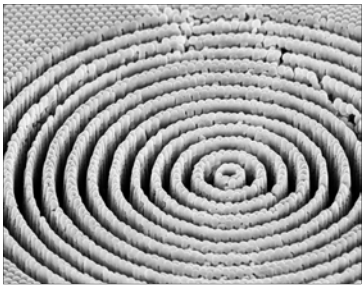

Figure 1: 2D grating milled on top of a 3D electrosprayed colloidal crystal.

The structures were made using 360nm polystyrene nanobeads. This crystal's parameters produce a reflectivity peak around 900-950nm wavelength. Within these samples, some 2D structures were milled using a Focused Ion Beam, an example is shown in figure 1. This first tested structure consists in concentric circles of 500nm periodicity and 1 µm depth.

In order to measure the reflectivity of these photonic structures, samples were placed close to an optic fiber of 5µm, reading the reflectivity in the visible spectrum (up to 1□m wavelength) in function of angle. The method used to measure the optical properties of the samples is based in Fourier imaging spectroscopy [4]. Results of the measurements are shown in figure 2.

References

[1] E. Yablonovitch and T.J. Gmitter, Physical Review Letters, 58 (1987) 2059.
[2] C. Palmer and E. Loewen. Diffraction Grating Handbook. (2005)
[3] S.Bermejo, A.Coll, L.Castañer: "Procedimiento para el depósito ordenado de capas de metamateriales a partir de soluciones coloidales de micro o nano esferas" Patent PCT/ES2012/070476
[4] M. López-García; J. F. Galisteo-López,; C. López. Angle and polarization resolved optical characterization of photonic structures through Fourier imaging spectroscopy. Submitted for publication.

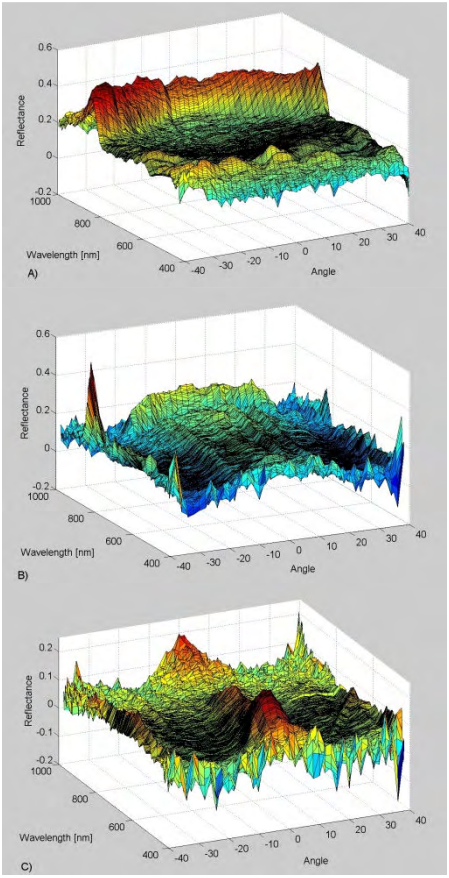

Figure 2: Reflectance measurements of the 3D colloidal structure (a) compared with reflectance at the edge (b) and center (c) of the FIB patterned grating shown in Fig. 1.

Nanocomposite based on gold nanoparticles embedded into ZnO films

Diana Fragua[1*], Rafael Abargues[2], Esteban Pedrueza[1] and Juan P. Martinez-Pastor[1]

[1]UMDO (www.uv.es/umdo), Instituto de Ciencia de los Materiales, Universidad de Valencia, PO Box 22085, 46071 Valencia, Spain
[2]Intenanomat S.L., Catedrático José Beltrán 2, 46980 Paterna, Spain

diana.fragua@uv.es

Metal-dielectric nanocomposites have attracted much attention in the last years because is a very promising approach towards multifunctional materials since they combine the unique electromagnetic properties of noble metal nanoparticles (NPs) with the characteristics of polymeric or metal-oxide host matrices [1,2]. As a result, nanocomposite thin films show high potential in diverse fields such as sensing [2] and photovoltaics [3], as many other. The control of the size and shape of NPs as well as their concentration and distribution within the host solid matrix is compulsory to achieve high-performance multifunctional materials for most of these applications.

Among the existing metal oxide matrices, ZnO has received enormous interest, because it exhibits various superior properties applicable to devices, such as wide direct band gap, large exciton binding energy, high optical transparency in the visible range, good electrical conductivity and piezoelectricity. Thus it has been widely used as a transparent electrode in optoelectronic devices, resistive gas sensors and SAW devices [4]. In this work we report on a novel sol-gel method for the synthesis of a nanocomposite based on Au NPs embedded into ZnO thin films. The procedure consists of spincoating an aqueous solution of $Zn(CH_3COO)_2$ and $HAuCl_4$ followed by a thermal annealing above 300 °C for several minutes (Figure 1). Both ZnO and Au NPs are synthesized in-situ during the hard bake. Film thickness and density of NPs in the resulting nanocomposite can be controlled by the concentration of the precursors in the wet process. Figure 2a shows the optical characterization of ZnO and Au-ZnO thin films. ZnO films show an absorption band at 362 nm, attributed to the exciton absorption peak, which corresponds to a bandgap energy of ≈3.4 eV (deduced by using an appropriate excitonic model for this direct gap semiconductor). On the other hand, the Au-ZnO nanocomposite nanocomposite exhibits two bands at around 350 and 553 nm, which are associated to the exciton absorption of ZnO (with a similar bandgap energy) and the localized surface plasmon resonance due to the presence of Au NPs, respectively. Therefore, ZnO conserves its intrinsic structural (demonstrated by X-Ray diffraction not shown here) and optical properties after the introduction of Au NPs in the film. A similar observation can be said with respect to the case of the electrical properties (Figure 2b): the conductivity of ZnO layers was found to be around 0.24 S/cm, whereas that of Au-ZnO films decreased by a factor two, may be due to a reduction of free carriers at ZnO grains or to an increase of potential walls at grain boundaries. The presence of Au NPs is clearly confirmed by TEM (Figure 3a), being their size around 40-60 nm in diameter, depending on the precursor concentration and baking temperature. We also observed a nanostructuring of the ZnO surface (see the SEM image in Figure 3b), in this case attributed to an average surface roughness (grain size) of ZnO of the order of 50 nm.

This work was supported by the EU-FP7 project NANOPV and the project PROMETEO/2009/074 from the Generalitat Valenciana.

References

[1] Pedrueza, E.; Valdés, J. L.; Chirvony, V.; Abargues, R.; Hernández-Saz, J.; Herrera, M.; Molina, S. I.; Martínez-Pastor, J. P. Adv. Funct. Mater. 2011, 21, 3502.

[2] Gradess, R.; Abargues, R.; Habbou, A.; Canet-Ferrer, J.; Pedrueza, E.; Russell, A.; Valdes, J. L.; Martinez-Pastor, J. P. J. Mater. Chem. 2009, 19, 9233.

[3] Atwater, H. A,; Polman, A. Nat. Mater. 2010, 9, 205.

[4] Özgür, U.; Hofstetter, D.; Morkoç, H. Proceedings of the IEEE 2010, 98, 1255.

Figure 1: Procedure of the synthesis of Au-ZnO nanocomposite thin film.

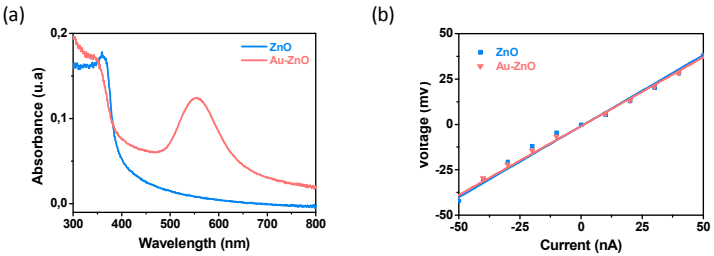

Figure 2: Optical and electrical characterization. a) UV-Vis spectra and of b) V-I Curve of ZnO and Au-ZnO films.

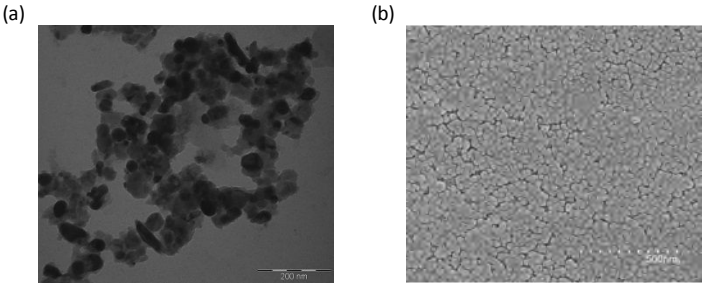

Figure 3: TEM (a) and SEM (b) images of Au-ZnO nanocomposite thin film.

Parabolic antennae at telecommunication infrared wavelengths

L. S. Froufe-Pérez,
R. Paniagua-Domínguez and
J. A. Sánchez-Gil

Instituto de Estructura de la Materia (CSIC),
Serrano 121, 28006 Madrid, Spain

Luis.froufe @ iem.cfmac.csic.es

Perhaps the most important wavelength interval in the IR is spanned in the range 1260nm – 1675nm because it is used in telecommunications. Hence, developing efficient compact highly directional antennas in this regime have a potential impact in the telecommunications industry [1].

In this regard, Silicon submicron-sized particles have attracted a lot of attention in recent years [2,3]. Silicon or Germanium, among other semiconductors widely used in the microelectronics industry, present a large refractive index and low absorption in the near IR. Hence, Semiconductors are particularly suitable materials to form the basis of new nano and micro devices in the near IR.

Altough well known, Mie scattering theory [4] is somehow being rediscovered. There are several reasons for this. On the one hand, microfabrication techniques allow for a fine control on the production of massive amounts of monodisperse Si particles with prescribed dimensions [5]. On the other hand, assembly of different materials or compound micro and nano devices is also possible and relatively affordable in a conventional laboratory and, even, can be thought to be transferred to industrial production factories [6].

Appropriate combinations of different semiconductor spherical particles have been recently proven to be excellent Yagi-Uda Antennas. In particular, these assemblies of particles present strong directionality in the angular scattering pattern [7]. Also, placing a single emitter between the reflector and the first director of the antenna, the radiation emission pattern can be strongly directional [8].

Following the conventional approach of tailoring well known concepts in the radiowave regime to the optical and IR one, we propose a parabolic antenna made of submicron sized silicon particles.

In this work we show that the parabolic microantenna present a strong directionality (ratio of the maximum power emitted divided by the average one) and low backward emission in a wide range of wavelengths. Actually this range covers 5 of the 6 more widely used bands in IR telecommunications.

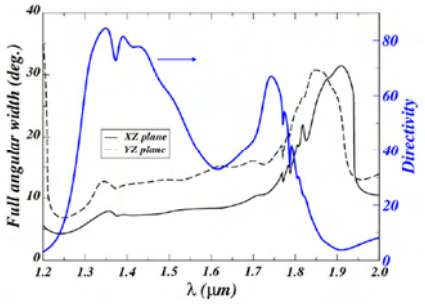

Figure 1: Full angular width and directivity of a parabolic antenna made of ~100 Si spherical particles or radius 250nm.

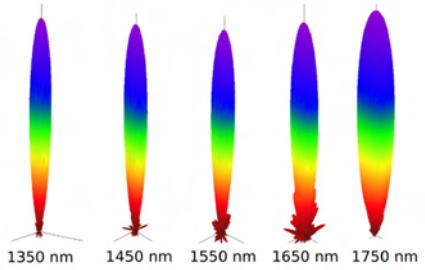

Figure 2: Emission patterns of the system emitter-antenna at different wavelengths (indicated in the legends). The emitter is a point dipole source placed at the parabola focus. The dipole points perpendicular to the emission patterns.

In figure 1 we show the spectral dependence of the directionality of the parabolic antenna (right scale), as well as the full angular width of the radiation pattern (left scale). As can be seen in this figure, the directionality varies by a factor ~2, while the angular spreading remains below 15 degrees in a wide frequency band.

In order to better illustrate this behavior, we present in fig. 2 the 3D angular spectrum of radiation for several wavelengths. It is pretty clear from these plots that the antenna behaves reasonably well in a wide band covering the telecommunications rage.

Interestingly, the angular radiation patterns are quite insensitive to the orientation of the emitter (placed at the focus of the parabola). This behavior is rather different to what is expected in other antenna configurations.

References

[1] P. Biagioni et al., Rep. Prog. Phys. 75 (2012) 024402.

[2] A. García-Etxarri et al., Opt. Express 19 (2011) 4815.

[3] A. I. Kuznetsov et al. Sci. Rep. 2 (2012) 492.

[4] C. F. Bohren and D. R. Huffman, Absorption and Scattering of Light by Small Particles (John Wiley &Sons, 1998).

[5] M. Ibisate et al., Adv. Mat. 21 (2009) 2899; Lei Shi et al.,ibid doi:10.1002/adma.201201987 (2012).

[6] J. F. Galisteo-López et. al., Adv. Mat. 23 (2011) 30.

[7] W. Liu et al. , ACS Nano 6 (2012) 5489.

[8] A. E. Krasnok et al., Opt. Express 20 (2012) 20599.

Photoinduced Local Heating in Silica Photonic Crystals for Fast and Reversible Switching

Francisco Gallego-Gómez,
Álvaro Blanco and Cefe López

Instituto de Ciencia de Materiales de Madrid,
ICMM (CSIC),
c/ Sor Juana Inés de la Cruz 3,
28049 Madrid, Spain.

francisco.gallego@icmm.csic.es

A number of strategies have been proposed in order to achieve tunable photonic bandgaps in photonic crystals. Many of them imply filling of the voids of the photonic crystal with photo-, thermo- or electroresponsive systems like liquid crystals, isomerizable materials, hydrogels, etc., which generally is complicated and costly, and with slow response.

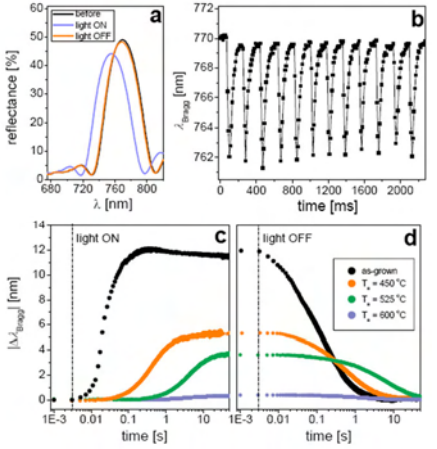

Figure 1: (a) Bragg reflectance peak of a dye-infiltrated as-grown silica opal before, under photoirradiation (for 200 ms) and after relaxation (for 2 s). (b) Modulation of λ_{Bragg} by photoswitching (laser on/off in 30/150 ms periods). Spectra were measured every 10 ms. (c, d) Temporal evolution of $|\Delta\lambda_{Bragg}|$ in infiltrated as-grown (black symbols) and annealed (at 450, 525 and 600 ºC; orange, green and blue lines) opals. The laser was turned on/off 2 ms after beginning the measurement (denoted by the dashed lines). In all cases, photoirradiation was performed on an area of 0.002 mm^2 at intensity of 20 W cm^{-2}.

We demonstrate [1] that just the inherent presence of adsorbed water in an artificial silica opal can be used for rapid and reversible switching of its photonic bandgap. Therefore, we provoked local heating by photoirradiating the opal, dyed with an absorbing chromophore, with a focused 488-nm laser, which induced fast evaporation of the water adsorbed between the opal spheres. As a consequence, the bandgap exhibited fast and highly reproducible shifts to shorter wavelengths. The effect was fully reversed without active cooling as water from the surrounding moisture was quickly readsorbed by the silica, which enabled efficient photoswitching of the photonic bandgap. The overall performance dramatically worsened in hydrophobic (thermally annealed) silica opals (Figure 1).

The observed effect on the bandgap was consistent with previous reports in which water was desorbed by heating the opal on a hot plate [2,3]. As an essential advantage of this approach, the laser-induced opal heating led to fast heating rates that enabled pronounced water desorption in milliseconds (unreachable by standard means), followed by spontaneous and rapid heat dissipation through the non-irradiated structure. The localized photoabsorption of the focused laser enabled such efficiency of both thermal concentration –leading to fast heating– and posterior thermal dissipation –as the opal acts as thermal reservoir regarding the small hot spot. In fact, the performance strongly enhanced by decreasing the photoirradiated opal volume, allowing bandgap shifts of 12 nm and response times of 20 milliseconds. The energy dissipation through the structure compromised the localization of the photoinduced heat, so some bandgap change was observable even at distances of 1.5 millimeter. However, the response times drastically decreased and the local character of the effect was basically preserved (Figure 2).

This very simple and cost-effective approach provides fast switching means in conventional silica photonic crystals, promising an inexpensive solution for a number of applications. This methodology also opens the possibility to study dynamic sorption phenomena.

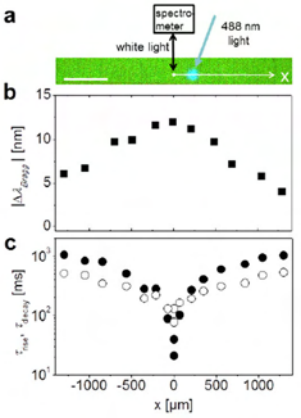

Figure 2: Local nature of the photoinduced PBG changes tested by displacing the irradiation spot from the measurement point a distance *x*. (a) Optical microscope image of the opal under 488 nm laser excitation (lighter spot); scale bar is 500 μm. Scheme of the setup and the defined *x*-axis were added. The white circle denotes the point at which the opal PBG was measured (area of ~ 20 μm^2). (b) *x* dependence of $|\Delta\lambda_{Bragg}|$ and (c) rise and decay half-times. Experiments were performed on an area of 0.002 mm^2 at intensity of 20 W cm^{-2} in an infiltrated as-grown opal.

References

[1] F. Gallego-Gómez, Á. Blanco, C. López, Adv. Mater. (2012), DOI: 10.1002/adma.201202828.

[2] F. Gallego-Gómez, Á. Blanco, V. Canalejas-Tejero, C. López, Small 7 (2011), 1838.

[3] F. Gallego-Gómez, Á. Blanco, C. López, J. Phys. Chem. C 116 (2012), 18222.

Water-Dependent Micromechanical and Rheological Properties of Silica Colloidal Crystals Studied by Nanoindentation

Francisco Gallego-Gómez[1], Víctor Morales-Flórez[2], Álvaro Blanco[1], Nicolás de la Rosa-Fox[3] and Cefe López[1]

[1]Instituto de Ciencia de Materiales de Madrid, ICMM (CSIC), Madrid, Spain
[2]Instituto de Ciencia de Materiales de Sevilla, ICMS (CSIC-Univ. Sevilla), Sevilla, Spain
[3]Departamento de Física de la Materia Condensada, Univ. Cádiz, Cadiz, Spain

francisco.gallego@icmm.csic.es

Solid colloidal crystals (CCs) have many applications in *e.g.* photonics, energy conversion, sensing and as templates, for which diverse mechanical requirements are mandatory, so that the study of issues like the stability against deformation is essential. They are also used for modeling of atomic systems, where mechanical features may impart relevant information. However, mechanical testing of CCs is not well-established and very little is known about their mechanical properties and governing factors.

We show the suitability of nanoindentation to study in detail the micromechanical response of CCs made of bare (without extrinsic ligands) submicrometer silica spheres [1]. The sensitivity to displacements smaller than the spheres size, even resolving discrete events and superficial features, revealed particulate features with analogies to atomic crystals (Figure 1). Significant robustness, long-range structural deformation and large energy dissipation were found. In silica CCs, the hydrophilic character of the particles leads to the presence of abundant physisorbed water (about 8 wt. %), and capillarity becomes relevant as water forms liquid bridges, which anticipates a link to wet granular matter. Experiments on heated opals (up to 150 °C), in which the water content was easily controlled, elucidated the influence of capillary cohesion on the mechanical strength (Figure 2). Rate-dependent nanoindentation revealed that the adsorbed water endowed silica CCs with properties of wet granular materials like viscoplasticity (Figure 3). A novel 'non-granular' CC was fabricated by substituting capillary bridges with silica necks to directly test non-water-dependent mechanical response. Silica CCs, as specific (nanometric, ordered) wet granular assemblies with well-defined configuration, may be useful model systems for granular science and capillary cohesion at the nanoscale.

References

[1] F. Gallego-Gómez, V. Morales-Flórez, Á. Blanco, N. de la Rosa-Fox, C. López, Nano Letters, 12 (2012) 4920–4924.

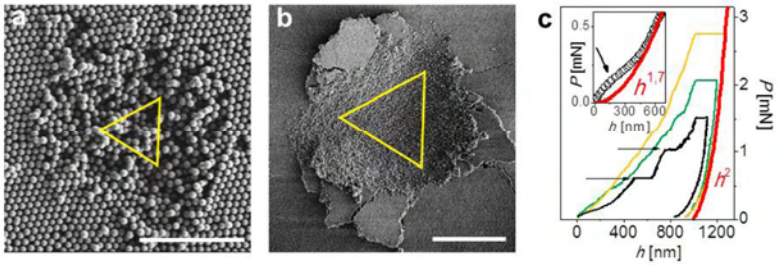

Figure 1: (a, b) SEM micrographs of residual indents at h_{max} = 500 and 4600 nm (scale bars are 5 and 20 µm), respectively. Yellow triangles delimit the intersection areas of the Berkovich indenter (at maximum penetration h_{max}) with the surface plane. (c) Typical load-depth curves with h_{max} = 1000 nm performed at different load rates (5, 50 and 500 µN/s –black, green and orange lines, respectively). Two pop-in events, designated by arrows, are visible at the lowest rate. Inset: zoom-in of the loading curve at early penetration stage (rate of 50 µN/s); the arrow indicates a characteristic initial displacement burst. Red curves are fitting power-law functions.

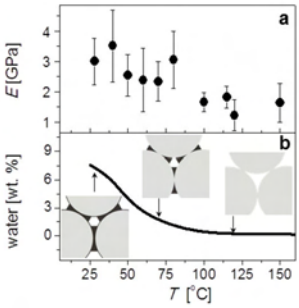

Figure 2: Temperature-dependence of the Young modulus E (a) measured at h_{max} = 600 nm, and content of adsorbed water in the CC (b). Sketches in (b) depict the distribution of water (black) between the opal spheres (gray) at T = 28, 70 and 120 °C (proportions are maintained).

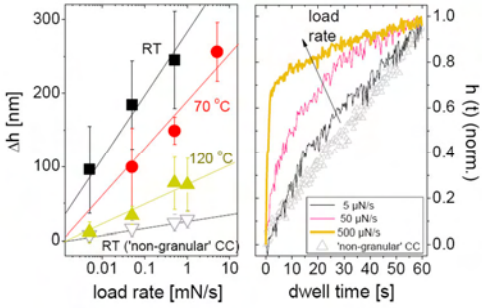

Figure 3: (a) Creep displacement Δh after dwell time of 60 s as function of the load rate (symbols) and linear fits (lines), measured in CCs at RT, 70 and 120 ºC, and in the modified, 'non-granular' CC (at RT). (b) Normalized transient creep h (t) measured at RT in CCs at 5, 50 and 500 µN/s and in the modified CC (at 50 µN/s). All experiments were performed at constant load P = 1.5 mN.

High magneto optical activity and low optical losses in metal–dielectric Au/Co/Au-SiO_2 magnetoplasmonic nanodisks

J.C. Banthí, D. Meneses, F. García, M.U. González, **A. García-Martín**, A. Cebollada and G. Armelles

IMM-Instituto de Microelectrónica de Madrid (CNM-CSIC), Isaac Newton 8, PTM, E-28760 Tres Cantos, Madrid, Spain

antonio@imm.cnm.csic.es

Magnetoplasmonics deals with the study of systems where the plasmonic and magneto-optical (MO) properties coexist and show a distinct interaction between them. In this kind of systems, the plasmonic properties can become tunable upon application of a magnetic field [1,2], or the MO effects can be largely increased by plasmon resonance excitation, as a consequence of the enhancement of the electromagnetic (EM) field in the MO component of the structure [3].

The study of the enhanced MO activity in structures with subwavelength dimensions is especially interesting since they may be viewed as nanoantennas in the visible range with MO functionalities. The light harvesting properties of these systems upon plasmon resonance excitation brings as a consequence an enhanced EM field in its interior, and more interestingly in the region where the MO active component is present. In fact, it has been recently demonstrated that the MO enhancement can be directly linked with the amount of EM field inside the MO layer, in such a way that this layer can be used as a probe to determine the EM field distribution inside a nanostructure [4].Therefore, optimizing the EM field distribution within the structure by maximizing it in the MO regions while simultaneously minimizing it in all the other, non MO active, lossy components, will allow for the development of novel systems with larger MO activity and reduced optical absorption, becoming an alternative to state of the art dielectric MO materials, like garnets.

Here we will present our approach to face this problem, based on the insertion of a dielectric layer in Au/Co/Au magnetoplasmonic nanodisks. The resulting nanostructure consists of two metallic nanodisks coupled through the dielectric layer, with one of the nanodisk being purely Au and the other one Au/Co (see Figure 1(a)). This kind of systems presents two hybridized localized plasmon resonance modes [5], showing two peaks in both the extinction and the MO spectra (see Figure 1(b)). Moreover, the EM field inside the nanostructure is strongly redistributed, being strongly concentrated in the nanodisk composed only of pure noble metal (Figure 1(c)). By optimizing the internal architecture (position of the Co layer), a configuration where the system exhibits large MO activity and low optical extinction in the same wavelength range can be obtained, as it can be seen in the right side of Figure 1(b) for the high wavelength peak [6].

References

[1] V.V. Temnov, G. Armelles, U. Woggon, D. Guzatov, A. Cebollada, A. Garcia-Martin, J.M. Garcia-Martin, T. Thomay, A. Leitenstorfer, and R. Bratschitsch, Nat. Photonics 4, 107 (2010).

[2] D. Martín-Becerra, J. B. González-Díaz, V.V. Temnov, A. Cebollada, G. Armelles, T. Thomay, A. Leitenstorfer, R. Bratschitsch, A. García-Martín and M.U. González, Appl. Phys. Lett. 97, 183114 (2010).

[3] G. Armelles, A. Cebollada, A. Garcia-Martin, J.M. Garcia-Martin, M.U. Gonzalez, J.B. Gonzalez-Diaz, E. Ferreiro-Vila, and J.F. Torrado, J. Opt. A: Pure Appl. Opt. 11, 114023 (2009).

[4] D. Meneses-Rodríguez, E. Ferreiro-Vila, P. Prieto, J. Anguita, M.U. González, J.M. García-Martín, A. Cebollada, A. García-Martín, and G. Armelles, Small 7, 3317 (2011).

[5] A. Dmitriev, T. Pakizeh, M. Käll, and D.S. Sutherland, Small 3, 294 (2007).

[6] J.C. Banthí, D. Meneses-Rodríguez, F. García, M.U. González, A. García-Martín, A. Cebollada, and G. Armelles, Adv. Mater. 24, OP36 (2012).

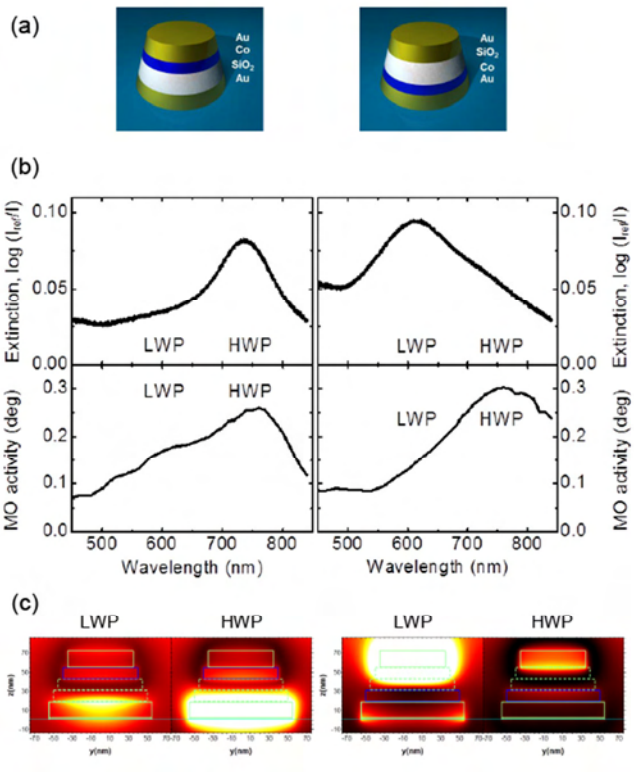

Figure 1: (a) Sketch showing the two kinds of fabricated magnetoplasmonic metal-dielectric nanodisks. (b) Extinction and magneto-optical (MO) activity spectra of the two kinds of nanodisks. (c) EM field distribution at the two resonance peaks, low wavelength (LWP) and high wavelength (HWP), for both kinds of nanodisks.

Silicon nanostructures and devices for advanced LEDs

J. M. Ramírez[1], Y. Berencén[1], A. Anopchenko[2], N. Prtljaga[2], A. Tengattini[2], L. Pavesi[2], P. Rivallin[3], J. M. Fedeli[3] and **B. Garrido**[1]

[1]Departament d'Electrònica, Universitat de Barcelona, Carrer Martì i Franquès 1, Barcelona 08028, Spain
[2]Nanoscience Laboratory, Department of Physics, University of Trento, Via Sommarive 14, Povo (Trento) 38123, Italy
[3]CEA, Léti, Minatec campus 17 rue des Martyrs, 38054 Grenoble cedex 9, France

Silicon based devices have been demonstrated as a potential alternative for photonic applications, providing several advantages towards the monolithic integration using the mainstream CMOS manufacturing tools [1].

However, there are still some needs that must be overcome such as the development of an efficient silicon-based and monolithically integrated light source (LED or a LASER) electrically pumped. Although this matter has attracted much attention and has been widely studied during the last years [2, 3] there is still room for improvement in this field, especially when using Si nanostructures (Si-ns) in combination with rare earth ions. The influence of Si-ns into Er ion excitation is well known due to its benefits either under optical (increase of the excitation cross-section) or electrical pumping (lowering of the tunnelling barrier height) and provides a good scenario for the realization of cost-effective light emitting devices with different operation ranges.

In this paper we present an overview of the work done towards the implementation of an integrated and efficient Er doped light source coupled to a slot waveguide and to an output coupler for wafer testing. The optimization of the material was previously performed by means of the electro-optical characterization in MOS capacitors replacing the oxide by the active layers. The transport properties [4], the power efficiency and the response to a pulsed excitation [5] were also investigated in these layers, providing valuable information of the best and more convenient fabrication parameters to be used for the coupled system.

Finally, a road map for the next generation of Si-based devices in our research group will be highlighted, displaying and appealing future work to be done in silicon based light sources.

References

[6] R. Soref, IEEE journal Selected topics in quantum electronics 12(6) (2006) 1678.
[7] A. J. Kenyon, et. al. Progress in Quantum electronics 26 (2002) 225.
[8] D. J. Lockwood and L. Pavesi, Silicon fundamentals for photonics applications 94 (2004) Springer Verlag.
[9] O. Jambois, et. al. J. Phys. D : Appl. Phys. 45 (2012) 045103.
[10] J. M. Ramírez et. al. Nanotechnology 23 (2012) 125203.

Magnetic modulation of surface plasmon modes in magnetoplasmonic Metal-Insulator-Metal cativies

E. Ferreiro-Vila, J. M. García-Martín, A. Cebollada, G. Armelles and **M. U. González**

IMM-Instituto de Microelectrónica de Madrid (CNM-CSIC), Isaac Newton 8, PTM, E-28760 Tres Cantos, Madrid, Spain

maria-ujue.gonzalez@csic.es

An external magnetic field is able to modify the properties of surface plasmon polaritons (SPP); in particular, when applied parallel to the interface but perpendicular to the SPP propagation direction, it modifies the SPP wavevector and introduces non-reciprocity in the dispersion relation [1]. This property has been known since the early '70s, but in the last decade it has received a renewed attention due to its potential for the development of integrated photonic devices, such as modulators [2] or optical isolators [3], as well as magneto-optical SPR sensors with increased sensitivity [4]. So far, the most often analyzed configuration consists of a single metal-dielectric interface where a magnetic element is introduced to increase the magneto-optic response, namely a ferromagnetic metal in a metallic noble metal/ferromagnetic metal multilayer [2,5-7] or a ferromagnetic dielectric [3,8]. However, very few studies have been devoted to more complex configurations composed of interacting interfaces.

In this work, we present, both experimentally and theoretically, the analysis of the magnetic modulation and non-reciprocity effects for the surface plasmon modes sustained by a metal-insulator-metal (MIM) cavity. The designed magnetoplasmonic MIM cavities consist of two metallic multilayers of Ag or Ag/Co with a SiO_2 spacer of different thickness. All upper metallic multilayers are capped by a thin Au layer to prevent oxidation. Three series of MIM cavities have been analyzed: with only one Co layer in the bottom metallic barrier, Co_{down}; with only one Co layer in the top metallic barrier, Co^{up}; and with one Co layer in each barrier, 2xCo (see sketches in Figure 1). As MIM cavities are known to support two modes, symmetric and antisymmetric [9], we have analyzed the magnetic modulation for each mode as a function of the thickness of the SiO_2 spacer for the three series. Figure 1 shows the obtained results. For only one Co layer present in the structure, a net modulation is observed, being it higher for the AM mode than for the SM mode. We attribute this to the difference in confinement between the two modes. For the 2xCo system, the modulation is reduced for both modes, mainly due to non-reciprocal effects.

References

[1] R.F. Wallis, J.J. Brion, E. Burstein, and A. Hartstein, Phys. Rev. B 9, 3424 (1974).

[2] V.V. Temnov, G. Armelles, U. Woggon, D. Guzatov, A. Cebollada, A. Garcia-Martin, J.M. Garcia-Martin, T. Thomay, A. Leitenstorfer, and R. Bratschitsch, Nat. Photonics 4, 107 (2010).

[3] B. Sepúlveda, L.M. Lechuga, and G. Armelles, J. Lightwave Technol. 24, 945 (2006).

[4] B. Sepúlveda, A. Calle, L.M. Lechuga, and G. Armelles, Opt. Lett. 31, 1085 (2006).

[5] J.B. González-Díaz, A. García-Martín, G. Armelles, J.M. García-Martín, C. Clavero, A. Cebollada, R.A. Lukaszew, J.R. Skuza, D.P. Kumah, and R. Clarke, Phys. Rev. B 76, 153402 (2007).

[6] E. Ferreiro-Vila, J.B. González-Díaz, R. Fermento, M.U. González, A. García-Martín, J.M. García-Martín, A. Cebollada, G. Armelles, D. Meneses-Rodríguez, and E. Muñoz-Sandoval, Phys. Rev. B 80, 125132 (2009).

[7] D. Martín-Becerra, V.V. Temnov, T. Thomay, A. Leitenstorfer, R. Bratschitsch, G. Armelles, A. García-Martín, and M.U. González, Phys. Rev. B 86, 035118 (2012).

[8] V.I. Belotelov, I.A. Akimov, M. Pohl, V.A. Kotov, S. Kasture, A.S. Vengurlekar, A.V. Gopal, D.R. Yakovlev, A.K. Zvezdin, and M. Bayer, Nature Nanotech. 6, 370 (2011).

[9] J.A. Dionne, L.A. Sweatlock, H.A. Atwater, and A. Polman, Phys. Rev. B 73, 035407 (2006).

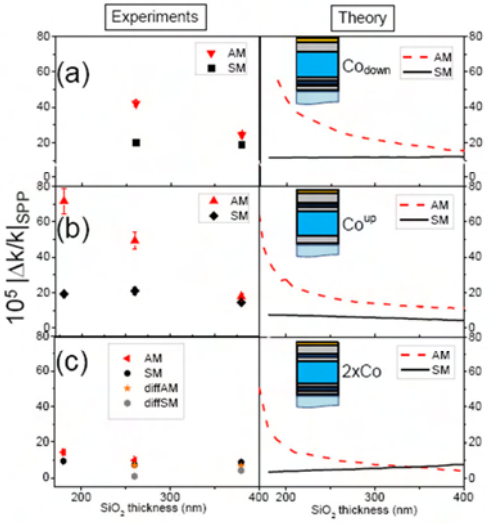

Figure 1: Experimental (left column) and simulated (right column) absolute values of the relative magnetic modulation of the SPP wavevector ($|\Delta k/k|_{SPP}$) as a function of SiO_2 thickness for antisymmetric, AM (red triangles and dashed lines) and symmetric, SM (black symbols and solid lines) plasmonic modes in (a) Co_{down}, (b) Co^{up}, and (c) 2xCo, magnetoplasmonic MIM cavities. The experimental $|\Delta k/k|_{SPP}$ values of the 2xCo series are also compared to the absolute difference between the Co_{down} and Co^{up} series modulation values for both modes (AM-star symbols, SM- hexagonal symbols) to establish the contribution of non-reciprocity.

Waveguides based on colloidal QDs embedded in PMMA and SU8

H. Gordillo, I. Suárez, P. Rodríguez-Cantó, R. Abargues, S. Albert, and J. Martínez-Pastor

UMDO (Unidad Asociada al CSIC-IMM), Instituto de Ciencia de los Materiales, Universidad de Valencia, PO Box 22085, 46071 Valencia, Spain

Henry.gordillo@uv.es

Nanocomposites based on the integration of colloidal quantum dots (CQD) into a polymer matrix are a very potential material to develop novel integrated photonic devices, because such a multicomponent material combines the properties of CQD with the technological feasibility of polymers. CQD are semiconductor nanostructures synthesized by colloidal chemistry and they present the advantages of joining the three dimensional confinement of carriers characteristic of quantum dots (QDs) with the tuning of the emission and absorption wavelength just by controlling the size and shape during their chemistry process [1]. In addition, as a consequence of their small size (1 nm to 10 nm) these nanostructures show strong quantum confinement, being its emission practically temperature independent [2]. Moreover, chemical methods allow controlling the emission wavelength by changing not only the NQDs size but also their base material without modifying the preparation method. In this way the NQDs emission can cover a broad range of the optical spectrum using CdS [3], CdTe [4] and CdSe [5] in the visible range, and PbS [6], PbSe and InAs [7] in the near infrared. For these reasons, NQDs are interesting candidates to be incorporated as active medium in new optoelectronic devices. However, in order to make these nanostructures compatible with the photonic technology they have to be embedded in a solid state matrix. In this way, the use of polymers as a host material seems to be a good choice, because they are cheap, flexible and they can be easily processed into films by coating techniques and patternable by UV or e-beam lithography [8].

In this work NQD-PMMA nanocomposite films are proposed as novel material to implement active waveguides. For this purpose The NQD-PMMA films (with thickness between 1 and 2 µm) were deposited on a SiO_2/Si substrate (see inset of figure 2). Since the refractive index of PMMA (1.489 at 600 nm) is higher than the one of SiO2 (1.458 at 600 nm) the nanocomposite can act as core layer of the waveguide. As result, if the appropriate concentrations of QDs in the polymer are chosen their PL can be coupled to the waveguide modes when the structures are optically pumped [9]. In addition, wavelength tunability of the NQDs allows the control of the active wavelength (from 400 nm to 2 µm) just by changing the material of the dots and their size [10] without modifying the fabrication conditions. In this way waveguiding of the PL of CdS (450 nm), CdSe (600 nm), CdTe (550 nm) and PbS (1100 nm) is demonstrated. Moreover, when more than one QD family is embedded in the polymer the structure can present multicolor waveguiding [8-9]. For example, figure 1 shows the guided PL spectra in a waveguide embedding CdS (blue, 452 nm), CdTe (green, 539 nm) and CdSe (red, 601 nm) QDs. It is worth noting that it was critical to adjust the relative amounts of QDs into the matrix in order to avoid (or compensate) reabsorption between QDs families. The pictures at the top of Fig. 1 correspond to the three color waveguiding of the three CQDs families.

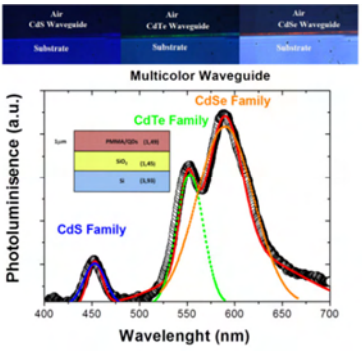

Figure 1: Bottom. PL wave-guided spectra of QD/PMMA planar waveguide with three QDs families (CdS, CdTe and CdSe). Top. Photographs of the waveguided light. The inset shows the waveguide structure.

Although PMMA is cheap and allows a trouble-free thin film processing, it is limited in the implementation of two dimensional waveguides due to the fact that it not allows patterning by UV lithographic methods. In this way SU8 seems to be a better choice because it is easily-patterned by using UV photolithography and also has a high refractive index (~1.5) interesting for waveguide applications. However, the main drawback of SU8 is its chemical incompatibility with as-syntesized QDs. In [11] the appropriate ligand exchange to disperse QDs in this polymer is proposed, making it possible to develop patterns with QD inside. Figure 2 shows a preliminary result of these new patterned structures. The spectra corresponds to the guided-PL of CdSe QDs in an 8 µm SU-8 ridge pumped with a 533 nm DSPP diode laser characterized by end fire coupling. The inset shows a photograph of the guided PL in waveguides with different widths. In all cases the structure is able to confine PL into two dimensions.

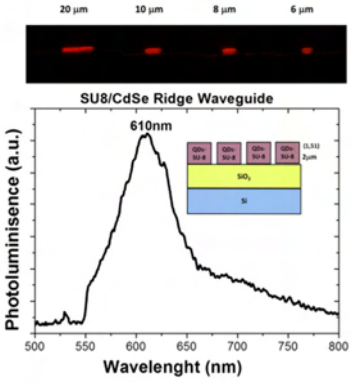

Figure 2: Top. Waveguiding PL spectrum of a CdSe-SU8 ridge waveguide. Bottom. Photographs of the waveguided light in structures with differents widths. The inset shows the waveguide structure.

Nanocomposites proposed in this work can be used as cores of active planar and stripe waveguides or in other application in organic photonic. Since they present the advantages of an easy processing and the possibility of tuning the active wavelength by the change of the base material, they are promising candidates for new integrated optic devices.

References

[1] Klimov V. I., "Nanocrystal quantum dots: from fundamental photophysics to multicolor lasing," Los Alamos Science, no. 28 (2003)., 214-220.

[2] Klimov V I, Mikhailovsky A A, Xu S, Malko A, Hollingsworth J A, Leatherdale C A, Eisler H J and Bawendi M G. "Optical Gain and Stimulated Emission in Nanocrystal Quantum Dots" Science, no. 290 (2000), 314-317.

[3] Chan Y., Stecke J. S. l., Snee P. T., Caruge J. M. , Hodgkiss J. M., Nocera D. G. And Bawendi M. G., "Blue semiconductor nanocrystal laser," Applied Physics. Letters, vol. 86, no. 7 (2005), 073102.

[4] D. Lourençoni Ferreira, F. Oliveira Silva, L. Cristina de Souza Viol, P. Licinio, M. Valadares, L. Alberto Cury, M. Antonio Schiavon and J. Luiz Aarestrup Alves, "Growth kinetics of CdTe colloidal nanocrystals," Journal of Chemical Phyics, vol. 131, no. 8 (2009), 084712.

[5] Chen Y., Herrsndorf J., Guiilhabert B., Zhang Y., Watson I. M., Gu E., Laurand N. And Watson M. D., "Colloidal quantum dot random laser," Optics Express, vol. 19, no. 4 (2011), 2996-3003.

[6] Sukhovatkin V., Musikhin S., Gorelikov I., Cauchi S., Bakueva L., Kumacheva E. and E. Sargent H., " Room-temperature amplified spontaneous emission at 1300 nm in solution-processed PbS quantum-dot films," Optics Letters, vol. 30, no. 2 (2005),171-173.

[7] Wu Z., Mi Z., Bhattacharya P., Zhu T. And Xu J., "Enhanced spontaneous emission at 1.55 µm from colloidal PbSe quantum dots in a Si photonic crystal microcavity," Applied Physics. Letters, vol. 90, no 171105 (2007).

[8] Uddin M. A. and Chan H. P., "Materials and process optimization in the reliable fabrication of polymer photonic devices," Journal of Optoelectronics and Advanced Materials, vol. 10, no. 1 (2008), 1-17.

[9] Suárez I.,Gordillo H., Abargues R., Albert S. and Martínez-Pastor J., "Photoluminiscence waveguiding in CdSe and CdTe QDs-PMMA nanocomposite films," Nanotechnology, vol. 22, no. 43 (2011), 435202.

[10] H. Gordillo, I. Suárez, R. Abargues, P. Rodríguez-Cantó, S. Albert, and J. P. Martínez-Pastor., "Polymer/QDs Nanocomposites forWaveguiding Applications", Journal of Nanomaterials, vol. 2012 (2012), 960201.

[11] To be published.

2D and 3D light absorption modeling of interdigitated full organic solar cells

P. Granero, V. S. Balderrama, J. Ferré-Borrull, J. Pallarès, and L. F. Marsal*

Nano-electronic and Photonic Systems (NePhoS), Department of Electronic, Electrical and Automatic Control Engineering, Universitat Rovira i Virgili, Av. Països Catalans 26 43007, Tarragona, Spain

*lluis.marsal@urv.cat

Introduction

A promising architecture for organic solar cells (OSC) is the interdigitated heterojunction approach, which joins the advantages of bulk heterojunction and planar bilayer devices. This approach provides a proper exciton dissociation interface without sacrificing direct paths for carriers' collection [1]. Several studies have demonstrated an increase in the efficiency of these cells [2]. Nevertheless, the interdigitated dissociation interface can be also a potential source of light trapping that can enhance OSC efficiency.

By means of numerical modelling, we investigate light absorption in interdigitated heterojunction full organic solar cells. Simulations are carried out by using the finite-element method [3], which allows evaluating the magnitudes on the devices as a function of the position. To determine the best configuration, we compare different cells which are obtained by varying the Donor-Acceptor interface geometry. The donor and the acceptor materials are poly(3-hexylthiophene) (P3HT) and 1-(3-methoxycarbonyl)-propyl-1-phenyl-(6,6)C_{61} (PCBM) respectively. This study is intended to improve our devices which are achieved via nanoporous anodic alumina templates (NAAT) [4,5] (Fig.1a and Fig.1b).

In this study we compare the absorbed light, from a standard AM1.5 light source model, in the P3HT layer by using two models: a 2D and a 3D one. The 2D one (Fig. 1c) is a simplification of a real 3D device where the nanostructured interface is composed of alternating blocks of each organic material. The advantages of this model over the 3D one are an easier geometry definition, shorter computing times and smaller simulation files. On the other hand, since it is a 2D definition, nanopillars are actually grooves. A more realistic 3D model is presented in Fig. 1d, where a more complex geometry represents the nanopillars. In both cases we model a structure of indium tin oxide (ITO), Poly(3,4-ethylenedioxythiophene) poly(styrenesulfonate) (PEDOT:PSS), P3HT, PCBM and a back contact of aluminium (Al). The parameters under study are α (nanopillar diameter), β (structure period (2D) or interpillar distance (3D), where β = 2α) and *T* (nanopillar height including the supporting base).

Results and discussion

Fig. 2 shows the total absorbed light power (Q_{TOTAL}) in the P3HT layer as a function of the nanopillars height (*T*) for several nanopillar diameters (α). Fig. 2a) corresponds to the 2D model. We can see that all the curves have a similar trend with two local maxima for *T* around 80 nm and 230 nm. A local minimum for *T* close to 130 nm is also present in all cases. The maximum absorption is achieved for α = 12.5 nm while the lower absorption is clearly for α = 125 nm.

Fig. 2b) shows Q_{TOTAL} for the 3D model. In this case we can see that not all the curves have the same trend. For α = 12.5 nm and 50 nm the maximum absorbed light take place for *T* = 70 nm and 260 nm while there is a local minimum for *T* = 150 nm. However, for the biggest diameters the local maxima are achieved for a pillar height of 50 nm and 190 nm, and the minimum Q_{TOTAL} take place for *T* = 110 nm. The amount of absorbed light for each height is also different, being higher for the 3D model.

So, if we compare the results of the two models, the 2D and the 3D ones, we can find some similarities. However, the fact that in one model we have grooves while in the other there are nanopillars introduces differences in the results. Hence, a 2D model of a real 3D interdigitated OSC can be a first approximation but it is not accurate enough to replace a 3D model.

This work was supported by the Spanish Ministry of Science and Innovation (MICINN) under grant number TEC2009-09551 and TEC2012-34397, CONSOLIDER HOPE project CSD2007-00007, and by the Catalan Authority under project 2009SGR549.

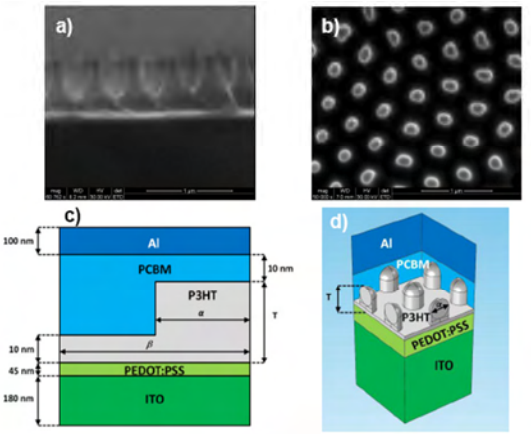

Figure 1: Environmental scanning electron microscopy (ESEM) images of P3HT nanopillars with the structure glass/ITO/PEDOT:PSS/P3HT-pillars made with NAAT, a) cross section and b) top view. Schematic unit cell (periodic conditions) of the structure ITO/PEDOT:PSS/P3HT/PCBM/Al for c) the 2D and d) the 3D models.

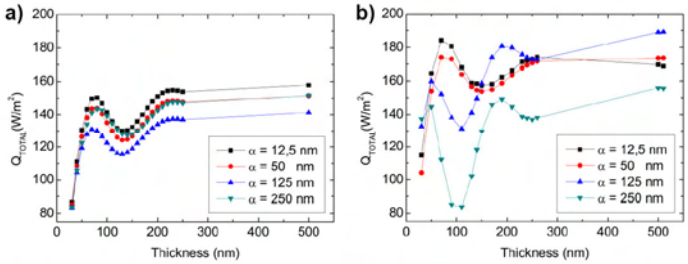

Figure 2: Total absorbed light power (Q_{TOTAL}) in the P3HT layer of a) the 2D and b) the 3D models as a function of the nanopillars height (*T*) for several nanopillar diameters (α).

References

[1] H. Hoppe, N. S. Sariciftci, J. Mater. Res., 19 (2004) 1924–1945.

[2] J. S. Kim, Y. Park, D. Y. Lee, J. H. Lee, J. H. Park, J. K. Kim, K. Cho, Adv. Funct. Mater., 20 (2010) 540–545.

[3] COMSOL (COMSOL Inc.), MA, USA. Available: http://www.comsol.com

[4] R. Palacios, P. Formentín, T. Trifonov, M. Estrada, R. Alcubilla, J. Pallarés, L. F. Marsal, Phys. Status Solidi Rapid Res. Lett., 2 (2008) 206–208.

[5] A. Santos, P. Formentín, J. Pallarés, J. Ferré-Borrull, L. F. Marsal, Sol. Energy Mater. Sol. Cells, 94 (2010) 1247–1253.

Annealing effect on the performance of PTB1: PCBM bulk heterojunction solar cells

P.L. Han, V.S. Balderrama, M. Alba, P. Formentin, J. Pallarés and L.F. Marsal*

Departament d'Enginyeria Electrònica, Elèctrica i Automàtica, Universitat Rovira i Virgili,
Av. Paisos Catalans 26, Tarragona, Spain

*lluis.marsal@urv.cat

Organic photovoltaic solar cells based on photonics technology have been widely investigated as they show the promise of solar energy conversion efficiencies at low cost and ease of fabrication [1-3]. In the past decades, much research has focused on device structure optimization and new materials synthesis to improve the efficiency of the device. In organic solar cells structure optimization, annealing of the polymer blend layer is an effective method to induce the crystallization, increase the phase separation and improve the transport across the interface between the active layer and electrode. Many efforts have been made to investigate the effect of temperature and scale on the thermal annealing in P3HT: PCBM hybrid system [4, 5]. Recently, a new series of the width spectral response polymer PTB1 have attracted much attention because of 6% high power conversion efficiency [6, 7]. In this work, we focus on the structure optimization of the PTB1: PCBM BHJ solar cell and discuss the influence of thermal annealing on the performance.

Photovoltaic (PV) devices were fabricated on pre-cleaned patterned ITO glass substrates. The ITOcoated glass substrate was cleaned stepwise in acetone, methanol, isopropanol, distilled water for 20min each. And then it was dried in an oven for 10 h at 60℃. A 30 nm hole extraction layer PEDOT:PSS was applied onto the substrates by spin coating. After being baked at 120℃ for 20 min, the PTB1:PCBM film with 1:1 weigh ratio and the PTB1 concentration of 10 mg/ml dissolved in 1, 2-dichlorobenzene was cast on the PEDOT: PSS layer at 1000 rpm for 30 s without further treatment inside a glove box. Subsequently, 100 nm Ag layer on top of 25 nm Ca layer were thermally deposited on the organic activity film under the vacuum of $1x\,10^{-6}$ using a thermal evaporator. The thermal annealing process was conducted at 100℃ for 20 min in the same glove box after cathode evaporation. The device efficient area was measured to be 0.09 cm^2. The current-voltage curves were measured using a Keithley 2400 source measure unit under AM1.5G illumination at 100 mW/cm^2. The light density was determined by a monosilicon detector to reduce spectral mismatch.

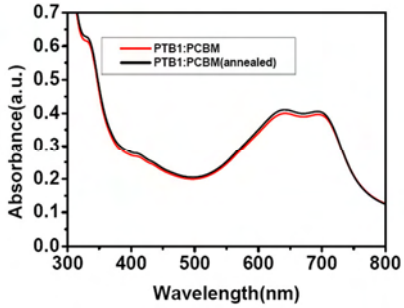

Figure 1: UV-vis absorption spectra of PTB1: PCBM 1:1pristine and annealed film at 100℃ for 20min.

Annealing is an indispensable step for the complete solar cell device fabrication in light absorption, phase separation and final efficiency. Figure 1 shows UV- Vis absorption spectra of PTB1: PCBM blend layer before and after the annealing at 100℃ for 20min. A broad peak in the 626-705 nm region is the characteristic π-π* transition of the PTB1. And the 325 nm peak comes from the absorption of PCBM. The results are in agreement with previous report [5]. In our experiment, light absorption of the PTB1:PCBM film is not significantly shifted after annealing at 100℃ for 20min compared with the results that Yu *et al.* has reported [6]. The different spectral response suggests that the rigid backbone of PTB1 is not changed after annealing as in P3HT system. Although the light absorption is not increased by annealing, the thermal annealing of the

activity layer changes the photovoltaic properties. Current density-voltage characteristic result shows that the Jsc of the device made from an annealed film dropped dramatically from 12.8 to 12.2 mA/cm^2 compared to the pristine PTB1: PCBM film. FF and PCE were calculated to decrease after annealing from 60.8% to 55.7% and from 4.44% to 3.9%, respectively (Figure.2). It is concluded that the Jsc and FF decreasing were a result of the improved phase separation and the reduced interfacial area between the donor PTB1 and the acceptor PCBM after annealing. This resulted in charge recombination and low transportation efficiency in the organic blends. In contrast, the Voc increased from 0.57 V to 0.58 V after annealing. Typically, the Voc is governed by the energetic relationship between the donor and acceptor as well as the contact form of polymer/electrode interface. And the energy level change is closely correlated to interchain interaction between the donor and the acceptor. However, the UV-Vis spectroscopy results (Figure 1) showed no absorption shift, which suggests that this interchain interaction between polymers does not altered. Therefore, the Voc increase can be explained due to an improvement of the ohmic contact of polymer/electrode interface in the PTB1: PCBM blend system.

This work was supported by the Spanish Ministry of Science and Innovation (MICINN) under grant number tec2009-09951, TEC2012-34937, CONSOLIDER HOPE project CSD2007-00007, by Catalan authority under project 2009 SGR 549.

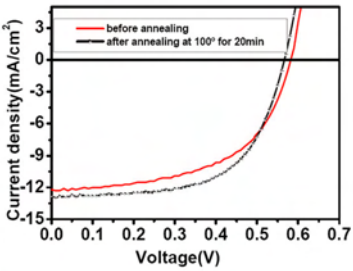

Figure 2: The typical current-voltage characteristic solar cell Device (ITO/PEDOT:PSS/PTB1:PCBM/Ca/Ag) made by PTB1: PCBM 1 : 1 pristine and annealed film under the AM 1.5 condition.

References

[1] B.Ecker, J. C. Nolasco, J. Pallares, L. F. Marsal, Adv. Funct. Mate, 15, (2005) 1617
[2] J.C.Nolasco, R.Cabre,J.Ferre-borrull, L.F.Marsal,Journal of Applied Physics, 107, (2010) 044505
[3] W. Gaynor, L. J. Yong, ACS Nano, 4, (2010) 30
[4] W. Ma, C.Yang, Adv. Funct. Mate, 15, (2005) 1617
[5] C. Renaud, S.J. Mougnier, Adv.Mater, 24, (2012) 219
[6] Y. Liang, Y. Wu, J. Am. Chem. Soc, 131, (2009) 56
[7] J. Guo, Y.Y. Liang, J. Phys. Chem. B, 114, (2010) 742

Tailoring the optical properties of nanoporous anodic alumina with geometry modification for further sensing applications

L. P. Hernández-Eguía, G. Macías, J. Ferré-Borrull and L.F. Marsal*

Departament d'Enginyeria Electrònica, Elèctrica I Automàtica, Universitat Rovira I Virgili,
Avda. Països Catalans 26 43007, Tarragona, Spain

*lluis.marsal@urv.cat

Nanoporous anodic alumina (NAA) is one of the smartest materials with considerable interest in recent years [1] due to their physico-chemical properties like thermal stability, environmental toughness or biocompatibility, and also to its easy fabrication to obtain a highly ordered and manageable porous assembly for purposes such as nanomaterials synthesis [2], photonics [3] or sensors [4].

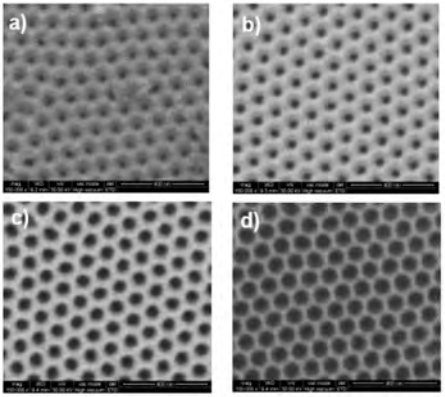

Figure 1: Set of ESEM top view images of the first group of GCA samples, 1.7 µm a) GCA-1 (PW=0 min); b) GCA-2 (PW=6 min); c) GCA-3 (PW=12 min); d) GCA-4 (PW=18 min).

Two batches of NAA samples, the second twice as thick as the first one (1.7 and 3.4 µm), have been prepared. Each set possess four samples with the same pore length but different porosities (figure 1) and have been studied by means of the Fabry-Pérot optical interferences both in reflectance, covering the UV-visible and the near infrared region of the spectrum, and in the UV-visible spectrum of photoluminescence. Changes in the two types of spectra are related to the different pore lengths and pore diameters.

Table 1 summarizes the geometric features of the samples and resumes the fabrication conditions.

Label	L_p (µm)	n	P (%)	D_p (nm)	EOT (µm)
GCA-1 / GCA-5	1.7/3.4	1.65	14.3	38.6	2.3/5.6
GCA-2 / GCA-6	1.7/3.4	1.58	23.1	51.2	2.7/5.4
GCA-3 / GCA-7	1.7/3.4	1.41	44.6	72.3	2.4/4.8
GCA-4 / GCA-8	1.7/3.4	1.20	71.2	90.9	2.0/4.0

Table 1: Optical and geometric characteristics of the eight GCA samples: fabricated in 0.3M oxalic acid at 40V. The interpore distance (D_{int}) was 102 nm for all the samples.

Oscillations appear in the optical spectrum of the nanoporous alumina when the pore geometry (pore length, L_p, and pore diameter, D_p) are suitable for the evidence of the Fabry-Pérot effect [5]. Figure 2a shows the reflectance spectra of the first sample of each group, GCA-1 and GCA-5, as an example. Furthermore, simulations have been also made using the effective medium approximation [6] to corroborate experimental results. We were able to fit pretty well the experimental data with simulations based on the effective medium approximation. Figure 2b depicts the simulation of reflectance compared with the experimental spectrum of sample GCA-1. NAA presents also interesting photoluminescence properties [7]. In figure 3 is represented the emission spectra of the same pair of samples.

We noticed that the capability of nanoporous anodic alumina is promising for being used as an accurate and sensible optical sensor employing either reflectance or fluorescence spectroscopy.

This work was supported by the Spanish Ministry of Science and Innovation (MICINN) under grant nº TEC2009-09551 and TEC2012-34397, CONSOLIDER HOPE project CSD2007-00007and AGAUR 2009 SGR 549.

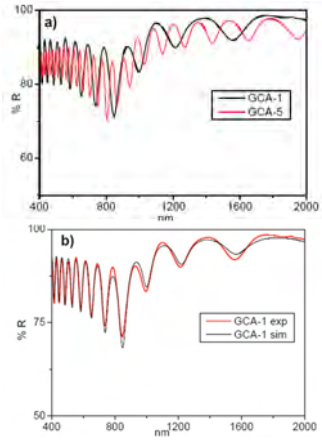

Figure 2: a) Comparison in the reflectance spectra of samples with the same porosity and the two different pore lengths, 1.7 and 3.4 µm, GCA-1 and GCA-5, black and red lines. b) Comparison in the reflectance spectra of the experimental sample, GCA-1, and the corresponding simulation, red and black lines respectively.

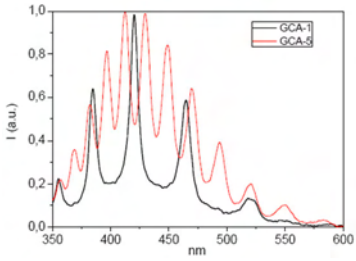

Figure 3: Fluorescence spectra of GCA-1 and GCA-5, black and red lines respectively, in the UV-visible region. The number of oscillations is multiplied by two in the sample with the double pore length.

References

[1] Losic D, Simovic S. Expert. Opin. Drug. Deliv., 6 (2009) 1363.

[2] Zhang Z, Shimizu T, Senz S, Gösele U. Adv.Mater, 21 (2009) 2824.

[3] Maksymov I, Ferré-Borrull J, Pallarès J, Marsal L F. Photon. Nanostruct. Fundam. Appl (2012) doi:10.1016/j. photonics.2012.02.003.

[4] Kim D-K, Kerman K, Yamamura S, Kwon Y S, Takamura Y, Tamiya E. Jap. J. Appl. Phys., 47 (2008) 1351.

[5] Lin V S Y, Motesharei K, Dancil K P S, Sailor M J, Ghadiri M R. Science, 278 (1997) 840.

[6] Bosch S, Ferré-Borrull J, Sancho-Parramon J. Solid-State Electronics, 45 (2001) 703.

[7] Santos A, Valderrama V S, Alba M, Formentín P, Ferré-Borrull J, Pallarès J, Marsal L F. Adv.Mater, 24 (2009) 1050.

Integration of gold nanoparticles in photonic crystals: effect of the interplay between plasmonic and optical cavity resonances

Alberto Jiménez-Solano[1], Carmen López-López[1], Olalla Sánchez-Sobrado[1], José Miguel Luque[1], Mauricio E. Calvo[1], Cristina Fernández-López[2], Ana Sánchez-Iglesias[2], Luis M. Liz-Marzán[2] and Hernán Míguez[2]

[1]Instituto de Ciencia de Materiales de Sevilla, CSIC-Universidad de Sevilla, Sevilla, Spain
[2]Departamento de Química Física, Universidad de Vigo, 36310 Vigo, Spain

alberto.jimenez@csic.es

Herein we show experimental examples of localized photon modes in periodical multilayer structures. [1,2] These experiments show the control of the spectral modification of the optical absorption of one-dimensional photonic crystal based resonators containing different types of gold nanoparticles. This control was achieved through the changes in the photonic environment of the gold nanoparticles by means of the interplay between planar optical cavity modes and localized surface plasmons [3].

Spin-casting of metal oxide nanoparticle suspensions was used to build multilayered photonic structures that host (silica-coated) gold nanorods and spheres (Figure 1). Strong reinforcement and depletion of the absorptance was observed at designed wavelength ranges, thus proving that our method provides a reliable means to modify the optical absorption originated at plasmonic resonances of particles of arbitrary shape and within a wide range of sizes. [4] Results are explained in terms of the calculated spatial distribution of the electric field intensity within the configurations under analysis.

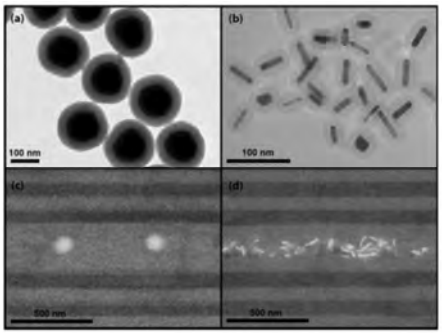

Figure 1: Top: TEM images of Au@SiO_2 nanospheres (a) and rods (b). Bottom: SEM backscattered electrons images of cross sections of optical resonators hosting Au@SiO2 nanospheres (c) and rods (d).

References

[1] Calvo, M.E., Colodrero, S., Rojas, T.C., Anta, J.A., Ocaña, M. and Míguez, H. Adv. Func. Mater. 18 (2008) 2708-2715.
[2] Colodrero, S., Ocaña, M. and Míguez, H. Langmuir 24 (2008) 4430-4434.
[3] Sánchez-Sobrado, O., Lozano, G., Calvo, M.E., Sánchez-Iglesias, A., Liz-Marzán, L.M. and Míguez, H. Adv. Mater. 23 (2011) 2108-2112.
[4] Jiménez-Solano, A., López-López, C., Sánchez-Sobrado, O., Luque, J.M., Calvo, M.E., Fernández-López, C., Sánchez-Iglesias, A., Liz-Marzán, L.M. and Míguez, H. Langmuir 28 (2012) 9161-9167.

Optimized integration of one-dimensional photonic crystals in dye solar cells

Carmen López-López,
Silvia Colodrero and Hernán Míguez

Instituto de Ciencia de Materiales de Sevilla, Consejo Superior de Investigaciones Científicas-Universidad de Sevilla, Américo Vespucio 49, 41092, Sevilla, Spain

carmen@icmse.csic.es

Dye solar cells (DSC) are photovoltaic devices in which the absorption of sunlight is realized by dye molecules attached to the surface of a titanium dioxide (TiO_2) electrode. In order to improve the light harvesting by the dye the optical design of these cells can be modify. It was already demonstrate that coupling nanoparticle one dimensional photonic crystal (1DPC) [1,2], which efficiently localize the incident light within the absorbing electrode in a targeted wavelength range, gave rise to increase of the power conversion efficiency of the cell. Such 1DPC showed no diffuse scattering, which allowed one to attain, for the first time, devices of enhanced efficiency while preserving the transparency. But the low photocurrent enhancement compared with theoretical predictions [3] and the fact that the fill factor of the cells decrease with the presence of these multilayers indicated that there may be an electrolyte diffusing problems.

New highly porous nanoparticle-based 1DPC [4] are attached to the working electrode. New porosity of these structures are the result of the incorporation of a polymeric porogen to the multilayer while being deposited and its subsequent removal by thermal annealing. In this way, not only the porosity is increase but also the pore size distribution is wider, thus the mass transport through the crystal is improved. Higher power conversion efficiency is obtained from the cells in which highly porous 1DPC are implemented [5].

References

[1] S. Colodrero, M. Ocaña, H. Míguez, Langmuir, 24 (2008) 4430.
[2] S. Colodrero, A. Mihi, L. Häggman, M. Ocaña, G. Boschloo, A. Hagfeldt, H. Míguez, Adv. Mater. 21 (2009) 764.
[3] G. Lozano, S. Colodrero, O. Caulier, M.E. Calvo, H. Míguez, J. Phys. Chem. C 114 (2010) 3681.
[4] C. López-López, S. Colodrero, S.R. Raga, H. Lindström, F. Fabregat-Santiago, J. Bisquert, H. Míguez, J. Mater. Chem., 22 (2012) 1751.
[5] S. Colodrero, A. Forneli, C. López-López, L. Pelleja, H. Míguez, E. Palomares, Adv. Funct. Mater. 22 (2012) 1303.

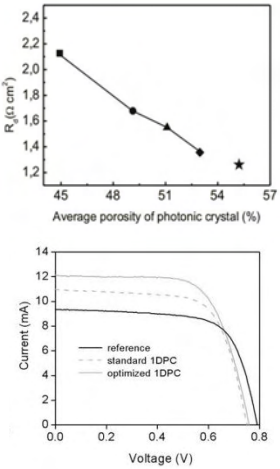

Figure 1: On the top diffusion resistance of nanoparticle based 1DPC built with different quantity of polymer porogen. At the bottom IV curves measured for DSSCs in which a non-modified 1DPC (grey dashed line), a highly porous 1DPC (grey solid line), and a reference cell (black solid line).

Fabrication and characterization of nanoporous anodic alumina bilayers for biosensing applications

G. Macias, L. P. Hernández-Eguía, J. Ferré-Borrull, J. Pallarès, P. Formentín and L.F. Marsal*

Departament d'Enginyeria Electrònica, Elèctrica I Automàtica, ETSE, Universitat Rovira I Virgili, Avda. Països Catalans 26, 43007 Tarragona, Spain

*luis.marsal@urv.cat

Nanoporous anodic alumina (NAA) with pore diameters between 15 and 300 nm have shown promising results in areas such as optoelectronics [1] and materials science [2]. However, recently there has been an increasing interest in their possible application in biosciences, especially in label-free detection of biomolecules. To date, the studied approaches rely on self-ordered anodic alumina monolayers. These studies show promising results, but further investigation has been focused on surface modification and protein immobilization instead of structure modification. Here, we present our results in self-ordered nanoporous anodic alumina bilayers, focusing on fabrication, characterization and data processing for a further application as a biosensing platform.

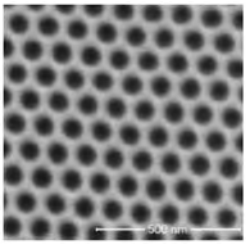

Figure 1: Top view of sample S2 showing highly ordered pores in a honeycomb-like manner.

Conventional two-step anodization [3] was performed on high-purity aluminium sheets (99.99% Ø20 mm 250 µm thick) purchased from Goodfellow Cambridge Ltd. Prior to anodization, a 4-min electropolishing pretreatment was performed in a mixture of ethanol (EtOH) and perchloric ($HClO_4$) acid 4:1 v/v at 20 V. Afterwards, the polished surface was anodized in oxalic acid ($H_2C_2O_4$ 0.3 M) at 40V and 4-6 ºC for 20 h in order to achieve self-ordering of pores. The grown aluminium oxide was then selectively dissolved in a mixture of phosphoric (H_3PO_4 6%wt.) and chromic acid (H_2CrO_7 1.8 %wt.) at 70 ºC for at least 3 h. A second anodization was performed under the same conditions but adjusted to obtain 1, 2, 3 and 4 µm respectively. Subsequently, pores were enlarged through wet chemical etching with phosphoric acid (5 %wt.) for 15 min. Finally, a third anodization took place under the same conditions in order to obtain a less porous 4-µm-thick second alumina layer. Fig.1 shows a top view of the samples.

Name	Layer 1 (µm)	Porosity 1 (%)	Layer 2 (µm)	Porosity 2 (%)
S1	1	50	4	10
S2	2			
S3	3			
S4	4			

Table 1: Sample structure characteristics.

Reflectance spectra were recorded for all samples in the 350-600 nm range using a PE Lambda 950 UV-Vis-NIR spectrometer at normal incidence (Fig.2). In order to establish the effective optical thickness (EOT) of each layer, fast Fourier transform (FFT) analysis was performed following a procedure described elsewhere [4].

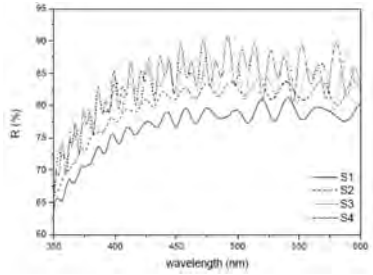

Figure 2: Reflectance spectra of NAA bilayers in the 350-600 nm range. The oscillations present in the spectra are not due to a single Fabry-Pérot effect, but to the combination of the intereference fringes of both layers.

According to literature regarding bilayers on porous silicon (PSi), three peaks should appear in the FFT graph, two of them referring to the first and second layers, and the last, to a combination of both [4]. However, the results obtained show just two peaks which refer to the second layer and the combination of layers (Fig.3). This may be a result of the overall shape of the NAA reflectance spectra (i.e. without the oscillations due to a Fabry-Pérot effect), which can mask low-frequency oscillations. Nevertheless, in-depth study must be undertaken to verify this theory.

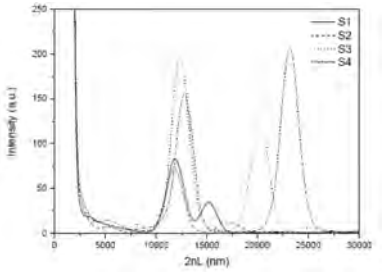

Figure 3: FFT plot of the reflectance spectra from Fig.2 of the NAA bilayers listed in Table 1. The peaks' position correspond to the EOT (i.e. 2nL=EOT) of the layer.

We have presented an easy approach for the fabrication of alumina bilayers with potential application in optical detection of biomolecules. FFT allows us to have a more robust and automated way of measuring the EOT. In addition, the FFT plot gives information in both axis. Peak position the EOT of the layer, while peak intensity is related with the refractive index contrast between two consecutive layers. Therefore, bilayers show promising results as they provide more information than monolayers thanks to their multiple FFT peaks which will be useful to follow functionalization and biomolecule immobilization. Finally, pore diameters can be tuned to promote or inhibit the entrance of certain macromolecules such as proteins and thanks to its funnel architecture give information of protein size.

This work was supported by the Spanish Ministry of Science and Innovation (ICINN under grant no. TEC2009-09551, CONSOLIDER HOPE project CSD2007-00007, AGAUR 2009 SGR 549 and TEC2012-34397.

References

[1] X.H. Wang, T. Akahane, H. Orikasa, T. Kyotani, Applied Physics Letters, 91 (2007) 011908.
[2] T. Yanagishita, K. Nishio, H. Masuda, Advanced Materials, 17 (2005) 2241-2243.
[3] H. Masuda, K. Fukuda, Science, 268 (1995) 1446-1448.
[4] S. Pace, B. Seantier, E. Belamie, N. Lautredou, M.J. Sailor, P.E. Milhiet, F. Cunin. Langmuir 28 (2012) 6960-6969.
[5] A. Santos, M. alba, P. Formentin, J. Ferré-Borrull, J. Pallarès, L.F. Marsal, Advanced Materials 24 (2012) 1050-1054.
[6] A. Santos, G. Macias, J. Ferré-Borrull, J. Pallarès, L.F.Marsal, ACS Applied Materials & Interfaces 7 (2012) 3584-3588.

Experimental demonstration of photonic confinement suspended square-lattice silicon photonic crystal cavities

Daniel Puerto[1], Amadeu Griol[1], José Maria Escalante[1], Bahram Djafari-Rouhani[2], Yan Pennec[2], Vincent Laude[3], Jean-Charles Beugnot[3] and **Alejandro Martínez**[2]

[1]Nanophotonics Technology Center, Universitat Politècnica de València, Valencia, Spain
[2]Institut d'Electronique, de Microélectronique et de Nanotechnologie, Centre National de la Recherche Scientifique, Lille, France
[3]Institut Franche-Comté Electronique Mécanique Thermique et Optique – Sciences et Technologies, Centre National de la Recherche Scientifique, Besançon, France

amartinez@ntc.upv.es

It has been shown that the square lattice is one the most suitable ones to produce simultaneous photonic and phononic band gaps on suspended silicon slabs [1]. The introduction of point defects on such "phoxonic" crystals should lead to an enhanced interaction between confined light and sound at the nanoscale. In this work we report on the experimental measurements of light confinement in cavities created on two-dimensional square-lattice silicon photonic crystal membranes. The dimensions of the fabricated structures are chosen to provide a "phoxonic" bandgap, where the photonic bandgap (PBG) for even modes occurs at wavelengths around 1550 nm. To obtain the "phoxonic" bandgap, the silicon layer is a thicker that in conventional triangular-lattice photonic crystals (around 220 nm): around 325 nm for the square lattice. The radius of the holes is *r*=230 nm and the lattice period is a=540 nm. We fabricated the "phoxonic" crystal structures by using a direct writing photolithography process carried out with standard nanofabrication tools. Cavities are created by removing N holes in the transversal direction. Figure 1 shows scanning electron micrographs images of the released regions in a fabricated sample with two cavities (N=3 and N=11). Transmission spectra were taken in the 1260-1630 nm wavelength range by using a conventional end-fire technique. Transmission results of a fabricated sample are shown in figure 2, where it can be seen the appearance of transmission peak inside the PBG corresponding to the excitation of cavity modes. Computations of the N=3 cavity using the Finite Element Method show the existence of three localized photonic modes around 1550 nm and four localized phononic modes around 6 GHz. Moreover, computations using the 3D-FDTD method permit us to observe a great agreement between experimental and theoretical results. Our results lead us to conclude that cavities implemented in square lattice "phoxonic" (or optomechanical) crystals are a very suitable platform to observe an enhanced interaction between propagating photons and phonons.

This research has received funding from the EC Seventh Framework Programme (FP7/2007-2013) under grant agreement number 233883 (TAILPHOX).

References

[1] Y. Pennec et al., "Simultaneous existence of phononic and photonic band gaps in periodic crystal slabs," Opt. Express 18, 14301-14310 (2010).

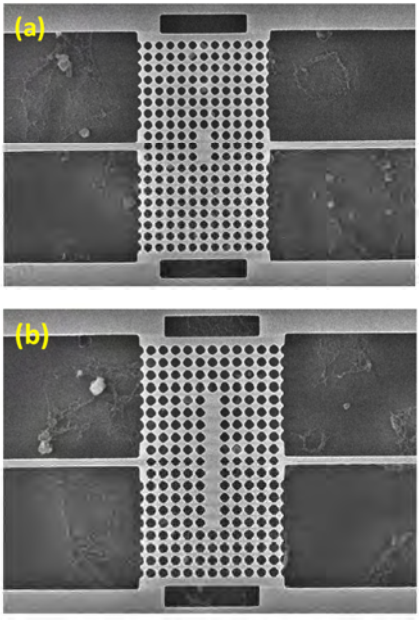

Figure 1: SEM images of a suspended square lattice silicon phoxonic crystals with cavities created by removing N holes in the transversal direction. (a) N=3 and (b) N=11.

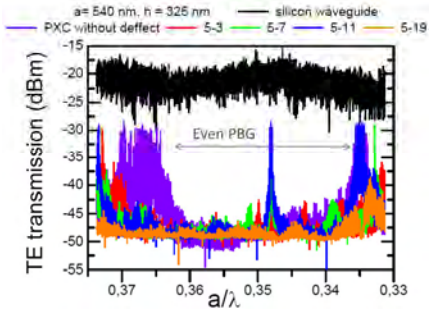

Figure 2: Measured spectra of a fabricated sample. The calculated PBG for even modes is shown. The peaks appearing in the PBG correspond to modes localized in the cavities.

In-situ synthesis of conducting polymers and gold nanoparticles into PMMA

M. L. Martinez-Marco[1], P. J. Rodriguez-Canto [1,*], R. Abargues[2], V. Latorre-Garrido[1] and J. P. Martinez-Pastor[1]

[1]Materials Science Institute, University of Valencia, P.O. Box 22085, 46071 Valencia, Spain
[2]Intenanomat S.L., Catedrático José Beltrán 2, 46980 Paterna, Spain

*pedro.j.rodriguez@uv.es

Hybrid nanocomposites are multicomponent materials in which nanoparticles are dispersed in the polymer matrix. These materials represent an adequate solution to many present and future technological demands, because they combine the novel properties of the nanoparticles with the unique characteristics of polymers (mechanical properties, thin film processing, conductive/dielectric properties, low cost…). In particular, metal nanoparticle-polymer composite materials are generating interest in many fields, such as optoelectronics and photonics, because of the plasmonic effect exhibited by metallic nanoparticles (Au, Ag) hosted in the nanocomposite [1]. Moreover, conducting polymers (CPs) have received much attention due to their interesting electronic and optical properties and potential applications in microelectronics, optoelectronics, photonics, photovoltaics, fuel cells and sensing. The successful application of CPs in many of the above given applications will depend on exploiting their low-cost potential by the innovative design and development of materials for scalable and inexpensive methods to pattern these CPs over different substrates. Thus, the combination of the excellent properties of metal NPs and CPs is of special interest in order to develop new multifunctional advanced materials for the fabrication of more complex devices for the next decade.

On previous works [2,3], we reported on the in-situ polymerization of terthiophene (3T) with $Cu(ClO_4)_2$ inside several host polymers to form an interpenetrating polymer network (IPN). Homogeneous conducting IPN films in the order of 10^{-4} to 150 S/cm were obtained depending on the specific IPN composition. The strong advantage of this approach is to combine properties of the host matrix with those of the in situ synthesized conducting polymers. This was demonstrated using a negative-tone novolak photoresist as a host polymer. Conductive micropatterns were generated by means of UV lithography after proper formulation of a negative-tone Novolak photoresist with 3T and $Cu(ClO_4)_2$.

In this work, we present a novel conducting nanocomposite containing gold nanoparticles. This time, the in-situ polymerization of 3T is carried out using $HAuCl_4$ as oxidizing agent inside PMMA and a negative-tone novolak photoresist. During the bake step, the gold salt is also reduced from Au (III) to Au (0) generating Au nanoparticles in the IPN system. We found that this novel multifunctional resist combines electrical conductivity and plasmonic properties with the potential lithographic capability provided by the host matrix. The resulting nanocomposites was investigated by TEM and UV-Vis spectroscopy. Electrical characterization was also conducted for different concentration of 3T and Au(III) following a characteristic percolation behaviour. We believe this synthetic approach is of potential application to modify the conductivity of numerous insulating polymers and synthesize Au NP preserving to some extent their physical and chemical properties.

References

[1] R. Abargues, K. Abderrafi, E. Pedrueza, R. Gradess, J. Marqués-Hueso, J. L. Valdés ,and J. Martínez-Pastor, New J. Chem., 33 (2009), 1720–1725.
[2] R. Abargues, U. Nickel, P. J. Rodriguez-Canto, Nanotechnology, 19 (2008), 125302.
[3] R. Abargues, P. J. Rodríguez-Canto, R. García-Calzada, and J. Martínez-Pastor, J. Phys. Chem. C, 116 (2012), 17547−17553.

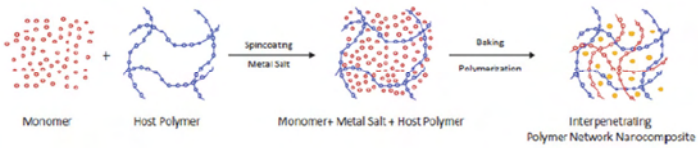

Figure 1: Scheme of in-situ synthesis of the conducting polymer and gold nanoparticle in a host polymer.

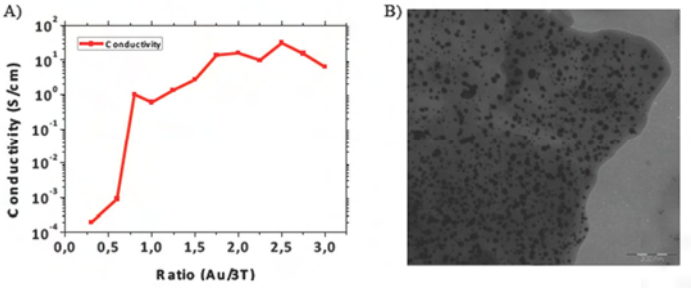

Figure 2: A) Dependency of IPN conductivity on Au/3T molar ratio. B) TEM image of the nanocomposite

Optical optimization for high performance polymer solar cells

Alberto Martínez-Otero[1], Xavier Elias[2], Rafael Betancur[1] and Jordi Martorell[1,2]

[1]ICFO-Institut de Ciencies Fotoniques, Mediterranean Technology Park, Castelldefels, Spain
[2]Departament de Fısica i Enginyeria Nuclear, Universitat Politecnica de Catalunya, Terrassa, Spain

alberto.martinez-otero@icfo.es

When using low-bandgap polymers with extended solar spectrum harvesting properties, efficiencies above 7% have been reached when a fine tuning of the electrical material properties or an optimized architectural device construction has been implemented. In direct architecture bulk hetero-junction devices, the work function of ITO and the metal electrodes can be finely tuned by an electron blocking layer and a hole blocking layer (HBL), respectively.

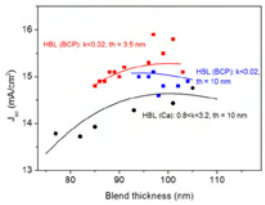

Figure 1: Calculated J_{SC} as a function of the PBDTTT-C:PC71BM blend thickness (solid lines) and experimentally determined J_{SC} for devices with top electrode composed of: 3.5 nm of BCP and 90 nm of Ag (red squares), 10 nm of BCP and 90 nm of Ag (blue squares) and 10 nm of Ca and 90 nm of Ag (black dots).

In the current work we show that the optical material constants of the HBL play a key role in determining the final power conversion efficiency (PCE) of the device. We demonstrate that by a proper selection of the imaginary and real parts of the refractive index, light harvesting can be largely optimized. For the study, we chose benzodithiophene derivatives (PBDTTT-C, PTB7) as the low-bandgap donor materials. Its low laying HOMO energy level is ideal to achieve a large difference with the LUMO of the acceptor. Indeed, PCEs of 6.4% for PBDTTT-C [1] and up to a 7.4% for PTB7 [2] has been reported when using the direct ITO/PEDOT:PSS/POLYMER:PC71BM/Ca/Al architecture. We performed a numerical optical optimization of the light harvesting which demonstrated that a reduced extinction coefficient (k) for the HBL is essential to achieve an optimal light absorption by the active layer. In accordance, in the device architecture indicated above, we replaced the typical back metal electrode composed of a thin 10-20 nm Ca layer and a thicker Al layer by a few nanometer thick bathocuproine (BCP) layer and a thick Ag layer.

BCP, which is a widely used exciton blocking layer in organic devices such OLEDs and small molecule solar cells, possess a k value that is close to zero for a broad range of wavelengths. This enhanced the reflectivity of the back Ag electrode which resulted in an increase of the short circuit current. Light harvesting could be further improved by adjusting simultaneously the thickness of both the BCP and the active layer to achieve an optimal optical interference. Such combined tuning of k and the real part of the refractive index (n) implied an 8% increase in short circuit current. In addition, we observed that when using the BCP/Ag electrode, the photovoltaic parameters of the cell not directly related to photon harvesting such as the open circuit voltage and fill factor also improved. Taking advantage of the optical optimization and the slight improvement in the electrical properties, we were able to fabricate cells with PCEs of 7.5% for the PBDTTT-C and up to 8.1% for the PTB7. In conclusion, we demonstrated that an optimization of the optical properties of the layers in the polymer solar cell is essential to achieve high performance thin film OPV devices.

References

[1] H. Y. Chen, J. H. Hou, S. Q. Zhang, Y. Y. Liang, G. W. Yang, Y. Yang, L. P. Yu, Y. Wu , G. Li , Nat. Photon. 3, (2009), 649.

[2] Y. Liang, Z. Xu, J. Xia, S.-T. Tsai, Y. Wu, G. Li, C. Ray, L. Yu, Adv. Mater. 22, (2010), E135.

Optical characterization of 1D and 2D Silicon PhoXonic crystals with an evanescent light coupling technique

D. Navarro-Urrios[1], J. Gomis-Bresco[1], F. Alzina[1], C. Sotomayor-Torres[1], D. Puerto[2], A. Griol[2] and A. Martinez[2]

[1]Catalan Institute of Nanotechnology (ICN), Campus UAB, Edifici CM3, 08193 Bellaterra, Spain
[2]Nanophotonics Technology Center, Universitat Politècnica de València, Valencia, Spain

dnavarro@icn.cat

Phononic and photonic crystals have been subject of an extensive investigation during the last decades. Structures with the existence of both photonic and phononic gaps (also called PhoXonic crystals) enable the simultaneous localization of acoustical and optical modes, thus enhancing acousto-optical and opto-mechanical interactions.

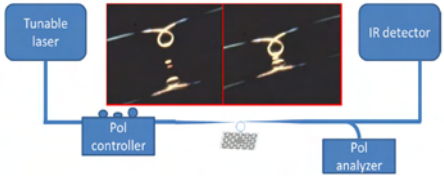

Figure 1: Experimental setup for optical transmission measurements. The two photos show a lateral view of the real fiber away from the sample (left) and close to the sample (right). The mirror image of the fibre can be seen reflected in the sample.

In this work, we will present the optical characterization of 1D and 2D PhoXonic (PX) crystal Silicon membranes fabricated with standard CMOS compatible techniques by means of an optical transmission technique.

The 1D structures are strip waveguides in which each unit cell contains one hole in the middle and two stubs on the sides. [1] The 2D structures are honey-comb lattices with just one type of holes. [2] Both PX crystal geometries have been fabricated without and with single defects, the latter case to provide PX mode localization within the gaps and the defect region.

The experimental setup exploits the evanescent light coupling from a microlooped tapered fiber into the PX structures. The relatively high spatial resolution provided by the loop shape (~1µm) allows the local excitation of the supported optical modes within the gap.

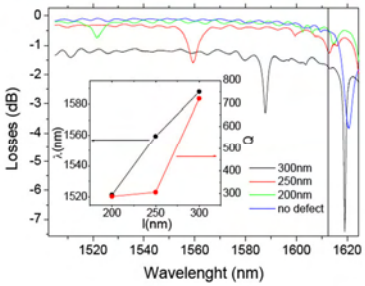

Figure 2: TE polarized transmission curves for different defect lengths for the 1D structures. Spectral position of the resonance for different defect lengths (inset, left) and the corresponding quality factor (inset, right).

On the 1D structures, we will present a study of the effect of the defect length on the spectral position of the resonant localized mode within the gap, while on the 2D structures we will show the effect of changing the pitch and diameter of the holes.
We will discuss on the expected opto-mechanical interaction in these structures on the basis of the experimental results.

This work was supported by EC through the project ICT-FP7-233883 TAILPHOX.

References

[1] Y. Pennec, B. Djafari Rouhani, C. Li, J. M. Escalante, A. Martinez et al. AIP Advances 1 (2011) 041901

[2] Y. Pennec, B. Djafari Rouhani, E. H. El Boudouti, C. Li, Y. El Hassouani, J. O. Vasseur, N. Papanikolaou, S. Benchabane, V. Laude, and A. Martinez, Optics Express 18, 13, (2010) 14301

Graphene supports the propagation of subwavelength optical solitons

M. L. Nesterov[1,2], J. Bravo-Abad[1], A. Yu. Nikitin[2], F. J. Garcia-Vidal[1] and L. Martin-Moreno[2]

[1]Departamento de Fisica Teorica de la Materia Condensada, Universidad Autónoma de Madrid, E-28049 Madrid, Spain
[2]Instituto de Ciencia de Materiales de Aragon and Departamento de Fisica de la Materia Condensada, CSIC-Universidad de Zaragoza, E-50009 Zaragoza, Spain

nesterovml@gmail.com

Nonlinear optical materials have fascinated physicists for decades, due to the fundamental interest of the unique phenomena that they display (such as frequency mixing, supercontinuum generation, and optical solitons) [1,2], as well as their important applications, such as higher-harmonic generation and optical signal processing [3,4]. Recently, a very high nonlinear response has been theoretically predicted [5, 6] and experimentally verified [7] in monolayer graphene. In this work we show that the large intrinsic nonlinearity of graphene at optical frequencies enables the formation of quasi onedimensional self-guided beams (spatial solitons) featuring subwavelength widths at moderate electricfield peak intensities [8]. We illustrate this capability by analyzing two arrangements leading to solitons with different polarizations: a graphene monolayer embedded into a conventional dielectric waveguide and a graphene sheet placed on top of a metal-dielectric structure. We also demonstrate a novel class of nonlinear self-confined modes resulting from the hybridization of surface plasmon polaritons with graphene optical solitons. We analyze in detail the formation of spatial solitons and the relation between soliton width and input power, showing that the subwavelength scale can be reached by using values for the beam peak intensity below the laser-induced damage threshold of graphene. Finally, we also develop a quasi-analytical model that is able to capture the basic ingredients of the numerical results.

References

[1] R. W. Boyd, Nonlinear Optics (Academic Press, San Diego, 1992).
[2] Y. Kivshar and G. Agrawal, Optical Solitons (Academic Press, New York, 2003).
[3] M. Nielsen and I. Chuang, Quantum Computation and Quantum Information (Cambridge University Press, Cambridge, 2000).
[4] G. P. Agrawal, Nonlinear Fiber Optics. (Academic Press, San Diego, 2001).
[5] S. A. Mikhailov, Europhys. Lett. 79 (2007) 27002.
[6] K. L. Ishikawa, Phys. Rev. B 82 (2010) 201402.
[7] E. Hendry, P. Hale, J. Moger, A. Savchenko, and S. Mikhailov, Phys. Rev. Lett. 105 (2010) 097401.
[8] M. L. Nesterov, J. Bravo-Abad, A.Y. Nikitin, F.J. Garcia-Vidal, and L. Martin-Moreno. Submitted.

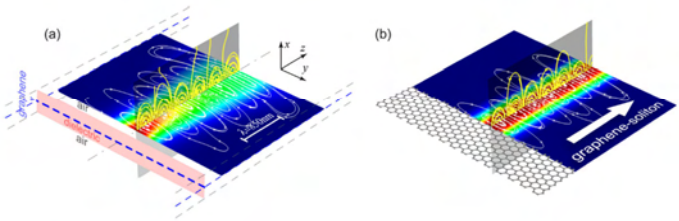

Figure 1: An optical beam propagates inside a dielectric waveguide including a graphene monolayer located in the center, for low (a) and high (b) input powers. Panels (a) and (b) show slices of the beam intensity evaluated at the graphene layer, the yellow lines represent magnetic vector field whereas white lines depict the electric vector field.

Silicon sub-wavelength structures for refractive index and dispersion engineering

Robert Halir[1,2,*], **Alejandro Ortega-Moñux**[1,2], Diego Pérez-Galacho[1], Alejandro Maese-Novo[1], Luis Zavargo-Peche[1], Íñigo Molina-Fernández[1,2], Gonzalo Wangüemert-Pérez[1] and Pavel Cheben[3]

[1]Dpto. Ing. Comunicaciones, ETSI Telecomunicación, Universidad de Málaga, 29010 Málaga, Spain
[2]BIONAND, Severo Ochoa 35, Parque Tecnologico de Andalucia, E-29590 Malaga, Spain
[3]National Research Council of Canada, Ottawa, K1A 0R6, Canada

*robert.halir@ic.uma.es

We show that using sub-wavelength structures both refractive index and dispersion can be locally engineered in integrated silicon photonic waveguides. These concepts are exploited to enhance of the coupling efficiency of fiber-to-chip grating couplers by more than 3dB without increasing fabrication complexity, and to achieve a five-fold broadening of the bandwidth of directional couplers.

Silicon nano-photonics is becoming a platform of mayor interest in both research and industry, because it enables the fabrication of photonic devices with the same infrastructure used to mass-produce CMOS electronics and microprocessors. In fact, it is considered an ideal candidate for optical interconnects that will overcome the copper-wire bandwidth limitation in next generation computing systems [1]. The high precision with which silicon photonic structure can be fabricated enables the use waveguides consisting of a periodic array of two media with a sub-wavelength period. As predicted more than half a century ago such structures should completely suppress diffraction and exhibit an effective refractive index lying between the refractive indices of the two media [2]. Recently such sub-wavelength grating (SWG) waveguides consisting of segments of silicon and air arrayed along the direction of light propagation (see Fig. 1) were experimentally shown to indeed exhibit these characteristics [3]. In the following we describe how SWGs can be exploited for refractive engineering in fiber-to-chip grating couplers and dispersion engineering in directional couplers.

Fiber-to-chip grating couplers are fundamental devices for efficient light injection and extraction from silicon photonic chips. As shown schematically in Fig. 2(a) they operate by placing an optical fiber over the chip and using a grating to change the direction of propagation of light into the horizontally oriented waveguide. If the grating is defined with the same full etch as the waveguide, it becomes very strong and the overlap between the fiber mode and the grating field is poor, limiting coupling efficiency to about -7.7dB, as shown in Fig. 2(b) [4]. However, an SWG arrayed perpendicular to the direction of propagation in the grating grooves [shown in red in Fig. 2(a)], acts as an artificial medium with an intermediate refractive index controlled by the duty-cycle of the SWG [referring to Fig. 1 the duty-cycle of these structures is defined as DC=a/(Λ-a)]. This allows for a better control of the grating strength which results in a more than 3dB enhancement in coupling efficiency, as seen from the measurements in Fig. 2(b). By apodizing the duty-cycle of the SWG, as shown in Fig. 2(c), a further improvement in coupling efficiency as achieved as seen in Fig. 2(b) [5].

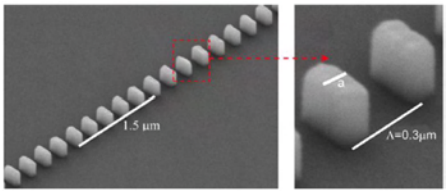

Figure 1: SEM image of a sub-wavelength waveguide, with a blowup of two segments.

Directional couplers are widely used devices in integrated optics, but their bandwidth is limited to around 20nm. As we showed in [6] this limitation arises from the wavelength dependence of the beat length of the coupler's two supermodes, labelled ϕ_1 and ϕ_2 in Fig. 3(a). We insert an SWG arrayed along the direction of propagation in the coupling region as highlighted in red in Fig. 3(a). By adequately designing the pitch this SWG and making use of the fact that its effective refractive index increases significantly as the Bragg wavelength is approached, the wavelength dependence of the beat length can be cancelled. 3D FDTD simulations show that this method flattens the insertion losses of the device over a bandwidth of almost 100nm, yielding fivefold bandwidth broadening compared to a coupler without SWG.

References

[1] M. Asghari, A. V. Krishnamoorthy, Nat. Photon., 5 (2011) 268

[2] S. M. Rytov, Sov. Phys. JETP, 2 (1956) 466

[3] P. Cheben, D.-X. Xu, S. Janz, and A. Densmore, Opt. Express, 11 (2006) 4695

[4] R. Halir, P. Cheben, S. Janz, D.-X. Xu, Í. Molina-Fernández, and J. G. Wangüemert-Pérez, Opt. Letters, 9 (2009) 1408

[5] R. Halir, P. Cheben, J. Schmid, R. Ma, D. Bedard, S. Janz, D. Xu, A. Densmore, J. Lapointe, and Í. Molina-Fernández, Opt. Letters , 19 (2010) 3243-3245

[6] R. Halir, A. Maese-Novo, A. Ortega-Moñux, I. Molina-Fernández, J.G.Wangüemert-Pérez, P. Cheben, D.-X. Xu, J. H. Schmid, and S. Janz, Opt. Express, 12 (2012) 13470.

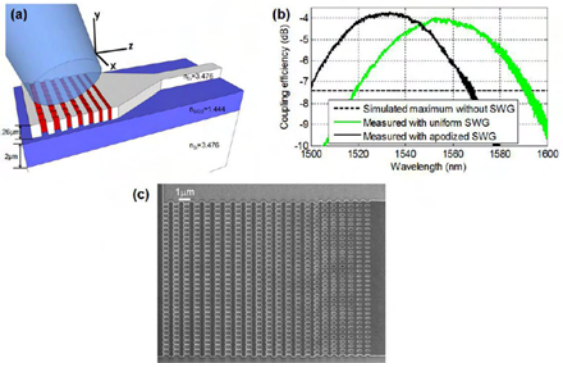

Figure 2: (a) Schematic of a fibre-to-chip grating coupler. (b) Coupling efficiencies of different gratings as a function of wavelength. (c) SEM image of an apodized fibre-to-chip grating coupler.

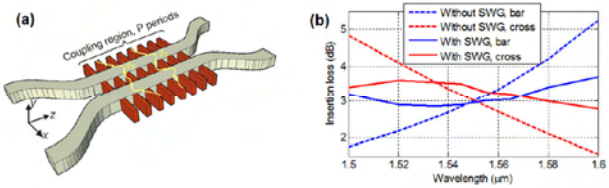

Figure 3: (a) Schematic of a SWG directional coupler. (b) Simulated insertion losses of a conventional coupler and a SWG directional coupler as a function of wavelength.

Optical analysis of 1D diffraction gratings patterned on nanocrystalline titania electrodes for enhanced photovoltaic conversion

R. Ortiz-Marchena, S. Colodrero, M.C. López-López and H. Míguez

Instituto de Ciencia de Materiales de Sevilla,
Consejo Superior de Investigaciones Científicas-Universidad de Sevilla,
Américo Vespucio-49, Sevilla, Spain

reyesortiz@gmail.com

Soft lithography is a useful technique that employs elastomeric stamps to fabricate or replicate different types of nanostructures with surface relief patterns. Two layer composite stamps, made of both PDMS and a thin layer of h-PDMS, allow replicating such kind of structures with high fidelity. [1-2]. In our work, we employ 1D diffraction gratings structures for molding nanocrystalline titania. These patterns give rise to optical diffraction of incoming light in the cell, increasing its optical path and thus enlarging the probability of absorption. We find experimental evidence of the improvement of solar to electric energy conversion efficiency as a result of this optical design.

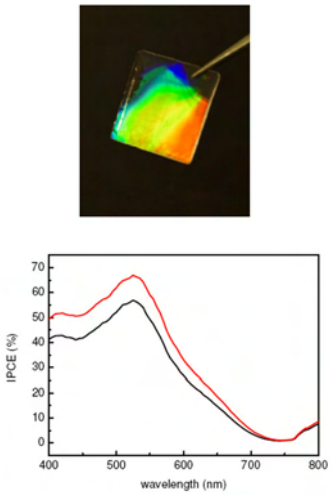

Figure 1: Top: View image of H-PDMS film that has been periodically patterned with a 1D diffraction grating. Bottom: Incident Photon to Collected Electron (IPCE) Efficiency Curves corresponding to the reference (black line) and to the solar cell (red line) of patterned titania.

References

[1] T.W. Odom, J.C. Love, D.B. Wolfe, K.E. Paul, G.M. Whitesides, Langmuir, 13 (2002) 5314.
[2] D. Qing, Y. Xia, G.M. Whitesides, Nature Protocols, 3 (2010) 491.

Au and Ag nanoparticle-doped-TiO_2 thin films: structural and optical characterization and antireflective properties

Esteban Pedrueza[1], Jordi Sancho-Parramon[2,4], Carlos Diaz-Egea[3], Manolo Dominguez[5], Rafael Abargues[1], José Luis Valdés[1], Sergio I. Molina[3], Salvador Bosch[4] and Juan P. Martinez-Pastor[1]

[1]UMDO (www.uv.es/umdo), Instituto de Ciencia de los Materiales, Universidad de Valencia, Valencia, Spain
[2]Rudjer Boskovic Institute, Zagreb, Croatia
[3]Departamento de Ciencia de los Materiales e I. M. y Q. I.,Facultad de Ciencias, Univ. de Cádiz, Cádiz, Spain
[4]Applied Physics and Optics Department, Universitat de Barcelona, Barcelona, Spain
[5]ADepartamento de Física de la Materia Condensada, Facultad de Ciencias, Univ. de Cádiz, Cádiz, Spain

esteban.pedrueza@uv.es

Metal-dielectric nanocomposite (MNC) thin films have attracted much attention in the last years due to its unique electromagnetic behavior and high potential in diverse fields like photovoltaics [1] and sensing [2], other than metamaterials, photodetectors, catalysis, sub-wavelenght imaging, etc. The special electromagnetic properties of the MNC are primarily dominated by the localized surface plasmon resonance (LSPR) typical of noble metal nanoparticles (NPs). The control of the size, shape and density of these NPs embedded in a given solid matrix is needed for most of these applications.

Embedded in-situ Au nanoparticles (NPs) in solid dielectric matrices of SiO_2 and TiO_2 has been recently developed using a sol-gel method implemented for spin-coating deposition. The average diameter and the density of the NPs can be changed varying the metal precursor concentration. Larger Au NPs (of around 40 nm) can be obtained in TiO_2 films than in SiO_2 (around 13 nm) [3], this may be important for photovoltaic (PV) applications, because light scattering predominates over light absorption for larger metal NPs. After a treatment with a weak wet-chemical etching, formation of a pores structure in the film takes place, which is translated, for films deposited over Si substrates, in a strong anti-reflectance effect in comparison with non-etched films, meanwhile an intensity decrease and blue shift of the extinction spectra is clearly appreciable for samples deposited over glass substrates (fig. 1); this is consistent with the formation of the porous structure developing from the film surface towards the Si-interface, because the overall refractive index decrease over the curve measured by ellipsometry before etching.

More recently, we have extended this method to the case of Ag NPs by varying the metal precursor concentration [5]. The structural characterization, performed by HRTEM, HAADF-STEM, SEM and AFM techniques, reveals a succesful formation of Ag NPs inside and onto the film surface (figs. 2a-b). Optical measurements (reflectance, extinction, ellipsometry) have been performed, revealing a LSPR extinction peak appearing at ~520 nm, due to the high effective medium dielectric function. Again, if we apply a similar wet-chemical etching process explained above, a minimum in the overall reflectance curve will be observed (fig. 2c), making these films good candidates for antireflective coatings in PV applications, due to the low cost of making solar cells using silver rather than gold. In both cases the method is simple, easy to scale up and enables a certain control over size and density of NPs by changing the precursor concentrations, humidity and temperature.

This work was supported by the EU-FP7 project NANOPV and the project PROMETEO/2009/074 from the Generalitat Valenciana, through JAE-Predoc grant program (CSIC), the Spanish MINECO (projects TEC2011-29120-C05-03 and CONSOLIDER INGENIO 2010 CSD2009-00013), the Junta de Andalucía (PAI research group INNANOMAT TEP-946), and the "Beatriu de Pinos" grant 2009 BP-B 00294 from the Generalitat de Catalunya.

References

[1] Atwater, H. A,;Polman, A., Nat. Mater., 9 (2010) 205.

[2] Gradess, R.; Abargues, R.; Habbou, A.; Canet-Ferrer, J.; Pedrueza, E.; Russell, A.; Valdes, J. L.; Martinez-Pastor, J. P., J. Mater. Chem., 19 (2009) 9233.

[3] Pedrueza, E.; Valdés, J. L.; Chirvony, V.; Abargues, R.; Hernández-Saz, J.; Herrera, M.; Molina, S. I.; Martínez-Pastor, J. P., Adv. Funct. Mater., 21 (2011) 3502.

[4] Pedrueza, E.; Sancho-Parramon, J.; Valdés, J.L. ;Bosch, S.; Martinez-Pastor, J. P., to be published.

[5] Pedrueza, E.; Diaz-Egea, C.; Sancho-Parramon, J.; Dominguez, M.; Abargues, R.; Valdés, J. L.; Molina, S. I.; Bosch, S.; Martinez-Pastor, J. P., to be published.

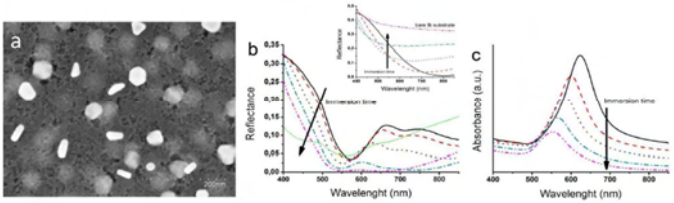

Figure 1: a) Planar view SEM image of etched Au-NPs/TiO_2 thin film, b) reflectance spectra (film deposited over Si substrate) with different times of etching (in the inset, the reflectance of an etched TiO_2 bare layer), c) extinction spectra of the same film (deposited over glass substrate).

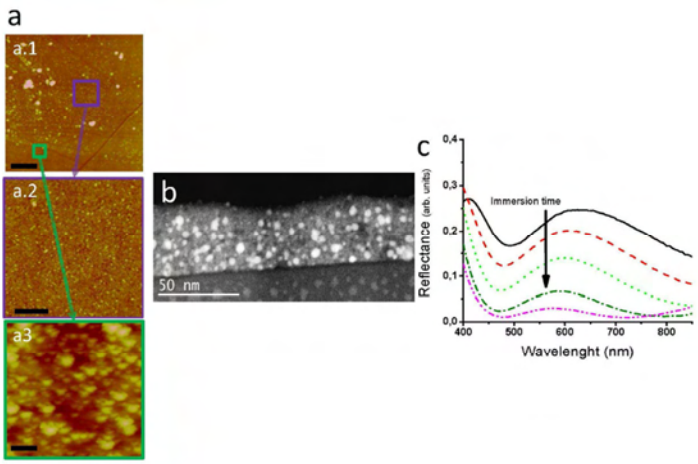

Figure 2: a) AFM images with different zooms of the surface of a Au-NPs/TiO_2 thin film (the black line represents the scale of a.1) 2 µm, a.2) 500 nm and a.3) 100 nm). b) HAADF-STEM cross section image showing the Ag NPs inside the layer. c) Reflectance spectra of film when it is applied the wet chemical etching process.

Direct ink writing of ZnO three-dimensional terahertz photonic crystals

Carmen Rial[1], José Ramón Salgueiro[2], Francisco Guitián[1] and Álvaro Gil[1]

[1]Instituto de Cerámica, Universidade de Santiago de Compostela, , Santiago de Compostela, Spain
[2]Departamento de Física Aplicada, Universidade de Vigo, Ourense, Spain

mdelcarmen.rial@usc.es

Photonic crystals are materials with periodic modulation in the dielectric constant that exhibit bandgaps in which the electromagnetic waves propagation is forbidden. There is a broad research on photonic crystals in the visible and infrared range, however this research is limited on the terahertz band. Recent developments in the generation and detection of terahertz waves and new technologies based in this range of frequencies have risen the interest in developing materials for guidance and processing of this kind of radiation.

In recent years, an intensive effort has been made to obtain photonic crystals that can be patterned in one single step. Direct ink writing (DIW) technique enables to fabricate three-dimensional photonic crystals in a single step [1,2]. This technique relies on direct writing of a continuous filament in a layer-by-layer built sequence.

This work is on the fabrication and characterization of periodic structures -photonic crystals- to guide and process radiation in the terahertz spectral range. We report three-dimensional photonic crystals for terahertz frequencies patterned by direct-ink writing in one-step and further sintering at 900 °C using ZnO. ZnO is a very suitable material to use in the THz frequencies due to its high dielectric constant [3]. Among the structures that support complete photonic bandgaps, the diamond and related woodpile structures stand out due to its wide and robust bandgap even with a moderate dielectric contrast. To fabricate our photonic crystal we chose the woodpile structure in order to get a complete bandgap [4]. The photonic crystal of woodpile structure was designed using CAD software.

A ZnO aqueous colloidal suspension was developed for DIW. Woodpile structures with rod diameter of 200 µm were fabricated from these inks by using DIW (Fig.1). The preparation and rheological behaviour of aqueous inks and the sintering process were systematically studied. Furthermore, the critical parameters for the design of a woodpile structure, such as the rod width and the rod spacing were determined by optimizing the bandgap in the THz frequency range.

(a)

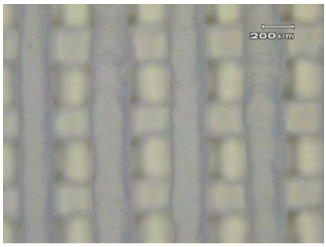

(b)

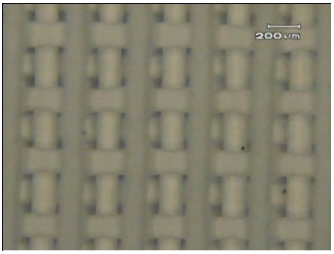

Figure 1: Optical microscopy image of a 3D woodpile structure assembled from aqueous ZnO ink. a) dried and b) after sintering at 900 °C for 2.5 hours.

References

[1] G. M. Gratson, M. Xu and J. A. Lewis, Nature, 428 (2004) 386.
[2] J. E. Smay, J. Cesarano III and J. A. Lewis, Langmuir, 18 (2002) 5429.
[3] Y. Kim, K. Ahn, B. G. Kim and D. Yee, Japanese Journal of Applied Physics, 50 (2011) 030203.
[4] M. Maldovan, E. L. Thomas, and C. W. Carter, Applied Physics Letters, 84 (2004) 362.

Single photons emitted by quantum dots: towards all-optical q-gates

D. Rivas, G. Muñoz-Matutano, J. Canet-Ferrer, and J. Martínez-Pastor

UMDO (Unidad Asociada al CSIC-IMM), Instituto de Ciencia de los Materiales, Universidad de Valencia, PO Box 22085, 46071 Valencia, Spain

david.rivas@uv.es

Self-assembled quantum dots (QDs) are nanostructures that confine electrons and holes in all three dimensions. This induces a zerodimensional density of states and a discrete spectrum of single-carrier energy levels [1,2]. Recently, we demonstrated that emission wavelength of single InGaAsQDs can be tuned over a wide range of interest for telecommunications (900 – 1300 nm) byan appropriate engineering of the growth conditions [3]. Other than applications in standard optoelectronics, these kinds of QDsare particularly promising for future emitters of single/entangled photons [4,5] and quantum logic elements [6] in quantum information processing and computing.

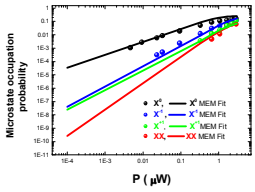

Figure 1: is presented the intensity evolution when exciting. Solid circles correspond to experimental data for the principal excitonic complexes and solid lines correspond to the results obtained with the models.

In this work, we present an adaptation of the Master Equations forthe Microstates (MEM) to reproduce the capture and recombination dynamics of the ground exciton states (quasi particles) confined in a single QD [7].This model considers that QDs are charged via 2D-statesof the wetting layer (WL), where pumping light is producing carriers, in two different ways: exciton capture (correlated e^- - h^+ capture) and uncorrelated (e^-,h^+) capture. The main input parameters of the model are (once considered that capture times are very fast compared to the other time constants): uncorrelated (e^-,h^+) escape times out of the QDs (te_e,te_h), the generation rates of correlated and uncorrelated carriers, G_X and G_{eh}, and the radiativo life times for the different exciton species (τ_r).Not all of these parameters are free and we can fix the experimentally measured radiative lifetimes of the different exciton species (τ_r of neutral and charged excitons, and biexciton).The other parameters (generation rates and escape times) are used as free fitting parameters to reproduce the power evolution of the emission intensity for the different exciton species, as shown in Fig. 1 for fitting parameters listed in Table 1. This procedure can be also applied to different single QDs with different charge environment. The latter condition can be simulated by introducing an extra reservoir of electrons to be transferred into the QD ground states (through an extra generation rate, G_I) if selective pumping is used [8].

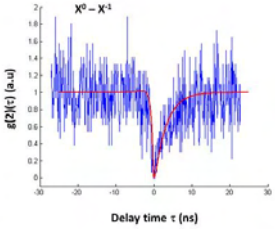

Figure 2: In blue the measured photon correlation function (g(2)(τ)) a single QD for $X^0 - X^{-1}$, and red line correspond the theoretical fit.

The output of the MEM model can be used to quantify the experimentally mesured second-order correlation function, g(2)(τ), both self- and cross-correlations, using the Hanbury-Brown-Twiss experiments, as shown in Fig. 2 for the case of neutral exciton and trioncross-correlations. Finally, we also conducted two-color experiments to measure cross-correlations between neutral

excitons and trions, but now generated with different pumping lasers, demonstrating a NAND-gate operation using single photons, again quantitatively corroborated byour MEM model.

References

[1] Hartmann, Y. Ducommun, E. Kapon, U. Hohenester and E. Molinari, Phys. Rev. 84, 5648 (2000).

[2] [E. Dekel, D. Gershoni, E. Ehrenfreund, J. M. Garcia, and P. M. Petroff, Phys. Rev. B 61, 11009 (2000).

[3] L. Seravalli, G. Trevisi, P. Frigeri, D. Rivas, G. Muñoz-Matutano, I. Suárez, B. Alén, J. Canet, and J. P. Martínez-Pastor, applied physics letters 98, 173112 (2011).

[4] Michler P, Kiraz A, Becher C, Schoenfeld W V, Petroff P M, Zhang L D, Hu E and Imamoglu A 2000 Science 290,2282.

[5] Santori C, Pelton M, Solomon G, Dale Y and Yamamoto Y 2001 Phys. Rev. Lett. 86, 502 (2011).

[6] Chen P, Piermarocchi C and Sham L J 2001 Phys. Rev. Lett. 87, 067401 (2010).

[7] J. Gomis-Bresco, G. Muñoz-Matutano, J. Martínez-Pastor, B.Alén, L. Seravalli, P. Frigeri, G. Trevisi, and S. Franchi, New J. Physics 13, 023022 (2011).

[8] G. Muñoz-Matutano, B. Alén, J. Martínez-Pastor, L. Seravalli, P. Frigeri, and S. Franchi, Nanotechnology 19, 145711 (2008).

te_e	te_h	$\tau_r(X^0)$	$\tau_r(X^{-1})$	$\tau_r(X^{+1})$	$\tau_r(XX)$	G_x	G_{eh}
5.5ns	3.5ns	0.85ns	0.892ns	0.892ns	0.539ns	0.046 excitones ns^{-1}	0.0061 $e^- - h^+$ ns^{-1}

Table 1: CW fitting parameters corresponding to figure 1 and 2.

Application of nanophotonic biosensors for the detection of traces of DMMP

Francisco Cuesta-Soto[*], **Manuel Rodrigo**, Jose Sansano, Antonio Varriale, Sabato D'Auria, Nuria Sanchez, Francisco Lopez-Royo, Benny Siegert, Karine Bonnot, Nelly Piazzon and Denis Spitzer

[1]DAS Photonics S.L., Camino de Vera s/n, Valencia, Spain
[2]Instituto di Biochimica delle Proteine (IBP), CNR, Napoli, Italy
[3]Nanophotonics Technology Center (NTC), Universidad Politécnica de Valencia, Valencia, Spain
[4]Nanomatériaux pour les Systèmes Sous Sollicitations Extrêmes (NS3E), UMR 3208 CNRS/ISL, Saint Louis, France

[*]fcuesta@dasphotonics.com

Abstract

Label free measurement systems are developed for the implementation of more sensitive and reliable solutions for detection purposes. The specific detection of some chemical compounds is specially challenging due to the small size of the target molecules. In this work it is shown the detection of chemicals with interest in defence and security applications. By means of a photonic refractive index sensor coated with biospecific bovine odorant binding protieins (b-OBP) direct measurements of ultra low concentrations (20 ppb) of DMMP has been achieved.

Introduction

The detection of traces and ultra-traces of toxic and harmful compounds in air by using networks of small sensors like MEMS (Micro Electro Mechanical Systems) or Lab-on-Chip devices, has led to a challenging research in these last years. Developments in biosensing solutions seek for the implementation of faster, more reliable sensing solutions with an ever increasing sensibility and at the same time easiness in the operation. These general features are valid for a big variety of fields in which the biosensors can be applied such as the medicine, veterinary or industrial applications. The molecular recognition approaches show outstanding performances with big biospecificity and are the ones with bigger expansion in commercial applications. Some of the most spread techniques, such as the well known ELISA (Enzyme-linked immunoSorbent assay) or ELFA (Enzyme-linked fluorescent assay), rely on the use of labelling molecules in the process of detection. These approaches require a labelling process that increases the complexity of the measurement. When the target of the sensing application consists of small chemical molecules these techniques fail due to the existence of only a single antigenic determinant. Therefore these kinds of techniques are no more valid for detection of chemicals with very small sizes.

Optical technology is one of the solutions widely used for implementation of transduction systems to monitor the sensing of a pollutant. Coupled to bio-recognition, nanoscale photonic Lab-on Chip systems permit both (i) the integration in one single device of several parts such as the probe, the transduction and the sampling system; and (ii) the development of a powerful detection and analysis tool with advantages of low cost and portability. Label free photonic biosensors have vast applications, especially in environmental and industrial monitoring.

This work, carried in under the project of the EDA JIP-ICET NANOCAP, deals with the detection of Dimethyl methylphosphonate (DMMP) as a stimulant of Sarin Gas for defence and security sensing applications.

Experiment and results

The sensing structure employed in the measurements consists of photonic integrated

circuits [1] implemented with Si_3N_4 strip waveguides with a cross section of 0.3x1.1µm. The transduction is implemented with a ring resonator (RR) structure with a total length of 654 µm. SEM micrographs of the fabricated RR are shown in Fig.1. The Si_3N_4 layer was deposited using low pressure chemical vapor deposition (LPCVD) and was patterned using i-line photolithography and dry etching. The ring resonator was functionalized with bovine odorant binding proteins (b-OBP) whose amino acid sequence was modified to selectively bind DMMP [2].

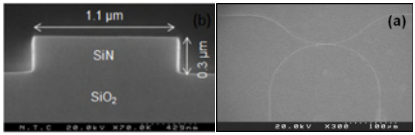

Figure 1: SEM images of the cross section of the SiN waveguide (left) and the ring resonator structure employed for the transduction of the biochemical binding (rigth).

A constant flow of 200 mL/min of N_2 is employed in the measurement for transporting the traces of DMMP. First the sensor is stabilized with the N_2 flow and then injections of 20 ppb of DMMP are performed to test the sensor. To demonstrate the selectivity binding of the b-OBP and check that there is no inespecific adsorption, the experiment was implemented in three different chips: one functionalized for DMMP with the b-OBP, a second raw chip without functionalization and finally a chip with a functionalization with other proteins. Results from the experiments are shown in Fig. 2 a, b and c respectively.

As it is shown in the graphs of Fig. 2 the flow of DMMP leads initially to a transient drift in the wavelength in the three cases but only the chip functionalized for detection of DMMP shows a stable signal (wavelength shift of ~20pm) due to the binding. The absence of a signal in the raw chip and in the one functionalized with proteins shows that there is no unspecific adsorption to the chip and neither to the proteins. In all the experiments all the conduction tubes and the measuring cell where heated up to 80 ºC to prevent the adsorption.

Conclusion

In this work it is shown the capabilities of nanophotonic biosensros for the detection of traces of DMMP (20 ppb) in gas medium. The implementation of a direct measurement without labelling process permits the direct detection of small molecules with a single epitope. The technique shows high sensitivity but at the same time simplicity since it measures the target DMMP directly in gas phase without the need of preconcentration systems and the transportation to liquid phase.

These are key features for the implementation of defence and security applications in the surveillance of environmental conditions.

This work was supported by the NANOCAP project A-1084-RT-GC that is coordinated by the European Defence Agency (EDA) and funded by 11 contributing Members (Cyprus, France, Germany, Greece, Hungary, Italy, Norway, Poland, Slovakia, Slovenia and Spain) in the framework of the Joint Investment Programme on Innovative Concepts and Emerging Technologies (JIP-ICET).

References

[1] Jokerst, N., Royal, M., Palit, S., Luan, L., Dhar, S., Tyler, T. J. Biophoton. 2(4) (2009) 212–226.

[2] Bañuls, M.J., González-Pedro, V., Barrios, C.A., Puchades, R., Maquieira, A. Biosens. Bioelectron. 25(6) (2010) 1460–1466.

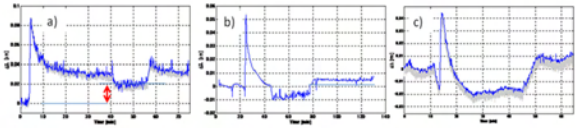

Figure 2: SEM images of the cross section of the SiN waveguide (left) and the ring resonator structure employed for the transduction of the biochemical binding (rigth).

Plasmonic layers of colloidal Ag nanoparticles for enhancement of light trapping in silicon solar cells

Raúl García-Calzada[1,*], **Pedro Rodríguez-Cantó**[1], Vladimir Chirvony[1], Rafael Abargues[2] and Juan P. Martínez-Pastor[1]

[1]Instituto de Ciència de los Materiales, Universidad de València, Apartado de Correo 22085, 46071 Valencia, Spain
[2]Intenanomat S.L., Catedrático José Beltrán 2, 46980 Paterna, Spain

raul.garcia@uv.es

During the last decade, extensive studies have been undertaken concerning a possibility to use Au and Ag nanoparticles (NPs) supporting localized surface plasmons (LSP) for achieving enhanced light absorption in silicon solar cells [1]. In particular, theoretical studies made significant progress in optimizing the design of Si solar cells containing plasmonic NPs and in understanding the mechanisms of increasing their efficiency, whereas experimental investigations of plasmonic effects in Si-based photovoltaics are much less developed. Primarily this is due to the lack of simple and reliable methods of incorporation of plasmonic NPs layers into silicon solar cell structures.

Until now the mostly often used method of metal NPs incorporation into Si solar cell structures is the thermal-evaporation induced formation of metal thin films with subsequent annealing to form NPs [2]. Although the method provides good physical contact between metal NPs and a substrate, it possesses such considerable disadvantages as an inability to vary the NPs shape and difficulties of varying the NP size and obtaining big NPs with narrow size distribution: the latter is very important since only big-size NPs demonstrate high-efficiency light scattering whereas light absorption prevails in case of small-size NPs.

The present work is devoted to the development and investigation of the other method of metal NPs incorporation into Si solar cell structure, namely the deposition of colloidal metal NPs from liquid suspension with subsequent solvent evaporation. Although this method has been formally used in the middle of 2000s by one group to deposit big-size Au NPs on top of several types of solar cells [3, 4], the very low level of surface covering by NPs (about 1%) as well as the absence of any optical data (reflectance spectra) in these publications suggest that hardly the metal NPs plasmonic properties were responsible for the observed improvements of Si solar cells efficiencies. In view of the above our first task was to achieve high levels (at least 10%) of solar cell surface covering by metal NPs and confirmation of this level of covering by optical (reflectance spectra) and direct SEM measurements.

(a)

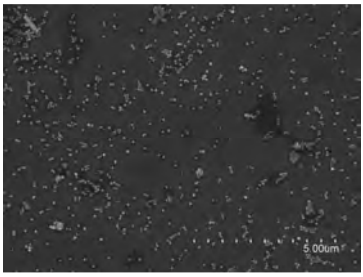

(b)

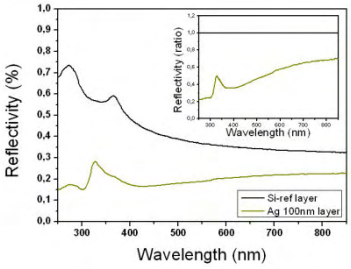

Figure 1: (a) SEM image of Ag NPs layer deposited on silicon. The covering factor is about 6%. (b) Reflectance spectra of the Si substrate before (upper curve; the reference spectrum) and after (lower curve; the working spectrum) 100-nm Ag NPs deposition. The inset shows a ratio of the working spectrum to the reference one and demonstrates antireflection properties of the silver NPs layer.

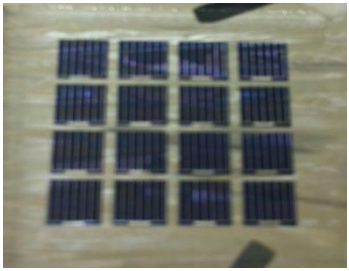

Figure 2: Layout of a set of 16 aSi/cSi solar cells on one common glass substrate.

We used 100-nm diameter colloidal Ag NPs (NanoComposix, USA) to prepare the plasmonic layers. We used two types of Ag NPs bearing different organic ligands on their surface, either citrate anions or polyvinylpyrrolidone. Two methods of deposition were used: (i) the deposition on bare substrates, and (ii) the deposition on preliminary functionalized substrates. To the best of our knowledge, this is the first time when the functionalization method, which results in covalent attachment of Ag NPs to substrate surfaces through a chemical linker (3-mercaptopropyltriethoxysilane in our case) is used for metal NPs deposition onto solar cells. Having in mind the necessity of Ag NPs incorporation into different solar cell structures, we carried out deposition of colloidal Ag NPs on Si, ZnO, and SiNx surfaces and investigated SEM images and optical reflectance spectra of the corresponding substrates. A regime of multiple deposition as well as a post-deposition heating of substrates were applied to achieve high values of the covering factor. Fig. 1 shows SEM image and reflectance spectra of Si substrate before and after covering by a layer of 100-nm Ag NPs. As one can see, a considerable decrease of reflectance is observed over all spectral region investigated (250-850 nm).

As the next step, we carried out the deposition of colloidal Ag NPs on ZnO surface of heterojunction aSi/cSi solar cells (the layout of a set of such cells is shown in Fig. 2). The effect of Ag NPs deposition on the solar cell optical properties as well as external quantum efficiency will be presented in our poster.

References

[1] G. M. Gratson, M. Xu and J. A. Lewis, Nature, 428 (2004) 386.

[2] J. E. Smay, J. Cesarano III and J. A. Lewis, Langmuir, 18 (2002) 5429.

[3] Y. Kim, K. Ahn, B. G. Kim and D. Yee, Japanese Journal of Applied Physics, 50 (2011) 030203.

[4] M. Maldovan, E. L. Thomas, and C. W. Carter, Applied Physics Letters, 84 (2004) 362.

Disordered macroporous silicon as optical filter in the medium infrared region

E. Romano, M. Alba, J. Ferré-Borrull and L. F. Marsal

Universitat Rovira I Virgili, DEEEA,
Avda Paisos Catalans 26, 43007 Tarragona, Spain

elisabetta.romano@urv.cat

The ability to modify the properties (electromagnetic, optical, thermal and so on) of a material tailoring them for target applications is a powerful tool for the maximization of the performances of ultimate devices. Micro- [1] and even more efficiently nano-technology [2] have certainly boosted the development of that field. Porous silicon is a prototypical example: whereas crystalline silicon is not photoluminescent, porous silicon shows tunable visible photoluminescence, strictly related to the structural parameters of thickness, porosity, pore shape and size (from few nanometers to microns), and to the chemical termination of the inner surface [3].

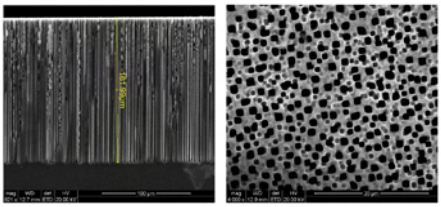

Figure 1: Cross (left) and top (right) view SEM images of disordered macroporous layer, sample 1.

Due to the huge impact on the world of optoelectronics, the optical response of porous silicon in the region from visible to near infrared radiation has been thoroughly studied [3,4]. Since in the mid-infrared (mid-IR, 2.5–25 μm) its optical behavior does not differ from that of crystalline silicon, but the surface-to-volume ratio can be increased up to 3 orders of magnitude, for a long time porous silicon has been used as an easy tool for the vibrational analysis of organic monolayer grafted onto the Si surface [3]. More recently, ordered arrays of macropores [5,6] have shown the ability to block the transmission of specific wavelength ranges in the mid-IR, working as filters.

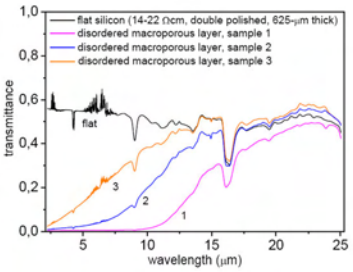

Figure 2: IR transmittance spectra before and after the formation of a layer of disordered macropores. The layer thickness and the porosity range are: sample 1, 162μm and 25-45; sample 2, 64μm and 19-36; sample 3, 20 μm and 13-30. In all cases the reference is the spectrum of the empty chamber.

Here we report preliminary results about the lowering of the transmittance in the 2–10 μm region when the IR beam crosses a disordered macroporous layer (Fig. 1) along the pore direction. The pores are obtained via electrochemical etching in a solution of HF in dimethylformamide [6] without any photolithographic pre-patterning of the surface. Fig. 2 shows that the filtering efficiency varies with both the thickness and the percentage of void space in bulk silicon (porosity), being the two characteristics strictly coupled in disordered macroporous layers.

This work was supported by the Spanish Ministry of Science and Innovation (MICINN) under grants No TEC2009-09551 and TEC2012-34397, CONSOLIDER HOPE project CSD2007-00007 and AGAUR 2009 SGR 549.

References

[1] B. G. Lee, Y.-T. Lin, M.-J. Sher, E. Mazur, H. M. Branz, proceeding of 2012 IEEE Photovoltaic Specialists Conference Austin, Texas June 3–8, 2012.

[2] Y. He, G. Galli, Phys. Rev. Lett., 108 (2012) 215901.

[3] M. J. Sailor, Porous Silicon in Practice: Preparation, Characterization and Application, 2011, Wiley-VCH: Weinheim, Germany.

[4] K. A. Salman, Z. Hassan, K. Omar, Int. J. Electrochem. Sci., 7 (2012) 376.

[5] T. Trifonov, L. F. Marsal, A. Rodríguez, J. Pallarès, R. Alcubilla, Phys. Stat. Sol. C, 2 (2005) 3104.

[6] M. Garín, T. Trifonov, A. Rodríguez, L. F. Marsal, R. Alcubilla, Mat. Sci. Eng. B, 149 (2008) 275.

Plasmonic Fano resonances on single nanorods: Application to refractive index sensing

F. López-Tejeira, R. Paniagua-Domínguez, R. Rodríguez-Oliveros and **J. A. Sánchez-Gil**

Instituto de Estructura de la Materia (CSIC), Serrano 121, 28006 Madrid, Spain

j.sanchez@csic.es

Metal nanoparticles exhibit a rich optical phenomenology due to the excitation of localized surface plasmons (LSPs). A special type of LSP resonances are highly promising for potential applications due to the extremely narrow (asymmetric) line shapes and fine sensitivity to environment changes: Fano LSP resonances [1]. Fano LSP resonances require typically complex multi-particle configurations involving wide, dipolar modes with narrow, dark modes.

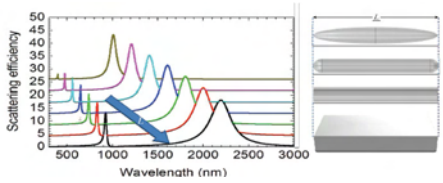

Figure 1: Calculated scattering efficiency spectra for a single Ag spheroid (top right) surrounded by glass (ε_d=2.25). Incident field is p-polarized and perpendicular to the rotation axis of the spheroid. Different curves correspond to increasing values of L (diameter D=30 nm). Right: Nanorod geometries for which evidence of Fano LSP is found in [2].

Contrary to such common assumption that coupling between nanoparticles is required to excite Fano LSP resonances, we show analytically and numerically in this work [2] that (single) elongated Ag nanoparticles such as nanospheroids, nanorods, and rectangular nanowires, suffice to exhibit asymmetric (Fano) resonances as a consequence of the interference between the broad, (dipole-like) half-wavelength mode, with dark, higher-order modes (see Fig. 1). We make use of explicit analytical expressions for light scattering by spheroids to conclude that not only spectral but also spatial overlap (i.e. non-orthogonality) between interacting modes underlies the emergence of such single-rod resonances [2].

Potential applications in (Fano) LSP sensing are discussed that exploit the simplicity of the required nanostructures, resulting in turn in large figures of merit [3]. In particular, two configurations are proposed based on elongated nanorods: colloidal nanorice and nanobelts on a substrate (see Fig. 2).

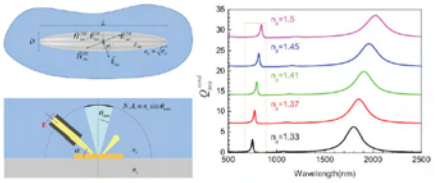

Figure 2: Left: Configurations proposed for refractive index sensing based on Fano LSP resonances: Colloidal Ag nanorice (top) and Au nanobelt on a substrate (bottom). Right: Scattering efficiencies for random orientation for a single nanospheroid (L=345 nm, D=30 nm) embedded in a medium with different index of refraction n_d [3].

Acknowledgements: Spanish "Ministerio de Economía y Competitividad" (CSD2008-00066 and FIS2009-11264), "Comunidad de Madrid" (S2009/TIC-1476), and CSIC (JAE-Pre grant).

References

[1] A. Miroshnichenko, S. Flach, and Y. Kivshar, Rev. Mod. Phys. 82 (2010) 2257.

[2] F. López-Tejeira, R. Paniagua-Domínguez, R. Rodríguez-Oliveros, and J. A. Sánchez-Gil, New. J. Phys. 14 (2012) 023035.

[3] F. López-Tejeira, R. Paniagua-Domínguez, and J. A. Sánchez-Gil, ACS Nano in press (2012).

Light Harvesting at the Infrared

F. Villate-Guío[1], F. López-Tejeira[2], F.J. García-Vidal[3], L. Martín-Moreno[1] and F. de León-Pérez[1,4]

[1]Instituto de Ciencia de Materiales de Aragón and Departamento de Física de la Materia Condensada, CSIC-Universidad de Zaragoza, Zaragoza, Spain
[2]Instituto de Estructura de la Materia (IEM-CSIC), Madrid, Spain
[3]Departamento de Física Teórica de la Materia Condensada, UAM, Madrid, Spain
[4]Centro Universitario de la Defensa de Zaragoza, Zaragoza, Spain

fvillateguio@gmail.com

New developments in optoelectronics and chemical sensing are based on a single subwavelength aperture drilled in an opaque metallic film, which surface is sculpted at the scale of the wavelength. In systems, like the slit-groove array (SGA) sketched in Fig. 1, surface corrugation acts like an antenna to couple the incident light into surface modes that squeeze the electromagnetic energy into the aperture [1, 2]. Surface modes are responsible of the light harvesting process. Transmission resonances can be controlled adjusting the geometric parameters of the SGA [3].We study SGA of Fig.1 in order to identify simple design rules for optimal light transmittance. Such rules are developed from the physical mechanism responsible for squeezing light into the aperture. The light harvesting process is also optimized using the conjugate gradient (CG) algorithm which uses as seed optimal values taken from simulations based on the physical intuition. We shall consider uniform and periodic groove arrays as well as nonuniform and non periodic ones. The calculations are done in the framework of the coupled-mode method with surface boundary conditions [2]. We compute the intensity of the light radiated to the far field and normalize it to the light incident on the area of the slit, this quantity, called η, accounts for the efficiency of the light harvesting process. Fig.2 shows η as a function of groove period (a), the distance from the slit to the nearest groove (b) and the groove width (c), for an optimal SGA with N_g= 10, w_s= 0.36μm, h_s = 1.28μm, P = 3.81μm, d_{sg} = 3:64μm and wavelength λ = 4.0μm. We find that Fabry-Perot(FP) and cavity modes should be at the same spectral position for the whole IR regime. For subwavelength apertures at a given λ, the position and intensity of the FP modes are controlled by metal thickness and aperture size, respectively. The spectral position for the cavity modes is mainly determined by groove depth and pitch. We also observe that transmission efficiency of a uniform SGA in the infrared is practically independent of λ. In contrast, the enhancement provided by nonuniform SGA decreases with λ. A chirped groove array enhances the transmittance between 15% and 39% for decreasing λ (not shown but discussed in [4]).

References

[1] C. Genet and T. W. Ebbesen, Light in tiny holes, Nature (London) 445, 3946 (2007).
[2] F. J. Garc´ıa-Vidal, L. Mart´ın-Moreno, T. W. Ebbesen, and L. Kuipers, Light passing through subwavelength apertures, Rev. Mod. Phys. 82, 729787 (2010).
[3] O. T. A. Janssen, H. P. Urbach, and G. W. Hooft, Giant optical transmission of a subwavelength slit optimized using the magnetic field phase, Phys. Rev. Lett. 99, 043902 (2007).
[4] F. Villate-Gu´ıo, F. L´opez-Tejeira, L. Mart´ın-Moreno, and F. de Le´on-P´erez. arXiv:1207.6031 [physics.optics] (2012).

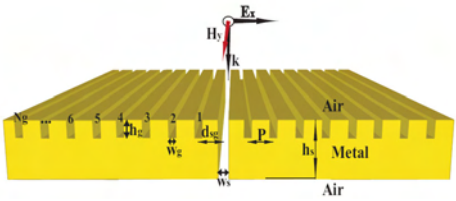

Figure 1: (Color). Schematic representation of the slit-groove array on a free-standing gold film of thickness h_s. The slit of width w_s is surrounded by $2N_g$ grooves (width w_g, depth h_g, and period P). The distance from the slit to the first groove, d_{sg}, is in principle different from P.

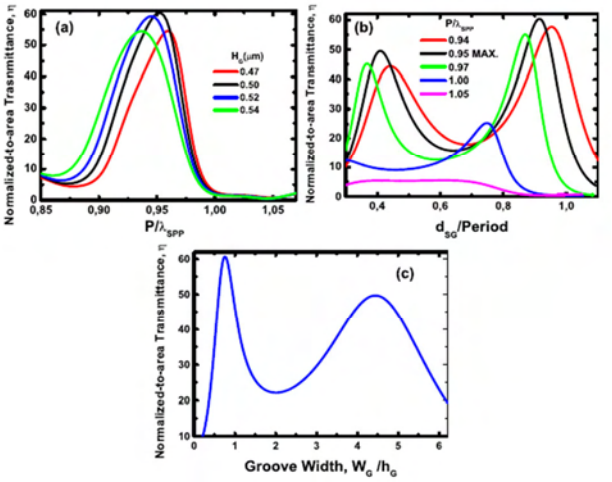

Figure 2: (Color). (a) Normalized-to-area transmittance (η) for a SGA as a function of the groove period P for groove depth increasing from h_g=470 nm to 540 nm at λ = 4:0 μm. P is normalized to λ_{spp} = 3:997 μm. (b) η as a function of the slit-first groove distance d_{sg} for several values of P/λ_{spp} taken from the black curve of (a) (h_g = 0.5μm). (c) η versus the aspect radio ($r = w_g/h_g$) for the optimal geometry of (b): P = 0.95 λ_{spp} and P = 0.91P.

Perturbative approach for the statistical scattering of waves in disordered waveguides: closed channels contributions and the effective medium approximation

M. Yépez and J. J. Sáenz

Condensed Matter Physics Department and Centro de Investigación en F´sica de la Materia Condensada (IFIMAC), Universidad Autónoma de Madrid, Fco. Tomás y Valiente 7, 28049-Madrid, Spain

miztli.yepez@uam.es

We study the statistical properties of wave scattering in a disordered waveguide. The statistical properties of the disordered system of length *L*, that we call the "Building Block", are derived from a random potential model, which is constructed as a sequence of *n* statistically independent scattering units in the propagation direction. The scattering units consist of thin potential slices, idealized as delta potentials in the longitudinal direction of the waveguide, while the variation of the potential in the transverse direction is arbitrary. The theoretical results were obtained in the short-wave-length or weak disorder approximation (where the wave number k and the mean free path ℓ satisfy the condition $k\ell >> 1$), assuming weak scattering units and by using two perturbative methods: Born series and the transition matrix method. The theoretical results were compared with numerical simulations when the waveguide supports $N = 2$ open channels (traveling modes) and $N' = 0;1;2;3$ closed channels (evanescent modes) were considered in the calculations.

Born series method predicts that the closed channels contributions are crucial for the statistics of the scattering amplitudes, while the statistic of the corresponding coefficients are insensitive to those contributions. Unfortunately, this perturbative method is only valid in the ballistic regime ($L >> \ell$), where its predictions are in good agreement with the numerical simulations; however, Born series predictions suggest that the closed channels contributions are relevant for the scattering amplitudes even beyond the ballistic regime, what is confirmed by the numerical simulations: see Fig. 1.

In order to give a more general description than Born series method, a perturbative method based on the transition matrix $\mathcal{T}$ method was performed. This method explains the intriguing contributions of the closed channels in the statistics of the scattering amplitudes, considers explicitly the multiple scattering processes and gives an excellent agreement with the numerical simulations even beyond the ballistic regime: see Fig. 2. In addition, when the waveguide admits a very large number of open channels $N >> 1$, the transition matrix method predicts that the Building Block can be replaced by an effective potential, whose real part is too sensitive to the number of closed channels considered in the calculations. On the other hand, if the number of open channels is $N \sim 1$, it is not possible to approximated the Building Block by an effective medium, what is due to the recurrent multiplescattering.

References

[1] A. Ishimaru, Propagation and Scattering in Random Media, Academic Press, New York, 1978.

[2] P. Sheng, Introduction toWave Scattering, Localization and Mesoscopic Phenomena, Academic Press, New York, 1995.

[3] P. A. Mello and N. Kumar, Quantum Transport in Mesoscopic Systems. Complexity and Statistical Fluctuations,Oxford University Press, Oxford, 2004.

[4] L. S. Froufe-Pérez, M. Yépez, P. A. Mello and J. J. Sáenz, Phys. Rev. E, 75, 031113, (2007); M. Yépez, P. A. Mello and J. J. Sáenz, AIP. Conf. Proc., 1319, 49, (2010).

[5] U. Frisch, Annales d'Astrophysique, 30, 565, (1967).

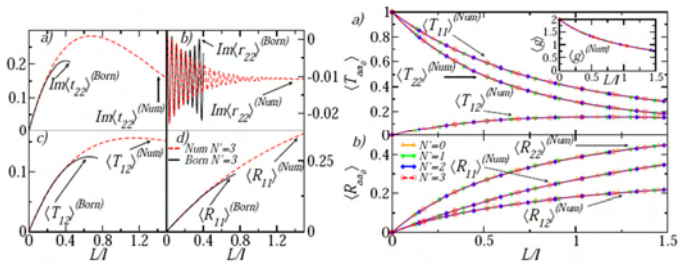

Figure 1: Left: Born series and numerical results for the expectation values of scattering amplitudes and coefficients when the waveguide supports N=2 open channels and N'=3 closed channels were considered in the calculations. Right: Numerical results for the expectation values of the coefficients.

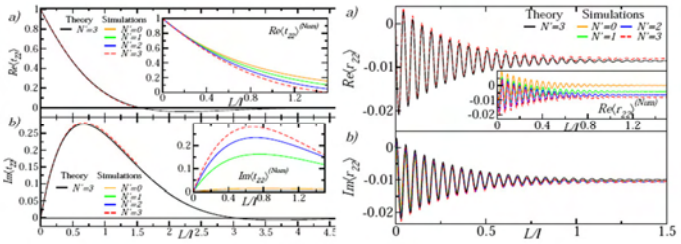

Figure 2: Transition Matrix and numerical results for the scattering amplitudes when the wave guide supports N = 2 open channels and N'=3 closed channels were considered in the calculations.

Organisers

Universitat
Rovira i Virgili

UNIVERSITAT
POLITÈCNICA
DE VALÈNCIA